HIGHWAY RESEARCH RECORD

Number 147

Bridges and Structures

9 Reports

Subject Classification

27 Bridge Design
32 Cement and Concrete

HIGHWAY RESEARCH BOARD
DIVISION OF ENGINEERING NATIONAL RESEARCH COUNCIL
NATIONAL ACADEMY OF SCIENCES—NATIONAL ACADEMY OF ENGINEERING

Washington, D. C., 1966 Publication 1422

Department of Design

W. B. Drake, Chairman
Assistant State Highway Engineer for
Planning, Research and Materials
Kentucky Department of Highways, Lexington

HIGHWAY RESEARCH BOARD STAFF

F. N. Wray, Engineer of Design

R. C. Edgerton, Assistant Engineer of Design

BRIDGE DIVISION

J. N. Clary, Chairman
Bridge Engineer
Virginia Department of Highways, Richmond

COMMITTEE ON BRIDGE DESIGN

(As of December 31, 1965)

Vernon J. Burns, Chairman
Deputy Chief Engineer (Design)
New York State Department of Public Works, Albany

R. J. Posthauer, Secretary
Senior Civil Engineer (Design)
New York State Department of
Public Works, Bridge Subdivision, Albany

W. C. Anderson, Chief, Research and Development Engineer, The Union Metal Manufacturing Company, Canton, Ohio
Louis M. Bjorn, Bridge Engineer, Vermont Department of Highways, Montpelier
Arthur L. Elliott, Bridge Engineer, California Division of Highways, Sacramento
T. R. Higgins, Director of Engineering and Research, American Institute of Steel Construction, New York, N.Y.
John J. Hogan, Consulting Structural Engineer, Portland Cement Association, New York, N.Y.
Nelson C. Jones, Engineer of Bridge and Road Design, Michigan State Highway Department, Lansing
Adrian Pauw, Professor of Civil Engineering, University of Missouri, Columbia
Sidney L. Poleynard, Bridge Design Engineer, Louisiana Department of Highways, Baton Rouge
Charles F. Scheffey, Chief, Structures and Applied Mechanics Division, U. S. Bureau of Public Roads, Washington, D.C.
C. P. Siess, Professor of Civil Engineering, University of Illinois, Urbana
J. R. Stemler, Manager, Highway Products and Structural Section, Sales Development Division, Aluminum Company of America, New Kensington, Pennsylvania
Ivan M. Viest, Structural Engineer, Sales Engineering Division, Bethlehem Steel Corporation, Bethlehem, Pennsylvania

COMMITTEE ON STEEL SUPERSTRUCTURES

(As of December 31, 1965)

M. N. Quade, Chairman
Consulting Engineer
Parsons, Brinckerhoff, Quade and Douglas
New York, N.Y.

Frederick H. Dill, Assistant to Vice President, Engineering, American Bridge Division, United States Steel Corporation, Pittsburgh, Pennsylvania
Arthur L. Elliott, Bridge Engineer, California Division of Highways, Sacramento
John W. Fisher, Research Assistant Professor, Fritz Laboratory, Lehigh University, Bethlehem, Pennsylvania
Carl H. Gronquist, Partner, Steinman, Boynton, Gronquist and London, New York, N.Y.
T. R. Higgins, Director of Engineering and Research, American Institute of Steel Construction, New York, N.Y.
William H. Munse, Jr., Department of Civil Engineering, University of Illinois, Urbana
Sidney L. Poleynard, Bridge Design Engineer, Louisiana Department of Highways, Baton Rouge
A. A. Toprac, Professor of Civil Engineering, University of Texas, Austin
Ivan M. Viest, Structural Engineer, Sales Engineering Division, Bethlehem Steel Corporation, Bethlehem, Pennsylvania

COMMITTEE ON CONCRETE SUPERSTRUCTURES

(As of December 31, 1965)

W. E. Baumann, Chairman
Engineer of Bridge and Traffic Structures
Illinois Division of Highways, Springfield

Harry N. Wenke, Secretary
Bridge Engineer
Portland Cement Association, Chicago, Illinois

Raymond Archibald, Otis, Oregon
James W. Baldwin, Rust Engineering Company, Pittsburgh, Pennsylvania
Carl E. Ekberg, Head, Department of Civil Engineering, Iowa State University, Ames
E. S. Elcock, Wichita, Kansas
Phil M. Ferguson, Department of Civil Engineering, University of Texas, Austin
R. S. Fountain, United States Steel Corporation, Pittsburgh, Pennsylvania
John J. Hogan, Consulting Structural Engineer, Portland Cement Association, New York, N.Y.
C. L. Hulsbos, Department of Civil Engineering, University of New Mexico, Albuquerque
T. W. Jennings, Assistant State Highway Engineer (Structures), Florida State Road Department, Tallahassee
Alan H. Mattock, Department of Civil Engineering, University of Washington, Seattle
Paul F. Rice, Technical Director, Concrete Reinforcing Steel Institute, Chicago, Illinois
W. T. Robertson, Bridge Design Engineer, Washington Department of Highways, Olympia

COMMITTEE ON SUBSTRUCTURES, RETAINING WALLS AND FOUNDATIONS

(As of December 31, 1965)

Wayne Henneberger, Chairman
Engineer of Bridge Design
Texas Highway Department, Austin

Raymond Archibald, Otis, Oregon
F. M. Fuller, Assistant Vice President, Raymond International, Inc., New York, N. Y.
H. D. Gibbons, The Union Metal Manufacturing Company, Canton, Ohio
W. T. Hunzicker, Assistant Bridge Engineer, Arizona Highway Department, Phoenix
Joe S. Robinson, Chief Engineer, Delaware State Highway Department, Dover
Charles B. Trueblood, Armco Steel Corporation, Armco Division, Middletown, Ohio

Foreword

The nine papers in this RECORD report research on several different subjects related to highway structures. They will be of interest to all who are involved in highway bridge design.

The design and erection of the large signs required on Interstate Highways has focused attention to the need for better information for the design of anchor bolts. Dr. Breen reports on thirty-six tests on anchor bolts ranging from $1\frac{1}{4}$ to 3 in. in diameter under different conditions.

The next two papers are concerned with piling. Dr. Hirsch describes and discusses the phenomena which can cause cracking and spalling of concrete piles during driving. He also outlines the fundamentals of good design and confirms several items of good driving practice including the protection of the pile head with a wood driving cap and the reduction of driving stresses by the use of a heavy ram with a low impact velocity.

Mr. Yang presents a review and analytical approach to pile buckling including piling with free-standing ends and piling subjected to lateral loads. He reports that under normal foundation conditions, only a little soil confinement is required to prevent the buckling of a pile unless the free-standing length becomes excessively long and that the reduction of elastic stability is more critical for a pile subject to a definite horizontal force than due to the increase of free-standing length.

The paper by Fisher, Kulak and Beedle reports on tension tests on long structural splices connected by high-strength bolts. In addition to the usual concept of bolted joints, the paper presents data on slip resistance for use in designing friction-type connections.

Slutter and Fisher give the results of fatigue tests on three different mechanical shear connectors, $\frac{3}{4}$-in. and $\frac{7}{8}$-in. diameter studs and channel connectors, and present a tentative design procedure for shear connectors.

In his study of splices in tensile reinforcing bars, Dr. Segner gives the results of eight different splicing systems applied to No. 9, 10, 11 and 14s deformed bars. These results will be valuable in the evaluation of systems and in design.

Professor Ferguson reports on an investigation of bond and shear in the cantilever ends of bent caps. He found that shear much higher than allowed by current specifications was feasible under some loading conditions and that vertical stirrups added no perceptible strength but horizontal web steel was effective.

The paper by Khachaturian and Gurfinkel develops requirements for strength and ductility in prestressed concrete beams and presents a method of beam design based on these factors.

Professor Beecroft presents a final report on the long term physical properties of two lightweight concretes that have been kept under compressive stress for five years in some cases and eight years in others. He also compares these properties with these of normal concrete specimens that were maintained under similar conditions. Under conditions of relaxing prestress, he finds the loss of prestress to be 50 percent greater in prisms of lightweight concrete than in normal weight concrete prisms.

Contents

Development Length for Anchor Bolts

JOHN E. BREEN, Associate Professor of Civil Engineering, University of Texas, Austin

This paper summarizes findings of a research program to study design criteria for the proper lengths for anchor bolt embedment into drilled shafts. The program included a series of tests on 36 anchor bolts ranging from 1¼ to 3 in. in diameter which were embedded near the edge of a square shaft specimen and were under a combination of flexural tension, bond, and splitting conditions approximating those in the prototype. Loaded-end slip behavior was determined at nominal working loads, at first yielding, and in many cases at ultimate capacity. Important trends affecting design practices are indicated.

•THE GENERAL purpose of this investigation was to establish the development length or the embedment length required to develop the tensile yield capacity of ASTM A 7 anchor bolts. At the same time it was desired to explore the effect of various types of end anchorages and certain other variables. A substantial amount of recent test data have been compiled on the proper development length for ASTM A 305 deformed reinforcing bars. Very little material is available concerning the length required to develop the strength of large-size anchor bolts. The main information existing is a series of concentric pullout tests reported by Abrams (1) which involved plain bars anchored with nuts and without washers. As has been shown by Ferguson et al. (2), the results of such concentric pullout tests, in which the concrete around the bolt is under compression, do not reflect the bond-slip behavior of elements in the tension zone of beam or pier members, such as the prototype sign support drilled shaft foundations.

In order to simulate the behavior found in typical sign support structures, the test specimen shown in Figure 1 was developed. The bolt is embedded near the edge and tension is applied through a flexural loading. In this type of specimen, the concrete around the anchor bolt is under a combination of tension, bond, and splitting conditions approximating those in the prototype structure. However, the shear distribution is different because of the absence of a soil pressure distribution.

This investigation reports on tests of 12 shaft specimens containing a total of 36 bolts. The anchor bolt sizes ranged from 1¼ in. to 3 in. with embedment lengths of 10 and 15 diameters. End anchorages consisted of either a standard nut or a combination of a standard nut and washer. Each bolt in a given shaft specimen was loaded in turn until yielding occurred, and after all bolts in a specimen had yielded several bolts were reloaded until ultimate was attained.

SPECIMENS

All of the specimens used in this program were of the same general type. When 1¼-in. through 2-in. diameter bolts were used, 4 anchor bolts were embedded in each specimen. However, only 2 bolts were used with the 2½-in. and 3-in. sizes. The individual specimens are designated by a 4-part code symbol. The first number represents the nominal bolt diameter. This is followed by the letter N for a specimen with a nut anchorage only, W for a specimen with a nut and washer anchorage, and S for the series with special type of end anchorage. This letter is followed by a number which is the embedment length in terms of number of bar diameters. The final letter indicates

Paper sponsored by Committee on Bridge Design and presented at the 45th Annual Meeting.

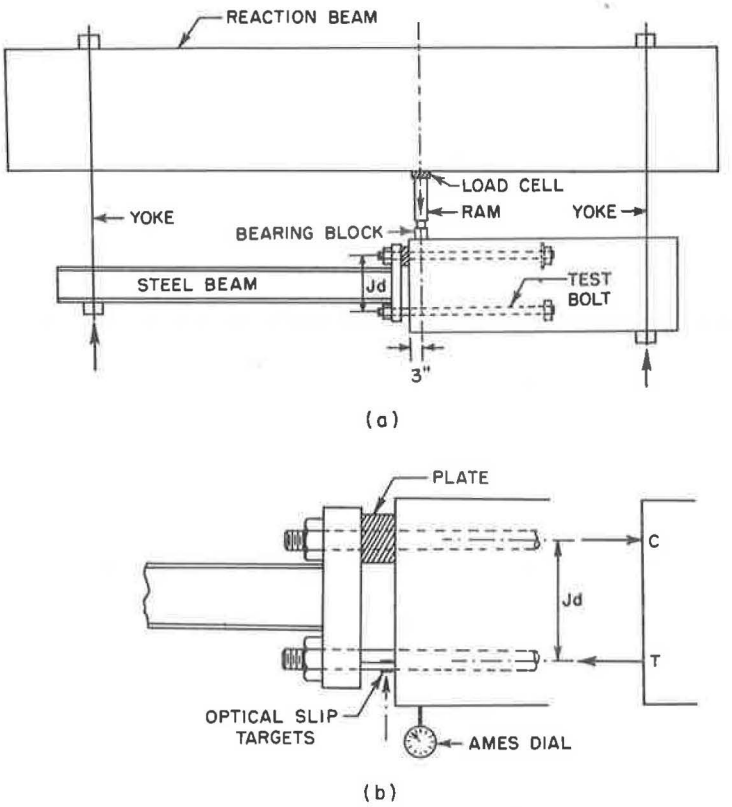

Figure 1. Test arrangement.

the designation of individual companion specimens. For example, the designation 1¼ W 10a designates a specimen in which a 1¼-in. bolt with a nut and washer anchorage was embedded for 10 diameters. The a indicates that it was the first of this type tested. Figures 2, 3 and 4 show the entire set of test specimens with critical dimensions. A tabulation of the important variables and summary of the test results is provided in the Appendix.

MATERIALS

Concrete

A concrete conforming to Texas Highway Department "Class A" concrete was used (3). The 1¼-in. and 1½-in. specimens were cast with a job-mixed concrete. The 1¾-in. through 3-in. specimens were cast with a ready-mixed concrete. High-early-strength cement (type III) was used with a cement factor of 5 sacks per cubic yard and a slump range of 3- to 4-in. Maximum aggregate size was 1 in. In general, the water-cement ratio was 7 gallons per sack.

Anchor Bolts

The anchor bolts were specified to be manufactured from ASTM A 7 steel with a minimum yield strength of 33 ksi. The bolts were fabricated locally with USS threads from round bar stock and were not galvanized. Figure 5 shows typical stress-strain curves for the bolts used. In one set of 1¾-in. bolts, the shape of the stress-strain curve as shown in Figure 6 indicated that a high carbon or other alloy steel was substituted and the yield point was 91 ksi.

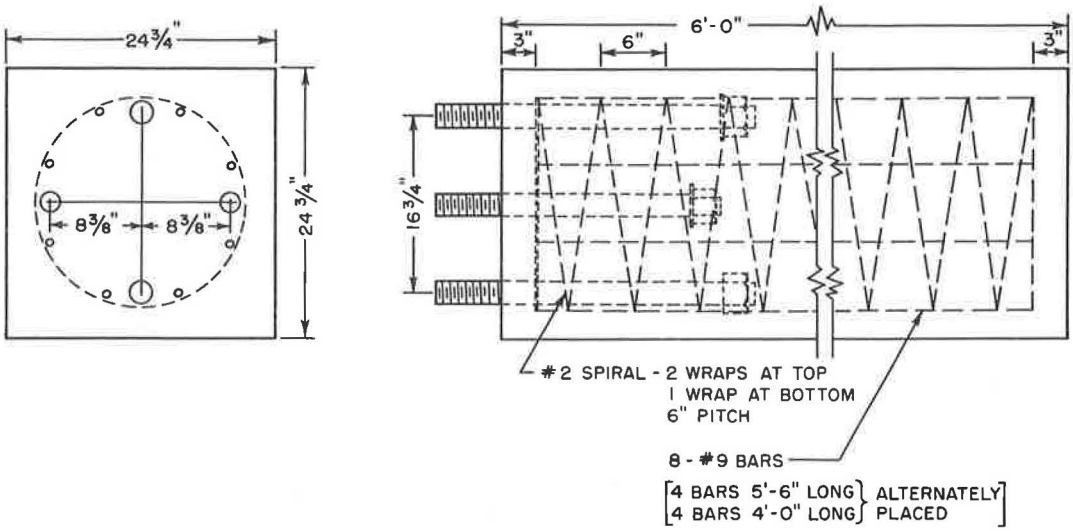

Figure 2. Typical specimen detail.

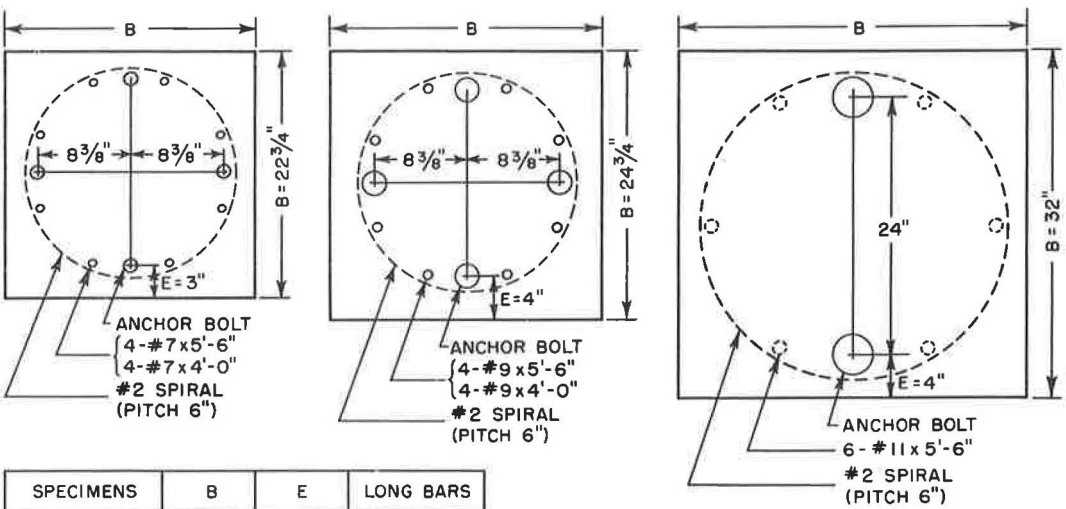

SPECIMENS	B	E	LONG BARS
ALL 1¼", 1½"	22¾"	3"	8-#7
ALL 1¾", 2"	24¾"	4"	8-#9
ALL 2½"	32"	4"	8-#9
ALL 3"	32"	4"	6-#11

Figure 3. Specimen details.

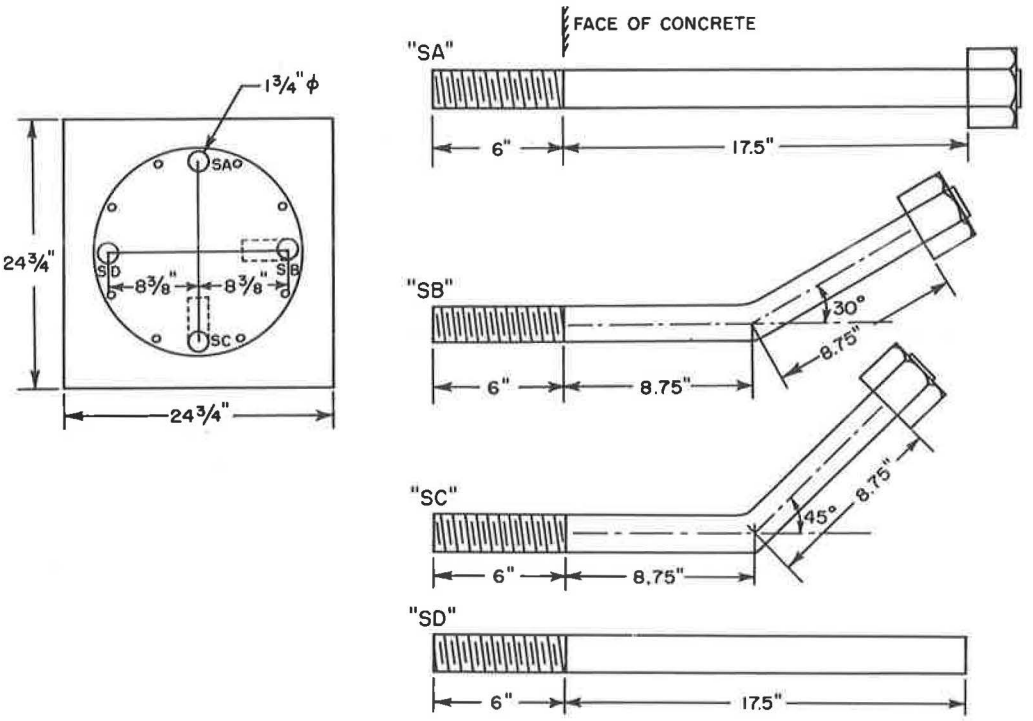

Figure 4. Details of special anchorage, series "S".

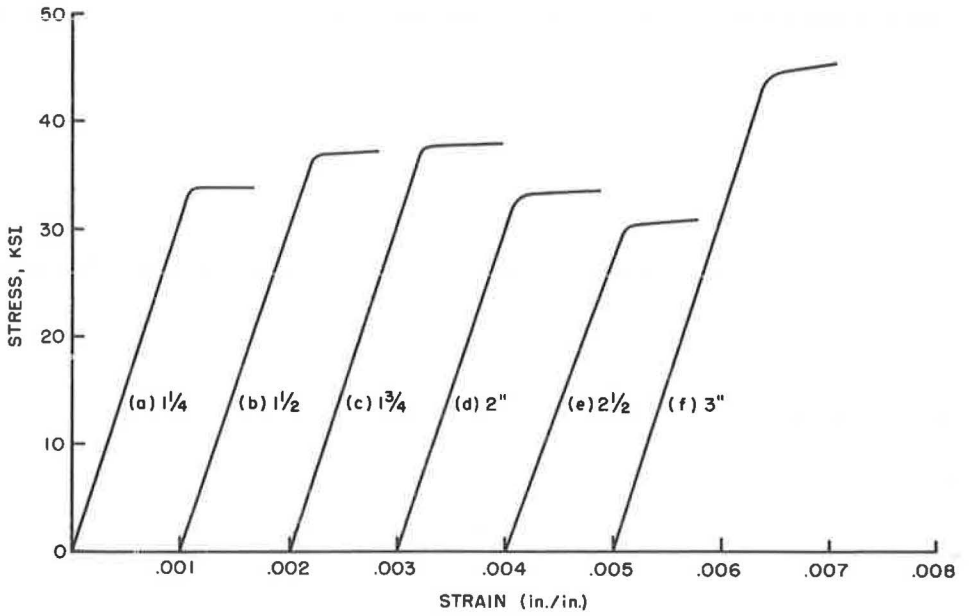

Figure 5. Mild steel anchor bolt stress strain diagrams.

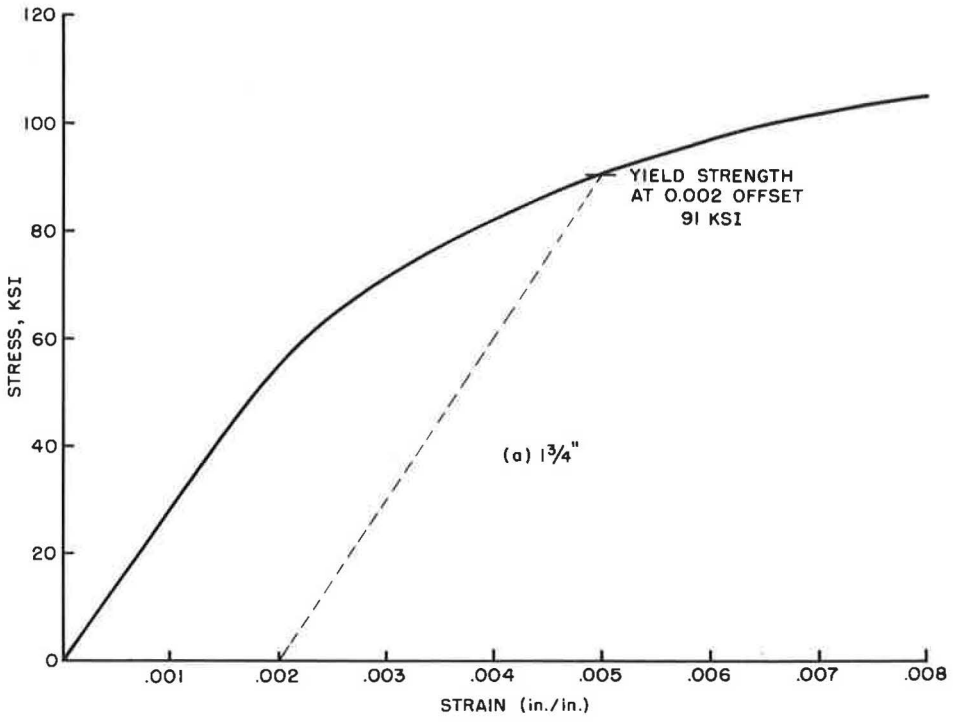

Figure 6. High strength anchor bolt stress strain diagram.

Reinforcing Steel

The main reinforcing steel used met ASTM A 305 and A 15 intermediate grade specifications. The spirals were made from the same grade steel.

Forms

All the specimens were cast in wooden forms as shown in Figure 7. The bolts were cast in a vertical position at the top of the forms. In all specimens the overall height was maintained at 6 ft to insure that the water gain effect would remain relatively constant in all tests and would closely approximate that found under field conditions.

Casting Procedure

The concrete was vibrated into place with a large internal vibrator. Standard compression test cylinders were cast from the batch which was placed in the top half of the specimen. Because of the 3- to 4-in. slumps used, good compaction was obtained.

Curing

The specimens were troweled and then left with a piece of moist burlap placed over the open end of the form. On the sixth day, the burlap and side forms were removed and the specimen was prepared for testing. At no time was the specimen lifted by the embedded anchor bolts.

Test Procedure

A calibrated hydraulic ram (A) and an electronic load cell (B) were inserted between the specimen and a reaction beam as shown in Figures 1 and 8. The ram load was distributed to the specimen through a thick steel bearing plate (C). Then a steel wide-

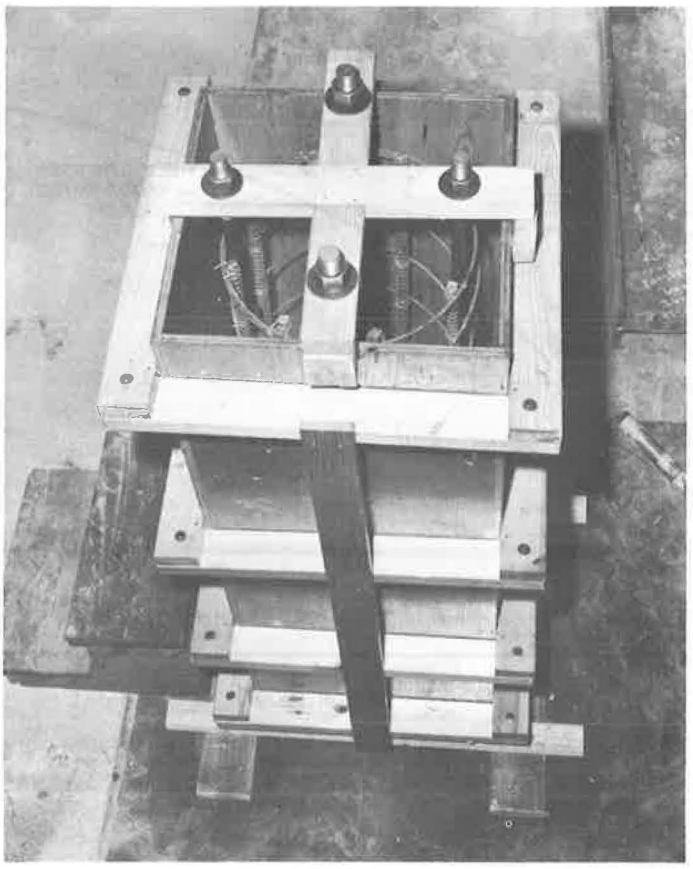

Figure 7. Specimen prior to concrete placement.

flange section (D) was attached. Reaction straps (E, F) were positioned to yoke the test assembly to the reaction beam (G). A heavy plate assembly was provided to concentrate the compression force over a relatively shallow area. This insured an accurate determination of the location of the compression centroid.

The instrumentation utilized was relatively simple. Dial gages were used at H, I, and J to measure the deflection at the reaction straps and directly under the applied load. An optical micrometer mounted on the theodolite shown at K in Figure 9 was used to measure the relative slip between the anchor bolt and the concrete face. Targets were mounted above and below the bolt on steel rods embedded in the concrete. A third target was mounted on the bolt next to the face of the concrete (L). The optical micrometer was used to read the relative displacement between the targets with a sensitivity of 0.001 in.

The loads were applied in increments and held until the instrumentation was read and any cracking recorded. Loading for a particular test required approximately 1 to 2 hours. Because each shaft contained more than one anchor bolt, the loading pattern had to be varied to preserve the specimen until all bolts were tested. This was accomplished by initially loading a bolt until yielding occurred. Then the specimen was unloaded, rotated, and the next bolt loaded to yielding. This continued until the last anchor bolt in a specimen, which would be loaded until complete failure occurred. If the condition of the specimen still permitted, it would be rotated and other bolts would be retested until complete failure occurred. However, since the specimens with $2\frac{1}{2}$-in. and 3-in. sizes contained only 2 bolts in each footing and since the overall specimen was not

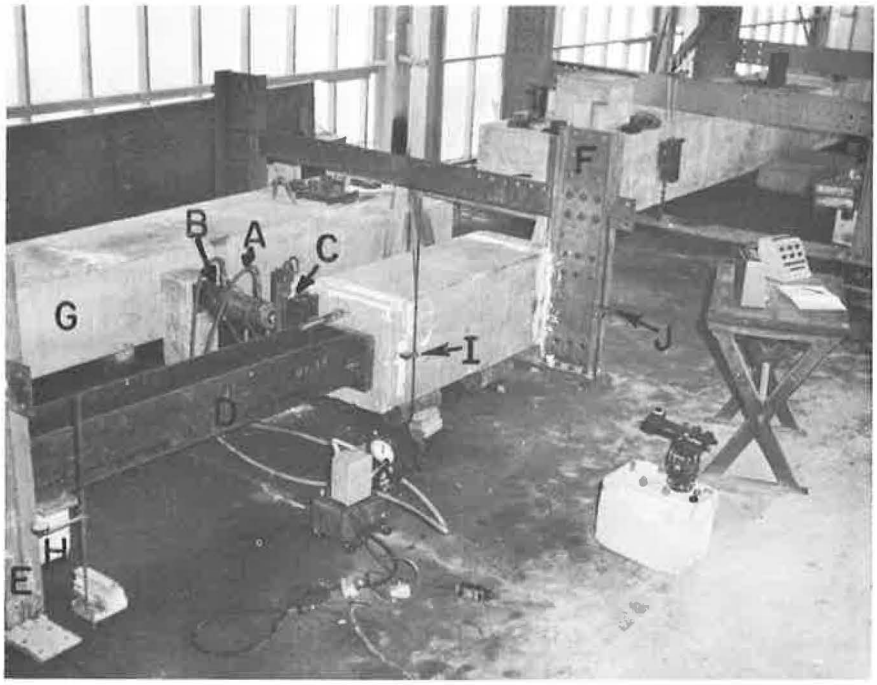

Figure 8. Loading arrangement.

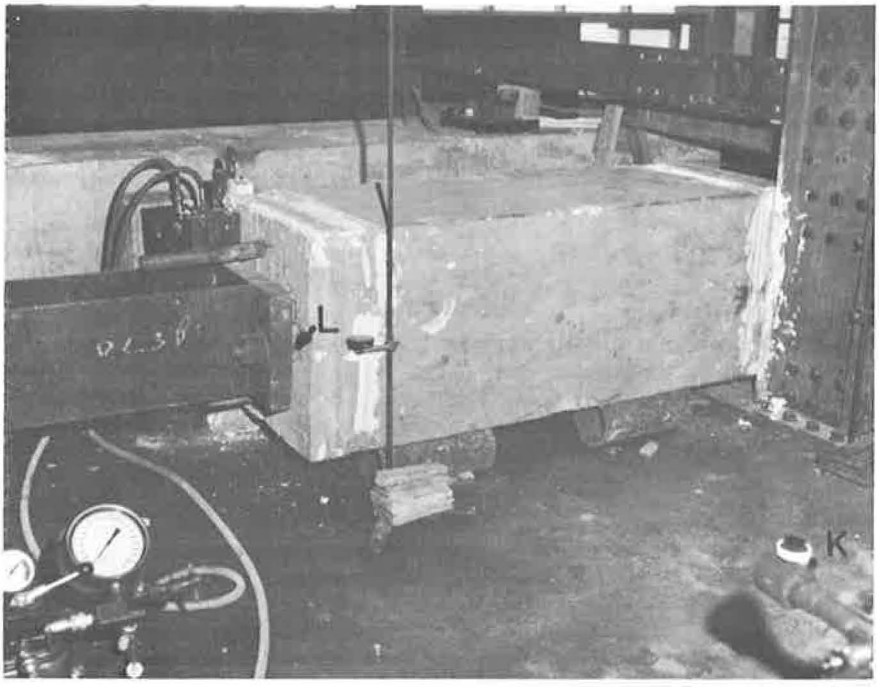

Figure 9. Slip measurement system.

too badly damaged after failure of one bolt occurred, these were taken to failure without retesting.

SPECIMEN BEHAVIOR AND FAILURE

Loaded-end slip started almost immediately upon initial loading and progressed with gradually increasing slip increments for equal increases in load. In a few cases splitting of the cover started over the bolt at the loaded end and progressed towards the anchored end. In most cases very definite flexural cracks opened up across the tension face. Usually the largest flexural crack occurred in the vicinity of the anchorage of the bolt. The final failure of those specimens which were taken to ultimate fell into 3 different classes:

Figure 10. Splitting failure.

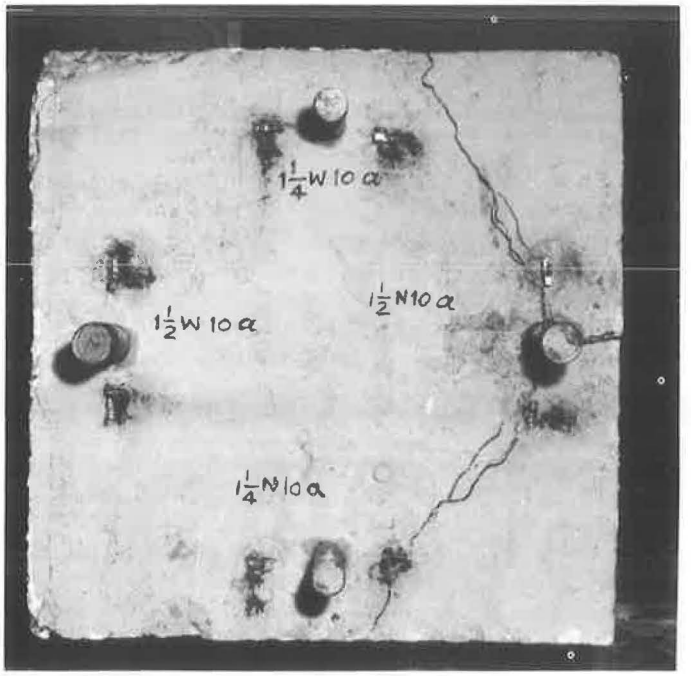

Figure 11. Splitting failure—end view.

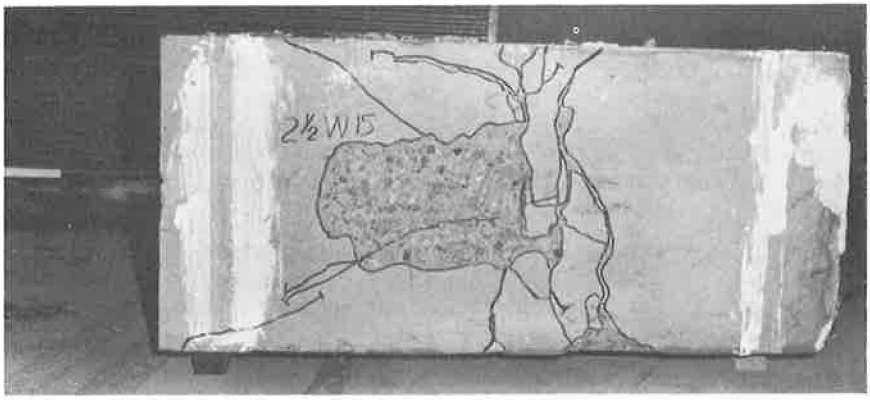

Figure 12. Crushing and spalling failure.

1. Specimens in which very definite and pronounced splitting appeared along the full length of the bolt at ultimate load, as shown in Figures 10 and 11. A very wide spitting crack extends from the bolt to the face of the specimen. The concrete cover over the bolt tends to break off into 2 distinct wedges. This is similar to failures found in pullout tests of deformed bars.
2. Specimens in which very little longitudinal splitting appeared prior to or at failure but in which very intensive spalling and crushing of the concrete in the vicinity of the anchorage of the bolt appeared. Most of the spalling and crushing did not become apparent until failure occurred. A typical case is shown in Figure 12.

Figure 13. Fracture of bolt inside concrete.

3. Specimens in which the full tensile strength of the bolt was developed and failure occurred in the steel anchor bolt itself. Two types of such failures were observed: (a) in 2 specimens the bolt failed inside the concrete in the root of the thread immediately in front of the anchor nut (Fig. 13); and (b) in 2 other specimens the bolt failed outside of the concrete at the root of the thread where the loading nut was attached. Although these 4 cases were the only ones in which the full ultimate tensile strength of the bolts was developed, the nominal yield points of the bolts were developed in all but 2 of the specimens tested.

In addition to these 3 general cases there was one other specialized type of failure. One anchor bolt was used which had no anchorage (i. e., it was just a smooth round bar). This specimen failed by simply pulling out of the concrete at a fairly low stress.

BASIC CALCULATIONS

Since the loading system was statically determinate, the applied moment at the concrete bearing face was known. The calculated steel stress, f_s, can be found approximately as $f_s = M/(A_s jd)$. It was decided that the values for calculated steel stress should be computed for the mean thread area as recommended by ASTM standards (4). Tests have shown that the strength computed on the area at the root of the thread gives a fictitiously high value, whereas strength computed on the pitch area gives a fictitiously low value. Slaughter (5) has observed that the mean diameter is closer to the diameter of an equivalent bar in tension than either of these other 2 diameters. This was confirmed by comparative tests on threaded and unthreaded samples of the bolt stock used in this series (6). The mean area can be calculated from

$$A_{sm} = 0.7854\left(D - \frac{0.9743}{n}\right)^2 \qquad (1)$$

where

A_{sm} = mean stress area,
D = the nominal diameter of the bolt, and
n = threads per inch.

Because the compression force was concentrated on a very small line area of the compression zone, the lever arm jd was known within an accuracy of 5 percent. Thus all steel stresses could be fairly accurately calculated.

TABLE 1

ANCHORAGE DETAILS

Bolt Diameter, in.	Nut Diameter, in.[a]	Washer Diameter, in.	Clear Cover, in.	Clear Cover / Diameter
1¼	1⅞[b]	3[d]	2⅜	1.90
1½	2¼[b]	3½[d]	2¼	1.50
1¾	2¾[c]	4[d]	3⅛	1.79
2	3⅛[c]	4½[d]	3	1.50
2½	3¾[b]	5[e]	2¾	1.10
3	4⅝[c]	5½[f]	2½	0.83

[a] Measured across flats.
[b] Finished hexagon nut (7).
[c] Heavy semifinished hexagon nut (7).
[d] Type B, regular series (8).
[e] Type A (8).
[f] Type B, narrow series (8).

VARIABLES

The primary variables were bolt diameter, bolt length, and type of end anchorage. Accompanying the variation in bolt diameter was the corresponding variation in the size of the standard nuts and washers used for the end anchorages. A complete tabulation of these dimensions is given in Table 1.

In addition, 3 secondary variables were introduced owing to the nature of the test specimens used and to the construction practices. The first is the ratio of the clear cover over a bolt to the bolt diameter. Following standard practice of the Texas Highway Department, bolts in a shaft specimen of a given depth were located with a fixed center-to-center dimension. Inherent in this method of detailing is a decreasing clear cover for larger bolt sizes. This can be represented both as an absolute decrease in cover and as a decreasing ratio of cover-to-bolt diameter. These values are also given in Table 1.

The concrete strength varied somewhat during the test program. The average f_c' was 4650 psi. However, in 2 shafts a substantial deviation from this value was noted. Although in many bond investigations using deformed bars a correction for variation in concrete strength has been made assuming that the bond strength will vary as the square root of f_c', there is no evidence that this same relationship would apply for the steel or bond stress developed at a given slip in these specimens. The basic test data were not corrected for the variation in concrete strength.

Finally, 2 of the anchor bolts tested were made from a high strength steel with no well-defined yield point.

LOADED END SLIP

The plot of total slip against either load, bolt stress, or bond stress gives the same curve shape for any given specimen since a combination of given bolt size and length establishes fixed ratios between load, tensile stress, and average bond stress.

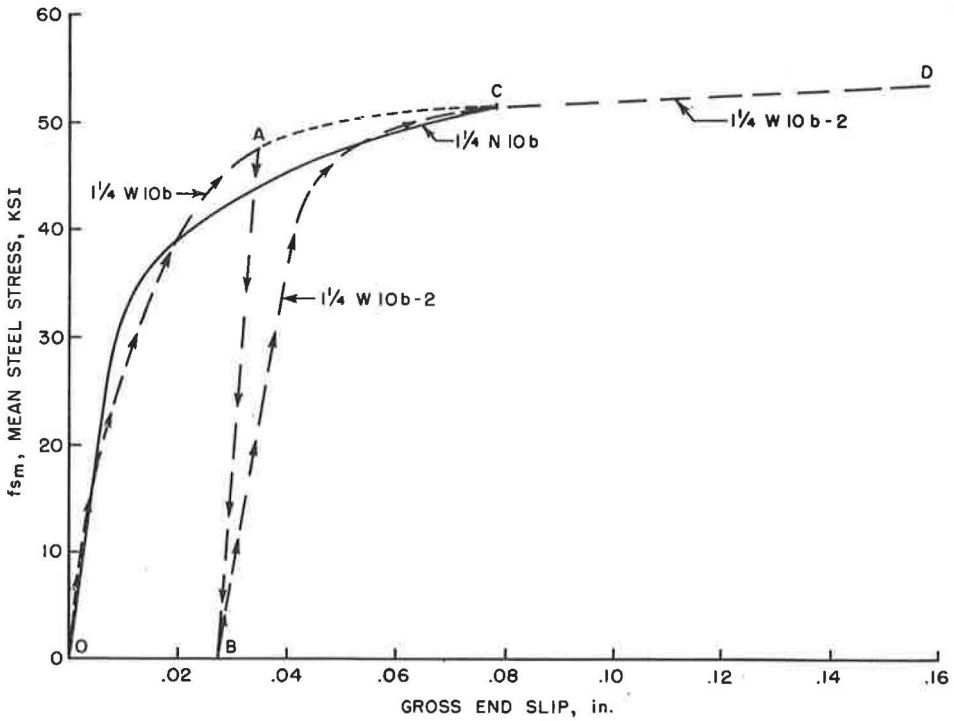

Figure 14. Effect of interrupted loading on steel stress-slip relation.

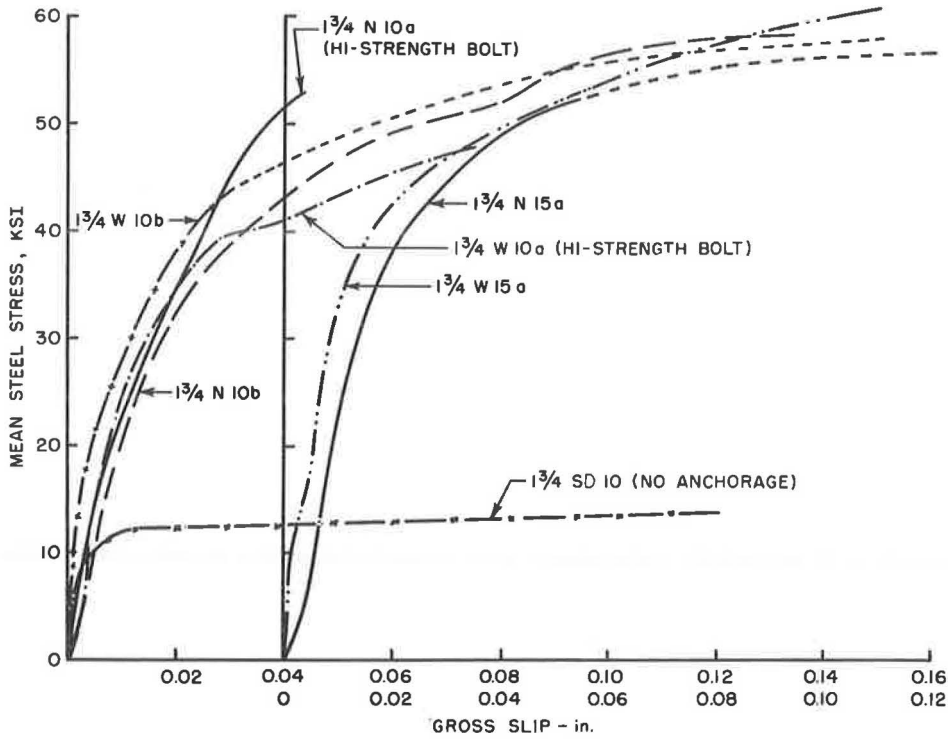

Figure 15. Steel stress-slip curves for $1\frac{3}{4}$-in. bolts.

Many of the specimens were loaded initially only until apparent yielding. Then the specimens were unloaded and a corresponding set of zero load readings were taken. Upon completion of the testing of the other bolts in the specimen, many of the bolts were reloaded until failure occurred. From the data in these tests it was found that all of the reloaded specimens seemed to have a common behavior. The steel stress-slip curve OA in Figure 14 shows the results of the initial testing of specimen $1\frac{1}{4}$ W 10b. Testing was discontinued at A and the load released. The total permanent slip OB upon removal of the load was observed as indicated by the descending branch AB. After testing the other bolts, bolt $1\frac{1}{4}$ W 10b-2 was reloaded. In this test the steel stress-slip curve BCD was observed. The results of a generally similar test specimen in which the bolt was initially tested to a much higher slip level is shown by curve OC. If one extends curve OA by the light dashed line shown until it intersects curve CD, it is reasonable to assume that a credible cumulative steel stress-slip curve for this specimen is described by the resulting total curve OACD. Such a construction was used to eliminate the unloading and reloading branches of the steel stress-slip curves, since this construction always took place substantially above the nominal yield point value. This hypothesized curve serves as a reasonable indication of the measure of ductility observed.

Steel stress-slip curves for all the specimens tested are given elsewhere (6). A typical pattern is indicated in Figure 15 where the results of the $1\frac{3}{4}$-in. diameter bolt tests are shown. It is especially interesting to note the performance of specimen $1\frac{3}{4}$ SD 10 in which no end anchorage at all was provided. The bolt barely developed 13 ksi in bond through friction and adherence before pulling out. The inclusion of end anchorage completely changes the load capacity, although at the expense of much increased slips.

END SLIP AT CRITICAL STEEL STRESSES

To illustrate service load behavior, the measured end slip corresponding to a steel stress of 20 ksi is shown in Figure 16 as a function of the bolt diameter. The 10 D bolts exhibit slightly greater slip than the 15 D lengths. However, in several cases the longer bolts actually show a greater slip. Except with the 3-in. bolts, the combination nut and washer anchorage (W) shows somewhat less slip than the plain nut anchorage (N). The reverse is true for the 3-in. bolts and is probably due to the reduced cover over the washers. Based on crack width limitations used with deformed bars, a good justification may be given for selecting the limiting service load value of slip as 0.02 in. for this type application. All of the bolts would meet this criterion.

Figure 17 shows the observed slip at the 33 ksi nominal yield point of the bolts. All specimens except 3 of the 3-in. bolts exhibit less than 0.03-in. end slip. In the case of the 3-in. bolts, the specimens with 10 D embedment length had failed (as indicated) at less than 33 ksi, while the 15 D specimen with nut and washer anchorage had a slip of approximately 0.046 in. at this stress level. It can again be noted that generally the 15 D specimens with washers show the least amount of slip at this stress level. In the 10 D specimens, slip does not seem to vary consistently with the type of end anchorage. In some cases, specimens with nuts show less slip than specimens with nuts and washers. The opposite is true in other cases.

To provide a qualitative indication of the relation between slip and elastic elongation, 2 additional curves are given in Figures 16 and 17. Assuming that the anchor bolt is completely unbonded, the theoretical elastic elongation is shown for both embedment lengths. In Figure 16, some of the 10 D bolts indicate an end movement fairly close to that which might be expected if no bond were present, while the 15 D bolts indicate substantially lower movements. In Figure 17, the 10 D bolts generally show an even greater end movement than that calculated. This indicates two important factors. The first is that the effect of bond at this level must be very small. Since the $1\frac{3}{4}$-in. bolt with no end

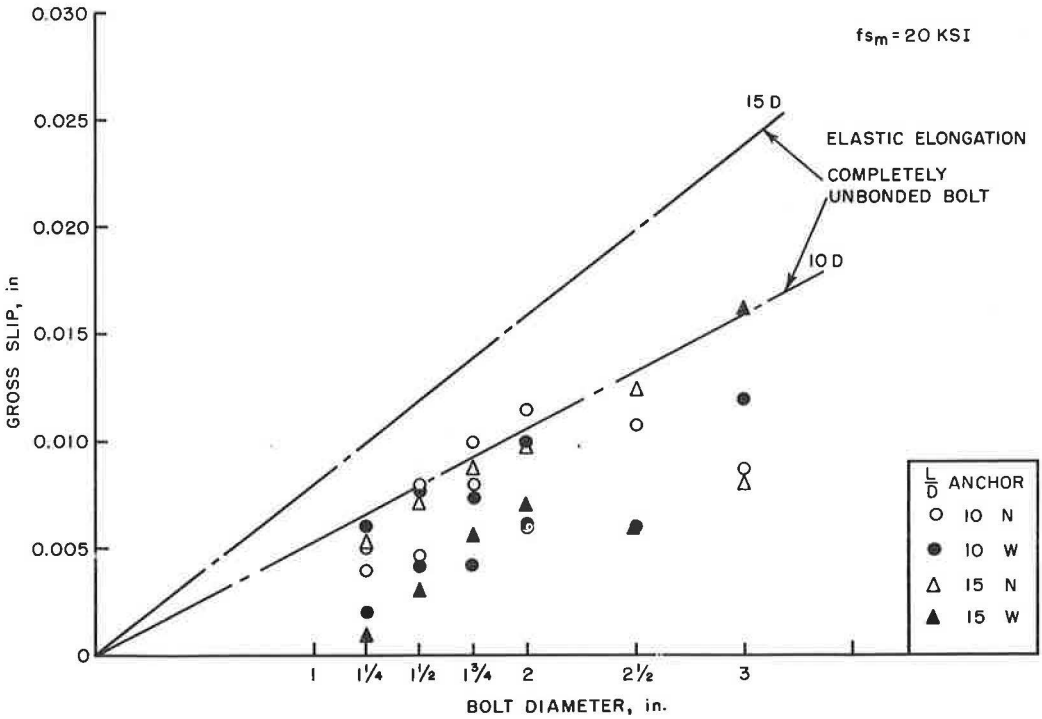

Figure 16. Slip at a steel stress of 20 ksi.

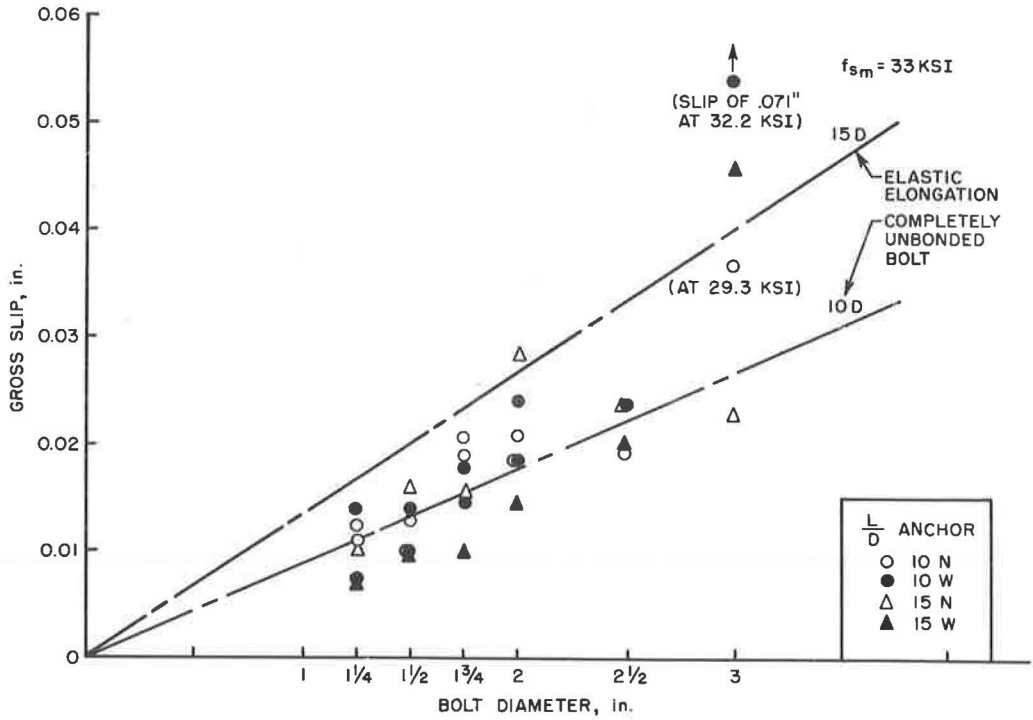

Figure 17. Slip at a steel stress of 33 ksi.

anchorage and a 10 D embedment length pulled out of the specimen at a stress of about 13.6 ksi, the major portion of the tensile development must be by bearing on the end anchorage device. Only a minor portion can be credited to friction bond. Second, since the measured end movement is greater than the total elastic elongation computed assuming zero bonding, the end anchorage device must have moved. After completion of the testing, the cover over the bolts was carefully removed. In many cases a definite separation was visible between the rear end of the nut and the concrete immediately adjacent to it. With nut and washer anchorages both a gap behind the nut and a definite bending of the washer around the nut were observed. This reinforces the conclusions arrived at by Abrams (1) that a certain amount of slip is essential to bring the end anchorage into action, and that the amount of movement required to bring this end anchorage into bearing will almost completely destroy the bar's adhesion and sliding resistance.

ULTIMATE STRENGTH BEHAVIOR

In addition to meeting service load requirements, it is important that bolts not fail due to loss of end anchorage or bearing capacity prior to development of full yield point stress. Even though the extreme amounts of slip occurring at high loads might be undesirable, a study has been made of the ultimate strength characteristics of the specimens.

Figure 18 shows the ultimate steel stress, f_{su}, as a function of the bolt diameter, D. All specimens tested to failure except the 10 D 3-in. bolts developed the 33 ksi nominal yield point. The 15 D embedment was much less effective than the 50 percent increase in embedment length. The larger bolt specimens with less cover failed due to the concrete over the anchor. After an attempt to relate ultimate steel stress to clear cover proved unsatisfactory, it was decided to compare ultimate steel stress and ratio of clear cover divided by bolt diameter, α (Fig. 19). Comparison with

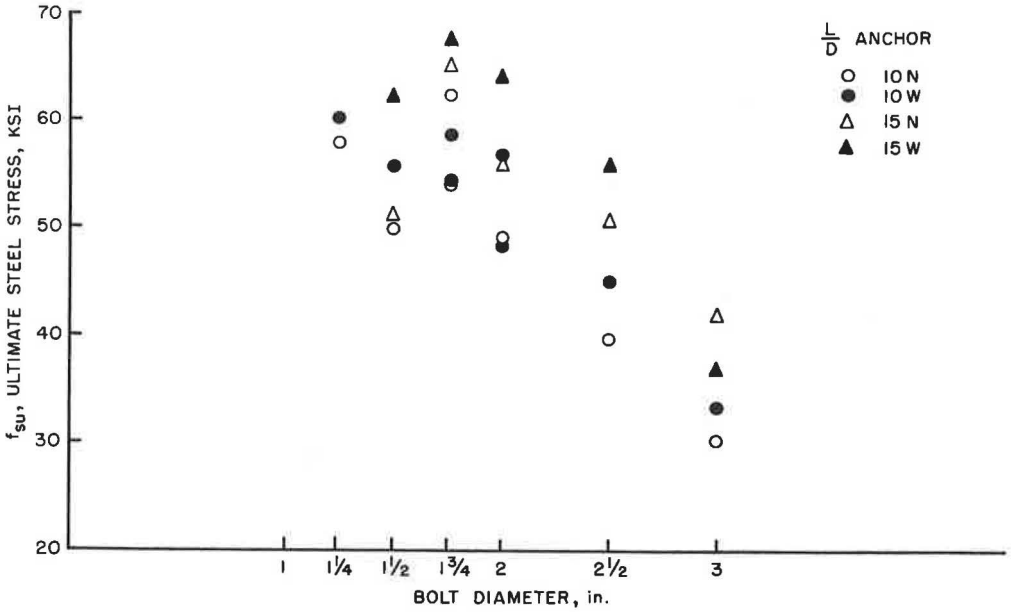

Figure 18. Ultimate steel stress.

Figure 18 indicates that clear cover as a function of bolt size seems to be a significant parameter. Two distinct curves are visible, one for the 10 D and the other for the 15 D embedment length. With low cover-to-diameter ratios, failure usually occurs due to crushing and spalling in the vicinity of the anchor. With higher cover-to-diameter ratios, the failure occurs due to splitting above the bolt. Unless sufficient cover is

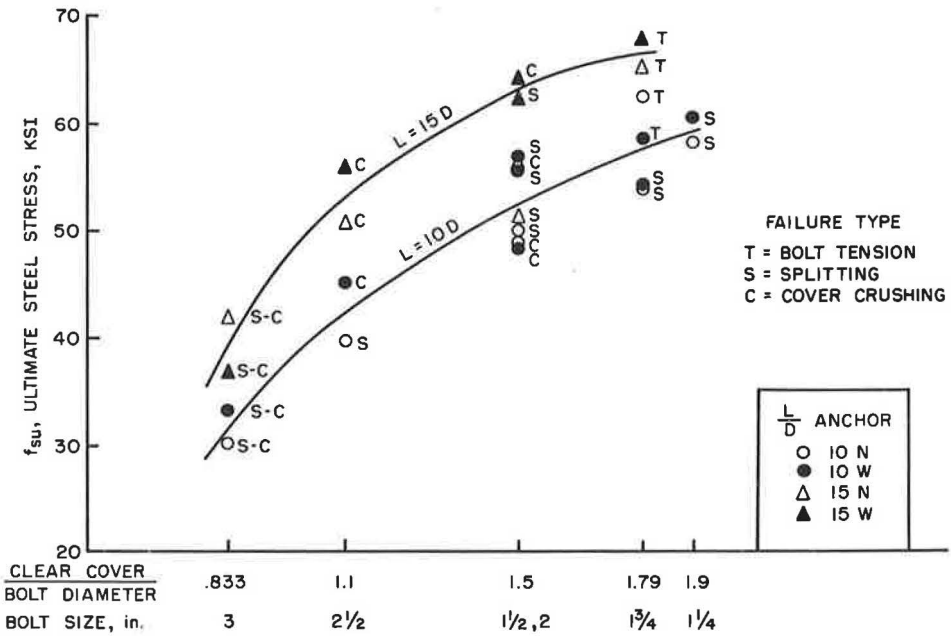

Figure 19. Ultimate steel stress as a function of clear cover.

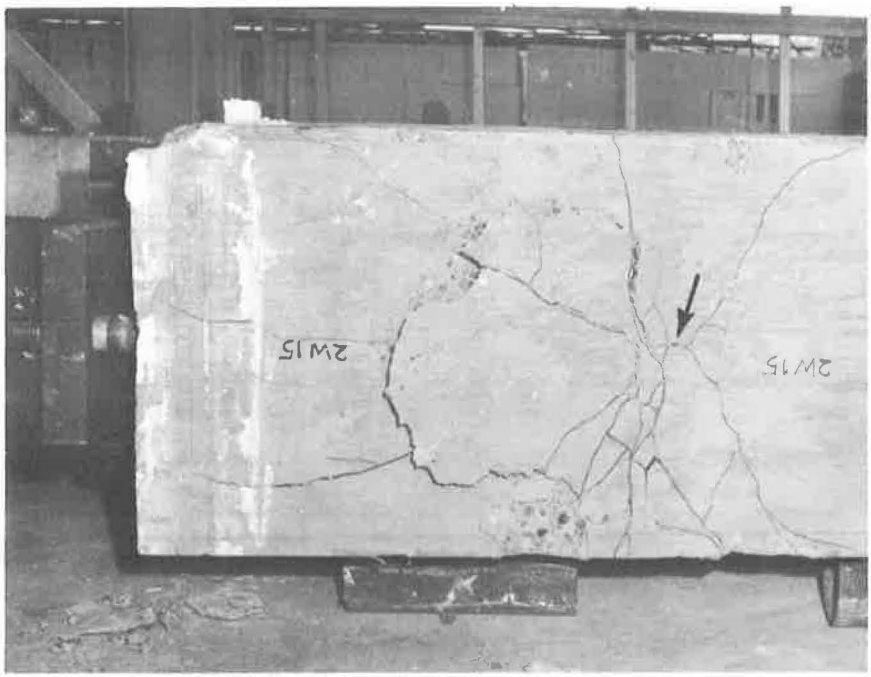

Figure 20. Spalling over anchor.

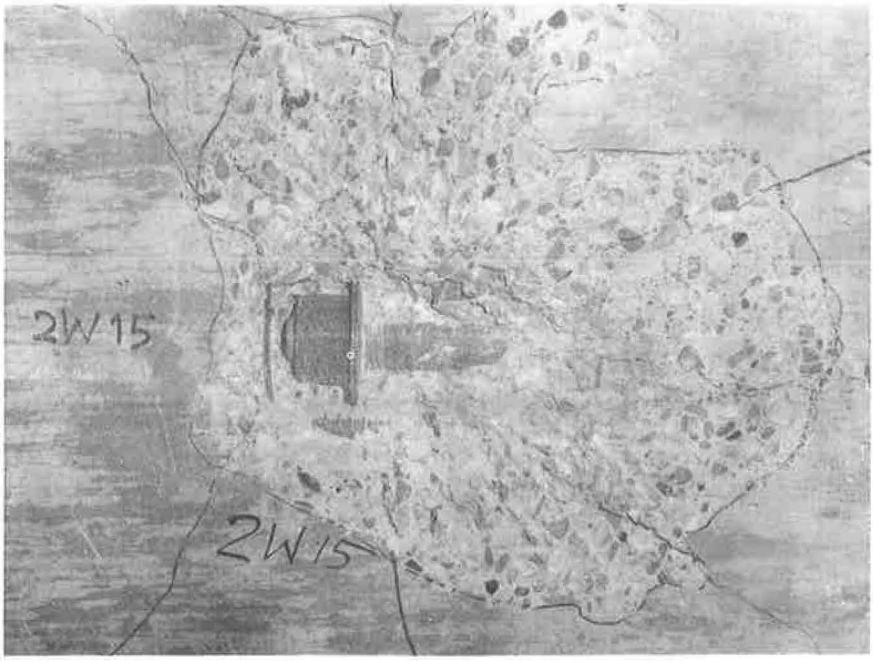

Figure 21. Anchor after removal of cover.

provided, the concrete above the anchor will crush prior to splitting of the cover or development of the tension capacity of the bolt.

BEARING STRESSES

In Abrams' study of the concentric pullout specimen, he had reported bearing stresses of as much as 13,000 psi in the specimens with nut anchorages. With f_c' of about 1850 psi, the calculated bearing stresses would be as high as $7.0 f_c'$. This is a case of a concrete element under a great deal of confinement and it should be possible to develop very high compressive stresses. Still, such magnitudes of stress are surprising.

In order to check the general magnitude of the ultimate bearing stresses developed by the anchorage devices, a simplified set of computations was made. Since the ultimate bond characteristics of the $1\frac{3}{4}$-in. bolt without an anchorage device were comparatively small, it was assumed that at failure the total tension force in the bolt was taken by the anchor device. With nut anchorages, the computed bearing stresses range from 15,000 to 32,000 psi. Since average f_c' is about 4650 psi, this ranges from 3 to 6 f_c' and is in reasonable agreement with Abrams' tests. It should be noted that in both Abrams' tests and in these specimens, spiral reinforcement was provided. This will be extremely helpful in containing internal splitting. For the specimens with nut and washer anchorages, the bearing stresses developed are approximately 2 to 3 f_c' if the full area of the washer is used. However, since so many of the specimens displayed

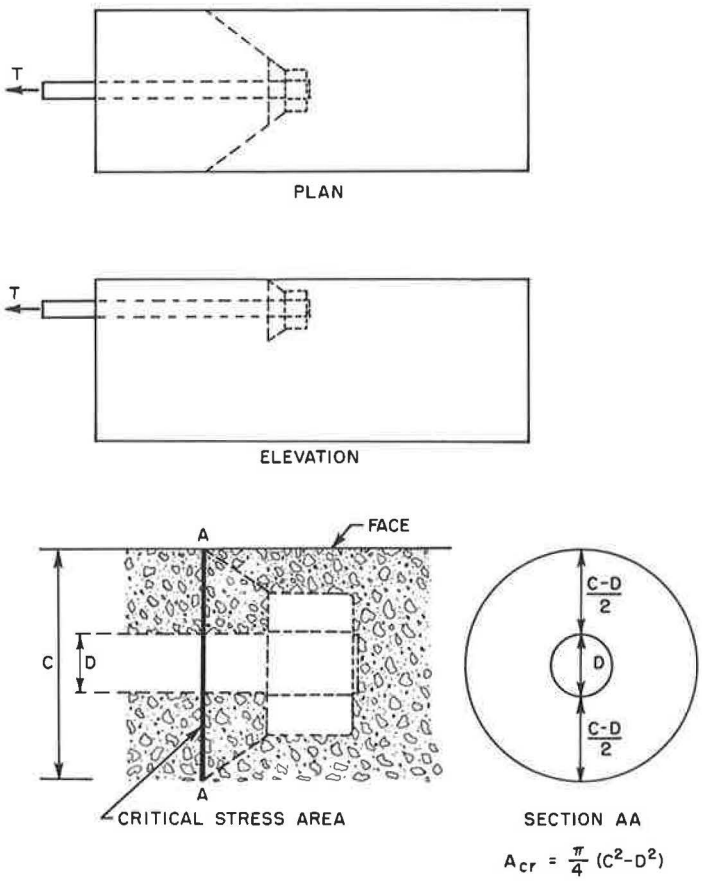

Figure 22. Critical bearing area hypothesis.

only a slight increase in ultimate steel stress when the washers were used, it can be concluded that the total area of the washer was not fully effective in developing bearing. Examination of the specimens after failure showed that the washers were generally bent back over the nuts.

EFFECT OF CLEAR COVER

In the cases in which failures occurred prematurely (i. e., before the tensile strengths of the bolts were developed) the failure seemed to be one of compression crushing and spalling of the cover immediately over the anchor device as seen in Figures 20 and 21. The location of the nut and washer is indicated by the arrow in Figure 20. The crushing seems to radiate from the anchor in a pyramidal pattern at angles somewhere between 30 and 45 degrees. Postulating that this same type of stress distribution might be taking place in 3 dimensions leads to the idea of a truncated cone of stress radiating out from the head.

The following hypothesis is advanced: Assume that the critical stress area for bearing will occur not at the end anchor, but on the base of the cone defined where the cone of stresses intersects the surface of the specimen as illustrated in Figure 22. This critical stress area can be computed as

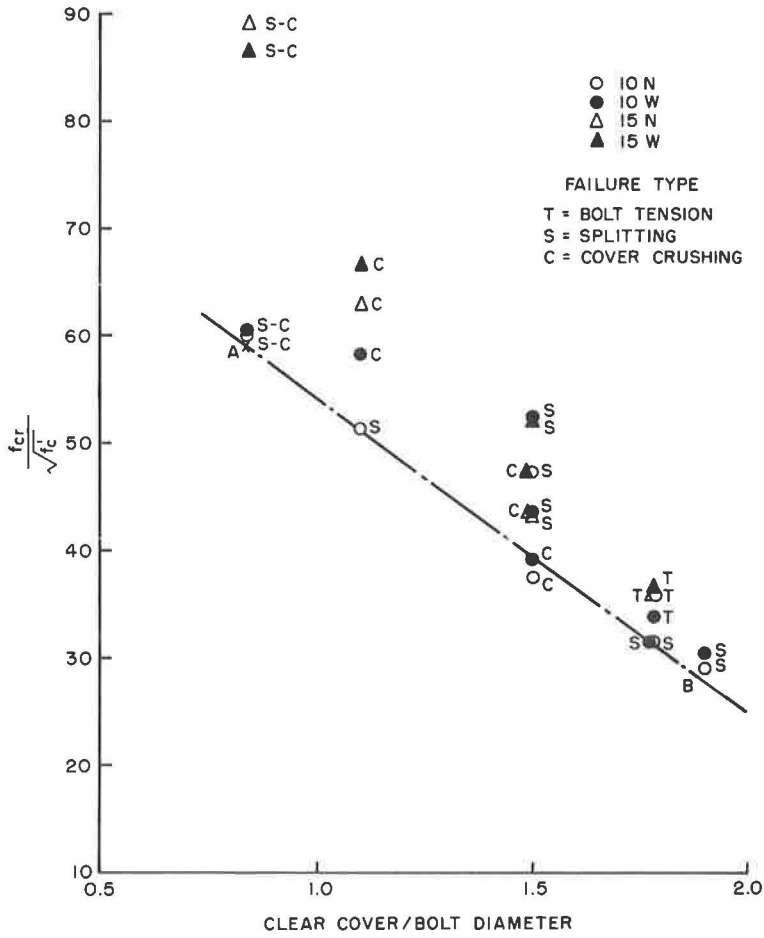

Figure 23. Critical bearing stress related to concrete strength.

$$A_{cr} = \frac{\pi}{4}(C^2 - D^2) \quad (2)$$

where C/2 is the total cover measured from the center line of the bolt and D is the diameter of the bolt. The fictitious ultimate bearing stresses on this section, f_{cr}, have been computed and are given in the Appendix.

In order to recognize the variation of the concrete strength in the specimens, the data were corrected for variation in cylinder strength. Since many of the failure phenomena involved splitting and since this is affected to a great extent by the tensile strength, the square root of f_c' was used. In Figure 23 the data for all specimens tested to ultimate are shown as a function of the ratio $f_{cr}/\sqrt{f_c'}$ and the parameter clear cover/bolt diameter, α.

The relation shown can be used in formulating some rough guides for design criteria. Since it is desirable that any such criteria be on the conservative side, a lower envelope was drawn in the form of the straight line AB. This line can be expressed by the equation

$$\frac{f_{cr}}{\sqrt{f_c'}} = 80 - 28\alpha \quad (3)$$

The limits and the overall shape of the curve were also investigated. As C approaches D, the clear cover approaches zero. For a bolt with a finite value of tensile force, $f_{cr}/\sqrt{f_c'}$ must approach infinity. Similarly, as C becomes much greater than D, then A_{cr} approaches infinity, and the stress must approach zero. Hence the overall form of the relationship should be a hyperbola, as shown in Figure 24. The straight line portion AB may only be valid for the very small range of variables in the present series. However, a few other points are available. In a pilot series of tests run prior to this investigation, a specimen was tested with a $1\frac{3}{4}$-in. anchor bolt, approximately 10 D embedment, a standard nut and washer anchor, and increased clear cover. This bolt failed in tension and the results are plotted on Figure 24. In addition, in Abrams' original set of pullout specimens he tested some $\frac{3}{4}$-in. bars with a nut and washer anchorage embedded for 8 in. in an 8-in. diameter concrete specimen. For these

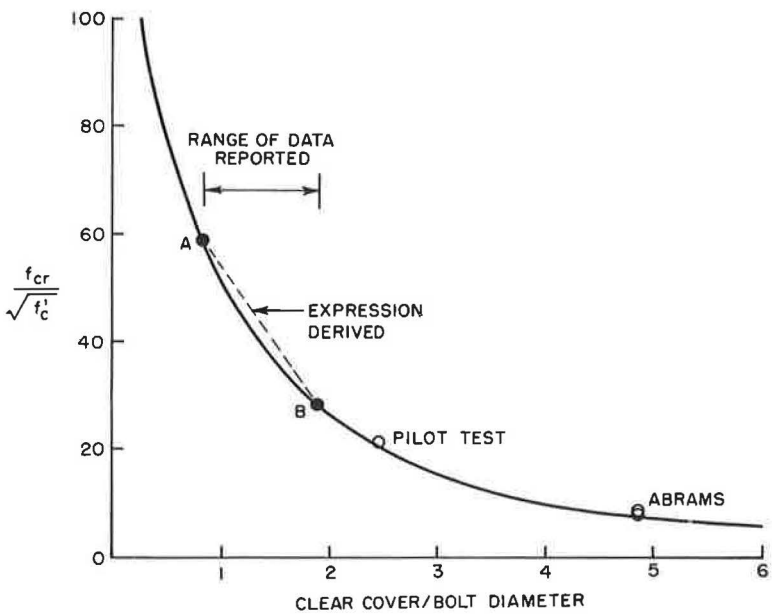

Figure 24. Probable general form of critical bearing stress-cover relationship.

specimens α is 4.84. The specimens failed by splitting of the concrete. These results are also shown and tend to indicate the general trend. However, it must be emphasized that any conclusions as to the desirable amount of cover deduced from these results are only approximate and should be considered within the limits of test data available. As in all empirical expressions, a great danger exists in extrapolating limited test results. However, in this case it is felt that an attempt should be made to give some guidance as to the magnitude of adjustment of cover in order to increase anchor bolt performance. Further testing to validate such changes is presently underway.

PILOT TESTS—BENT BOLTS

In order to get an idea of the effect of bending the bolt to get more cover over the anchorage zone, a limited series of tests was run. A single specimen was used (Fig. 4). Two of the 4 bolts were bent, a third had no anchor and the other was a standard bolt. The specimen with no end anchorage (SD) simply slipped out at a very low stress level. The standard specimen (SA) behaved the same as similar specimens. The bent specimens (SB and SC) showed a slightly stiffer load-slip response but did not develop as high an ultimate strength. Possibly this was due to very severe internal splitting. The higher bearing stresses developed in the other specimens could not be obtained. Another possibility is that the bend in the bar reduces the effective embedment length and causes a stress raiser with an adverse effect. Unfortunately, the results of this series must be regarded as inconclusive in that, while the bending of the bolt seems to give somewhat better service load characteristics, the ultimate strengths found were lower than in the unbent anchor bolts.

PILOT TESTS—HIGH STRENGTH BOLTS

The bolts used for specimens $1\frac{3}{4}$ N 10a and $1\frac{3}{4}$ W 10a had no well-defined yield point, as shown in Figure 6. Their yield strength, based on 0.002 offset, was 91 ksi. As can be seen in Figure 15, the specimens were loaded until end slips greater than 0.02 in. developed. Shortly after this the specimens failed by splitting. Both bolts developed an ultimate steel stress of 54.1 ksi. Their companion specimens with A 7 bolts failed in the thread area at the face of the anchor nut at ultimate steel stresses of 62.7 and 58.9 ksi. Since the high strength bolts did not develop as high an ultimate stress as the A 7 bolts owing to failure of the concrete, it might initially appear that there is no advantage in their use. However, design for A 7 bolts would be based on a minimum yield point of 33 ksi, which is less that 60 percent of the ultimate steel stress developed. Design for higher strength bolts would be based on a higher stress level and could be based on the more realistic limit of concrete control. However, it is important to note the observed reduction in ductility when high strength bolts are used. This might be adverse in some structures.

CONCLUSIONS AND RECOMMENDATIONS

The test series included anchor bolts ranging from $1\frac{1}{4}$ in. to 3 in. in diameter with embedment lengths of 10 and 15 diameters. The bolts were anchored with a standard nut or a combination of a standard nut and washer. All specimens had a No. 2 intermediate grade spiral at 6-in. pitch. Only a limited range of clear cover was investigated. All conclusions must be restricted to this range of physical dimensions. The following conclusions were reached:

1. The pullout tests indicated that A 7 (33 ksi yield point) steel anchor bolts can be fully developed with a 15-diameter embedment length and a standard nut anchor in all bolt sizes. (Steel stress computations are based on the mean diameter stress area.)
2. Anchor bolts of A 7 (33 ksi yield point) steel with diameters of $2\frac{1}{2}$ in. or less can be fully developed with a 10-diameter embedment length and a standard nut anchor.
3. An important variable affecting the developable tensile strength is the amount of clear cover. Results of calculations based on a limited empirical expression indicate that the clear cover should be increased for the $2\frac{1}{2}$-in. and 3-in. diameter bolts over the $2\frac{3}{4}$-in. and $2\frac{1}{2}$-in. used in these tests.

As a result of the evaluation of this test series, it is recommended that:

1. The clear cover over the large bolts ($2\frac{1}{2}$-in. and 3-in. diameter) should be increased if possible. The clear cover should be at least as great as that used with the smaller ($1\frac{3}{4}$-in. and 2-in. diameter) bolts. An indication of the cover required can be found using Eq. 3.
2. Additional specimens should be tested to investigate the effect of clear cover, particularly with respect to the development of large bolts. The data provided by this program are quite limited in this respect.
3. Consideration should be given to the effect of repeated loadings on the anchorage characteristics. Literature searches have indicated that very little information is available in this area.
4. Further study should be given to the use of higher strength steel bolts. The limited pilot tests indicate these may be more efficient at service load levels than the corresponding larger bolts. It is possible that some of the cover modifications associated with the very large diameter bolts could be partially avoided by providing reduced diameter, high strength bolts.

ACKNOWLEDGMENTS

The tests described here were conducted as part of the overall research program of the University of Texas Center for Highway Research. The work was sponsored jointly by the Texas Highway Department and the U. S. Bureau of Public Roads. The project was materially aided by effective liaison with the Texas Highway Department through the advisory committee consisting of Wayne Henneberger, Larry G. Walker, and DeLeon Hawkins.

REFERENCES

1. Abrams, D. A. Tests of Bond Between Concrete and Steel. Univ. of Ill. Eng. Exp. Sta. Bull. No. 71, pp. 97-99, Dec. 1913.
2. Ferguson, P. M., Turpin, R. D., and Thompson, J. N. Minimum Bar Spacing as a Function of Bond and Shear Strength. Jour. ACI, Vol. 50, pp. 869-888, June 1954.
3. Texas Highway Department. Standard Specifications for Road and Bridge Construction. Jan. 2, 1962.
4. American Society for Testing Materials. Low Carbon Steel Externally and Internally Threaded Standard Fasteners (A 307-58T) 1958 Standards, Part I, p. 749.
5. Slaughter, E. M. Tests on Threaded Sections Show Exact Strengthening Effect of Threads. Metal Progress, Vol. 23, No. 3, pp. 18-20, March 1963.
6. Breen, J. E. Development Length for Anchor Bolts. Univ. of Tex. Center for Highway Research Rept. 3-5-63-53, April 1964.
7. Square and Hexagon Bolts and Nuts. American Standard ASA B18. 2-1960, published by ASME.
8. Plain Washers. American Standard ASA B27. 2-1958, published by ASME.

Appendix

SUMMARY OF DATA

Specimen	f_c' (ksi)	f_y (ksi)	f_s at Slip = 0.01 (ksi)	f_s at Slip = 0.02 (ksi)	Slip at f_s = 20 (in.)	Slip at f_s = 33 (in.)	f_{su} (ksi)	Failure[a]	f_{cr} (psi)	$\frac{f_{cr}}{\sqrt{f_c'}}$	Clear Cover / Diameter
1¼N10a	3.16	33.7	30	40	0.005	0.012	43.5	D	1560	27.9	1.9
1¼N10b	5.04	33.7	32	39	0.004	0.011	58.0	S	2085	29.3	1.9
1¼W10a	3.16	33.7	37	—	0.002	0.007	41.2	D	1480	26.5	1.9
1¼W10b	5.04	33.7	27	39	0.006	0.014	47.3	D	1700	24.0	1.9
1¼W10b-2	5.04	33.7					60.3	S	2170	30.6	1.9
1¼N15a	4.04	33.7	33	40	0.005	0.010	41.9	D	1520	24.0	1.9
1¼W15a	4.04	33.7	37	42	0.002	0.007	42.7	D	1540	24.5	1.9
1½N10a	3.16	37.0	26	40	0.008	0.013	50.0	S	2640	47.2	1.5
1½N10b	5.04	37.0	33	40	0.005	0.010	41.1	D	2170	30.6	1.5
1½W10a	3.16	37.0	32	41	0.004	0.010	41.6	D	2200	39.2	1.5
1½W10a-2	3.16	37.0					55.8	S	2950	52.8	1.5
1½W10b	5.04	37.0	23	39	0.008	0.014	38.9	D	2060	29.0	1.5
1½N15a	4.04	37.0	25	37	0.007	0.016	41.1	D	2170	34.5	1.5
1½N15a-2	4.04	37.0					51.1	S	2700	43.2	1.5
1½W15a	4.04	37.0	33	41	0.003	0.010	62.2	S	3280	52.2	1.5
1¾N10a	4.66	91.0	22	34	0.008	0.019	54.1	S	2140	31.6	1.785
1¾N10b	4.74	38.0	20	32	0.010	0.021	62.7**	T	2480	36.0	1.785
1¾W10a	4.66	91.0	24	34	0.008	0.018	54.1	S	2140	31.5	1.785
1¾W10b	4.74	38.0	28	38	0.004	0.014	43.8	D	1740	25.3	1.785
1¾W10b-2	4.74	38.0					58.9**	T	2340	34.0	1.785
1¾N15a	5.30	40.5	24	38	0.008	0.015	51.6	D	2050	28.2	1.785
1¾N15a-2	5.30	40.5					65.3**	T	2590	35.6	1.785
1¾W15a	5.30	40.5	33	42	0.006	0.010	67.9**	T	2690	36.7	1.785
2N10a	4.66	36.7	18	32	0.011	0.021	42.5	D	2260	33.2	1.5
2N10b	4.74	30.6	24	34	0.006	0.018	38.5	D	2045	29.7	1.5
2N10b-2	4.74	30.6					49.0	C	2600	37.8	1.5
2W10a	4.66	36.7	20	34	0.010	0.018	50.3	D	2670	39.3	1.5
2W10a-2	4.66	36.7					48.3	C	2570	37.8	1.5
2W10b	4.74	30.6	24	31	0.006	0.024	38.5	D	2045	29.8	1.5
2W10b-2	4.74	30.6					56.8	S	3020	43.8	1.5
2N15a	5.17	33.5	21	29	0.009	0.027	41.8	D	2220	43.2	1.5
2N15a-2	5.17	33.5					56.2	C	2990	41.5	1.5
2W15a	5.17	33.5	28	37	0.007	0.016	45.7	D	2430	33.6	1.5
2W15a-2	5.17	33.5					64.0	C	3400	47.3	1.5
2½N10a	4.63	30.7	19	34	0.011	0.019	39.7	S	3510	51.5	1.1
2½W10a	4.68	30.7	25	30	0.006	0.024	45.0	C	3980	58.4	1.1
2½N15a	5.06	30.7	16	30	0.011	0.024	30.7	C	4470	63.0	1.1
2½W15a	5.46	30.7	24	32	0.006	0.021	55.9	C	4940	66.8	1.1
3N10a	4.88	45.0	21	26	0.008	—	30.4	S-C	4200	60.1	0.833
3W10a	4.75	45.0	19	24	0.012	—	33.3	S-C	4600	60.8	0.833
3N15a	4.18	45.0	23	31	0.008	0.023	42.0	S-C	5800	89.2	0.833
3W15a	3.55	45.0	15	23	0.016	0.046	36.9	S-C	5100	86.5	0.833
1¾SD10	4.90	35.5	12	12	—	—	16.1	SL	640	9.1	1.785
1¾SA10	4.44	35.5	16	32	0.012	0.022	36.5	D	1450	21.8	1.785
1¾SA10-2	4.90	35.5					43.3	S	1720	24.6	1.785
1¾SB10	4.44	35.5	29	—	0.007	0.012	34.0	S	1350	20.2	1.785
1¾SC10	4.44	35.5	21	41	0.010	0.015	44.1	S	1750	26.2	1.785

[a]T = bolt tension; S = splitting; C = crushing over anchorage; D = discontinued after apparent yield; SL = bolt sliding out.
**Average tensile ultimate of 3 companion specimens-63.8 ksi.

Discussion

W. C. ANDERSON, Chief Research & Development Engineer, the Union Metal Manufacturing Co., Canton, Ohio—The subject covered in Prof. Breen's paper is very timely and gives data regarding means for obtaining more economical anchorages. Particularly in the Sign Support program the general specifications are those of AASHO, and I don't believe there is any reference to allowable stress in bonding or bearing in concrete of anchor bolts. American Concrete Institute Building Code (June 1963) gives some bond stresses and bearing values which are not really applicable but can be used as guides.

The study is particularly pertinent to shallow steel reinforced foundations and low strength bolts (A 7). It further establishes that the real bearing value of concrete in compression is many times the generally accepted allowable compression stress, if the concrete is sufficiently contained. The data support "clear cover" distances which are rational to diagonal shear stress analyses. The study also shows that washers as bearing plates on top of the nuts must be adequate in thickness to support the loads imposed or they have little value.

Other related information needed includes further investigation of shear bond stresses with higher strength steels with specifically noted surface conditions. The value of nuts embedded in deep foundations should be studied.

An examination of different styles of foundations helps show where the greatest interest should lie. Spread or slab type footings are classic with bridge engineers. These are ideal to support vertical loads. Here short anchor bolts have a real advantage. Cylindrical foundations will generally cost one-tenth or less as much as a slab foundation to support a vertical cantilever. Here the anchor bolts have been long, nearly to the bottom of the cylinders and have eliminated the need for any other reinforcing. In this case the greatest economy points to a yield of at least 55,000 psi, which is now readily available at no premium.

In the steel pole industry there have been many thousands of installations of deep cylindrical foundations over the last 40 years with loads up to 1,000,000 ft-lb that we know of, and I don't know of a single structural failure.

Getting back to the main subject, I would like to see some adoption of engineering specifications which would permit the designer to use the most economical anchor bolts in the most economical overall design. The anchoring value of a nut on the bottom of a rod might make a real contribution.

JOHN E. BREEN, Closure—Mr. Anderson's discussion is timely in pointing out the need which exists for extending the study to include the effects of higher strength steel bolts and deep cylindrical foundations. In an extension of the project reported on in this paper, both variables are under investigation as well as a study of the effect of repeated loads at service load levels.

Fundamental Design and Driving Considerations for Concrete Piles

T. J. HIRSCH, Associate Professor and Head of Structural Research Department, Texas Transportation Institute, Texas A&M University

•THE PURPOSE of this paper is to describe and discuss briefly the phenomena which can cause cracking and spalling of concrete piles during driving and to outline procedures which will prevent these problems. In some cases of driving of concrete piles, cracking and spalling have been encountered and in most instances these problems can be avoided by apply certain fundamentals of good design and driving practices.

TYPES OF PROBLEMS

In general, the problems of cracking and spalling of concrete piles which may occur during driving can be classified into 4 types:

1. Spalling of concrete at the head of the pile due to high compressive stress;
2. Spalling of concrete at the point of the pile due to hard driving resistance at the point;
3. Transverse cracking or breaking of the pile due to tensile stress wave reflected from the tip or head of the pile; and
4. Spiral or transverse cracking due to a combination of torsion and reflected tensile stress wave. This type cracking is sometimes accompanied by spalling at the crack.

CAUSES OF PROBLEMS

Compression

Spalling of concrete at the head of the pile is caused by very high or irregular compressive stress concentrations. This type problem can occur from a variety of conditions:

1. Insufficient cushioning material between the pile driver's steel helmet or cap and the concrete pile will result in a very high compressive stress on impact of the pile driver ram.
2. When a pile is struck by a ram at a very high velocity, or from a very high drop, a stress wave of high magnitude is produced. This stress is directly proportional to the ram velocity.

If the pile is idealized as a long elastic rod, with an elastic cushion on top as shown in Figure 1(A), equations for the compressive stress can be developed (10, 22), using the following notation:

σ_c max = maximum compressive stress at pile head, psi;
W = ram weight, lb;
$V = \sqrt{2gh}$ = ram impact velocity, ips;
h = ram free fall, in.;
g = acceleration due to gravity, 386 in./sec^2;
$K = \frac{A_c E_c}{t_c}$ = cushion stiffness, lb/in.;

Paper sponsored by Committee on Substructures, Retaining Walls and Foundations and presented at the 45th Annual Meeting.

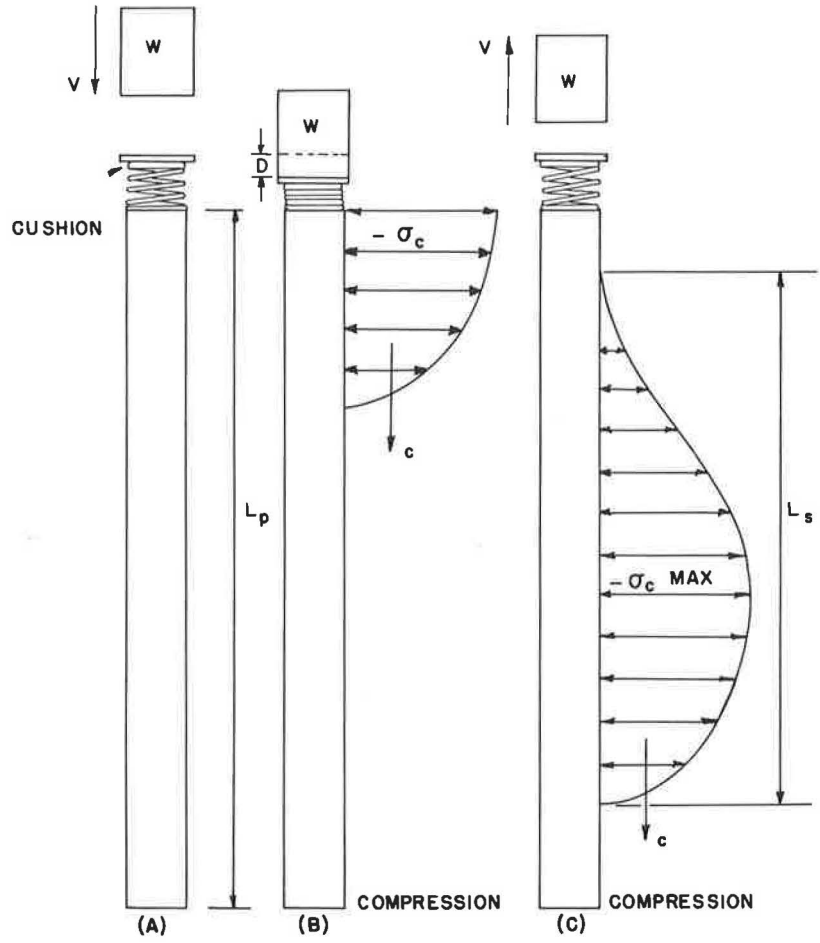

Figure 1. Idealized stress wave produced when ram strikes cushion at head of concrete pile.

A_c = cross-sectional area of cushion, in.^{2};
E_c = modulus of elasticity of cushion, psi;
t_c = initial uncompressed thickness of cushion, in.;
t = time, sec;
A = cross-sectional area of pile, in.^{2};
E = modulus of elasticity of pile, psi;
γ = unit weight of pile, lb/in.^{3};

$$n = \frac{K}{2A}\sqrt{\frac{g}{E\gamma}}; \text{ and}$$

$$p = \sqrt{\frac{Kg}{W}}.$$

Omitting the mathematics, the approximate equations for the maximum compressive stress at the pile head are as follows:

Case I—$n < p$:

$$\sigma_c \text{ max} = \frac{-KV\, e^{-nt}}{A\sqrt{p^2-n^2}} \sin\left(t\sqrt{p^2-n^2}\right) \qquad (1)$$

where t is found from the expression

$$\tan\left(t\sqrt{p^2-n^2}\right)=\frac{\sqrt{p^2-n^2}}{n}$$

Case II—n = p:

$$\sigma_c \text{ max} = -\left(\frac{KV}{nA}-\frac{W}{A}\right)e^{-1} \tag{2}$$

Case III—n > p:

$$\sigma_c \text{ max} = -\frac{KV\,e^{-nt}}{A\sqrt{n^2-p^2}}\sinh\left(t\sqrt{n^2-p^2}\right) \tag{3}$$

where t is found from the expression

$$\tanh\left(t\sqrt{n^2-p^2}\right)=\frac{\sqrt{n^2-p^2}}{n}$$

Equations 1, 2, or 3 can be used to determine the maximum compressive stress at the pile head. For most practical pile problems n will be less than p and Eq. 1 will be used. However, this is not always the case. For a given pile these equations can be used to determine a desirable combination of ram weight W, ram velocity V, and cushion stiffness K so as not to exceed a given allowable compressive stress at the pile head. To illustrate the use of the equations consider the following situation. Given:

Concrete Pile
- 65 ft long
- $A = 200 \text{ in.}^2$
- $\gamma = 0.0868 \text{ lb/in.}^3$ (150 pcf)
- $E = 5.00 \times 10^6$ psi

Green oak cushion, grain horizontal
- $A_c = 200 \text{ in.}^2$
- $E_c = 45{,}000$ psi (for properties of wood see Table 1)
- $t_c = 3.0$ in.
- $K = \frac{A_c E_c}{t_c} = 3.0 \times 10^6$ lb/in.

Steel ram
- W = 5000 lb
- h = 36 in.
- $V = \sqrt{2gh} = 167$ ips
- $g = 386 \text{ in./sec}^2$

Calculations:

$$n = \frac{K}{2A}\sqrt{\frac{g}{E\gamma}} = 224 \text{ sec}^{-1}$$

$$p = \sqrt{\frac{Kg}{W}} = 481 \text{ sec}^{-1}$$

Since n < p, Eq. 1 of Case I applies.

$$\tan\left(t\sqrt{p^2-n^2}\right)=\frac{\sqrt{p^2-n^2}}{n}=\frac{425}{224}=1.896$$

TABLE 1

MODULUS OF ELASTICITY OF WOOD CUSHIONS LOADED PERPENDICULAR TO GRAIN[a]

Wood	E_c
Pine plywood	23,000 psi
Gum	27,000 psi
Fir plywood	35,000 psi
Oak	45,000 psi

[a]Typical values from Ref. 9.

so

$$t\sqrt{p^2-n^2} = 62.2^\circ \text{ or } 1.085 \text{ radians}$$

$$t = 0.00255 \text{ sec}$$

TABLE 2

VARIATION OF DRIVING STRESS WITH RAM WEIGHT AND VELOCITY

Results from Eq. 1 for 65-ft long pile, 200-in.^{2} area, and 3-in. wood cushion. Stresses shown are maximum compression at pile head. E_c = 45,000 psi.

Ram Weight (lb)	Ram Velocity (ft/sec), Stroke (ft)			
	11.4, 2	13.9, 3	16.1, 4	18.0, 5
2,000	1,790 psi	2,200 psi	2,540 psi	2,840 psi
5,000	2,380 psi	2,920 psi	3,380 psi	3,780 psi
10,000	2,830 psi	3,470 psi	4,000 psi	4,480 psi
20,000	3,250 psi	3,980 psi	4,600 psi	5,150 psi

TABLE 3

VARIATION OF DRIVING STRESS WITH RAM WEIGHT AND RAM ENERGY

Results from Eq. 1 for 65-ft long pile, 200-in.^{2} area, and 3-in. wood cushion. Stresses shown are maximum compression at pile head. E_c = 45,000 psi.

Ram Weight (lb)	Driving Energy (ft-lb)	
	20,000	40,000
2,000	4,010 psi	5,680 psi
5,000	3,380 psi	4,780 psi
10,000	2,830 psi	4,000 psi
20,000	2,290 psi	3,250 psi

From Eq. 1

$$\sigma_c \text{ max} = \frac{-KVe^{-nt}}{A\sqrt{p^2-n^2}} \sin\left(t\sqrt{p^2-n^2}\right)$$

$$= \frac{3 \times 10^6 \times 167\, e^{-224 \times 0.00255}}{200 \times 425} \sin 62.2^\circ$$

$$\sigma_c \text{ max} = 2920 \text{ psi}$$

Using these equations, Tables 2 and 3 were developed to illustrate the effect of ram weight and velocity on driving stresses. Table 2 shows the variation of the driving stress (compressive) with the ram weight and ram velocity. It can be seen that the stress magnitude also increases slightly with ram weight; however, this is usually not of serious consequence. Table 3 shows the variation of driving stress (compression) with ram weight and ram driving energy. At a constant driving energy the driving stress decreases as the ram weight increases. Therefore, it is better to obtain driving energy with a heavy ram and short stroke than use a light ram and large stroke.

3. When the top of the pile is not square or perpendicular to the longitudinal axis of the pile, the ram impacting force will be eccentric and cause very high stress concentrations.
4. If the reinforcing steel is not cut flush with the end of the pile, high stress concentrations in the concrete adjacent to the reinforcing may result. The ram impact force may be transmitted to the concrete through the projecting reinforcing steel.
5. Lack of adequate spiral reinforcing at the pile head and also pile point may lead to spalling or splitting. In prestressed concrete piles, anchorage of the strands is being developed in these areas, and transverse tensile stresses are present. If no spiral reinforcing is used the pile head may spall or split on impact of the ram.
6. Fatigue of the concrete can be caused by a large number of blows at a very high stress level.
7. If the top edges and corners of the concrete pile are not chamfered the edges or corners are likely to spall on impact of the ram.

Spalling of concrete at the point of the pile can be caused by extremely hard driving resistance at the point. This type resistance may be encountered when founding the pile point on bed rock. Compressive stress under such driving conditions can be twice the magnitude of that produced at the head of the pile by the hammer impact, as shown in Figures 2(B) and 4(B). Field measurements and the results from Eqs. 1, 2, and 3 indicate that stress magnitudes at the head of the pile due to hammer impact frequently reach 2,000 to 3,000 psi. Consequently, if the pile tip encounters hard rock the stresses there can develop 4,000 to 6,000 psi, which will probably produce spalling.

Tension

Transverse cracking of a pile due to a reflected tensile stress wave is a complex phenomenon. It may occur in the upper end, midlength, or lower end of the pile. It usually occurs in long piles (approx. 50 ft or over). It can occur when driving in a very soft soil or when the driving resistance is extremely hard or rigid at the point, such as in bearing on solid rock.

When a pile driver ram strikes the head of a pile or the cushion on top, compressive stress is produced at the head of the pile. This compressive stress travels down the pile at a velocity

$$c = \sqrt{E/\rho}$$

where

c = velocity of the stress wave, in./sec;
E = modulus of elasticity of the pile material, psi; and
ρ = mass density of the pile material, lb-sec^2/in.^{4}.

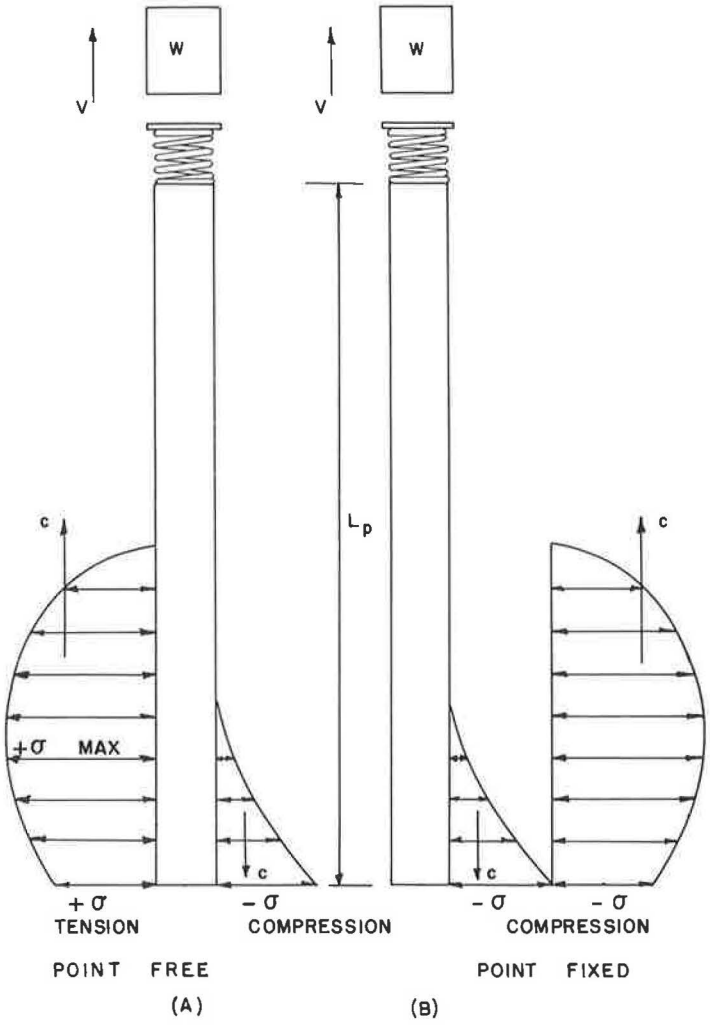

Figure 2. Reflection of stress wave at point of a long pile.

The intensity of the stress wave (σ_c max) can be determined by Eqs. 1, 2, or 3 and depends on the weight of the ram, velocity of the ram, stiffness of the cushion, and stiffness of the pile. Since in a given pile the stress wave travels at a constant velocity (about 13,000 to 15,000 ft/sec), the length of the stress wave (L_S) will depend on the length of time (t_S) the ram is in contact with the cushion or pile head. A heavy ram will stay in contact with the cushion or pile head for a longer time than a light ram, thus producing a longer stress wave. If a ram strikes a thick soft cushion, it will also stay in contact for a longer period of time than when it strikes a thin hard cushion. For Case I (when $n<p$, which is typical for most practical pile conditions), the length of the stress wave can be calculated by

$$L_S = ct_S$$

or

$$L_S = \frac{c\pi}{\sqrt{p^2-n^2}} \qquad (4)$$

where L_S is the length of stress wave in inches.

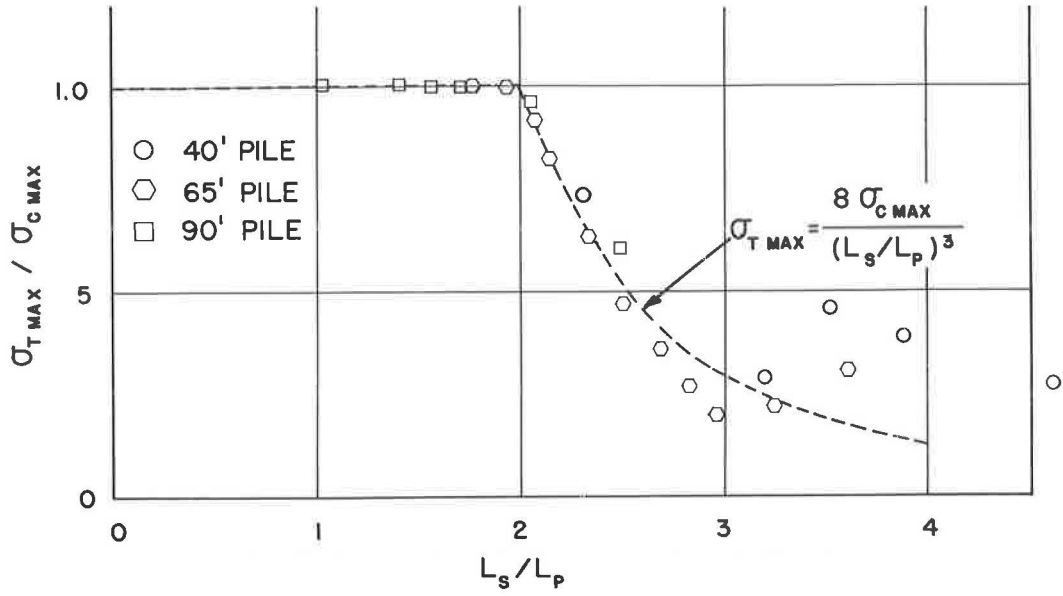

Figure 3. Effect of ratio of stress wave length to pile length on maximum tensile stress for pile with point free.

Figure 1(B) shows the compressive stress wave building up while the ram is in contact with the cushion. After the ram rebounds clear of the cushion, the compressive stress wave is completely formed and travels down the length of the pile as shown in Figure 1(C). When the compressive stress wave reaches the point of the pile, it will be reflected back up the pile in some manner depending on the soil resistance. If the point of the pile is experiencing little or no resistance from the soil, it will be reflected back up the pile as a tensile stress wave as shown in Figure 2(A). If the point of the pile is completely free, the reflected tensile wave will be of the same magnitude and length as the initial compressive wave. As shown in Figure 2(A), these two waves may overlap each other. The net stress at a particular point on the pile at a particular time will be the algebraic sum of the initial compressive (-) stress wave and reflected tensile (+) stress wave. Whether or not the pile will ever experience critical tensile stresses will depend on the pile length (L_p) relative to the length of the stress wave (L_s), and on material damping. If the pile is long compared to the length of the stress wave, critical tensile stresses may occur at certain points. When a heavy ram strikes a thick soft cushion, the stress wave may be around 150 ft in length. When a light ram strikes a thin hard cushion it may be only 50 or 60 ft in length.

The results of a theoretical study (10) on ideal piles with the point free of soil resistance has shown that the maximum reflected tensile stress (σ_t max) can be computed approximately by

$$\sigma_t \text{ max} = \sigma_c \text{ max} \tag{5}$$

when $L_s/L_p \leq 2$, and

$$\sigma_t \text{ max} = \frac{8\,\sigma_c \text{ max}}{\left(L_s/L_p\right)^3} \tag{6}$$

when $L_s/L_p \geq 2$.

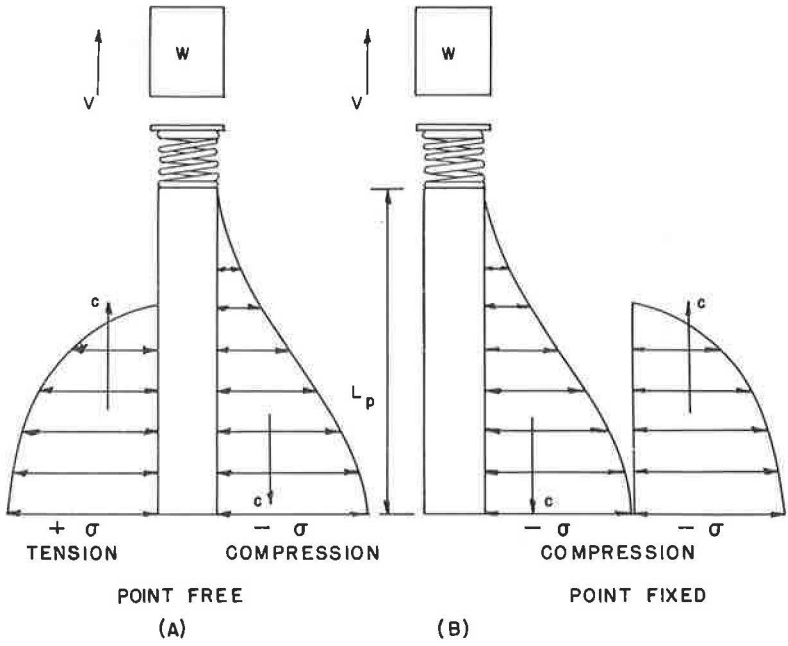

Figure 4. Reflection of stress wave at point of a short pile.

Figure 3 shows in dimensionless parameters how σ_t max is affected by σ_c max, the length of the stress wave L_S, and the length of the pile L_p. The data points shown were computed using stress wave theory (10) and piles with a free point. These values are conservative since material damping of the pile and soil will tend to reduce them.

If the point soil resistance is hard or very firm, the initial compressive stress wave traveling down the pile will be reflected back up the pile also as a compressive stress wave, as shown in Figure 2(B). If the point of the pile is fixed from movement, the reflected compressive stress wave will be of the same magnitude and length as the initial compressive stress wave. As shown in Figure 2(B), these 2 stress waves may overlap each other at certain points. The net compressive stress at a particular point at a particular time will be the algebraic sum of the initial compressive (-) stress wave and the reflected compressive (-) stress wave. (Note that under these conditions the maximum compressive stress at the pile point can be twice that produced at the pile head by ram impact.) Tensile stress will not occur here until the compressive stress wave is reflected from the free head of the pile back down the pile as a tensile stress wave similar to the reflection shown at the free point in Figure 2(A). It is possible for critical tensile stress to occur near the pile head in this case; however, internal damping characteristics of the concrete pile and surrounding soil may reduce the magnitude of this reflected tensile stress wave by this time. Such failures have occurred, however.

Figure 4 shows the reflection of the initial compressive (-) stress wave from the point of a relatively short pile. If the pile is short compared to the length of the stress wave (L_S) critical tensile stresses are not likely to occur. In Figure 4(A) the reflected tensile (+) stress wave overlaps the initial compressive (-) stress wave coming down the pile. Since the net stress at any point is the algebraic sum of the 2, they tend to cancel each other and critical tension is not likely to occur. A similar phenomenon will occur when the reflected compressive (-) stress wave from the point is likely to find the ram still in contact with the pile head when it arrives there. In such a case, little or no reflected tensile stress wave will occur. In Figure 4(B) the initial compressive (-) stress wave is being reflected from the fixed point also as a compressive (-) stress wave. In this case also, little or no reflected tensile stress will occur.

The cases illustrated by Figures 2 and 4 are highly idealized and simplified, but they should indicate some of the basic factors which can cause tensile stress failures in concrete piles. To summarize, tensile cracking of concrete piles can be caused by the following:

1. When insufficient cushioning material is used between the pile driver's steel helmet or cap and the concrete pile, a stress wave of high magnitude and of short length is produced, both characteristics being undesirable.
2. When a pile is struck by a ram at a very high velocity, or from a very high drop, a stress wave of high magnitude is produced; the stress is proportional to the ram velocity.
3. When the tensile strength of the concrete pile is too low to resist a reflected tensile stress, severe cracking will occur.
4. When little or no soil resistance at the point of long piles is present during driving, critical tensile stresses may occur in the lower half or near midlength of the pile.
5. When hard driving resistance is encountered at the point of long piles, critical tensile stresses may occur in the upper half of the pile when the tensile stress is reflected from the pile head.

Torsion

Spiral or transverse cracking of concrete piles is usually caused by a combination of torsion and reflected tensile stress. Diagonal tensile stress resulting from a twisting moment applied to the pile can by itself cause pile failure. However, if reflected tensile stresses occur during driving and they combine with diagonal tensile stress due to torsion, the situation can become even more critical. Torsion on the pile may be caused by the following:

1. The helmet or pile cap fitting too tightly on the pile, preventing it from rotating slightly due to soil action on the embedded portion of pile.
2. Excessive restraint of the pile in the leads and rotation of the leads.

SUMMARY

From the preceding discussion of types and causes of concrete pile problems which have occurred, some basic fundamental considerations have been revealed. These fundamentals for good design and driving practices for concrete piles can be summarized as follows:

1. Use adequate cushioning material between the pile driver's steel helmet or cap and the concrete pile head. Three or 4 in. of wood cushioning material (green oak, gum, pine or fir plywood, etc.) may be adequate for short (approx. 50 ft or less) piles with reasonably good point soil resistances. Six or 8 in. or more of wood cushioning material may be required when driving longer piles in very soft soil. The wood cushioning material should be placed on top of the pile with the grain horizontal and inspected to see that it is in good condition. When it begins to become highly compressed, charred or burned, it should be replaced. Some specifications require a new cushion on every pile. If driving is extremely hard, the cushion may have to be replaced several times during driving of a single pile. Use of an adequate cushion is usually a very economical means of controlling driving stresses.
2. Driving stresses can be reduced by using a heavy ram with a low impact velocity (short stroke) to obtain the desired driving energy rather than a light ram with a high impact velocity (large stroke). Driving stresses are proportional to the ram impact velocity. The maximum compressive stress can be determined approximately by Eqs. 1, 2, or 3.
3. Reduce the ram velocity or stroke during early driving when light soil resistance is encountered. Anticipate soft driving or at the first sign of easy driving reduce the ram velocity or stroke to avoid critical tensile stresses. This is very effective when driving long piles through very soft soil. When the point of the pile is free of resistance, the maximum tensile stress can be determined approximately by using Eqs. 5 or 6.

4. If pre-drilling or jetting is permitted in placing the piles, insure that the pile is well seated with reasonable soil resistance at the point before full driving energy is used. Driving and jetting should not be done simultaneously.

5. Insure that the pile driving helmet or cap fits loosely around the pile top so that the pile may rotate slightly without binding within the driving head to prevent torsional stress.

6. Insure that the pile is straight and not cambered because of uneven prestress or poor concrete placement during casting. High flexural stresses may result during driving of a crooked pile.

7. Insure that the top of the pile is square or perpendicular to the longitudinal axis of the pile.

8. Cut ends of prestressing or reinforcing steel flush with the end of the pile head to prevent their direct loading by the ram stroke.

9. Use adequate spiral reinforcing at the pile head and tip to reduce tendency of pile to split or spall.

10. Use adequate amount of prestress in prestressed piles or reinforcement in ordinary precast piles to resist reflected tensile stresses.

11. Chamfer top and bottom edges and corners of pile to reduce tendency of concrete to spall.

ACKNOWLEDGMENTS

The literature search, theoretical work, and field tests which led to this summary of fundamental design and driving considerations for concrete piles were sponsored cooperatively by the Texas Highway Department and the U. S. Bureau of Public Roads. E. A. L. Smith, chief mechanical engineer of Raymond International (now retired), served as a special consultant to the Texas Transportation Institute during the initial phase of this work. The guidance and support of Wayne Henneberger and Farland Bundy of the Bridge Division of the Texas Highway Department is also acknowledged.

REFERENCES

1. Donnell, L. H. Longitudinal Wave Transmission and Impact. Trans. ASME, Vol. 52, p. 153, 1930.
2. Gardner, S. V., and New, D. H. Some Experiences With Prestressed Concrete Piles. Proc., Inst. Civil Eng. (London), Vol. 18, pp. 43-66, Jan. 1961, and Vol. 21, pp. 867-891, April 1962.
3. Gerwick, B. C. Torsions in Concrete Piles During Driving. Jour. Prestressed Concrete Inst., Vol. 4, pp. 58-63, 1959.
4. Glanville, W. H., Grime, G., Fox, E. N., and Davies, W. W. An Investigation of the Stresses in Reinforced Concrete Piles During Driving. British Building Research Board Tech. Paper No. 20, Dept. of Sci. and Ind. Res., H. M. Stationery Office, London, 1938.
5. Hirsch, T. J. Stresses in Long Prestressed Concrete Piles During Driving. Rept. Texas Transportation Inst., Texas A&M Univ., Sept. 1962.
6. Hirsch, T. J. Computer Study of Variables Which Affect the Behavior of Concrete Piles During Driving. Rept. Texas Transportation Inst., Texas A&M Univ., Aug. 1963.
7. Hirsch, T. J. Field Tests of Prestressed Concrete Piles During Driving. Rept. Texas Transportation Inst., Texas A&M Univ., Aug. 1963.
8. Hirsch, T. J., Samson, C. H., and Lowery, L. L. Driving Stresses in Prestressed Concrete Piles. Presented at annual meeting of Structural Division of ASCE, San Francisco, Sept. 1963.
9. Hirsch, T. J., and Edwards, T. C. Impact Load-Deformation Properties of Pile Cushioning Materials. Rept. Texas Transportation Inst., Texas A&M Univ. (unpublished), July 1965.
10. Hirsch, T. J. Theoretical Development of Impact Stress Equations in a Long Slender Elastic Pile. Unpublished notes, 1965.

11. Hirsch, T. J., and Samson, C. H. Driving Practices for Prestressed Concrete Piles. Rept. Texas Transportation Inst., Texas A&M Univ. (unpublished), April 1965.
12. Portland Cement Association. Driving Problems with Prestressed Concrete Piles. Discussion published by Structural Bureau, PCA, Oct. 1962.
13. Samson, C. H., Jr. Pile-Driving Analysis by the Wave Equation (Computer Procedure). Rept. Texas Transportation Inst., Texas A&M Univ., May 1962.
14. Samson, C. H., Hirsch, T. J., and Lowery, L. L. Computer Study of Dynamic Behavior of Piling. Jour. Structural Div., ASCE, Vol. 89, No. ST4, pp. 413-449, Aug. 1963.
15. Smith, E. A. L. Pile Driving Impact. Proc. Industrial Computation Seminar, Sept. 1950, International Business Machines Corp., New York, 1951, p. 44.
16. Smith, E. A. L. Impact and Longitudinal Wave Transmission. Trans. ASME, Aug. 1955, p. 963.
17. Smith, E. A. L. What Happens When Hammer Hits Pile. Engineering News Record, Sept. 5, 1957, p. 46.
18. Smith, E. A. L. Tension in Concrete Piles During Driving. Jour. Prestressed Concrete Inst., Vol. 5, pp. 35-40, 1960.
19. Smith, E. A. L. Pile-Driving Analysis by the Wave Equation. Trans. ASCE, Vol. 127, Part I, p. 1145, 1962.
20. Siess, C. P. Dynamic Tests of Prestressed Cylinder Piles. Unpublished report to Raymond Concrete Pile Co., Jan. 15, 1958.
21. Strobel, G. C., and Heald, John. Theoretical and Practical Discussion of the Design, Testing and Use of Pretensioned Prestressed Concrete Piling. Jour. Prestressed Concrete Inst., Vol. 6, No. 3, p. 22, Sept. 1961.
22. Thornton, D. L. Mechanics Applied to Vibration and Balancing. Chapman and Hall, London, 1951.
23. Timoshenko, S., and Goodier, J. N. Theory of Elasticity, 2nd ed., p. 438. McGraw-Hill Book Co., Inc., New York, 1951.
24. Zollman, C. C. Investigation of Failure of Three Prestressed Concrete Piles. Concrete Briefs, Jour. ACI (Proc.), Vol. 58, No. 1, July 1961.

Buckling Strength of Pile

NAI C. YANG, Senior Design Engineer, The Port of New York Authority

Previous solutions for the buckling strength of piles are based on the assumptions that the piles are fully embedded and subject to no horizontal loads. In common engineering practice, the buckling of a pile is constantly associated with its freestanding length above the mud line. The solution of such problems requires the extrapolation of the analysis and the accuracy of the result is correspondingly affected.

In this paper, a review has been given of (a) the elastic stability of partially embedded piles by assuming that the buckling deflection is a half-sine curve; (b) the general equation of horizontal subgrade reaction based on the interaction of pile and foundation soil; (c) the relation between pile deflection and soil reaction; and (d) the effect of horizontal translation on the critical buckling strength of a pile.

When the critical buckling strength of a pile is greater than its compressive yield strength of material, the pile will not fail by elastic buckling. In normal foundation condition, only a little soil confinement is required to prevent the buckling of a pile unless the freestanding length becomes excessively long. The reduction of elastic stability is more critical for a pile subject to a horizontal force than due to the increase of freestanding length.

•THE PROBLEM of pile buckling usually does not exist when the piles are fully embedded. The early research on this subject was done in connection with the freestanding long piles used in waterfront construction where the piles are assumed to be fixed at a certain depth below the mud line, and Euler's formula is applied to determine the critical buckling capacity. Such an empirical approach has served very well in the past.

In recent years, however, high capacity piles have been widely adopted to serve both as structural columns and as load transfer media in the foundation soil. The common problems arising in the superstructure, such as rotation, translation and displacement of joints, become, then, inherent features of the pile design. While the buckling concept of piles is still in the development stage, some foundation difficulties would be anticipated.

In this paper, the theory of the elastic stability of piles is reviewed. The introduction of lateral soil resistance would be helpful in achieving a better understanding of the mechanics of the pile deflections. Four theoretical boundary conditions are separately discussed on the effect of pile fixities. For practical engineering applications, the degree of fixity of the pile head should be carefully studied. As demonstrated in this paper, a pile with its head fixed can withstand much greater load than one in which the head is free to rotate, and the horizontal translation of a pile head usually causes the worst condition of critical buckling.

ELASTIC STABILITY OF PILE

The previous solutions for the buckling strength of piles were based on the flexural equation

Paper sponsored by Committee on Substructures, Retaining Walls and Foundations and presented at the 45th Annual Meeting.

$$EI\frac{d^4y}{dx^4} + P\frac{d^2y}{dx^2} + k_h y = 0 \qquad (1)$$

in which EI is the flexural stiffness of the pile, P is the axial load and k_h is the subgrade modulus. In the earlier solution (1), the subgrade modulus k_h was assumed to be a constant and independent of depth of soil. The critical buckling capacity, P_{cr}, is given by the equation

$$P_{cr} = U_{cr}\frac{EI}{R^2} \qquad (2)$$

where U_{cr} is the coefficient of critical buckling load and the parameter R is equal to $(EI/k_h)^{1/4}$, which represents the interaction of pile and soil resistance. Davisson and Gill (2) found that an error of 100 percent in the deflections and moments may arise for the analysis of laterally loaded piles because of the assumption that k_h is constant with depth.

In his treatise on subgrade reaction, Terzaghi (3) recommends that the k_h value for granular soils be considered directly proportional to the depth x, and introduced a constant, n_h, to represent the rate of change of horizontal subgrade reaction. The validity of Terzaghi's recommendation has been demonstrated on a model test by Prakash. Peck and Davisson (4) have indicated that the assumption is also valid for normally loaded silts and clays. The solution for the buckling strength of piles with variable subgrade reaction has been given by Davisson (6). The governing differential equation is

$$EI\frac{d^4y}{dx^4} + P\frac{d^2y}{dx^2} + n_h xy = 0 \qquad (3)$$

The critical buckling capacity is expressed by the equation

$$P_{cr} = V_{cr}\frac{EI}{T^2} \qquad (4)$$

in which T is equal to $(EI/n_h)^{1/5}$ and V_{cr} denotes the axial load coefficient. The solution of V_{cr} for a fully embedded pile has been worked out by Davisson with the aid of an analog computer. The analytical results indicate that a great benefit can be obtained by restraining the pile head from rotation and translation.

For practical engineering analysis, the buckling problem of a pile is constantly associated with the freestanding length above the mud line. The solution of the problem requires extrapolation of the analysis and the accuracy of the result is correspondingly affected.

The general buckling strength of a compressive member within the limit of elastic stability is expressed by

$$P_{cr} = \frac{\pi^2 EI}{L^2} \qquad (5)$$

where L is the effective length of the compression member. For a partially embedded pile, the effective length consists of a portion or the entirety of the freestanding length and a portion of the embedded length. When the axial compression is less than P_{cr}, the pile is in a state of elastic equilibrium and there is, theoretically, no side deflection at any portion of the pile. However, when the axial compression approaches the buckling limit, P_{cr}, the side deflection increases plastically, having no definite relation to the intensity of load. At the beginning of the lateral deformation, the deflection is very small as compared with the length and can be assumed to be a half-sine curve or partial sine curve, depending on the relative fixity of each end, of the form $y = y_0 \sin(\pi x/L)$, where y_0 is the deflection amplitude of the sine curve.

As a result of lateral deflection of the pile, a lateral resistance would be developed in the surrounding soil. Consequently, the pile would be pushed back in the opposite direction of buckling. When the deflection attributable to soil resistance is just equal to the buckling deformation, the critical limit of elastic stability is established. This is the state of equilibrium known as critical buckling. A particular solution can be obtained when the boundary condition of a pile head is established. For practical engineering application, the boundary condition of a pile head should be evaluated in accordance with its connection details. The general guidelines outlined for the fixity of long columns could be a valuable reference. The general boundary conditions can be classified, theoretically, as (a) pinned top, non-translating; (b) fixed top, non-translating; (c) pinned top, translating; and (d) fixed top, translating. A detailed analysis for each boundary condition will be discussed in the following.

Pinned Top, Non-Translating

In Figure 1, the state of equilibrium is graphically illustrated for a pile having its top pinned against translation, but free to rotate. The unit soil reaction at a point x distance from the bottom of effective buckling length is

$$\Delta F = -n_h(\ell - x)\, y_0 \sin\frac{\pi x}{\ell + \ell_0}\,\Delta x \tag{6}$$

By using the principle of reciprocal theory, the center deflection due to the soil reaction ΔF is

$$\Delta y = \frac{(\ell + \ell_0)^3}{48\,EI}\sin\frac{\pi x}{\ell + \ell_0}\,\Delta F \tag{7}$$

By integrating Eq. 7, the total deflection at midpoint of effective buckling length due to the soil reaction is

$$y_c = \frac{(\ell + \ell_0)^5\, n_h y_0}{192\pi^2 EI}\left[\left(\frac{\pi\ell}{\ell + \ell_0}\right)^2 - \sin^2\frac{\pi\ell}{\ell + \ell_0}\right] \tag{8}$$

For the critical buckling strength $y_c = y_0$, and therefore

$$[a] = \frac{\ell}{T} = \left[\frac{192\pi^2}{\left(\frac{\pi\ell}{\ell + \ell_0}\right)^2 - \sin^2\frac{\pi\ell}{\ell + \ell_0}}\right]^{1/5}\frac{\ell}{\ell + \ell_0} \tag{9}$$

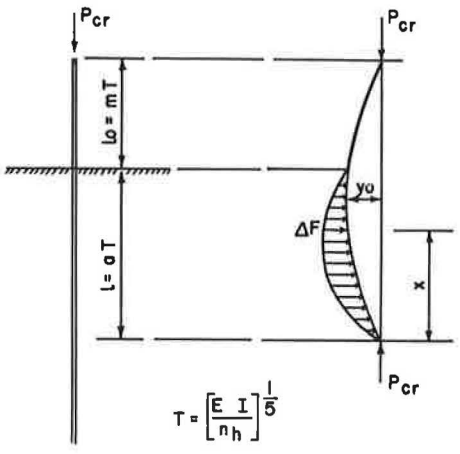

Figure 1. Buckling of pile, pinned top, non-translating.

By using $\ell/(\ell + \ell_0)$ as a parameter, the coefficient [a] of effective embedded length can be obtained. The relation between the length coefficients [a] and [m], which is equal to ℓ_0/T, is shown in Figure 2.

Substituting the relation of $\ell = aT$ and $\ell_0 = mT$, Eq. 5 can be rewritten as

$$P_{cr} = \frac{\pi^2 EI}{T^2}[G] \tag{5a}$$

in which [G] is equal to $1/(a + m)^2$. The buckling coefficient [G] has been computed and plotted in Figure 3 for various free-

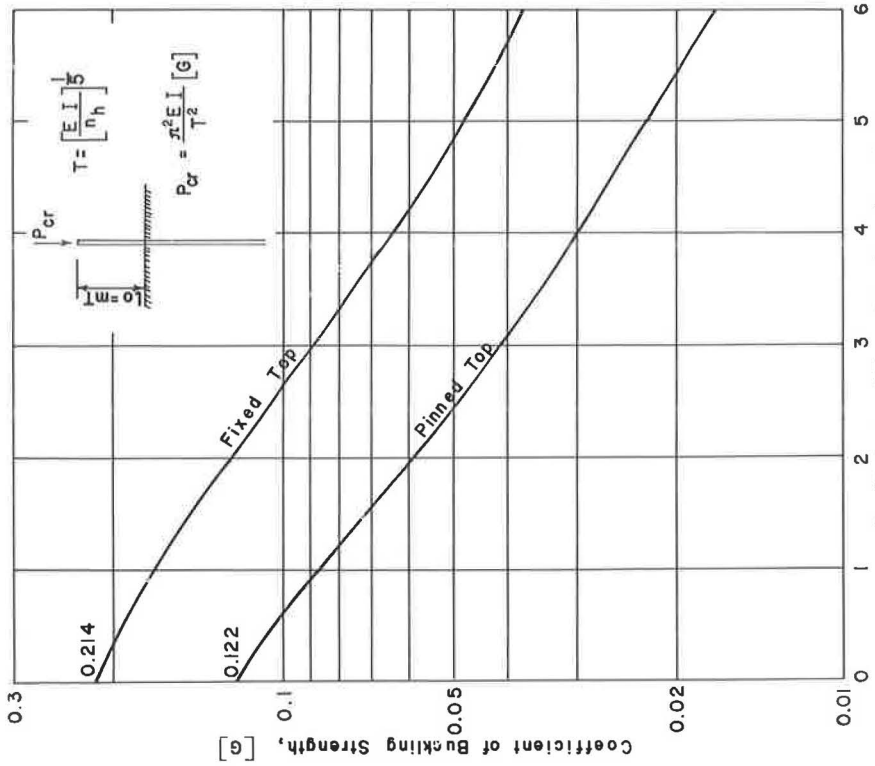

Figure 3. Coefficient of critical buckling strength.

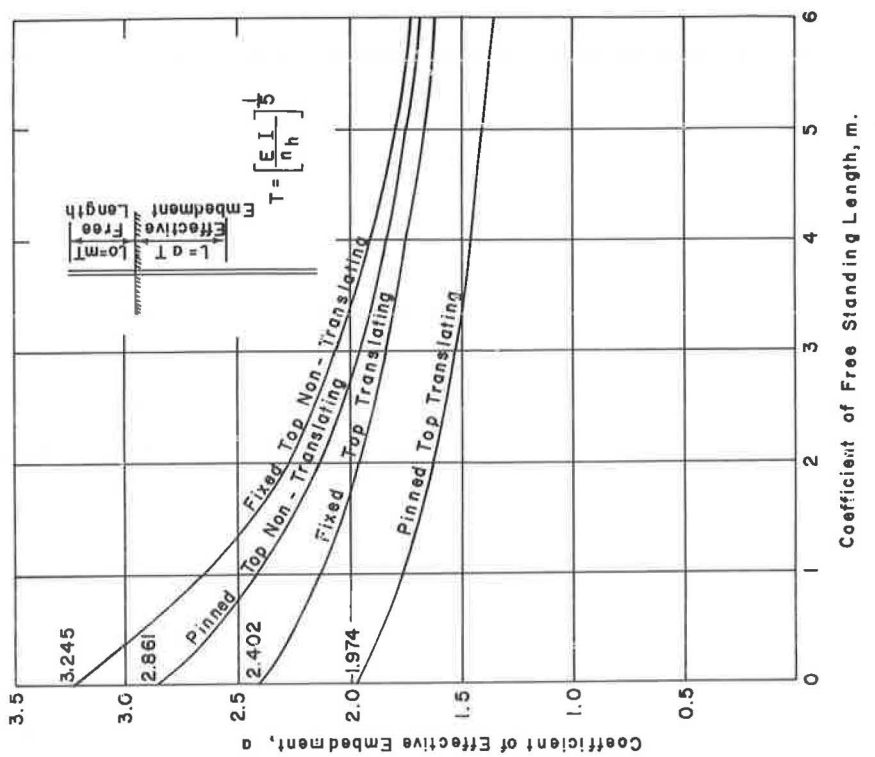

Figure 2. Effective embedment of pile at buckling.

standing lengths of a pile. It is noted that the buckling strength of the pile decreases rapidly as the freestanding length increases.

Fixed Top, Non-Translating

For a fixed pile top, the deflection curve is assumed to be of the shape shown in Figure 4. There is no rotation at the pile top. The deflection curve consists of three-quarters of a full sine wave. The soil reaction at a point x distance from the bottom of effective buckling length is

$$\Delta F = - n_h (\ell - x) y_o \left[\frac{x}{\ell + \ell_o} + \sin \frac{\pi x}{{}^2/_3(\ell + \ell_o)} \right] \Delta x \qquad (10)$$

By using the theory of reciprocal deflection, the deflection at the center of the lower half-sine wave due to the soil reaction is given by

$$\Delta y = \frac{(\ell + \ell_o)^3}{162\,EI} \left[\frac{x}{\ell + \ell_o} + \sin \frac{\pi x}{{}^2/_3(\ell + \ell_o)} \right] \Delta F \qquad (11)$$

The integration of Eq. 11 yields

$$y_c = \frac{n_h y_o}{48\pi^2 EI} \left[{}^2/_3(\ell + \ell_o) \right]^5 [k] \qquad (12)$$

where

$$[k] = \frac{3\pi^2}{16} \left(\frac{\ell}{\ell + \ell_o} \right)^4 + \frac{9\pi^2}{16} \left(\frac{\ell}{\ell + \ell_o} \right) + \frac{8}{3\pi} - \frac{1}{8} - 2 \left(\frac{\ell}{\ell + \ell_o} \right) \sin \frac{\pi \ell}{{}^2/_3(\ell + \ell_o)}$$

$$- \frac{8}{3\pi} \cos \frac{\pi \ell}{{}^2/_3(\ell + \ell_o)} + \frac{1}{8} \cos \frac{2\pi \ell}{{}^2/_3(\ell + \ell_o)}$$

At the critical buckling condition, $y_c = y_o$, Eq. 12 becomes

$$[a] = \frac{\ell}{T} = \left(\frac{48\pi^2}{k} \right)^{1/5} \frac{3\ell}{2(\ell + \ell_o)} \qquad (13)$$

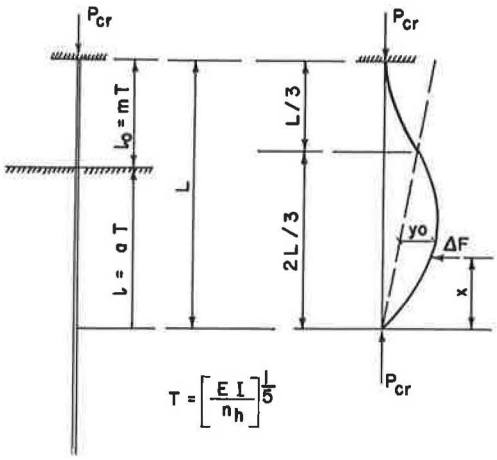

Figure 4. Buckling of pile, fixed top, non-translating.

By using the same parameter $\ell/(\ell + \ell_o)$, the dimensionless coefficient [a] and [m] are computed and shown in Figure 2. Similarly the dimensionless buckling coefficient $[G] = 9/[4(a + m)^2]$ can be determined for Eq. 5a (Fig. 3).

The validity of the above analysis depends primarily on the depth of pile penetration, which should at least be deeper than the value of [a] T. According to the experience of general foundation construction, the buckling problem is encountered only for piling in soft mud, in which the penetration of the pile is usually deep.

HORIZONTAL SUBGRADE REACTION

The evaluation of horizontal subgrade reaction has been reviewed and discussed

by Davisson (6) and Prakash (7), to a great extent on its effect on pile deflection. The general expression of the horizontal subgrade reaction (3) is

$$k_h = n_h \frac{x}{B} \tag{14}$$

where n_h is the coefficient of subgrade reaction and B is the width of pile. In their study regarding the effect of width of pile on the subgrade modulus, Davisson and Prakash have suggested that the soil reactions and deflections will be the same for piles of various widths, although the unit soil pressure across the face of the piles is different. The general equation of the horizontal subgrade reaction becomes

$$k_h = n_h x \tag{15}$$

The validity of the equation has been demonstrated by Peck and Davisson (4) on actual field measurements as well as model tests in the laboratory. A first glance at the conclusion would seem to indicate that the well-established concept of the pressure bulb and its influence on the load width is in question. In reviewing the studies, it is noted that the stiffness of pile has not been entered in the evaluation of horizontal subgrade reaction. From the point of view of the entire foundation structure, the embedded portion of pile is actually integral with the foundation soil. The interaction between pile and soil should be analyzed.

At the critical buckling condition, the stress in the pile reaches the yield strength of the material, i.e.,

$$\sigma_y = \sigma_{cy} \; 1 + \frac{y_0 c}{r^2} \tag{16}$$

where y_0 is the mid-height deflection of pile, r is the radius of gyration, and c is the distance from neutral axis to outer fiber of the pile. By using the critical buckling equation developed earlier (Eq. 5a), the mid-height deflection can be expressed by

$$y_0 = \frac{\sigma_y (\ell + \ell_0)^2}{\pi^2 E c} - \frac{r^2}{c} \tag{17}$$

Over the entire width of the pile, the soil reaction (psi per linear inch) at a distance x from the bottom effective compressive length (Fig. 1) is

$$F_x = - n_h (\ell - x) y_x \tag{18}$$

Substituting Eq. 17 in 18, and also assuming the pile deflection to be a half-sine curve, Eq. 18 can be rewritten as

$$F_x = - n_h (\ell - x) \left[\frac{\sigma_y (\ell + \ell_0)^2}{\pi^2 E c} - \frac{r^2}{c} \right] \sin \frac{\pi x}{\ell + \ell_0} \tag{18a}$$

For a fully embedded pile, i.e., $\ell_0 = 0$, the maximum subgrade reaction, E_x, is encountered at the depth where the first derivative of Eq. 18a is equal to zero, i.e. (for $\ell_0 = 0$),

$$F_{max} = - 0.58 \ell n_h \left(\frac{\sigma_y \ell^2}{\pi^2 E c} - \frac{r^2}{c} \right) \tag{19}$$

At the ultimate equilibrium of the soil, the maximum subgrade reaction shall not exceed the bearing capacity of soil, which is expressed by

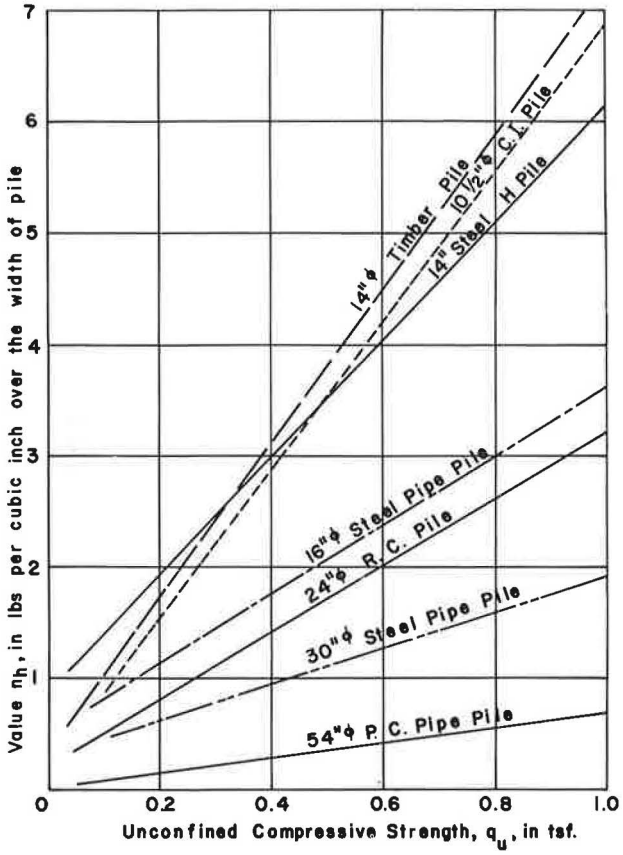

Figure 5. Horizontal subgrade reaction.

$$F_{max} \leq B\ S\ N_c \tag{20}$$

where S and N_c are the shearing strength and bearing capacity factor of the soil. The theoretical figure for the N_c value is 7.4, but Hansen and Mackenzie have observed that a value between 8 and 9 is appropriate for N_c. At the construction of the Brooklyn pier foundation, Verrazzano Narrows Bridge, the N_c value has been observed by the writer to vary from 5.9 to 6.5 under the continuous steel cutting edges. In the following computation, the N_c value is assumed to be 7.4. For the clayey soils, the shearing strength can be assumed to have a value of one-half that of the unconfined compressive strength. By consolidating Eqs. 19 and 20, and also substituting the effective compressive length $\ell = 2.861\ (EI/n_h)^{1/5}$, the following relation is established (for $\ell_0 = 0$):

$$n_h = 0.11(A\sigma_y)^{2.5}\ (EI)^{-1.5} \left(1 + \sqrt{1 + \frac{13.0\,E_c}{A\sigma_y^{\,2}}\,B\,q_u}\right)^{2.5} \tag{21}$$

The theoretical relation between n_h and q_u has been computed and plotted in Figure 5 for various types of pile in common foundation works. It is noted that the n_h is practically a linear function of the q_u value.

The above analysis has demonstrated that the width and elastic stiffness of pile are very significant on the evaluation of horizontal subgrade reaction. A particular value

of n_h should be developed for each type of pile. The field measurements observed by Peck and Davisson (4) on 14-in. steel H piles are in good agreement with the n_h-q_u curve of the same pile as shown in Figure 5.

PILE SUBJECT TO HORIZONTAL FORCE

The effect of a horizontal force on the stability of a pile has been an interesting subject since modern soil mechanics was in its infancy. Cummings and Chang (8) introduced the governing differential equation

$$EI \frac{d^4y}{dx^4} = - ky \qquad (22)$$

Chang attempted to solve the equation mathematically, but his effort was hampered due to the lack of evaluation of the k-value, the horizontal subgrade reaction. No significant progress on this subject was noted until the publication of a comprehensive study on the subgrade reaction by the late Karl Terzaghi. Reese and Matlock (5, 9) presented their study on the nondimensional solution for laterally loaded piles with the soil modulus assumed proportional to depth. Davisson and Gill extended the study for laterally loaded piles in a layered soil system. Since the publication by Cummings and Chang in 1937, the knowledge of subgrade reaction has been definitely improved and high-speed computers have been developed to aid in the direct solution of differential equations. According to their studies, the authors have prepared a set of influence charts which are very comprehensive. In some cases, the direct result from the computer may not be applicable. Broms (10) attempted to simplify the analysis and extend it to a pile with a freestanding length above the mud line. However, the final computation may be affected by the simplifying assumptions.

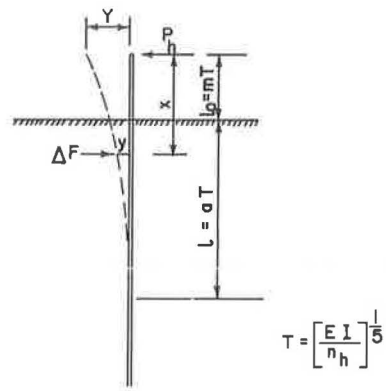

(A) PINNED TOP

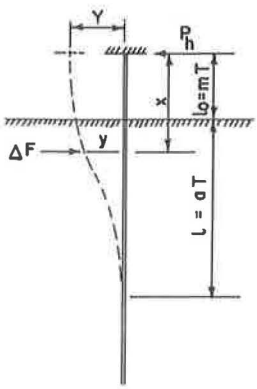

(B) FIXED TOP

Figure 6. Buckling of pile, translating head.

In studying the mechanics of piles under a horizontal force, the first step is the determination of the point of zero shear in the soil. The maximum bending moment and deflection of the pile can then be determined.

Pinned Top, Translating

In Figure 6, the load-deflection curve is illustrated for a free top cantilever type pile. The freestanding length of pile is ℓ_0 above the mud line and the point 0 is the location of zero shear. At a distance x below the top of pile, the free deflection, when no soil resistance is encountered, is

$$y = \frac{P_h}{6EI}\left[x^3 - 3(\ell+\ell_0)^2 x + 2(\ell+\ell_0)^3\right] \qquad (23)$$

The corresponding soil resistance is

$$\Delta F = n_h (x - \ell_0)\, y\, \Delta x \qquad (24)$$

The point of zero shear would be located where

$$P_h = \sum_{x=\ell_0}^{\ell+\ell_0} n_h (x - \ell_0) y \tag{25}$$

By substituting Eq. 23 in Eq. 24 and integrating Eq. 25, the dimensionless coefficient [a], indicating the point of zero shear, becomes

$$[a] = \left[\frac{120}{4 + 5\left(\frac{m}{a}\right)}\right]^{1/5} \tag{26}$$

By using (m/a) as a parameter, the relationship between [a] and [m] can be established and is plotted in Figure 2.. It can be seen that the [a] value decreases gradually with the increase of [m] value.

At the point of zero shear, the bending moment ΔM_r due to the soil reaction ΔF is expressed by

$$\Delta M_r = (\ell + \ell_0 - x)\ \Delta F \tag{27}$$

The total bending moment M_r produced by the soil reaction above the point of zero shear is

$$M_r = \frac{n_h P_h}{6 EI} \int_{\ell_0}^{\ell + \ell_0} (\ell + \ell_0 - x)(x - \ell_0) \left[x^3 - 3(\ell + \ell_0)^2 x + 2(\ell + \ell_0)^3\right] dx \tag{28}$$

Integrating Eq. 28 and incorporating Eq. 26, the bending moment due to soil resistance becomes

$$M_r = \frac{P_h \ell}{3} \left[\frac{7 + 9\left(\frac{m}{a}\right)}{4 + 5\left(\frac{m}{a}\right)}\right] \tag{29}$$

The resultant bending moment is the difference between pile moment without soil resistance and the moment from soil resistance alone. The relation between horizontal force P_h and the resultant bending moment M can be expressed by

$$M = P_h(\ell + \ell_0) - M_r = \frac{P_h T}{[H]} \tag{30}$$

where

$$[H] = \frac{3}{a}\left[\frac{4 + 5\left(\frac{m}{a}\right)}{5 + 18\left(\frac{m}{a}\right) + 15\left(\frac{m}{a}\right)^2}\right] \tag{31}$$

In Figure 7, the relation between [H] and [m] has been established by using (m/a) as a parameter of the computation.

For the deflection caused by the soil resistance, the small increment of deflection at the top of pile can be expressed by

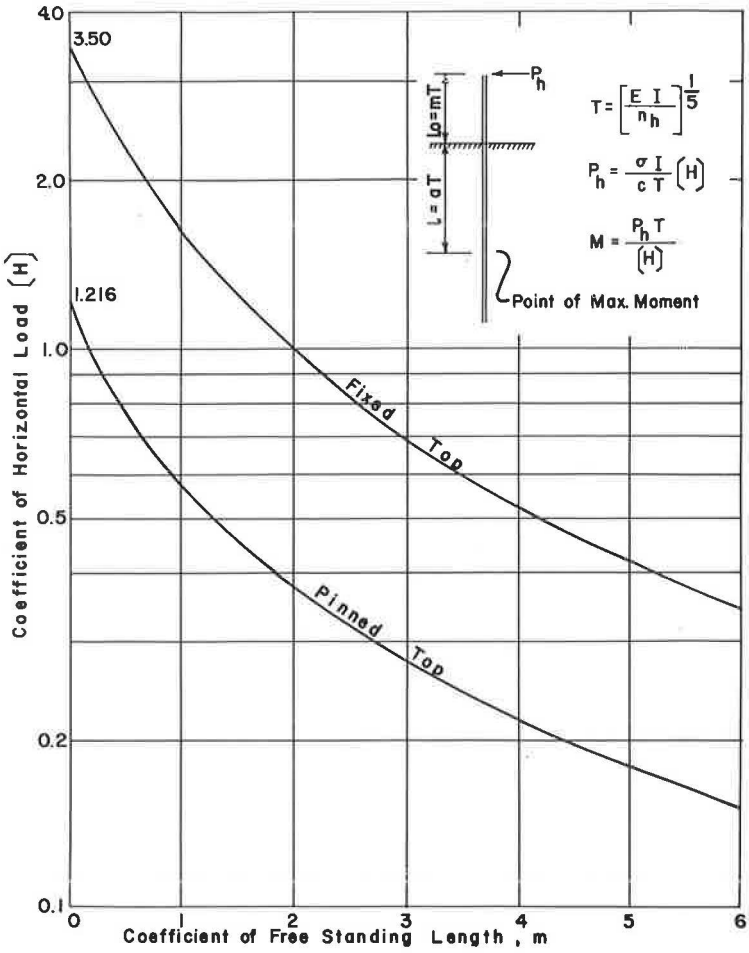

Figure 7. Coefficient of horizontal load capacity.

$$\Delta y_r = \frac{1}{6EI}\left[x^3 - 3(\ell + \ell_o)^2 x + 2(\ell + \ell_o)^3\right] \Delta F \tag{32}$$

By integrating the above equation and substituting Eq. 26, the total deflection caused by the soil reaction is

$$y_r = \frac{P_h T^3}{84 EI} \frac{a^3}{4 + 5\left(\frac{m}{a}\right)} \left[49 + 128\left(\frac{m}{a}\right) + 84\left(\frac{m}{a}\right)^2 - 560\left(\frac{m}{a}\right)^3\right] \tag{33}$$

The net deflection is the difference between pile with and pile without soil resistance, and is given by

$$Y = \frac{P_h T^3}{EI} [D] \tag{34}$$

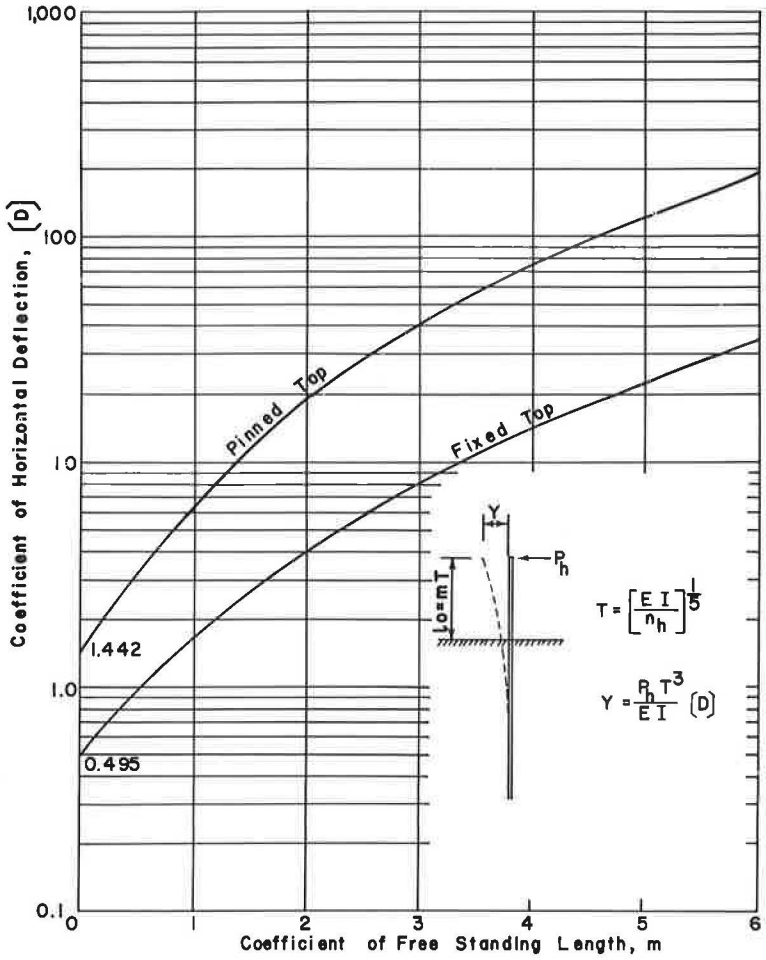

Figure 8. Coefficient of horizontal deflection.

where

$$[D] = \frac{a^3}{84\left[4 + 5\left(\frac{m}{a}\right)\right]}\left[63 + 348\left(\frac{m}{a}\right) + 672\left(\frac{m}{a}\right)^2 + 1092\left(\frac{m}{a}\right)^3 + 140\left(\frac{m}{a}\right)^4\right] \qquad (35)$$

The result of Eq. 35 has been computed and plotted in Figure 8. The charts indicate the relationship between the dimensionless coefficient of horizontal deflection with respect to the change of freestanding length, which is expressed by a dimensionless coefficient [m].

Fixed Top, Translating

The determination of bending moment and deflection for a fixed head pile is similar to those for a pinned head one, except a moment should be applied at the pile head to prevent its rotation during translation. The deflection of a free pile, without any lateral soil pressure, is

$$y = \frac{P_h}{12EI}\left[2x^3 - 3(\ell + \ell_0)x^2 + (\ell + \ell_0)^3\right] \tag{36}$$

at a point x below the pile top (Fig. 6). On the other hand, the subgrade resistance due to the deflection y is

$$\Delta F = n_h (x - \ell_0)\, y\, \Delta x \tag{37}$$

At the point of zero shear, P_h is equal to $\sum_{x=\ell_0}^{\ell+\ell_0} \Delta F$, and the depth ℓ is represented by [a] T in which [a] is a dimensionless coefficient

$$[a] = \left[\frac{240}{3 + 5\left(\frac{m}{a}\right)}\right]^{1/5} \tag{38}$$

It is noted that Eqs. 26 and 38 have the same basic form of variable. The relation of the dimensionless coefficients is shown in Figure 2.

At the point of zero shear, where the summation of bending moment will be the maximum, the increment of bending moment caused by the soil reaction ΔF is

$$\Delta M_r = \frac{(\ell + \ell_0)^2 - x^2}{2(\ell + \ell_0)}\,\Delta F \tag{39}$$

By integrating Eq. 39, the result will represent the total bending moment caused by the soil resistance from the mud line to the point of zero shear

$$M_r = \frac{P_h \ell}{21}\left[\frac{24 + 77\left(\frac{m}{a}\right) + 63\left(\frac{m}{a}\right)^2}{3 + 8\left(\frac{m}{a}\right) + 5\left(\frac{m}{a}\right)^2}\right] \tag{40}$$

The net bending moment, which will be the maximum at the point of zero shear, is therefore

$$M = \tfrac{1}{2}P_h(\ell + \ell_0) - M_r = \frac{P_h T}{[H]} \tag{30a}$$

in which

$$[H] = \frac{42}{a}\left[\frac{3 + 8\left(\frac{m}{a}\right) + 5\left(\frac{m}{a}\right)^2}{15 + 77\left(\frac{m}{a}\right) + 147\left(\frac{m}{a}\right)^2 + 105\left(\frac{m}{a}\right)^3}\right] \tag{41}$$

The dimensionless coefficient [H] is plotted in Figure 7 with respect to the coefficient of freestanding length [m].

The deflection at the top of pile is governed by

$$\Delta y_r = \frac{1}{12\,EI}\left[2x^3 - 3(\ell + \ell_0)\,x^2 + (\ell + \ell_0)^3\right]\Delta F \tag{42}$$

Integration of Eq. 42 will give the total deflection at the pile head, caused by the soil resistance above the point of zero shear, as

$$y_r = \frac{P_h T^3}{42\,EI}\,\frac{a^3}{3 + 5\left(\frac{m}{a}\right)}\left[6 + 22\left(\frac{m}{a}\right) + 21\left(\frac{m}{a}\right)^2\right] \tag{43}$$

The net deflection at the pile head can be expressed by the same formula

$$Y = \frac{P_h T^3}{EI}\,[D] \tag{34a}$$

where

$$[D] = \frac{a^3}{84\left[3 + 5\left(\frac{m}{a}\right)\right]}\left[9 + 54\left(\frac{m}{a}\right) + 126\left(\frac{m}{a}\right)^2 + 126\left(\frac{m}{a}\right)^3 + 35\left(\frac{m}{a}\right)^4\right] \tag{44}$$

The results of Eq. 44 have been computed and shown in Figure 8. They are dimensionless coefficients which can be used for general application.

BUCKLING OF PILE AT TRANSLATION

In the preceding analysis, two boundary conditions of the buckling problem have been given for the piles partially or fully embedded in the soil. The non-translating condition, under the section heading of "Elastic Stability of Pile," represents the state of stress for a perfectly straight pile subject to no eccentricity nor any bending moment. It is purely an academic condition. For practical foundation design, piles are always subject to bending and axial load caused by one or a combination of the following: imperfection in cross section and length, deviation due to pile driving, stress due to temperature change, horizontal force and overturning moment due to dead or live load, and many other reasons.

Similarly, the stress condition under the section heading "Pile Subject to Horizontal Force" is also hypothetical. All piles will be subject to an axial load of some intensity. Therefore, the actual application of the above analysis requires the proper blending of the interaction of horizontal force and vertical axial load.

According to the basic mechanics of elastic stability, the critical buckling strength, P_{cr}, without translation and dynamic excitation, is

$$P_{cr} = P'_{cr} + \frac{M\,c}{r^2} \tag{45}$$

in which P'_{cr} is the critical buckling strength under the influence of the bending moment M caused by the eccentricity of P'_{cr} or the horizontal force on the pile, or the combination of both. In the following analysis, the bending moment is assumed to be caused by

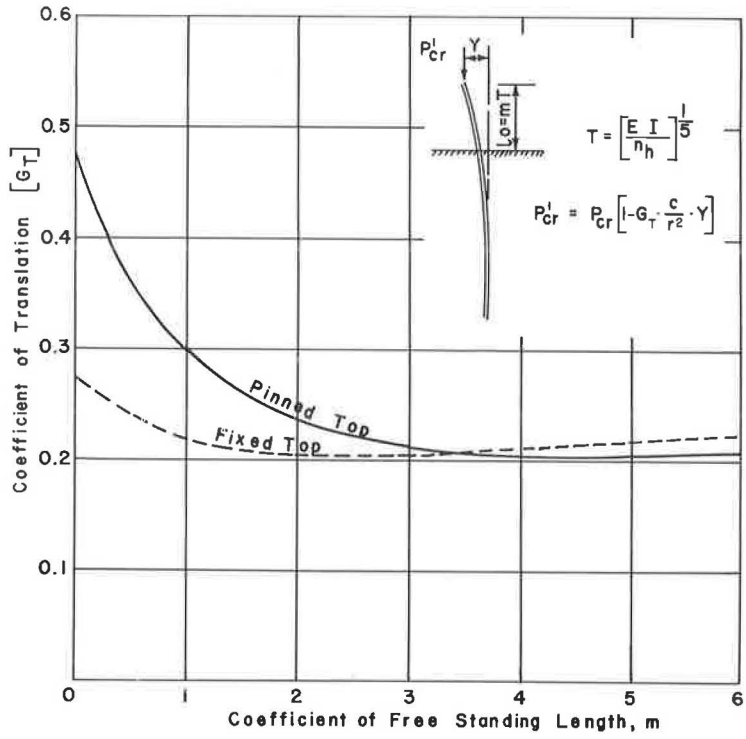

Figure 9. Coefficient of decrement of buckling strength.

the translation of the pile head, which includes the effect due to eccentricity of P'_{cr} at the pile head. The corresponding maximum bending moment at the point of zero shear is given by Eqs. 30 and 30a, and the deflection at pile head, which would be the eccentricity of axial load P'_{cr}, is given by Eqs. 34 and 34a. By substituting these equations in Eq. 45, the critical buckling load P'_{cr} at a translation of Y distance becomes

$$P'_{cr} = P_{cr} - \frac{EI}{T^2} \frac{Y}{[D][H]} \frac{c}{r^2} \tag{46}$$

where P_{cr} is the critical buckling strength of the pile without any translation. The above equation can be simplified as

$$P'_{cr} = P_{cr} \left(1 - G_T \frac{c}{r^2} Y\right) \tag{47}$$

in which $[G_T] = 1/\pi^2 [D][H][G]$, representing the coefficient of decrement of buckling strength. In Figure 9, the coefficient $[G_T]$ has been computed and plotted for various coefficients of freestanding length [m].

For piles subject to a given horizontal force, the bending moment in Eq. 45 would include those produced by the horizontal force and the eccentricity of vertical load; Eq. 47 should be rewritten as

$$P'_{cr} = \frac{P_{cr}\left(1 - G_T \frac{c}{r^2} \frac{P_h T^3}{EI}[D]\right)}{1 + \frac{c}{r^2} \frac{P_h T^3}{EI}[D]} \qquad (48)$$

It can be seen that the reduction of pile capacity is more critical for a pile subject to a definite horizontal force.

When the critical buckling capacity P'_{cr} is greater than the compressive yield strength $\sigma_y A$ of material, the pile will not fail by elastic buckling. In normal conditions only a little soil confinement is required to prevent the buckling of a pile, unless the freestanding length becomes excessively long or the pile head translates detrimentally.

ILLUSTRATIVE EXAMPLE

In designing a pier foundation, the bearing piles consist of 18-in. OD steel pipe having an effective wall thickness of ¼-in., and 4000-psi concrete fill. The foundation soil is predominantly a deep deposit of soft organic silt having an unconfined compressive strength ranging from 0.2 to 0.4 tsf for the uppermost 40 ft. It is a normally loaded deposit. The horizontal subgrade reaction is estimated to be 1.0 to 1.5 lb per cubic inch (Fig. 5). The range of soil reaction has been confirmed by field measurements on test piles. The piles will be installed in a depth of water varying from 25 to 42 ft. The freestanding lengths of the piles, therefore, vary from 30 to 48 ft. In the final structure, the piles will be subject to a horizontal translation of 3 in. due to temperature change of the superstructure.

The physical properties of the pile are as follows:

$$EI = 3.20 \times 10^{10} \text{ in.-lb}$$

$$\frac{c}{r^2} = 0.359 \text{ in.}^{-1}$$

$$T = \left[\frac{3.20 \times 10^{10}}{1.5}\right]^{1/5} = 116.4 \text{ in.}$$

For a 48-ft freestanding length, the coefficient [m] is

$$m = \frac{48 \times 12}{116.4} = 4.95$$

The coefficient of the critical buckling strength, [G] value from Figure 3, is 0.0227 for piles pinned at top and 0.0485 for piles fixed at top. The critical buckling capacity for pinned top would be

$$\frac{\pi^2 \times 3.20 \times 10^{10}}{116.4^2} \times 0.0227 = 530 \text{ kips}$$

and for fixed top

$$\frac{\pi^2 \times 3.20 \times 10^{10}}{116.4^2} \times 0.0485 = 1,130 \text{ kips}$$

For a 30-ft freestanding length, the critical buckling capacity for pinned top is

$$2.33 \times 10^7 \times 0.0383 = 890 \text{ kips}$$

and for fixed top

$$2.33 \times 10^7 \times 0.0860 = 2,000 \text{ kips}$$

The ultimate compressive strength of the material is computed to be 1, 280 kips. It can be said that the piles with fixed top will have no problem in elastic buckling, while every pile with a pinned top would tend to buckle rather than fail in compression.

The compressive strength of the material cannot be fully utilized in the pinned top pile.

At a 3-in. horizontal translation, the reduced critical buckling capacity is

$$P'_{cr} = P_{cr} \left(1 - G_T \frac{c}{r^2} Y\right)$$

Within the range [m] = 3.10 to 4.95, the [G_T] value is fairly constant. A value 0.21 is taken from Figure 9. The ratio of P'_{cr}/P_{cr} is

$$1.00 - 0.21 \times 0.359 \times 3.00 = 0.774$$

The critical buckling strength becomes:

Pile Top	Freestanding Lengths	Translation	Critical Buckling Strength
Pinned	48 ft	3 in.	0.774 × 530 = 410 kips
Fixed	48 ft	3 in.	0.774 × 1,130 = 875 kips
Pinned	30 ft	3 in.	0.774 × 890 = 690 kips
Fixed	30 ft	3 in.	0.774 × 2,000 = 1,550 kips

The above computation demonstrates the desirability of using fixed top piles in such foundation designs.

In an actual test, an 18-in. OD by ½-in. wall steel pipe was subjected to a horizontal force of 5,000 lb. There was no vertical load on the pile. The steel pipe was driven in the same organic silt as described above. The point of application of horizontal load was 39.8 ft above the mud line. The physical properties of the steel pipe are as follows:

$$EI = 3.05 \times 10^{10} \text{ in.-lb}$$

$$T = \left[\frac{3.05 \times 10^{10}}{1.5}\right]^{1/5} = 115.3 \text{ in.}$$

$$[m] = \frac{39.8 \times 12}{115.3} = 4.14$$

The coefficient of horizontal deflection, according to Figure 8 is [D] = 82 for pinned top pile. The horizontal deflection is

$$Y = \frac{5,000 \times 115.3^3}{3.05 \times 10^{10}} \times 82 = 20.6 \text{ in.}$$

The observed deflection was 19 in. The difference is about 8 percent, which is within the accuracy of assuming E and n_h values and also the surveying tolerance in the determination of load and deflection.

REFERENCES

1. Hetenyi, M. Beams on Elastic Foundations. Univ. of Michigan, 1946.
2. Davisson, M. T., and Gill, H. L. Laterally Loaded Piles in a Layered Soil System. Jour. Soil Mech. Found. Div., Proc. ASCE, Vol. 89, No. SM3, May 1963.
3. Terzaghi, Karl. Evaluation of Coefficient of Subgrade Reaction. Geotechnique, Vol. 5, pp. 297-326, 1955.
4. Peck, R. B., and Davisson, M. T. Discussion of Design and Stability Considerations for Unique Pier, by J. Michalos and D. P. Billington. ASCE Trans., Vol. 127, pp. 413-424, 1962.
5. Reese, L. C., and Matlock, H. Non-Dimensional Solution for Laterally Loaded Piles with Soil Modulus Assumed Proportional to Depth. Proc. Eighth Texas Conf. on Soil Mech. and Found. Eng., Austin, 1956.
6. Davisson, M. T. Estimating Buckling Loads for Piles. Proc. Second Pan-American Conf. on Soil Mech. and Found. Eng., July 1963.
7. Davisson, M. T., and Prakash, S. A Review of Soil-Pole Behavior. Highway Research Record No. 39, pp. 25-48, 1963.
8. Cummings, A. E., and Chang, Y. L. Discussions of Lateral Pile Load Tests, by L. B. Feagin. ASCE Trans, Vol. 102, pp. 272-278, 1937.
9. Matlock, H., and Reese, L. C. Foundation Analysis of Offshore Pile Supported Structures. Proc. Fifth Internat. Conf. on Soil Mech. and Found. Eng., Paris, 1961.
10. Broms, B. B. Lateral Resistance of Piles in Cohesive Soils. Jour. Soil Mech. Found. Div., Proc. ASCE, Vol. 90, No. SM2, March 1964.

Behavior of Large Bolted Joints

JOHN W. FISHER, GEOFFREY L. KULAK, and LYNN S. BEEDLE
Respectively, Research Assistant Professor, Research Assistant, and Director, Fritz Engineering Laboratory, Lehigh University, Bethlehem, Pennsylvania

This paper summarizes the results of tension tests of long structural splices of A 7 or A 440 steel connected by high-strength bolts (A 325 or A 490) which have provided background for parts of the specification of the Research Council on Riveted and Bolted Structural Joints. The influence of joint length, pitch, and relative proportions of the net tensile area of the plate to the bolt shear area on the ultimate strength of bearing-type connections is determined by theoretical studies and confirming tests. Data on the slip resistance are also presented for use in designing friction-type connections.

•WHEN THE A 325 high-strength bolt was first used, it was as a one-for-one replacement for the A 141 steel rivet. It was soon recognized that the bolt was stronger than the rivet and an extensive research program was initiated at Lehigh University in 1957 to determine the behavior of the A 325 bolt in large bolted butt splices and to help establish allowable stresses which recognized the superior strength of the bolt. Tests were conducted on compact joints to determine the proper ratio of shear area and net tension area to achieve a so-called balanced design (1). It was shown in these studies that the proper tension-shear ratio was 1 to 1.10 for A 325 bolts in A 7 steel joints. Thus, for bridge specifications, if the allowable tensile stress in the plate were 18 ksi, then the allowable shear stress in the bolts would be 20 ksi. These stresses imply a factor of safety of 3.3 against the ultimate strength of bolts and plate in a compact joint.

Subsequently, tests were conducted on long bolted joints which were proportioned using the tension-shear relationship that had been established for the compact joints (2). These tests showed that the longer joints were not able to effect a complete redistribution of the load because the end fasteners failed prematurely. This failure was not due to any deficiency of the fastener but was the result of the accumulated differential strains between the main and the lap plates. Since the end fasteners did not have the ability to deform sufficiently to accommodate these differential strains, equalization of load among all bolts could not take place.

The balanced design criterion was also used in recent tests to determine the relative proportions of shear area and net tensile area when A 325 bolts were used to connect A 440 steel plates (3). This work showed that the balanced design concept would yield a tension-shear ratio of 1 to 1.0 for material in the thickness range of $\frac{3}{4}$ to $1\frac{1}{2}$ in. Subsequent analytical studies (4, 5) and tests (6) indicated that the ultimate load was greatly affected by the relationship between the net tensile area of the plate (A_n) and the shear area of the bolts (A_s).

More recently, analytical studies and tests have been conducted on A 440 steel joints connected by A 490 bolts (7). This paper summarizes the results of these studies on large bolted connections and discusses the design criteria for bearing-type connections.

Paper sponsored by Committee on Steel Superstructures and presented at the 45th Annual Meeting.

TEST SPECIMENS

The research program summarized in this report consisted of static tension tests of large bolted joints. Twenty-four double shear, bolted, A 7 steel butt joints with from three to sixteen $\frac{7}{8}$-in., 1-in., or $1\frac{1}{8}$-in. A 325 bolts in line were tested. Four double shear, riveted A 7 steel butt joints with from five to thirteen $\frac{7}{8}$-in. A 141 steel rivets were tested for comparative purposes. Also, four bolted, A 7 steel lap joints with from two to ten $\frac{7}{8}$-in. A 325 bolts in a line were tested to verify single shear behavior. Additional details of these tests are given elsewhere (1, 2).

Eighteen double shear, bolted, A 440 steel butt joints with from four to sixteen $\frac{7}{8}$-in. A 325 bolts in line were tested to determine what effect grade of steel had on joint behavior (3, 6). Eight double shear, bolted A 440 shear butt joints with from four to nineteen $\frac{7}{8}$-in. A 490 bolts in line were tested to investigate the behavior of the new, higher strength A 490 bolt. Results of these tests were reported earlier (7).

FABRICATION AND ASSEMBLY

The joints were assembled by a local fabricator. Plates were first cut by torch and then machined to final dimensions. Loose mill scale was removed by hand brushing with a wire brush. Oil and grease were wiped from the plates with solvent in order to establish a faying surface condition which would be comparable to that likely in the field. Eight A 7 steel butt joints had all mill scale removed with a power tool. This resulted in a semi-polished surface representative of field conditions for friction-type joints. The plates were assembled into the required configuration, clamped together, and the 4 end holes subdrilled and reamed. Fitted pins were inserted to maintain alignment while the remainder of the holes were drilled through all plies of the assembly.

The bolting-up operation was carried out by a field erection crew of the fabricator. Bolts with grips less than 5 in. had the nuts tightened one-half from "snug." The nuts of A 325 bolts were torqued through a three-fourths turn and those of A 490 bolts a two-thirds turn from snug for bolts with grips of 5 in. or more. In all cases, bolt threads did not intercept the shearing planes.

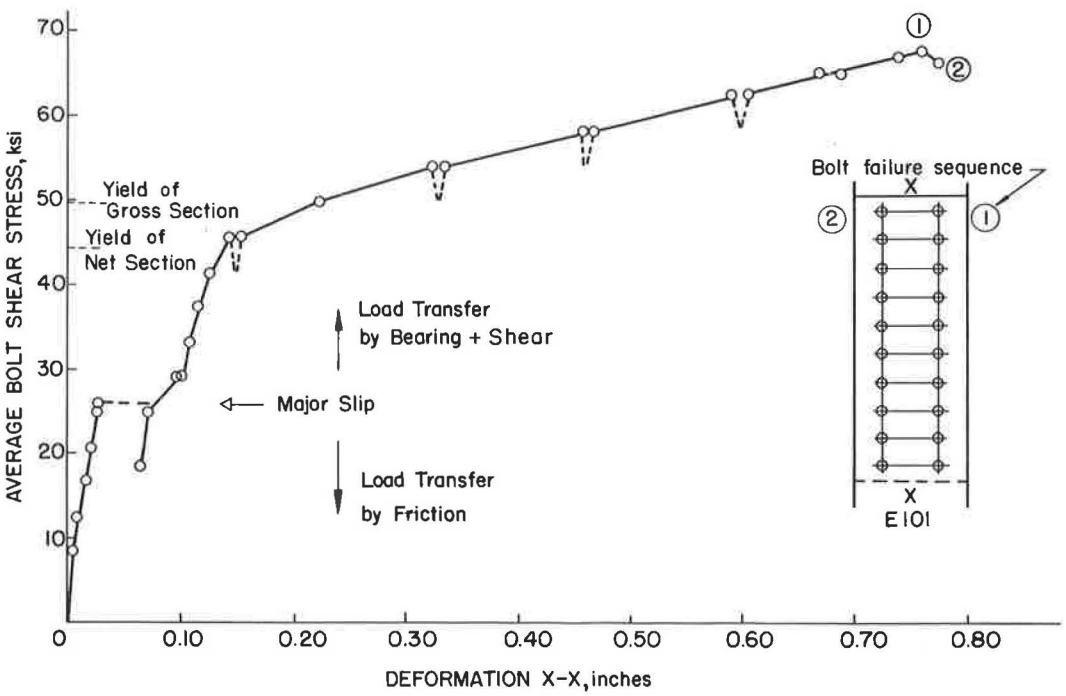

Figure 1. Typical load-deformation curve (A 440 steel joint connected by A 325 bolts).

TESTING

The joints were loaded in static tension using a 5000-kip universal testing machine with wedge grips. The progress of a test is well illustrated by load-deformation curves. Typical behavior is shown in Figure 1 for an A 440 steel joint with 10 A 325 bolts in line. As load was first applied, the load transfer mechanism was one of friction and linear response was observed up to the time of major slip. Usually the joint slipped into bearing instantaneously. After major slip, the principal load transfer mechanism was that of shear and bearing. As load was applied, inelastic deformations occurred in the bolts and plate until one of the end bolts failed, at which time the load was considerably above the yield load of the plate. Additional loading caused a second bolt to shear, at a slightly lower load in this case. This sequential failure of bolts, starting from the ends, is termed "unbuttoning."

EFFECT OF JOINT LENGTH AND VARIATIONS IN PLATE AREA

In many of the early tests of mild steel joints, the plate area at the net section was about 75 percent of the shear area of the bolts (1, 8). In these cases, failure usually occurred by tearing and fracture of the plate. The exception was one joint which had 13 fasteners in line. This failed by unbuttoning (8).

In shorter joints, failure occurred in the plate even when the plate area and the shear area were equal. Figure 2 shows a large mild steel splice connected by A 325 bolts. The plate area is equal to 96 percent of the bolt shear area.

Figure 3 shows the influence of joint length on the strength of double-lap, A 7 steel butt joints (1, 2). A plotted point is the reported average shear stress at failure for the given joint length. Bolts in a particular joint were from the same lot; however, several lots with differing strengths were used in the joint tests. The scatter in the experimental results is caused primarily by these variations. All bolts had strengths which exceeded the ASTM minimum and the tensile strength of the plate material was up to 9 percent greater than the minimum specified by ASTM.

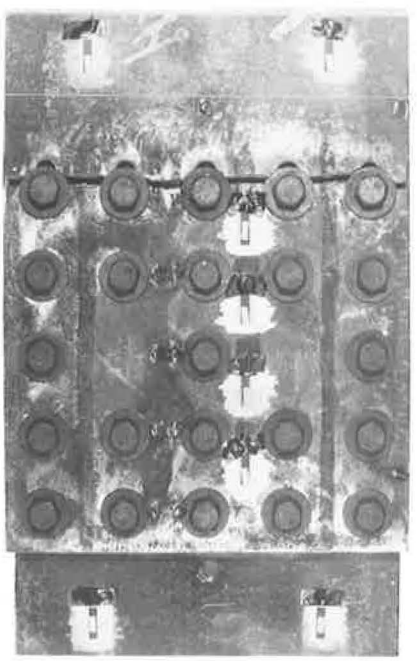

Figure 2. Tensile failure of large bolted joint.

Also shown in Figure 3 is the theoretical strength curve for failure of the bolts as found using the procedure developed by Fisher and Rumpf (5). The permissible shear stress of 20 ksi according to recent specifications is shown on the graph (9, 10). The theoretical calculations have been based on minimum strength A 325 bolts and A 7 steel plates. It is clear that the short, compact joints are substantially stronger than the longer joints.

The 4 A 7 steel joints connected by A 141 steel rivets tested for comparative purposes showed the same general behavior as the bolted joints. The results, illustrated in Figure 4, show good agreement between predicted (5) and test (2) values.

Initial tests on A 440 steel joints connected by A 325 bolts were performed on compact joints with 2 lines of 4 bolts each. These tests were designed to determine the shear strength of the bolts. In addition, it was desirable to know what influence variations in the net plate area had on the shear strength.

These tests showed that the shear strength of the bolts was about 70 ksi.

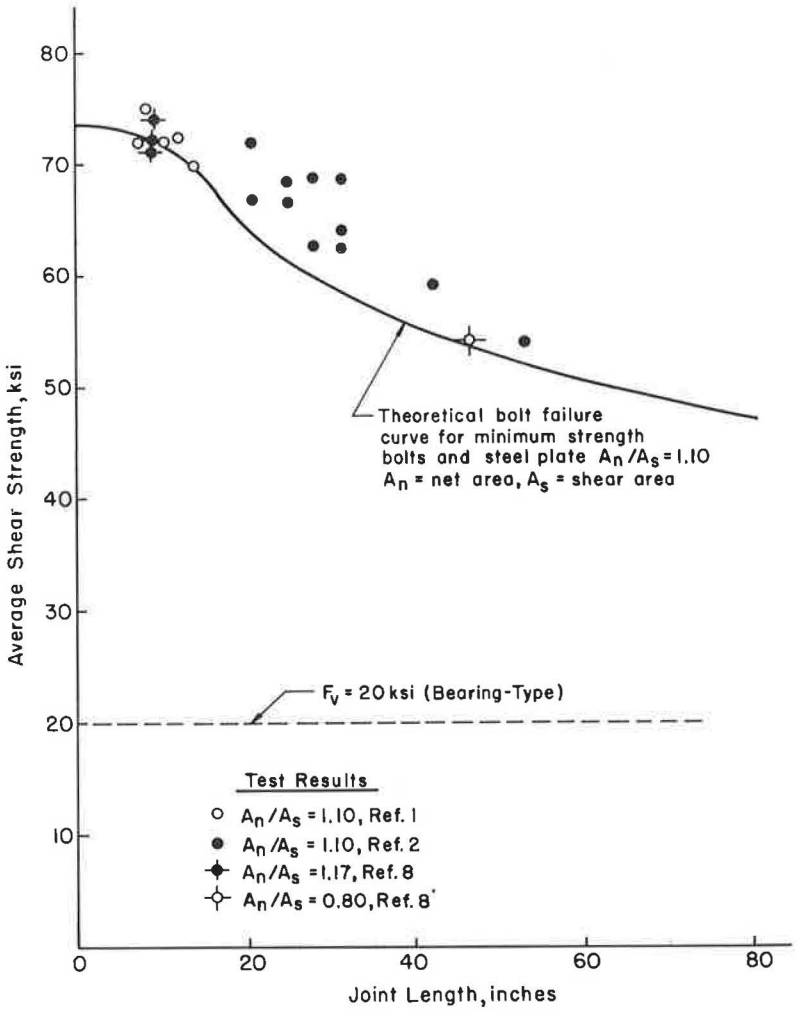

Figure 3. Comparison of computed failure curve with test results of A 7 steel joints connected by A 325 bolts.

The minimum ultimate strength of 1-in. A 440 steel plate is 67 ksi. Previous investigations of riveted and bolted joints had developed the concept of "balanced design," that is, at ultimate load the shear strength of the fasteners was equal to the tensile capacity of the plate. The compact joint tests indicated that when the portions of the load carried by the plate and by the fasteners were equal, the A_n/A_S ratio was nearly unity for this combination of bolt and plate material. Subsequent test specimens having from 7 to 16 bolts in a line were proportioned using ratios of either 0.8, 1.0, or 1.2. All bolts were installed in drilled and aligned holes and were tightened by the turn-of-nut method.

The results of these tests are summarized in Figure 5 (3, 6). The dashed horizontal line represents the shear strength of a single bolt. If the plate were perfectly rigid, complete redistribution would occur at all lengths. In the short joints, simultaneous shearing of all the bolts did occur. In the longer joints, however, one or more bolts in the lap plate end sheared due to their larger deformation before the full strength of all of the bolts could be achieved. The results are plotted in this figure with the average shear stress at failure as a function of joint length.

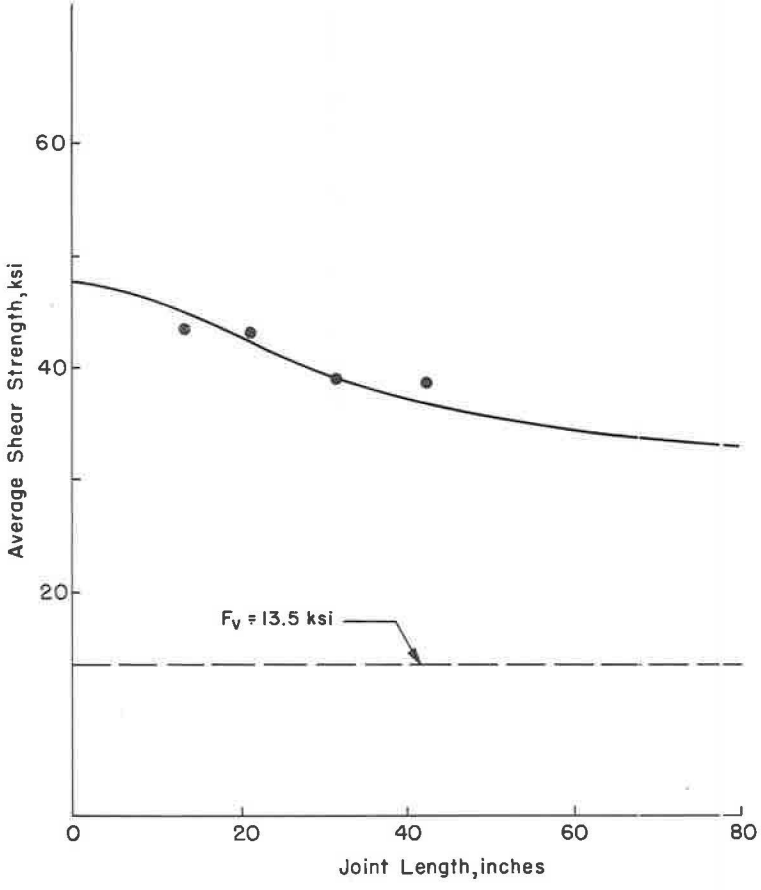

Figure 4. Comparison of computed failure curve with test results of A 7 steel joints connected by A 141 steel rivets.

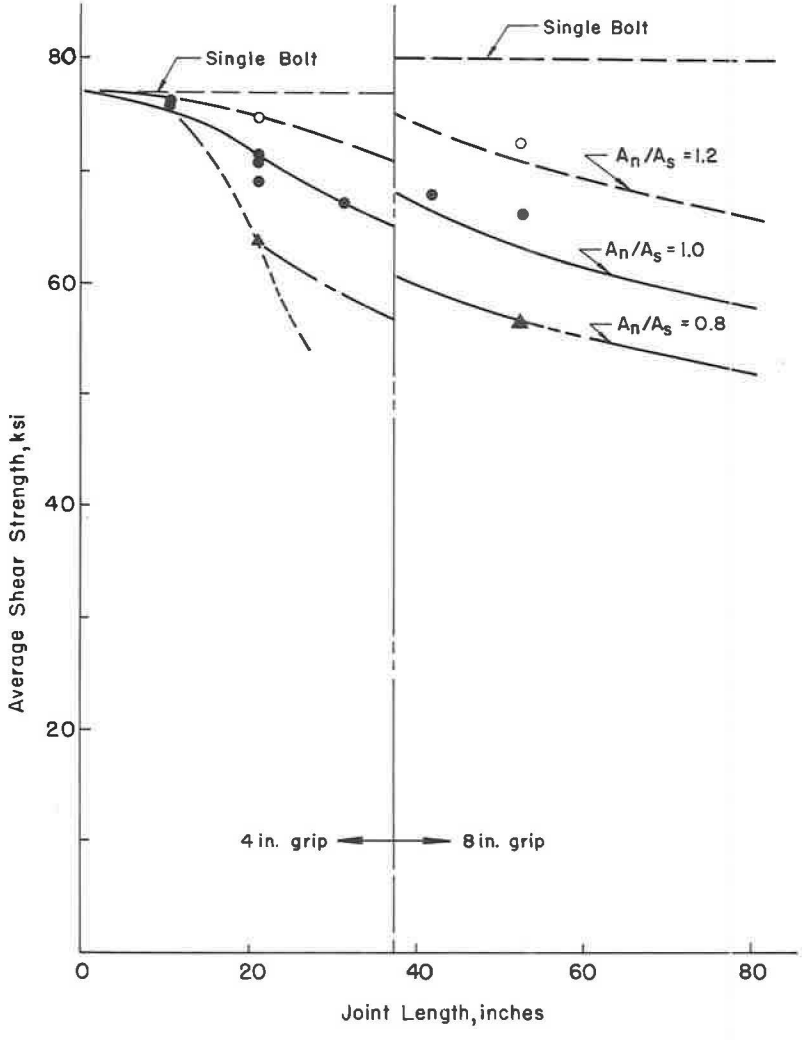

Figure 5. Comparison of computed failure curves with test results of A 440 steel joints connected by A 325 bolts.

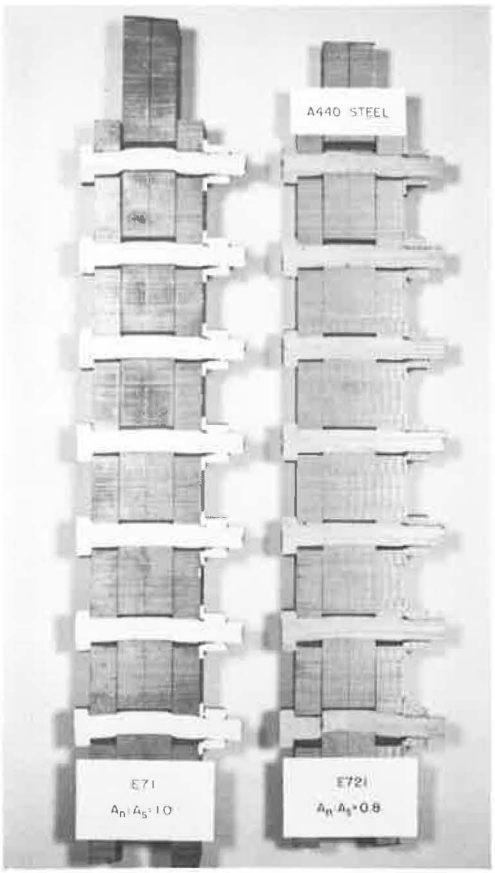

Figure 6. Sawed sections of test joints after failure.

As the net tensile area of the plate is increased relative to the bolt shear area, as would result from higher allowable bolt shear stresses, the average shear strength of the bolts in the longer joints increased.

When the net plate area of A 440 steel joints was only 80 percent of the bolt shear area (A_n/A_s = 0.80), short and medium length joints invariably failed by tearing of the plate. The predicted plate failure boundary is also indicated in Figure 5. In the longer joints, the accumulated differential strains between the main and lap plates caused a bolt failure before the plate failed.

Two sawed sections of joints with 7 A 325 bolts in line (Fig. 6) show the influence of the accumulated differential strains between the main plate and the lap plate. It is evident that the accumulated strains were much higher for joint E 721 with an A_n/A_s ratio of 0.8 than for joint E 71 in which A_n/A_s was 1.0. As judged by the deformations in the joints, the distribution of load among the fasteners is more nearly uniform in joint E 71. Joint A 722, of the same length and number of bolts but with A_n/A_s = 1.2, failed by an apparent simultaneous shearing of all the fasteners. This indicates that complete, or almost complete, redistribution of load had taken place.

Recent tests of joints using A 490 bolts installed in A 440 steel plate are summarized in Figure 7 (7). The behavior of these joints parallels those previously discussed.

EFFECT OF JOINT WIDTH

The effect of internal lateral forces caused by plate necking near the ultimate tensile strength of a wide joint was investigated with tests of 8 A 7 steel joints and 3 A 440 steel joints fastened with A 325 bolts (1, 3). These joints had from 4 to 6 lines of bolts with from 4 to 7 bolts in each line.

Generally, the behavior of these joints was directly comparable to joints with only 2 lines of fasteners and the same number of bolts in each line. For example, an A 440 steel joint with 6 lines of 4 bolts failed at exactly 3 times the ultimate load of a joint with 2 lines of 4 bolts. Similarly, the ultimate load of a joint with 4 lines of 7 bolts failed at twice the ultimate load of a joint with 2 lines of 7 bolts.

Approximately the same behavior was observed in A 7 steel joints, although in some cases plate necking was found to contribute to premature failure of corner bolts. In general, joint width did not significantly affect the joint behavior.

EFFECT OF NUMBER OF SHEAR PLANES

Although specifications have traditionally assigned to rivets a single shear value equal to one-half that for double shear, it seemed advisable to investigate this relationship experimentally for high strength bolts. Four lap joints of A 7 steel fastened with 2 lines of from 2 to 10 A 325 bolts each were tested. An external bracing system was

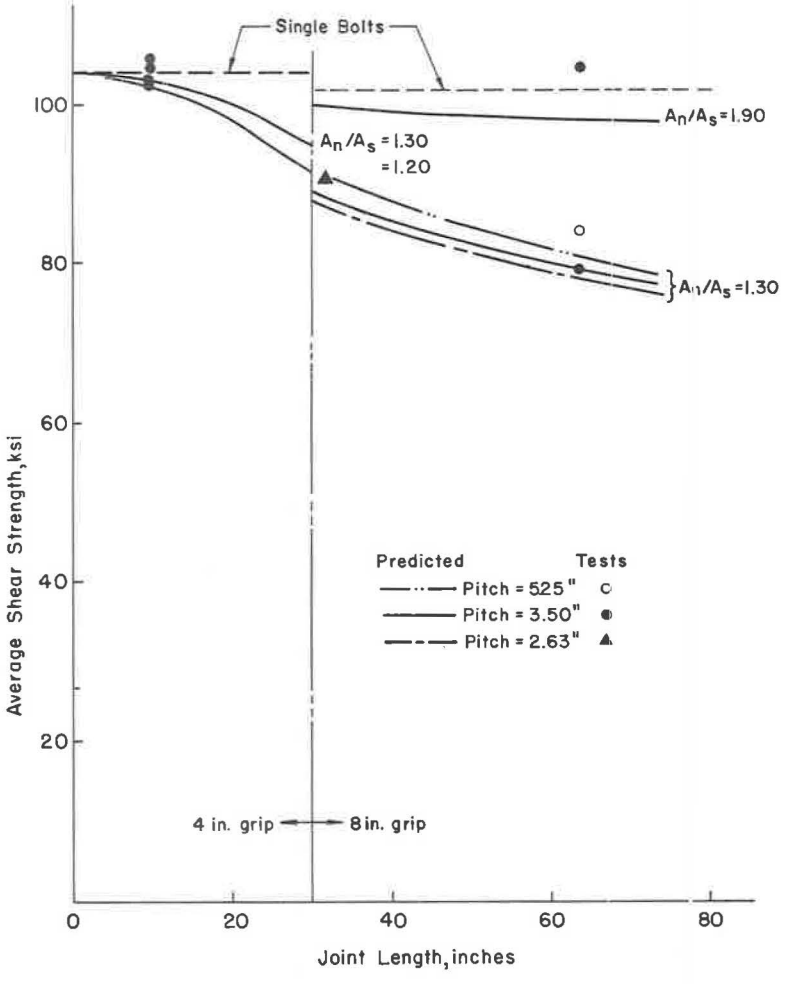

Figure 7. Comparison of computed failure curves with test results of A 440 steel joints connected by A 490 bolts.

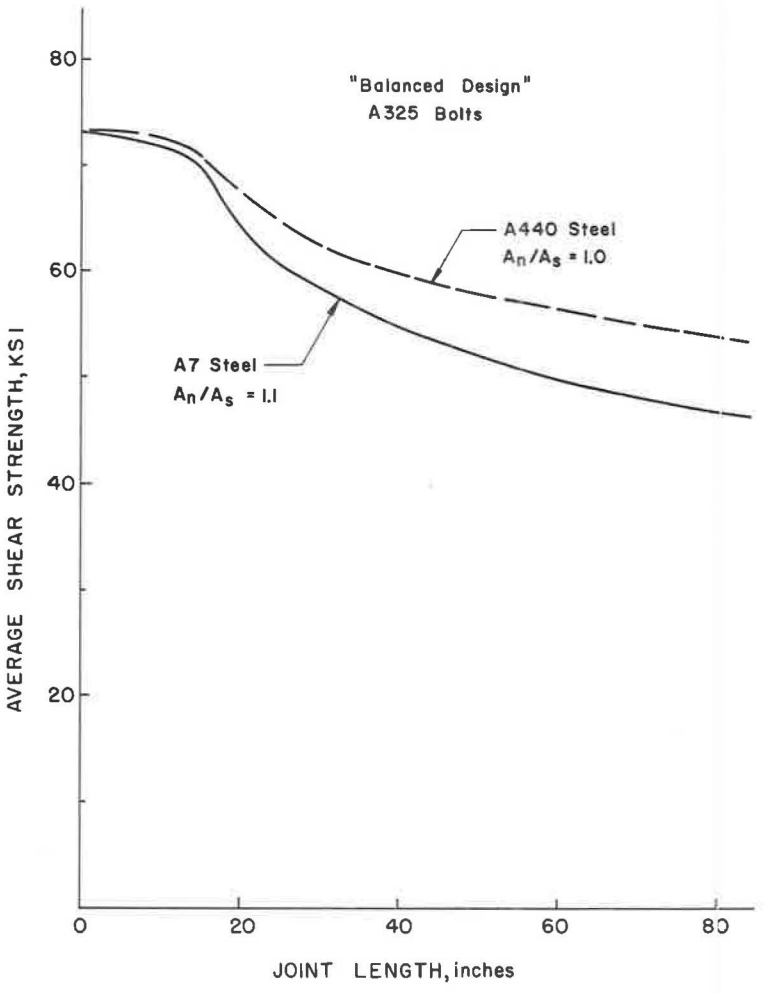

Figure 8. Effect of length on ultimate strength for balanced design.

used to eliminate the effects of the inherent eccentricity of the joints. Because of different tension-shear ratios, only one of these joints could be compared to a corresponding butt joint. In this case, the lap joint failed at almost exactly half the failure load of the butt joint.

DESIGN CRITERIA FOR BEARING-TYPE CONNECTIONS

The theory developed by Fisher and Rumpf (5) was used to compare the relative behavior of A 7 and A 440 steel joints fastened with A 325 bolts for the balanced design condition. Such a comparison is made in Figure 8, where the theoretical curve for A 7 steel joints with $A_n/A_s = 1.1$ is compared with the theoretical curve for A 440 steel joints with $A_n/A_s = 1.0$. This comparison shows that the A 325 bolts perform better in A 440 steel ($A_n/A_s = 1.0$) than in A 7 steel ($A_n/A_s = 1.1$) for these proportions. It should be noted again that balanced design was achieved only for very short joints. In the longer joints, the end bolts failed before the tensile strength of the plate was developed.

Since balanced design means that the same factor of safety against ultimate is applied to both the bolt and to the plate, this would imply (using the above ratios) that the allowable shear stress would be 20 ksi for A 325 bolts in A 7 steel and 25 ksi for A 325 bolts in A 440 steel. For compact A 7 steel joints where balanced design is achieved, the factor of safety would be about 3.3. The corresponding factor of safety would be 2.7 for compact A 440 steel joints. In both cases, an increase in joint length results in a decrease in the factor of safety. For long joints, the factor of safety is about 2.2 and is nearly independent of the grade of steel in the joints.

It is not reasonable to vary the allowable stresses for the same bolt depending on which material is being connected. A more rational approach is to establish working

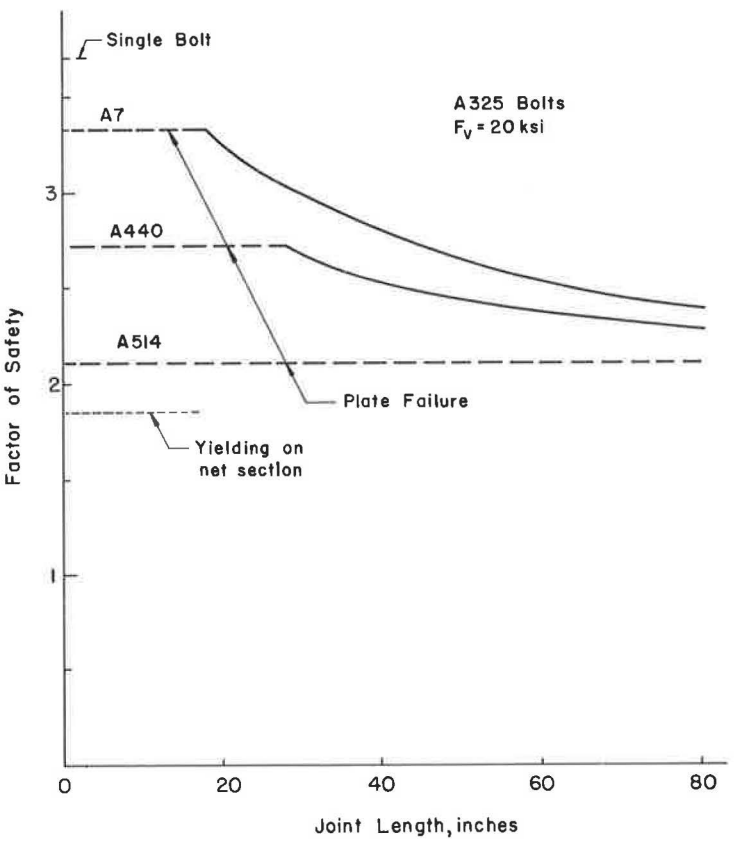

Figure 9. Current factor of safety for A 325 bolts in various steels.

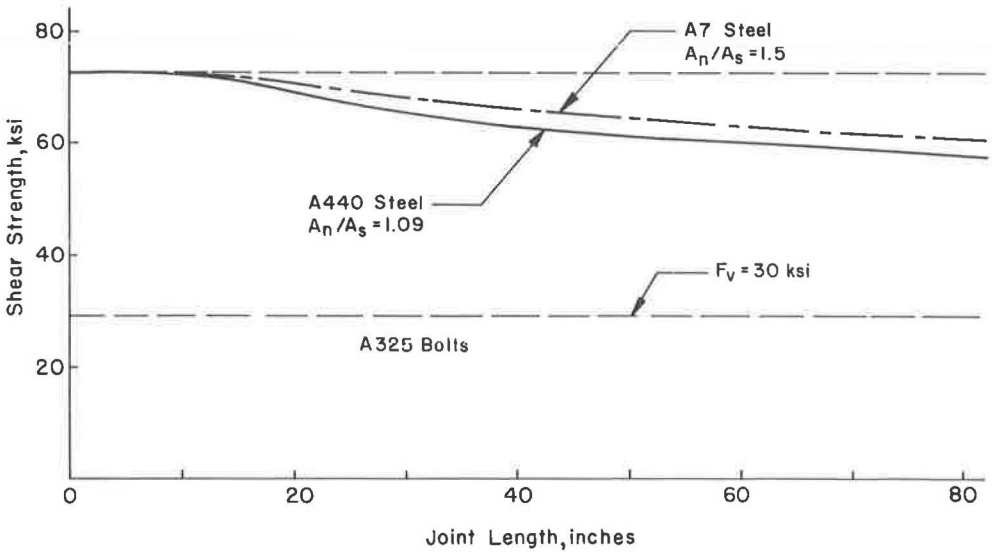

Figure 10. Predicted behavior of A 325 bolts designed for 30 ksi in bearing-type joints.

stresses based on the behavior of the bolt in the various steel joints (9). As shown in Figure 9, the behavior of the bolt for a given allowable stress (20 ksi) is nearly the same in the 2 different steels. Here the factor of safety is plotted as a function of joint length for the current allowable shear stress of 20 ksi for A 325 bolts installed in A 7, A 440, and A 514 steel plate (9, 10). The curves show the factor of safety against shear failure in the bolt, whereas the horizontal lines show the cut-off that would occur as a result of plate failure for the 3 types of steel.

For short joints (up to about 4 bolts in a line), the factor of safety against shear failure in the bolt is the same regardless of the type of connected steel, namely 3.7. For long joints, neglecting plate failure, the factor of safety is seen to vary depending on the joint length.

It can be noted that higher strength steel joints develop less strength for the given allowable bolt stress (Fig. 9) than the A 7 steel joints. This is contrary to the results shown in Figure 8 which described the balanced design condition. The same situation holds at other stress levels. If, for example, the allowable shear stress in the bolt were 30 ksi, the corresponding A_n/A_s ratio for A 7 steel is 1.50 and for A 440 steel it is 1.09. Figure 10 shows that the bolt shear strength in A 440 steel joints is slightly less than that of A 7 steel joints for this design stress level in the bolts. The factor of safety for the A 325 bolt in this instance varies from about 2.45 to 2.0 for both types of connected steels. This analysis has shown, and tests have verified, that the shear strength of A 325 bolts installed in compact joints of A 7 and A 440 steel is substantially the same. With increasing joint length, both A 7 and A 440 steel joints show a decrease in the bolt shear strength.

This examination has shown that the concept of balanced design leads to inconsistent allowable bolt shear stresses for different steels and the same bolt. For a given allowable bolt shear stress (20 ksi), the resulting geometric configurations for different steels provide ultimate joint strengths which decrease slightly with an increase in steel strength. A more logical criterion for design follows if the factor of safety is fixed against the shear strength of the fastener. It is apparent that increasing the allowable bolt shear stress in bearing-type joints would have no adverse effect on the minimum factor of safety. It would simply mean that the material would be used more efficiently. Additional discussion of this design criterion is presented elsewhere (11).

SLIP RESISTANCE

Although the primary objective of these studies of high strength bolts in bearing-type connection was to evaluate the ultimate strength of the joints, information was also obtained on their slip resistance. The factors which determine the load at joint slip are the bolt clamping force and the slip coefficient. The clamping force was determined from measurements of the bolt elongations taken during fabrication.

The slip coefficient, K_S, has been computed as

$$K_S = \frac{P_S}{mn\ T_i} \tag{1}$$

where P_S is the major slip load; m is the number of bolt shear planes; n is the number of bolts; and T_i is the average initial bolt tension (or clamping force) as obtained from a torqued tension calibration curve using the average elongation of all bolts in a joint. The resulting values of K_S are shown in Figure 11. The slip coefficient was not significantly affected by joint width, length, or grip.

The A 7 steel joints with clean mill scale had slip coefficients which ranged from 0.32 to 0.57 with a mean value of 0.44. The A 440 steel joints with clean mill scale had a mean slip coefficient of 0.32. The average value generally used for steel joints is 0.35 (9). The eight A 7 steel joints which had the mill scale removed with a power tool had slip coefficients which ranged from 0.22 to 0.35, with a mean value of 0.29. This emphasizes the importance of avoiding the over-polishing of faying surfaces in friction-type connections.

In addition to the A 440 steel joints connected by A 325 bolts, 8 A 440 steel joints connected by A 490 bolts were tested. The number of bolts in a line varied from 4 to 19. The steel plate for both series of tests was from the same heat. The slip coefficient ranged from 0.33 to 0.40, with an average value of 0.35. This was only slightly

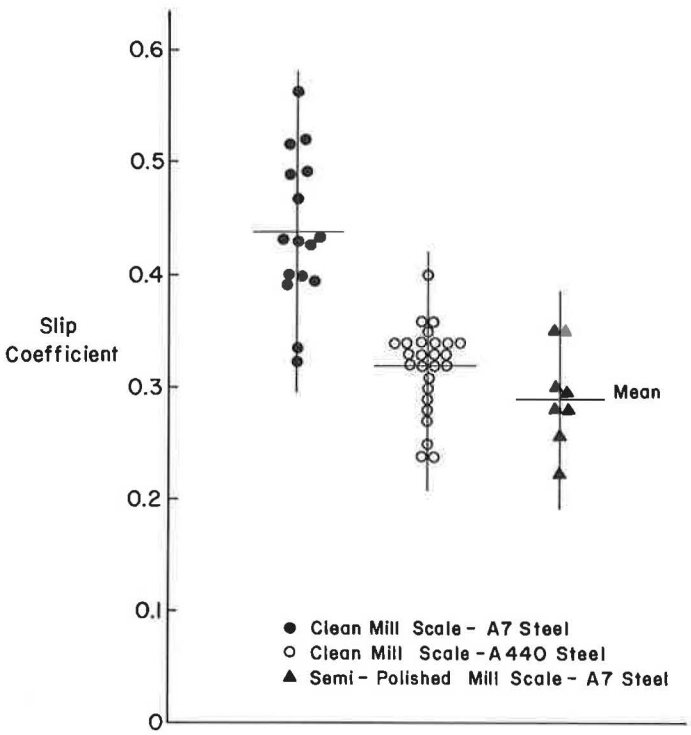

Figure 11. Slip coefficient for bolted joints.

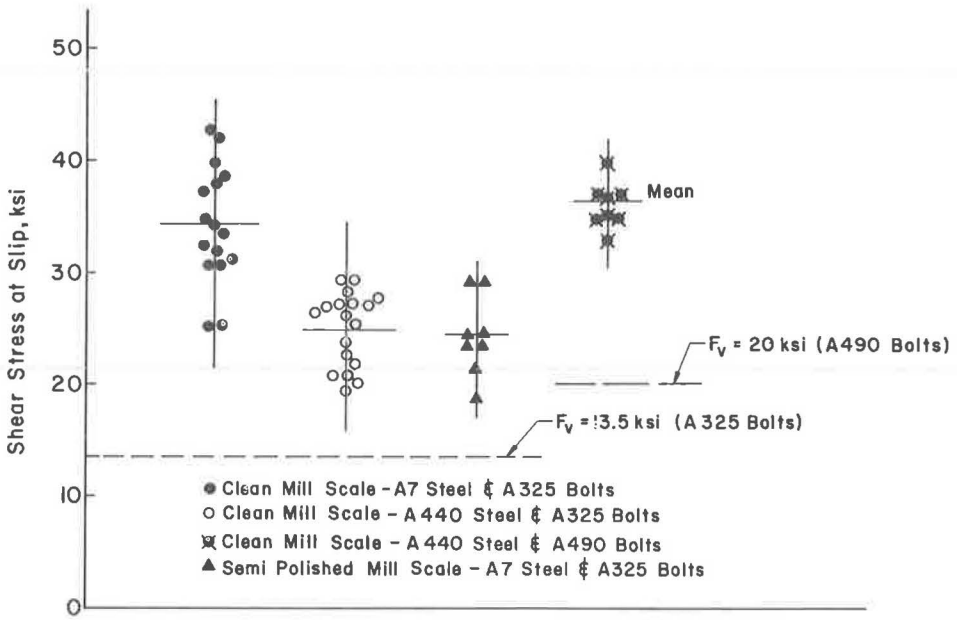

Figure 12. Slip resistance of bolted joints when bolts are tightened by turn-of-nut method.

higher than that obtained for the A 440 steel joints connected by A 325 bolts. Hence, the type bolt did not significantly affect the slip coefficient.

Although the bolts are not actually acting in shear, it has been convenient to regulate the design of friction-type connections by an allowable bolt shear stress (9). The average shear stress at time of major slip is plotted in Figure 12. The horizontal line extending across the graph at 13.5 ksi represents the working stress level for A 325 bolts. The horizontal line at 20 ksi is for A 490 bolts. It is readily apparent that all joints with clean mill scale faying surfaces had factors of safety against slip which exceeded the value of 1.55 described in Ref. 9. This was true for A 325 and A 490 bolts. All bolts were installed by the turn-of-nut method. The resulting internal bolt tension in A 325 bolts was about 30 percent greater than the minimum required tension. In A 490 bolts it was about 10 percent greater.

FURTHER RESEARCH

A number of studies are under way at Lehigh University to explore factors not covered. Among these are:

1. Studies of constructional alloy steel (A 514) joints fastened with A 325 or A 490 bolts.
2. Studies of joints in which 2 or more different grades of steel are joined.
3. Studies to determine the influence of joint flexibility on the installation of A 490 bolts.
4. Studies of the influence of slotted and oversize holes on slip resistance of joints and installation of bolts.
5. Studies of the influence of variations in clamping pressure and surface area on the slip resistance of bolted joints.

It is hoped that the results of this work will contribute to a better understanding of bolted joints and to further improvements in their use.

SUMMARY AND CONCLUSIONS

The following conclusions are based on the results of theoretical studies and of 54 confirming tests of large bolted joints conducted at Lehigh University and summarized herein. The principal items under investigation were the effect of joint length on the ultimate strength, the effect of variations in the net tensile area, the type of connected steel, and the type of fastener. Information was also obtained on the applicability of the turn-of-nut method, the effect of surface condition on slip resistance, the effect of pitch, the effect of joint width, the effect of number of shear planes, and long grip bolts.

1. Joints of A 440 steel with up to 4 A 325 fasteners in line were capable of developing about 96 percent of the shear strength of a single bolt. Similar joints of A 7 steel fastened with A 325 bolts behaved in substantially the same manner.
2. As joint length increased with an increasing number of bolts in a line, the differential deformations in the connected material caused the end bolts to shear before all bolts could develop their full shearing strength. The fastener pitch influences the shear strength mainly through its effect on joint length. This unbuttoning-type of failure was observed for all types of fasteners including rivets. It emphasizes the fact that joints should be kept as short as possible.
3. The decrease in strength with increasing joint length was slightly more for A 440 steel joints than for A 7 steel joints when the fasteners are proportioned to the same allowable shear stress.
4. Controlled variation in the plate area at the net section affected the bolt shear strength, as would be expected. As the plate area increased, greater rigidity was achieved and a correspondingly higher shear strength of the bolt groups resulted. This emphasizes the value of keeping the number of fasteners to a minimum.
5. An increase in joint width had no appreciable effect on the ultimate strength of A 440 steel joints and only slightly affected the strength of A 7 steel joints.
6. Good agreement was obtained between the test results and the theoretical analysis developed for determining the ultimate strength of bolted joints. The variation between the computed strength and the test result seldom exceeded 5 percent.
7. A more logical criterion for design evolves if the factor of safety is fixed against the shear strength of the fastener. The balanced design concept is shown to have no meaning because inconsistent allowable bolt stresses would result.
8. Bolts used in single shear have one-half the load-carrying capacity of comparable bolts in double shear, provided the shear planes act through the bolt shank.
9. The test confirmed that no special provision need be made for high strength bolts in long grips.
10. These tests indicated that a reasonable mean value of the slip coefficient for tight mill scale faying surfaces of A 7 or A 440 steel is about 0.35. Neither joint length nor width had any appreciable effect on the slip coefficient.
11. All bolts in these tests were tightened by the turn-of-nut method. The A 325 bolts had preloads about 1.3 times their specified proof load. The A 490 bolts had preloads about 1.1 times their specified proof load.

ACKNOWLEDGMENTS

The work described in this paper is part of an investigation of large bolted joints being conducted at the Fritz Engineering Laboratory, Department of Civil Engineering, Lehigh University. Professor William J. Eney is head of the Department and the Laboratory. The project is sponsored by the Pennsylvania Department of Highways, the U.S. Bureau of Public Roads, the American Institute of Steel Construction, and the Research Council on Riveted and Bolted Structural Joints. Committee 10 of the Research Council on Riveted and Bolted Structural Joints has provided technical guidance.

REFERENCES

1. Foreman, R. T., and Rumpf, J. L. Static Tension Tests of Compact Bolted Joints. Trans. ASCE, Vol. 126, p. 228, 1961.

2. Bendigo, R. A., Hansen, R. M., and Rumpf, J. L. Long Bolted Joints. Jour. Struct. Div., ASCE, Vol. 89, No. ST6, p. 187, Dec. 1963.
3. Fisher, J. W., Ramseier, P. O., and Beedle, L. S. Strength of A 440 Steel Joints Fastened With A 325 Bolts. Publications, IABSE, Vol. 23, p. 135, 1963.
4. Fisher, J. W. The Analysis of Bolted Butt Joints. PhD dissertation, Lehigh Univ., Bethlehem, Pa., 1964.
5. Fisher, J. W., and Rumpf, J. L. Analysis of Bolted Butt Joints. Jour. Struct. Div., ASCE, Vol. 91, No. ST5, p. 181, Oct. 1965.
6. Sterling, G. H., and Fisher, J. W. Tests of Long A 440 Steel Bolted Butt Joints. Fritz Engineering Laboratory Rept. No. 288.26, Feb. 1965.
7. Sterling, G. H., and Fisher, J. W. A 440 Steel Joints Connected by A 490 Bolts. Fritz Engineering Laboratory Rept. No. 288.30, Sept. 1965.
8. Vasarhelyi, D. D., Beano, S. Y., Madison, R. B., Lu, L. W., and Vasishth, U. C. Effect of Fabrication Techniques. Trans. ASCE, Vol. 126, Part II, p. 764, 1961.
9. Research Council on Riveted and Bolted Structural Joints. Specifications for Structural Joints Using ASTM A 325 or A 490 Bolts. 1964.
10. American Association of State Highway Officials. Standard Specifications for Highway Bridges. AASHO, Washington, 1961.
11. Fisher, J. W., and Beedle, L. S. Criteria for Designing Bolted Joints (Bearing-Type). Jour. Struct. Div., ASCE, Vol. 91, No. ST5 p. 129, Oct. 1965.

Fatigue Strength of Shear Connectors

ROGER G. SLUTTER, Research Instructor of Civil Engineering, and
JOHN W. FISHER, Research Assistant and Professor of Civil Engineering,
Fritz Engineering Laboratory, Lehigh University

An experimental investigation was undertaken at Lehigh University to determine the fatigue strength of shear connectors for steel and concrete composite beams. Factorial experiments were designed to provide information regarding the effect of stress range and minimum stress level on the cycle life.

Included are fatigue tests of 35 push-out specimens having the concrete slab connected to the steel beam section by $\frac{3}{4}$-in. stud connectors, 9 fatigue tests of push-out specimens using $\frac{7}{8}$-in. stud connectors and 12 fatigue tests of push-out specimens using 4-in., 5.4-lb channel connectors. The test data are described by mathematical equations which express the fatigue life as a function of the stress range.

Based on the reported fatigue tests and previous static and fatigue studies, a design criteria is proposed for the shear connectors of composite beams.

•COMPOSITE construction consisting of a concrete slab attached to steel beams by mechanical shear connectors is widely used for bridge spans of various lengths. Recent static (1) and fatigue studies (2, 3) of composite members have indicated that the currently used design procedure (4) for composite bridge beams is conservative. The wide use of this type of construction would indicate that worthwhile savings could be achieved by a better utilization of the connecting material.

The present design procedure for shear connectors is primarily based on static considerations (5). The useful capacity of connectors was derived from static tests of beams with shear connectors and from push-out specimens by limiting the magnitude of slip to a value which would preclude the yielding of connectors. Design values are obtained by dividing the useful capacity by a suitable factor of safety which insures that the ultimate strength of the member can be developed prior to yielding of connectors. Resulting designs were compared with available fatigue test results which indicated that fatigue failure was not a critical factor in the design. Since fatigue failure of connectors was not possible when this procedure was used, the spacing of connectors was determined from static load considerations. This results in a variable spacing of connectors which is proportional to the ordinate of the shear diagram.

Recent static studies have provided an approach for designing shear connectors so that the flexural strength of the member can be developed without requiring a limitation on the magnitude of slip or preventing yielding of the shear connectors (1). The investigation revealed that the number of connectors required to develop the ultimate strength of a member could be reduced considerably when compared with the requirements in the AASHO specifications. Also, the study showed that connectors need not be spaced in accordance with the intensity of static shear to develop the ultimate strength. Uniform spacing of connectors was satisfactory for most loading conditions and neither ultimate strength nor deflections were appreciably influenced by the uniform spacing of connectors.

Paper sponsored by Committee on Steel Superstructures and presented at the 45th Annual Meeting.

If the shear connector requirements are reduced by decreasing the factor of safety, fatigue failure of connectors may become the governing factor. Fatigue tests of composite beams at Lehigh University (2) and the University of Texas (3) revealed that no direct relationship exists between the static strength and the fatigue strength of connectors. Therefore, it is not advisable to retain the present design procedure and simply reduce the shear connector requirements. The test programs also indicated that when the number of shear connectors was adequate to prevent fatigue failure of connectors, the loss of interaction between slab and beam was not sufficient to cause appreciable increases in stresses and deflections in the beam. The initial fatigue studies did not provide complete information on the fatigue strength of connectors nor the effect of other variables on the fatigue strength.

The purpose of this investigation was to determine the fatigue characteristics of mechanical connectors for composite steel and concrete construction. Previous fatigue tests of composite beams had indicated that considerable variation could be expected in beam specimens, because it was difficult to assess the fatigue damage (2, 3, 6). The failure of one or two connectors could not always be detected and did not significantly affect the beam behavior as the shear was redistributed to other connectors. Also, in beam tests it was not feasible to determine the fatigue behavior of connectors subjected to stress reversal.

Pilot studies indicated that push-out specimens yielded results comparable to beam tests, so this type specimen was selected for the study. A push-out specimen had added advantages in that the loads to which the connectors were subjected could be more easily evaluated because redistribution was not significant. Also, a relatively large number of specimens could be tested more economically using push-out specimens.

EXPERIMENTAL STUDY OF ¾-INCH STUD CONNECTORS

The principal phase of the investigation involved push-out tests of ¾-in. stud connectors. The fatigue characteristics were evaluated by tests of 35 push-out specimens. Twenty-seven of these specimens formed the main experiment, 2 were pilot tests and 6 specimens were added to supplement the data of the main experiment. Each specimen consisted of a 20 by 26¾ by 6-in. reinforced-concrete slab attached by four ¾ by 4-in. stud connectors to an 8WF40 beam section as illustrated in Figure 1. The studs were attached to the ASTM A 36 steel beam sections by a local fabricator. The studs were inspected for soundness following the procedure outlined in a draft of "Recommendations for Materials and for Welding for Steel Channel, Spiral, and Stud Shear Connectors,"

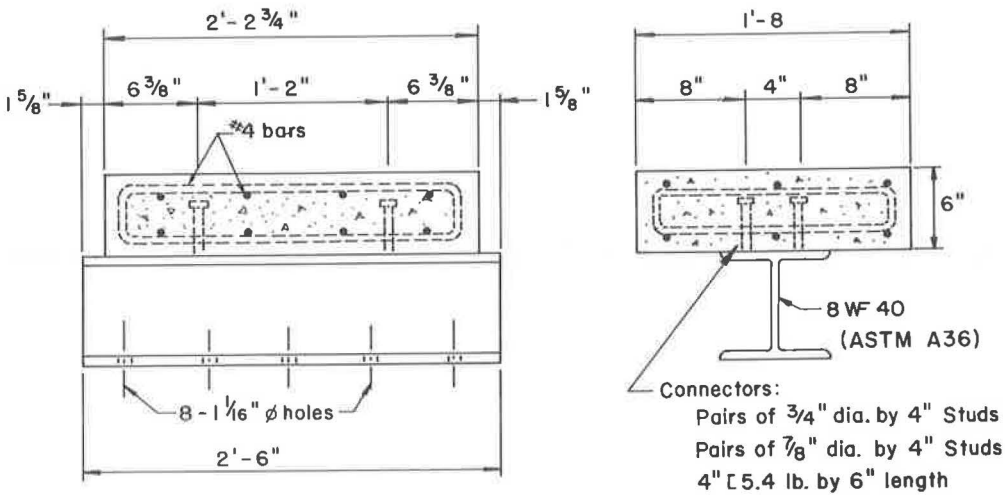

Figure 1. Details of test specimen.

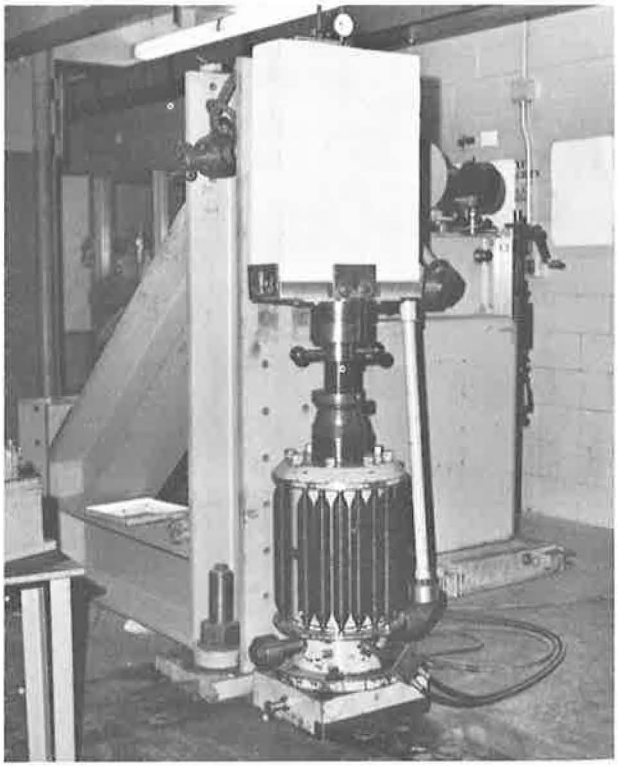

Figure 2. Test setup for loading in one direction.

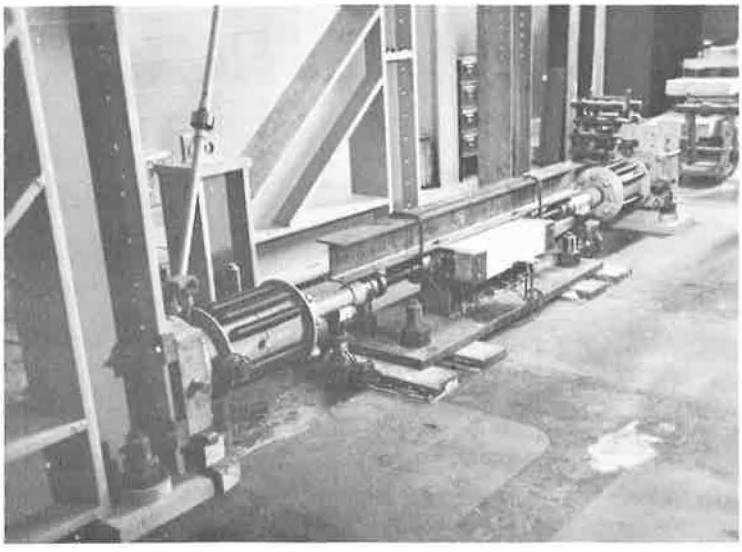

Figure 3. Test setup for stress reversal tests.

proposed by Subcommittee I of the ASCE-ACI Committee on Composite Construction and dated July 10, 1964. The push-out specimens were tested by applying load to the edge of the reinforced-concrete slab as shown in Figure 2. For stress reversal, load was applied to 2 edges of the slab (Fig. 3).

The specimens for the main experiment were cast in groups of 10. All slabs were cast in a horizontal position as in a normal bridge structure. The same concrete mix

TABLE 1

OUTLINE OF ¾-INCH STUD CONNECTOR EXPERIMENT

MAIN EXPERIMENT

Minimum Stress (ksi) \ Maximum Stress (ksi)	10	14	18	22	26
- 6	a 1 A b 1 A c 1 A	a 2 A b 2 A c 2 A	a 3 A b 3 A c 3 A		
2		a 2 B b 2 B c 2 B	a 3 B b 3 B c 3 B	a 4 B b 4 B c 4 B	
10			a 3 C b 3 C c 3 C	a 4 C b 4 C c 4 C	a 5 C b 5 C c 5 C

Minimum Stress (ksi) \ Stress Range (ksi)	8	12	16	20	24
- 6			a 1 A b 1 A c 1 A	a 2 A b 2 A c 2 A	a 3 A b 3 A c 3 A
2		a 2 B b 2 B c 2 B	a 3 B b 3 B c 3 B	a 4 B b 4 B c 4 B	
10	a 3 C b 3 C c 3 C	a 4 C b 4 C c 4 C	a 5 C b 5 C c 5 C		

SUPPLEMENTAL EXPERIMENT

Minimum Stress (ksi) \ Maximum Stress (ksi)	12	20
2	a 6 B b 6 B c 6 B	
10		a 6 C b 6 C c 6 C

Minimum Stress (ksi) \ Stress Range (ksi)	10
2	a 6 B b 6 B c 6 B
10	a 6 C b 6 C c 6 C

proportions were used for each casting. Two cylinders were tested at the beginning of each fatigue test. The specimens were 28 to 92 days old at the time of testing. The mean compressive strength of all cyclinders was 4300 psi, and the standard deviation of the concrete strength was 335 psi.

The tests were conducted with an Amsler hydraulic pulsator and jacks at the loading rates of 250 or 500 cycles per min. The rate of application of load was dependent on the specimen response. The average shear stress on the studs caused by the applied load was computed on the basis of the nominal cross-sectional area of the studs. Stress range is defined as the maximum horizontal shear stress minus the minimum horizontal shear stress in ksi on the cross-sectional area of studs or kips per inch of channel connector.

The main experiment was designed to evaluate 2 controlled variables—the stress range and the minimum stress. An outline of the main experiment design is given in Table 1. Five levels of maximum stress and stress range and 3 levels of minimum stress were selected on the basis of the previous beam experiments in order to establish the fatigue characteristics of the connectors for conditions that exist in bridge structures. Each minimum stress level was combined with 3 levels of maximum stress and stress range in such a manner that 2 complete 2 by 2 factorial experiments were included to obtain data on the effect of minimum stress on the maximum stress and minimum stress on the stress range. These four 2 by 2 factorial experiments are outlined by the dotted lines in Table 1. Three specimens were tested for each combination to provide replication.

Stress levels were assigned to the 27 specimens of the experiment at random and the specimens were assigned to 3 test blocks (a, b, c) as indicated in Table 1. Within each test block of the 2- and 10-ksi minimum stress levels a random order of testing was followed. All 3 test blocks of the reversal specimens (-6 ksi minimum stress) were randomized since a separate test setup was necessary. The random order of testing was followed to prevent variations caused by the controlled variables from being confounded with systematic variations due to uncontrolled variables such as the age of the specimens, behavior of testing equipment, etc.

The results of the main experiment indicated that range of stress rather than maximum stress was the more important variable. A stress range of 10 ksi appeared to be a suitable value for design. In an effort to obtain more data to supplement the main experiment, 6 additional specimens were tested with a stress range of 10 ksi and minimum stress levels of 2 and 10 ksi. This supplemental experiment is also shown in Table 1. The specimens for the supplemental tests were cast in one group. One cylinder was tested at the beginning of each fatigue test. The age of these specimens at the start of testing varied from 55 to 86 days. The mean compressive strength of all cylinders for this series was 3320 psi, and the standard deviation of the concrete strength was 110 psi. Hence, the additional test specimens also provided test data to help ascertain the influence of concrete strength on the fatigue life. In addition, 2 pilot tests are reported which were conducted to aid in the experiment design. The total number of push-out tests of $\frac{3}{4}$-in. diameter studs with minimum stress and range of stress as the major variables was 35.

EXPERIMENTAL STUDY OF $\frac{7}{8}$-INCH STUD CONNECTORS AND 4-INCH, 5.4-POUND CHANNEL CONNECTORS

The fatigue characteristics of $\frac{7}{8}$-in. stud connectors were evaluated by push-out tests identical to those for the $\frac{3}{4}$-in. stud connectors. Nine push-out specimens were designed and fabricated similar to the specimen shown in Figure 1. The specimens were tested in the same manner as the $\frac{3}{4}$-in. stud connectors.

The 9 test specimens for the factorial experiment were all cast at one time. One cylinder was tested at the beginning of each fatigue test and yielded a mean compressive strength of 4470 psi; the standard deviation was 80 psi. The age of the specimens at the start of testing varied from 53 to 63 days.

The experiment design was identical to that for the $\frac{3}{4}$-in. stud connectors except that only one test was made for each combination of stress conditions. An outline of the experiment design is given in Table 2.

TABLE 2

OUTLINE OF 7/8-INCH STUD CONNECTOR EXPERIMENT

Minimum Stress (ksi) \ Maximum Stress (kis)	10	14	18	22	26
- 6	e 1 G	e 2 G	e 3 G		
2		e 2 H	e 3 H	e 4 H	
10			e 3 I	e 4 I	e 5 I

Minimum Stress (ksi) \ Maximum Stress (ksi)	8	12	16	20	24
- 6			e 1 G	e 2 G	e 3 G
2		e 2 H	e 3 H	e 4 H	
10	e 3 I	e 4 I	e 5 I		

TABLE 3

OUTLINE OF 4-INCH, 5.4-POUND CHANNEL CONNECTOR EXPERIMENT

Minimum Stress (kips/in.) \ Maximum Stress (kips/in.)	3.0	3.5	4.0	4.5	5.0
-0.5	d 1 D	d 2 D	d 3 D		
+0.5		d 2 E	d 3 E	d 4 E	
+1.5			d 3 F	d 4 F	d 5 F

Minimum Stress (kips/in.) \ Stress Range (kips/in.)	2.5	3.0	3.5	4.0	4.5
-0.5			d 1 D	d 2 D	d 3 D
+0.5		d 2 E	d 3 E	d 4 E	
+1.5	d 3 F	d 4 F	d 5 F		

The fatigue characteristics of 4-in., 4.5-lb channel connectors was evaluated by tests of 12 push-out specimens. Nine of these specimens were part of the factorial experiment and 3 were pilot tests. Each specimen consisted of a reinforced concrete slab identical to that used for the stud connector specimens attached to the 8WF40 steel beam section by two 6-in. lengths of 4-in., 5.4-lb channels. One pilot test had the slab attached to the steel beam by only one 6-in. length of channel. Each channel was attached to the steel beam section by $\frac{3}{16}$-in. fillet welds placed along the length of the heel and toe. The specimens were tested in the same manner as the $\frac{3}{4}$-in. and $\frac{7}{8}$-in. stud shear connectors.

The 9 test specimens for the factorial experiment were all cast at one time. One cylinder was tested at the beginning of each fatigue test and yielded a mean compressive strength of 6045 psi, with a standard deviation of 80 psi. The age of the specimens varied from 28 to 76 days.

The tests were all conducted with the Amsler hydraulic pulsator and jacks at the rate of 250 cycles per min. The average force per inch of channel was computed by dividing the applied load by the total channel length. The load was applied to the test specimens of the main experiment by loading the edge of the concrete slab adjacent to the back face of the channel, since this is the orientation commonly used on construction. The load was applied to the opposite edge of the slab during the pilot studies.

The experiment design was the same as for $\frac{7}{8}$-in. diameter stud connectors; the outline of the main experiment is given in Table 3.

TEST RESULTS

All specimens were tested until failure occurred. For the stud shear connectors 2 different types of failure were apparent. Most of the fatigue failures were initiated at the reinforcement of the stud weld and penetrated into the beam flange causing a concave depression into the beam flange. In a few cases, the fatigue failure initiated at the reinforcement and penetrated through the weld. This latter condition was generally observed to occur when the weld penetration was incomplete. These typical failures are shown in Figure 4. Figure 4(a) shows failure through the weld. The concave depression into the beam flange is apparent in Figure 4(b). The crystalline texture of a typical fatigue fracture is readily apparent. The mode of failure was not a significant variable in these tests.

It was also apparent in the stud connector tests that 2 overall failure modes were evident for the push-out specimens. For the higher stress ranges and the lower minimum stress levels, the 2 studs nearest the applied load failed in fatigue. The remaining 2 studs were usually sheared off by the applied load as their ultimate static strength was exceeded before the machine could be stopped. For the lower stress range and higher stress levels, the applied load was more evenly distributed among the 4 studs and fatigue failures were evident in all 4 connectors.

For the channel shear connectors, the fatigue failure was generally initiated in one of the transverse fillet welds and propagated through the weld. In one instance, failure occurred in the channel web. No apparent stress raiser was noted for this case. With the channel connectors it was obvious that the channel nearest the applied load was carrying more load because the fatigue failure always initiated in this connector. The remaining channel was then pulled out of the slab as the static strength was exceeded. Figure 5 shows typical fatigue fractures of the channel connector nearest the applied load and shows the remaining connector that was pushed from the slab as its static strength was exceeded before the machine could be stopped. The specimen on the left is from the main experiment while the specimen on the right is a pilot specimen.

Because of this observed behavior, an additional pilot specimen was fabricated which had only one channel connecting the concrete slab to the steel beam section. No significant difference was observed in the cycle life between the one- or two-channel connector push-out specimens.

The experimental results for the $\frac{3}{4}$-in. stud connectors are summarized in Figure 6 in which the stress range is given as a function of the logarithm of the number of cycles to failure for each minimum stress level. The test data from the main experiment are

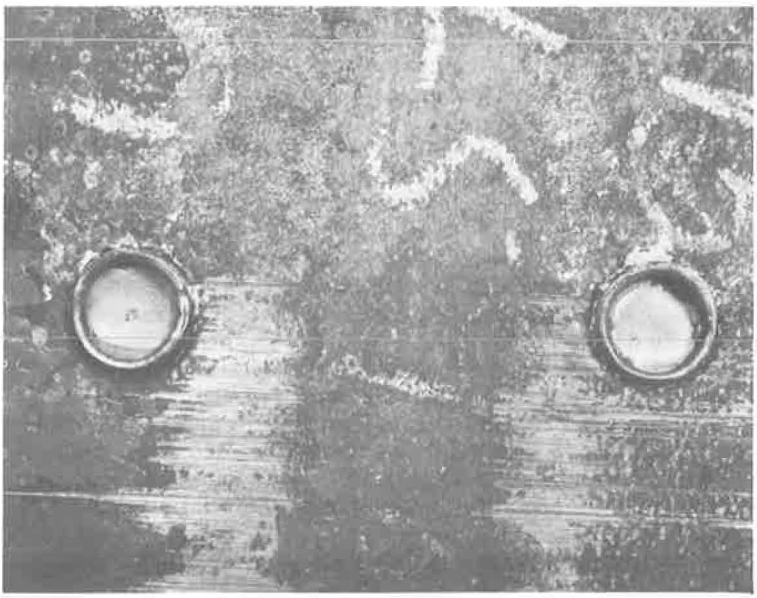

(a)

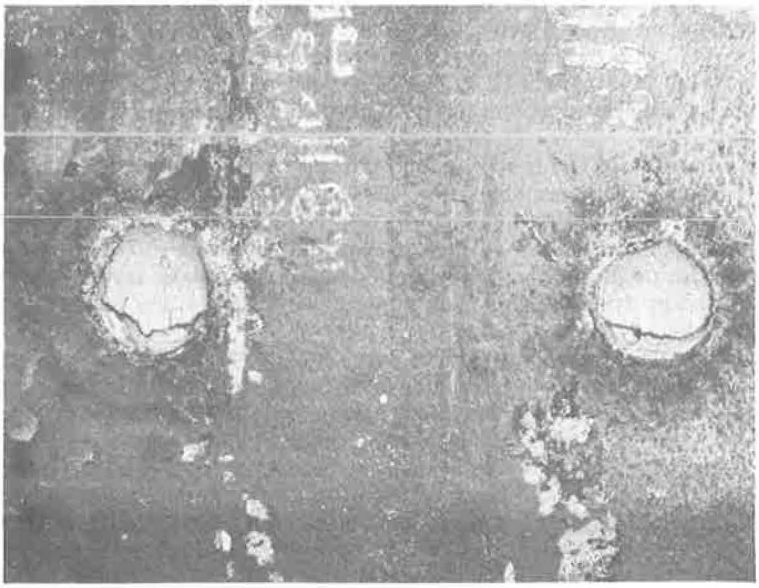

(b)

Figure 4. Typical failures of ¾-in. diameter studs: (a) failure through the weld; (b) failure penetrating into beam flange.

Figure 5. Failures of channel connectors.

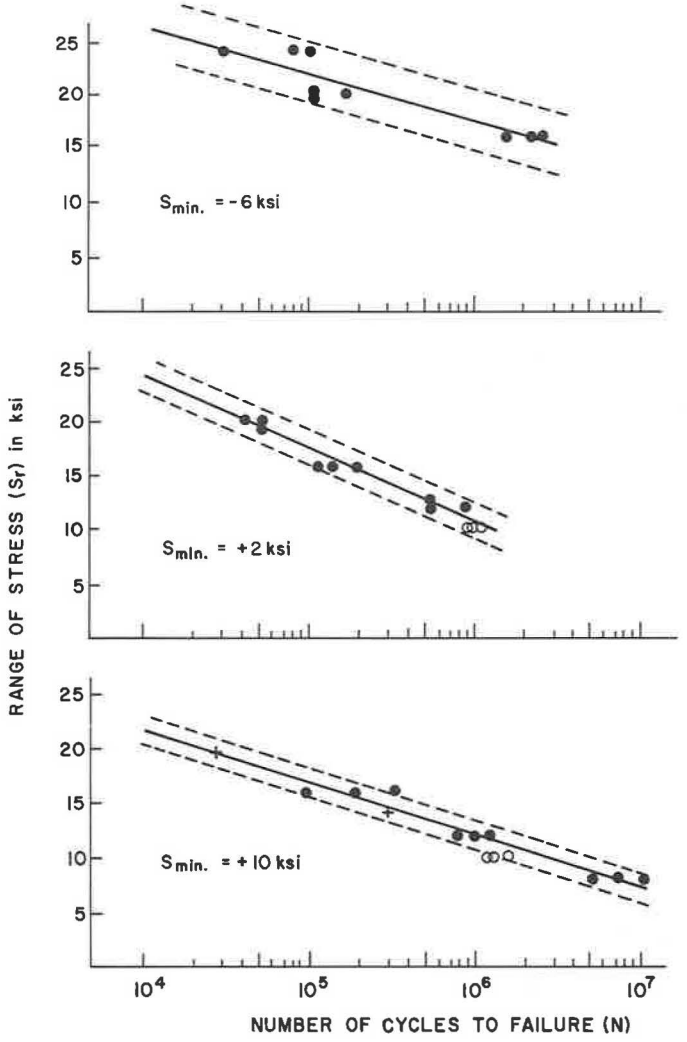

Figure 6. S-N curves for specimens with ¾-in. diameter studs.

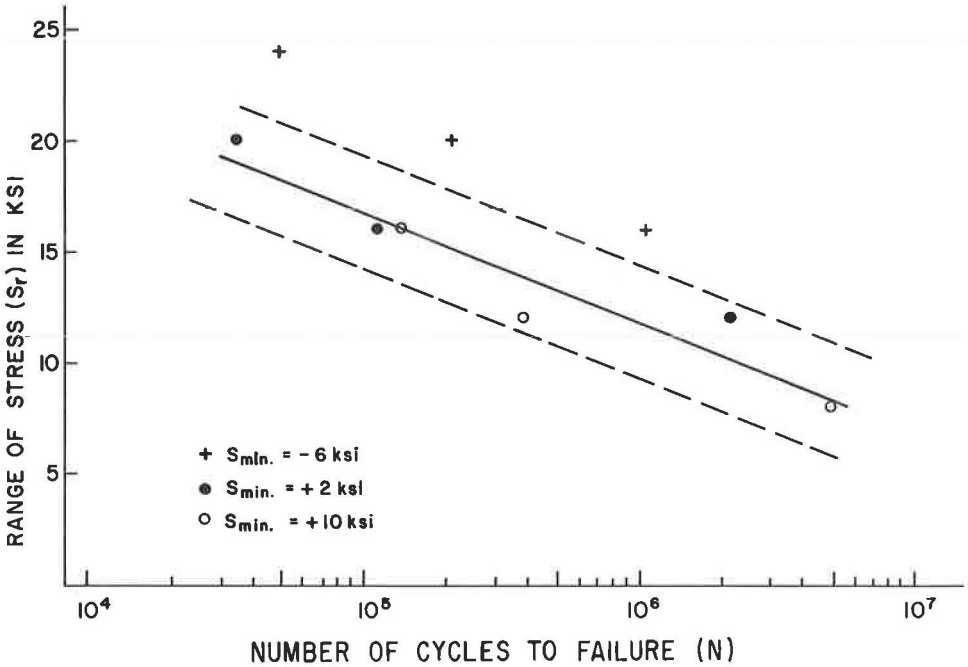

Figure 7. S-N curve for specimens with $\frac{7}{8}$-in. diameter studs.

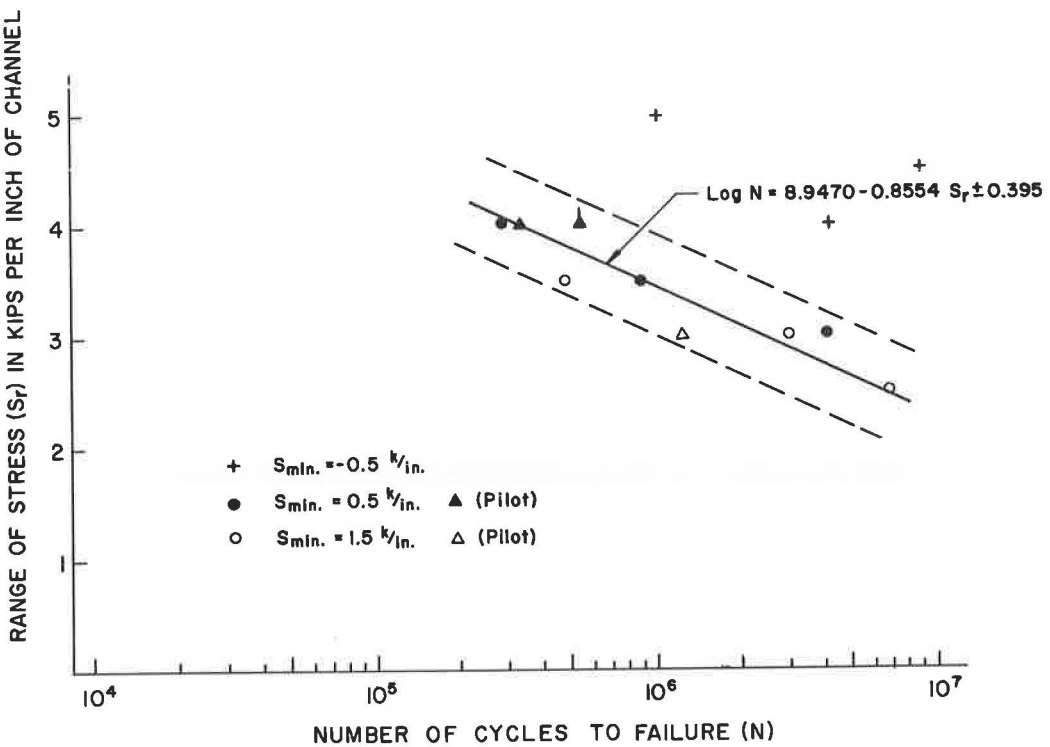

Figure 8. S-N curve for specimens with 4-in., 5.4-lb channels.

plotted as dots. The test data for the supplemental tests are plotted as circles and the pilot tests are plotted as crosses. The cycle life ranged from 27,000 up to 10,275,000 cycles.

The experimental results for the $\frac{7}{8}$-in. stud shear connectors are summarized in Figure 7. The test data for S_{min} = -6 ksi are plotted as crosses, the data for S_{min} = +2 ksi are plotted as dots and the data for S_{min} = +10 ksi are plotted as circles. The cycle life ranged from 33,000 to 4,885,100 cycles for the $\frac{7}{8}$-in. stud shear connectors. The experimental results for the 4-in., 5.4-lb channel shear connectors are summarized in Figure 8. The test data for S_{min} = -0.5 kips per in. are plotted as crosses, the data for S_{min} = +0.5 kips per in. are plotted as dots and the data for S_{min} = +1.5 kips per in. are plotted as circles. The cycle life ranged from 291,200 to 9,556,300 cycles for the channel shear connectors. The 3 pilot specimens of 4-in., 5.4-lb channel shear connectors are plotted as triangles. The specimen having the single channel connector has a vertical line attached above the triangle. It is obvious that the fatigue strength of the single channel specimen was equivalent to specimens with 2 channel shear connectors. Also, the orientation of the channel connector whether facing toward, as in the pilot tests, or away from the applied load, as in the main tests, had no significant influence on the fatigue life.

ANALYSIS OF TEST RESULTS

Earlier studies (2, 3) had indicated that the fatigue strength of the stud connectors could be represented by a mathematical model of the form

$$\log N = A + B S_r \qquad (1)$$

where S_r is the range of shear stress, N the number of cycles to failure and A and B empirical constants. The results of the beam tests are summarized in Figure 9 where circles represent data for $\frac{1}{2}$-in. diameter studs and dots represent data for $\frac{3}{4}$-in.

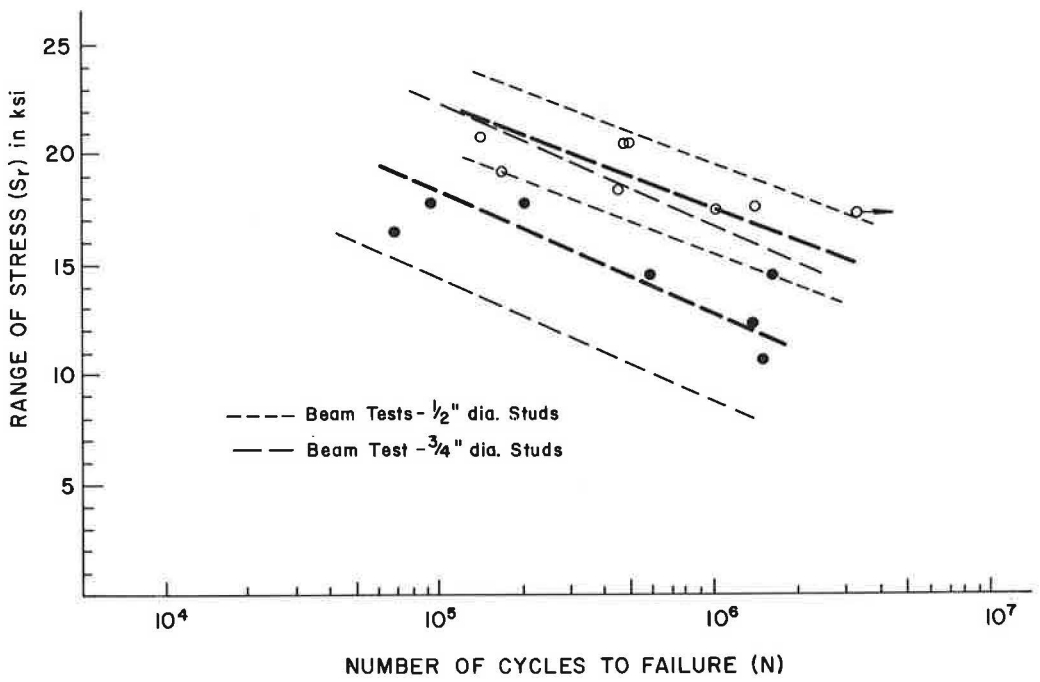

Figure 9. S-N curves for initial connector failure in beams with $\frac{1}{2}$-in. and $\frac{3}{4}$-in. diameter studs.

diameter studs. All specimens were tested with a low minimum stress level. No apparent leveling off of the S-N curves was noted in the beam tests. The mean regression lines in Figure 9 were developed from data reported earlier (2, 3). Also shown are the limits of dispersion of the test data. The failure criterion for the beam tests was taken as the initial fatigue fracture of the connectors. These tests indicated that ¾-in. stud connectors failed in fatigue at a lower stress than ½-in. stud connectors.

The factorial nature of the current experiments made possible independent determinations of the relative significance of the stress range and the minimum stress level. The analysis of the test data for ¾-in. stud shear connectors showed that the slopes of the S-N curves for the 3 minimum stress levels were not significantly different even at the 10 percent level. This indicated that the stress range affected the cycle life at each minimum stress level to the same degree. On the other hand, the analysis of variance indicated that the distances between the regression lines shown in Figure 6 were significantly different even at the 1 percent level—i.e., the minimum stress was a significant parameter. Hence, stress range and minimum stress accounted for the variations in the experiment.

An examination of the test data for the main experiment and the test data for the supplemental tests indicates that the strength of concrete had only a minor effect on cycle life. The supplemental test specimens with a mean concrete strength of 3320 psi were near the lower limit of dispersion of the test data for specimens with a mean concrete strength of 4300 psi, as can be seen in Figure 6. This was in agreement with the earlier fatigue tests of beam and push-out specimens which had concrete strength varying from about 3000 to 6000 psi (2, 3, 7, 8).

A further evaluation of the test data showed that the reason minimum stress had a significant effect on the cycle life was due to the stress reversal data. When all 3 curves are examined in Figure 6 it is apparent that the stress reversal curve is some distance above the other 2 levels of minimum stress. In fact, an analysis of variance of the test data for minimum stress levels of 2 and 10 ksi indicated that there was no significant difference in the test data and that minimum stress was not significant even at the 10 percent level.

Since the stress reversal specimens had significantly longer fatigue lives for the same stress range than the test data for 2- and 10-ksi minimum stress levels, it was concluded that a conservative estimate of the fatigue life could be obtained for all minimum stress levels by considering only the 2-ksi and 10-ksi minimum stress levels in the analysis. A regression analysis of the test data yielded

$$\log N = 8.072 - 0.1753\, S_r \qquad (2)$$

where

S_r = range of shear stress in ksi, $S_{max} - S_{min}$, and
N = number of cycles to failure.

The coefficient of correlation was 0.9323 and the standard error of estimate was 0.1940. The "goodness of the fit" may be judged from Figure 10 where the test data are compared with Eq. 2 shown as the solid line. The equation appears applicable for cycle lives which vary from 10^4 to 10^7. Equation 2 was developed by neglecting the stress reversal data. The limits of dispersion were taken as twice the standard error of estimate and are shown as 2 dashed lines parallel to the regression line. It is readily apparent that such an analysis will provide a greater margin of safety for the stress reversal case. This is not considered to be critical since most connectors will be subjected to a shear loading in only one direction. Also, when shrinkage of the concrete slab occurs, connectors designed for stress reversal may in fact be subjected to such a shear loading.

The results of the tests of ⅞-in. stud shear connectors were summarized in Figure 7. An examination of the test data shows that the ⅞-in. stud connectors behaved similarly to the ¾-in. stud connectors. Figure 11 compares the test data for the ¾-in. and ⅞-in. stud connectors. The data for ¾-in. connectors are shown as dots and for ⅞-in.

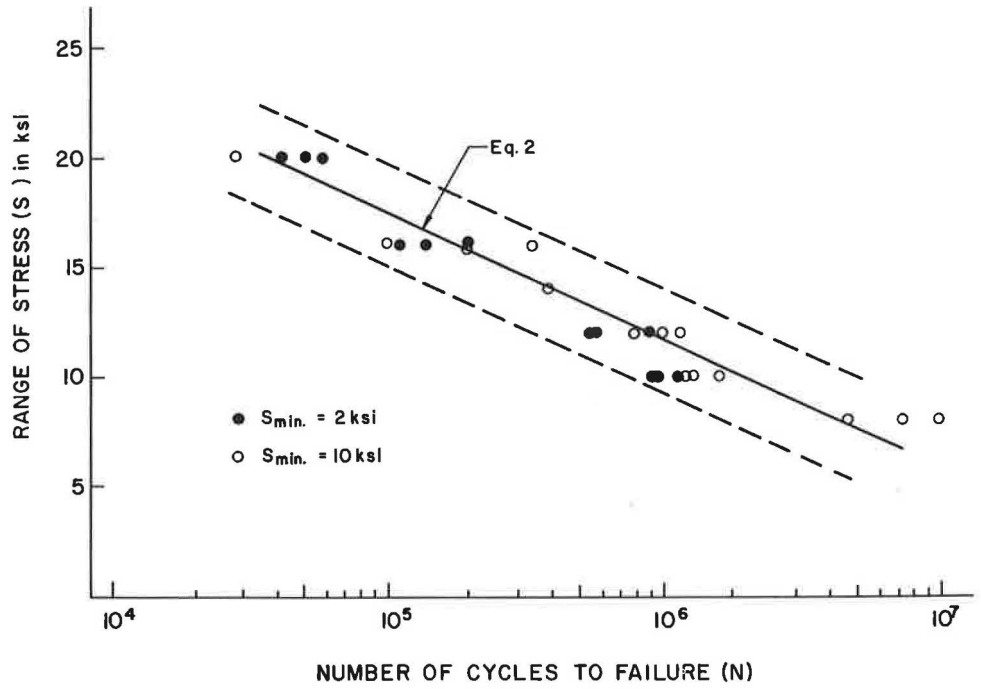

Figure 10. Regression curve for ¾-in. diameter studs.

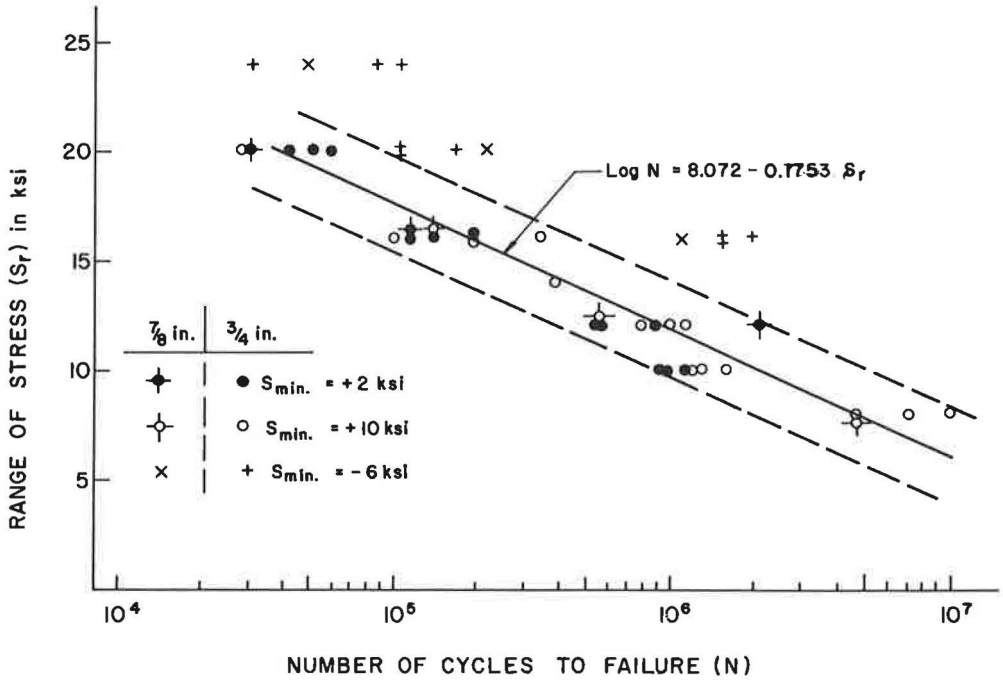

Figure 11. Comparison of push-out test data for ¾-in. and ⅞-in. diameter studs.

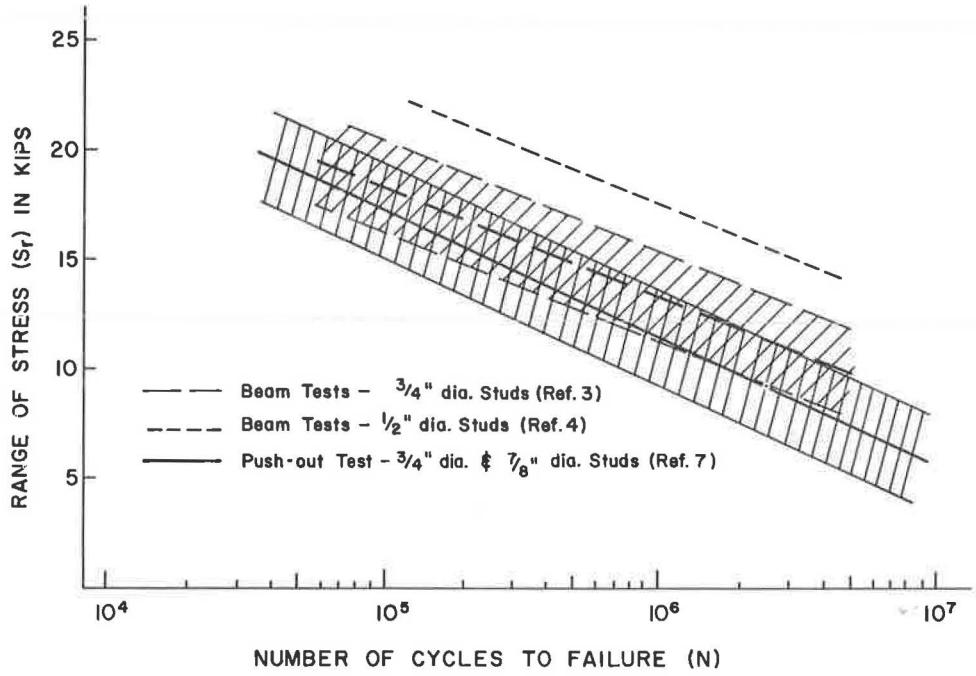

Figure 12. Comparison of S-N curves of beam tests and push-out tests.

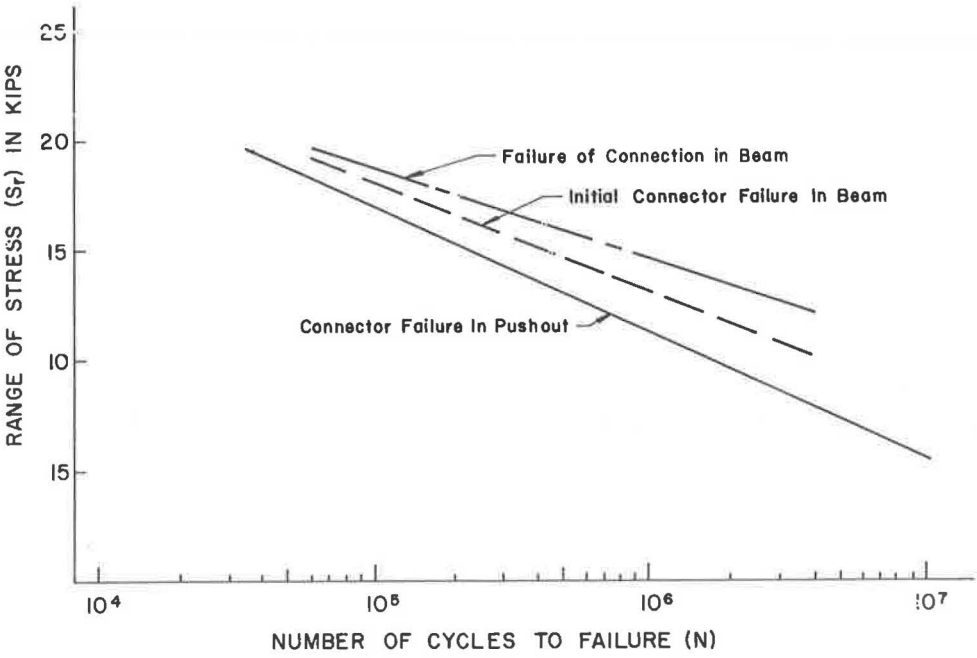

Figure 13. Comparison of initial connector failure and final failure of shear connection in composite beams.

connectors as circles. It is obvious and is verified by analysis that there are no significant differences between the fatigue strengths of $^3/_4$-in. and $^7/_8$-in. stud shear connectors.

The test data for the 4-in., 5.4-lb channel shear connectors plotted in Figure 8 also indicate that the stress reversal specimens had significantly greater fatigue strengths than the other 2 levels of minimum stress. Also, it is apparent that the test data for minimum stress levels of 0.5 k/in. and 1.5 k/in. are not significantly different. Hence, as with the stud shear connectors, a conservative estimate of the fatigue strength for all minimum stress levels can be obtained by neglecting the stress reversal data. A regression analysis of the test data for shear loading in only one direction yielded

$$\log N = 8.9470 - 0.8554\, S_r \qquad (3)$$

The coefficient of correlation was 0.8648 and the standard error of estimate 0.1975.

Figure 12 compares the regression curve for the push-out specimens reported herein with the beam tests reported earlier (2, 3). It is apparent that the lower limit of dispersion for the beam tests (taken as twice the standard error of estimate) overlaps the upper limit of dispersion for the push-out tests. Hence, the lower limit of dispersion of the beam tests is about equal to the mean behavior of the push-out specimens. This finding is reasonable because in the beam tests a loss of interaction was noted which allowed the connector forces to redistribute and resulted in a less severe stress condition than computed from elastic theory assuming complete interaction. In the push-out specimens the loading on the connectors was maintained at a reasonably constant level throughout the cycle life. Push-out tests therefore represent a lower bound for connector failure.

Also, it should be noted that the failure criteria for the beam test results plotted in Figures 9 and 12 were taken as the initial fatigue fracture of one or more connectors. Other studies (2, 3) have shown clearly that the failure of the first connectors has little effect on the beam response and that considerable additional life was available before the beam failed. This is illustrated in Figure 13 where the curve representing initial fatigue fracture of one or more connectors (plotted in Figs. 9 and 12) is compared with the curve relating the cycle life to failure of the connection in a beam (3). It is apparent that considerably longer cycle life was available before the composite beam failed due to the weakened shear connection.

Because the push-out tests provide a lower bound of fatigue strength it seems satisfactory to consider the mean curve shown in Figure 12 (Eq. 2) as the basis for the design of stud shear connectors. A suitable design value can be obtained from this curve for any desired cycle life. For example, if the expected life is 2 million cycles, the resulting allowable stress range is approximately 10 ksi. This value gives a suitable margin of safety with respect to beam test results.

On the basis of these data and rationale, a tentative design formula for the allowable range of load can be obtained from Eq. 2, with the result:

$$Z_r = \alpha\, d_s^2 \qquad (4)$$

where

Z_r = allowable range of shear force per stud in pounds;
d_s = diameter of the stud in inches; and
α = 13,800 for 100,000 cycles
10,600 for 500,000 cycles
7,850 for 2,000,000 cycles.

Equation 4 has been developed from tests of $^3/_4$-in. and $^7/_8$-in. stud shear connectors. An examination of Figure 12 indicates that it can be conservatively applied to smaller diameter stud shear connectors.

For the channel shear connectors, the fatigue failure was generally initiated in one of the transverse fillet welds and propagated through the weld. It was apparent that the critical parameter was the stress on the throat of the connecting fillet welds. For

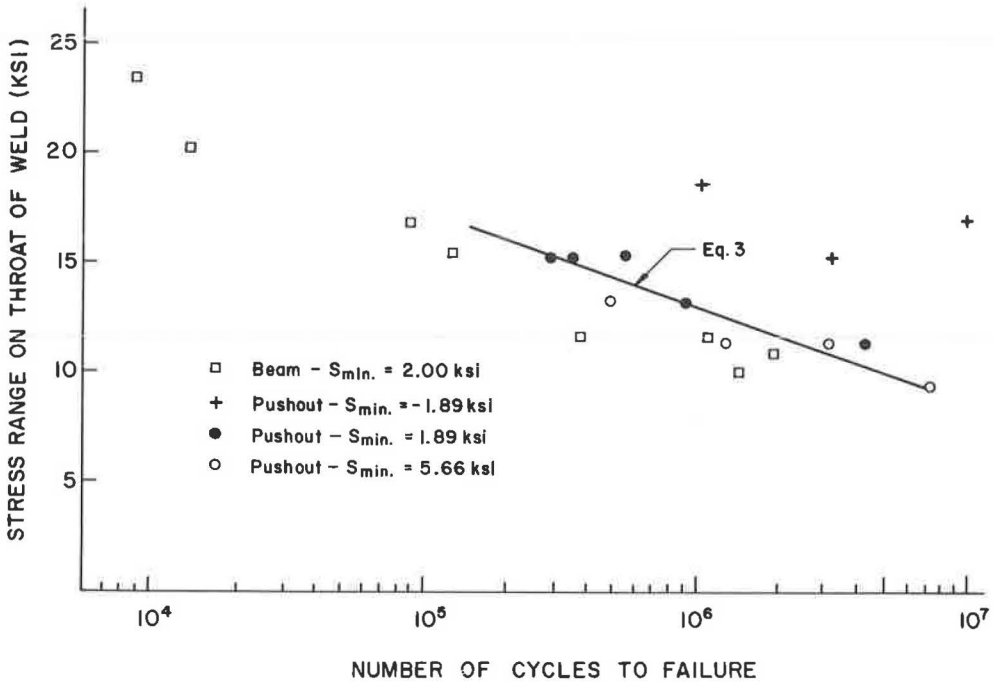

Figure 14. Comparison of Illinois beam test and push-out data for channels.

standard channel sections the thickness of the channel web is always equal to or greater than the thickness at the toe of the channel flange which is uniform at $^3/_{16}$ in. Since the thickness at the toe governs the weld size, it is to be expected that similar behavior should occur in other channels assuming that the same size $^3/_{16}$-in. fillet weld is placed at the heel and toe of the channel.

Equation 3 and the test data for the channel shear connectors are compared with small scale beam tests (6) in Figure 14. The average shear stress range on the throat of the fillet weld is plotted as a function of the logarithm of cycle life. Only those test beams which had shear connectors similar in geometry to the channels in this experiment were considered. Since the size of welds would normally be governed by the flange toe thickness, beams reported (6) with connectors which had the web area reduced so that the size of weld was greater than the web thickness were not considered applicable. In these latter tests the failure plane always occurred in the channel web.

For standard channel sections one should not attempt to place larger welds to provide an increase in the fatigue strength. The beam tests with channel connectors (6) showed that if larger welds were used premature failure would occur in the channel web. Obviously an increase in the fatigue strength of channel connectors could only be achieved if larger welds were used with channels having thicker webs.

Also, it should be noted that the concrete strength varied from about 2500 to 6000 psi in the beam tests. It is apparent that the concrete strength did not significantly influence the fatigue strength of the channel shear connectors which had geometric characteristics similar to the channel used in this experiment. Only when the web area was reduced, or the channel geometry substantially altered from the standard channel geometry, did the strength of concrete influence the cycle life.

It is readily apparent that channel shear connectors can be proportioned from the expected range of shear stress on the throat of the connecting fillet welds, since actual failure was due to fracture of the weld. For convenience, the range of shear in kips per inch of channel width was selected because all standard channels could be expected to behave in a similar manner if $^3/_{16}$-in. fillet welds were placed at the heel and toe.

On this basis, a tentative design formula for the allowable range of load for various cycle lives was developed from Eq. 3 using the lower limit of dispersion. The lower limit of dispersion was used because of the limited amount of test data and the absence of information on full-size beams:

$$Z_r = \beta w \tag{5}$$

where

Z_r = allowable range of shear force in kips per inch;
w = length of a channel shear connector in inches measured in a transverse direction on the flange of a beam; and
β = 4,000 for 100,000 cycles
3,200 for 500,000 cycles
2,600 for 2,000,000 cycles.

DESIGN CRITERIA FOR SHEAR CONNECTORS

It is apparent from the results reported here on the fatigue strength of shear connectors and from recent studies concerned with the ultimate load-carrying capacity of composite members (1) that a different design criterion is needed for the mechanical shear connectors used in composite bridge members. A rational philosophy of design should recognize that adequate static and fatigue strength is required in a bridge structure. Sufficient connectors should be provided to insure the proper fatigue strength. In addition, it is necessary to provide sufficient connectors such that the static ultimate strength of the composite member can be achieved.

Fatigue Considerations

The magnitude of the shear force transmitted by individual connectors has been found to agree closely with values predicted by theory assuming complete interaction within the elastic range (2). Tests have indicated that the difference between the computed values based on complete interaction and the experimental measurements is small. Although these measurements have indicated that connectors in regions of constant shear may not transmit equal forces, the maximum stress on any one shear connector seldom exceeds the value predicted from elastic theory assuming complete interaction.

Since fatigue is critical under repeated applications of working load, it is reasonable to determine the variation in shear stress using elastic theory. In other words the design criterion for fatigue is necessarily based on elastic considerations.

If complete interaction is assumed, the horizontal shear to be transferred by connectors for a given loading can be calculated as

$$H = \frac{VQ}{I} \tag{6}$$

where

H = horizontal shear per inch of length;
V = shear in kips acting on the composite section;
Q = statical moment of the transformed compressive concrete area about the neutral axis of the composite section, in.^{2}; and
I = moment of inertia of the composite section, in.^{4}

In regions of negative moment in continuous beams, the value of Q is the statical moment of the reinforcing steel and the moment of inertia is that of the steel beam and the reinforcing steel. In negative moment regions with continuous reinforcement, flexural conformance and action under working loads produces tensile stresses which are sufficiently large to cause cracking of the slab. Also, with passage of time, shrinkage will occur and hairline cracks will form. The composite bridges at the AASHO Road Test showed that even with large numbers of shear connectors, transverse shrinkage

cracks formed in the slabs of simple beams which allowed passage of water through the slab (9). Hence, it appears reasonable to only consider the cracked section of the concrete slab. It should also be noted that under initial loading when the slab may remain uncracked, in all probability high friction forces can be developed due to bond between the steel beam and the concrete slab. Hence, the connectors would not be required to transmit the greater range of shear alone. After cracking, this frictional force is reduced with continued application of loads as the bond is destroyed.

Placing the shear connectors in the negative moment regions should also assist in maintaining flexural conformance throughout the continuous beam. This also prevents the sudden transition from a composite to a non-composite section when they are omitted. Their placement should minimize the large differentials in deformation that might otherwise occur (as in a coverplated beam) and reduces the danger of fatigue failure in connectors adjacent to the negative moment region.

In simple span beams the range of shear stress throughout the span is dependent on the length of span and the type of loading. For spans up to about 70 ft the range of shear varies from a maximum at the end of the span to about 85 percent of the maximum near midspan. For longer spans this variation is not nearly as great, so that the range of shear is nearly constant throughout the span. This is illustrated by the shear envelopes

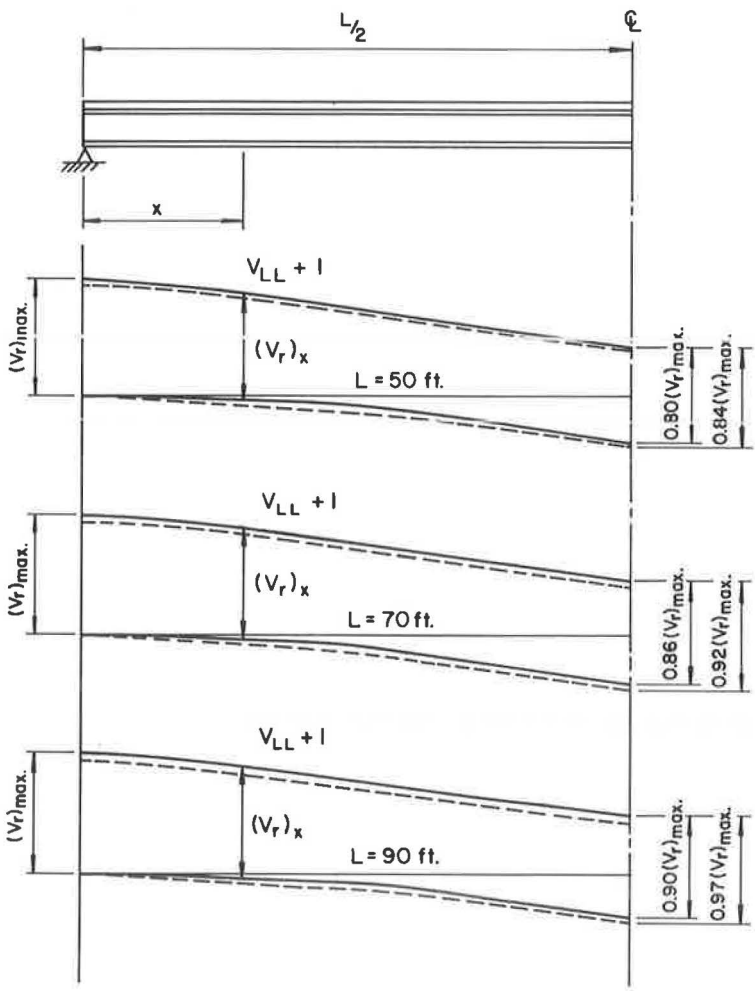

Figure 15. Typical shear envelopes for simple beams.

plotted in Figure 15. At the supports, the horizontal shear computed from Eq. 6 varies from zero to a maximum value as the live load moves onto the span. As is readily apparent from Figure 15, the range of horizontal shear stress will vary from zero to maximum at the supports to near full reversal at midspan. The dashed curves in Figure 15 indicate the maximum shear envelopes for loads moving in the opposite direction. At any section along the span the range of shear is the difference between the maximum and minimum shear envelopes and is indicated in Figure 15 as $(V_r)_x$.

The situation represented by the two outer shear envelopes in Figure 15 (the upper solid curves and the bottom dashed curves) is that of truck loads passing in both directions in the same lane. Although this is not a realistic condition, it is given here for purposes of discussion. The actual envelopes which apply to range of stress on connectors with traffic in one direction are the 2 solid or the 2 dashed curves, depending on the direction which the traffic is moving. The 2 outer shear envelopes could be used to establish a conservative approximation for the stress range throughout the span. For a 50-ft span the resulting range of shear at midspan is approximately 84 percent of the range of shear at the support and for a 90-ft span it is approximately 97 percent of the range of shear at the support. The difference in the resulting range of shear and the actual range of shear is usually less than 5 percent at midspan. This procedure is convenient to use since the actual range of shear is difficult to establish.

For design, an average of the range of shears at the support and at midspan could be used to ascertain the required number of shear connectors where the range of shear is the difference in the minimum and maximum shear envelopes for passage of the vehicle.

An alternate, more conservative, yet simpler procedure would result by considering only the maximum shear at the support. In longer span bridges, the range of shear is more nearly uniform than in the shorter spans so that such an approach would be more conservative for the short span structures. Using the shear at the support as the range of shear throughout the span results in a uniform spacing of the shear connectors. In many structures, the range of shear is nearly uniform and even if the actual shear range were used a nearly uniform spacing would result.

For continuous spans, the variation in the minimum-maximum shear envelopes along the lengths of the spans is usually somewhat greater than in simple spans. Figure 16 shows the moment and shear envelopes for a typical continuous bridge structure. If the variation in the shear stress range is significant, a variable spacing of the connectors is necessary. The range of stress on the connectors in the positive moment regions can be determined in the same manner suggested for simple span structures. The appropriate shear range and the usual composite beam properties of the cross section would be used.

In negative moment regions, the range of horizontal shear acting on the connectors is caused by the force in the reinforcing steel. This shear range can be evaluated from the shear envelopes $(V_r)_x$ and the cross-sectional properties of the beam in that region. As was noted, the value of Q will be the statical moment of the area of reinforcing steel, and the moment of inertia will be that of the steel beam and the reinforcing steel.

For unusual continuous span combinations, positive moments at an interior support may control and more shear connectors may be required to resist the resulting shear. In such instances, the range of shear would vary from zero to a maximum shear associated with the maximum positive moment. This condition only controls with 3- or 4-span continuous beams with odd span ratios such as 10:6:6 or 10:7:7:10.

Since the fatigue investigation reported here has indicated that stress range is the major variable influencing the fatigue strength of the shear connector, sufficient connectors can be provided for any desired cycle life.

The primary design consideration should be based on the fatigue criterion. The range of horizontal shear stresses is computed from Eq. 6. The spacing of the shear connectors is given by

$$P = \frac{\Sigma Z_r}{H_r} \tag{7}$$

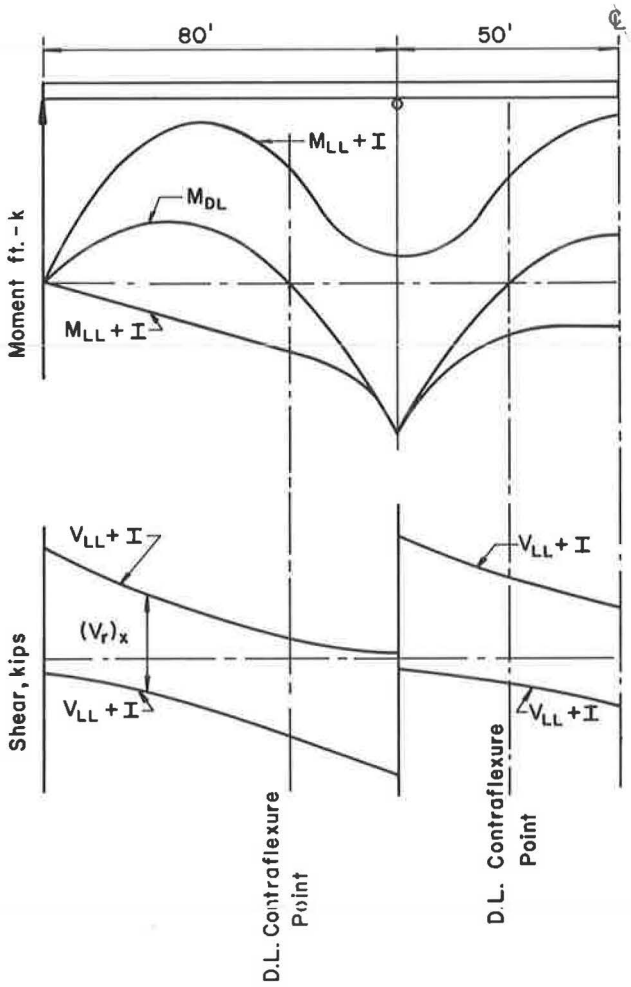

Figure 16. Typical shear and moment envelopes for continuous beams—from Viest et al. (10, p. 95).

where

H_r = the range of horizontal shear per inch of beam length at the junction of the slab and girder. [Note: The quantity H_r is determined from Eq. 6. As is noted in Figures 15 and 16, the range of shear due to live load and impact at any location is $(V_r)_x$.]

Z_r = allowable range of horizontal shear for the connector evaluated from Eqs. 4 or 5 (ΣZ_r is the resistance of all connectors at one transverse cross section of the girder).

P = spacing of shear connectors.

Equation 7 will determine the spacing in most designs. The spacing of connectors should never exceed 24 in. because connectors also perform the necessary function of holding the concrete slab in contact with the steel beam.

Flexural Strength Requirements

In addition to providing adequate fatigue strength, sufficient connectors should be provided to insure that the flexural strength of the composite member can be reached. Usually this requirement will be satisfied in most composite beams because fatigue considerations are usually critical except in cases of shored construction.

Recent research has shown that the flexural strength of composite beams can be achieved if sufficient connectors are provided to resist the maximum horizontal force in the slab (1). This study also confirmed that connector spacing was not critical and that connectors could be spaced uniformly without deleterious effects on the ultimate strength.

At the ultimate moment of a composite beam, 2 stress distributions are possible, as shown in Figure 17. Other studies (1) have demonstrated that the horizontal force required for the determination of the number of shear connectors is the compressive force in the concrete slab when the fully plastic stress distribution for the ultimate flexural strength is reached. For the two cases possible (Fig. 17), the maximum horizontal force is given by

$$H_1 = A_S F_y \tag{8}$$

$$H_2 = 0.85 f'_c bc \tag{9}$$

where

A_S = total area of the steel section including coverplates;
F_y = minimum yield point of the type of steel being used;
f'_c = compressive strength of concrete at 28 days;
b = effective width of the concrete slab; and
c = thickness of the concrete slab.

For any composite section the ultimate flexural strength will be governed by either Eq. 8 or Eq. 9. When the slab is large compared with the beam section, the yield strength of the steel section governs (Eq. 8). When the beam section is large compared with the slab, the ultimate compressive strength of the slab governs (Eq. 9). Obviously for any given composite beam the maximum possible compressive force in the concrete slab would necessarily have to be the smaller of the 2 values computed from Eqs. 8 and 9. Hence, between a point of maximum positive moment and the end of a beam or point of dead load contraflexure, sufficient connectors should be provided to resist the smaller value given by Eqs. 8 and 9.

For continuous beams an additional force in the slab between a point of dead load contraflexure and an adjacent interior support must be resisted, as indicated in Figure 18.

As the plastic moments of the continuous beam are approached and hinges develop, extensive cracks form over the supports of continuous composite beams. Therefore, in continuous beams the portion of the beam between a point of contraflexure and a point of maximum negative moment must be provided with sufficient shear connectors to resist the horizontal force, H_3, equal to the yield strength of the longitudinal reinforcement of the slab:

$$H_3 = A_S^r F_y^r \tag{10}$$

where

A_S^r = total area of reinforcing steel in the slab at the interior support, and

F_y^r = minimum yield point of reinforcing steel.

It has been shown (1) that the ultimate strength of shear connectors is given by the expressions

$$\text{Stud connectors} \quad q_u = 930 d_s^2 \sqrt{f'_c} \tag{11}$$

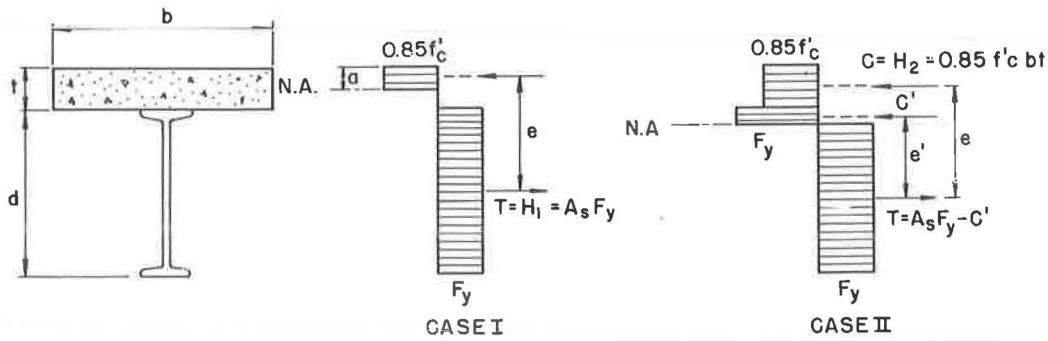

Figure 17. Stress distribution at ultimate load.

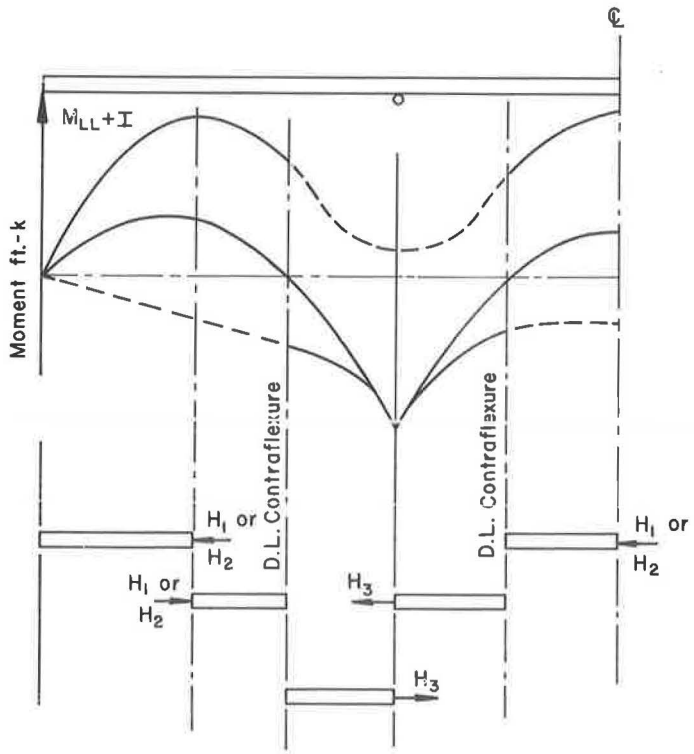

Figure 18. Forces acting on the slab of continuous beams.

$$\text{Channel connectors} \qquad q = 550\,(h + 0.5t)\,w\sqrt{f'_c} \tag{12}$$

To insure the development of the ultimate flexural strength of composite beams, a larger margin of safety against connector failure should be provided than is provided for the beam. Historically, the factor of safety for connections and fasteners has been larger than for the connected members. This assures that the connections do not fail before the main members. This margin can be accomplished by providing a load reduction factor (ϕ) to the ultimate shear strength of the shear connector. A ϕ value of

0.85 appears to be reasonable. Since the ultimate flexural capacity of composite bridge beams is usually 2.5 or more times the working load moment, the corresponding margin for the shear connection would be approximately 3 or greater.

Tests reported earlier (1) demonstrated that only a slight deformation in the concrete near the more heavily stressed connectors is needed to redistribute the horizontal shear to other less heavily stressed connectors. A few tests were reported by Culver and Coston (8) in which the loading positions for 2-point loading were changed in successive tests by moving the loads toward the supports. These tests have indicated that the maximum load can most likely move into the position of maximum moment without premature failure in a more heavily stressed connector because of these redistribution characteristics.

It should be noted that seldom will the maximum load criterion be the governing factor. The number of connectors required by the fatigue criterion will usually exceed the requirements for ultimate flexural strength.

In instances where the maximum load criterion represents the more critical condition, the use of the flexural strength requirements insures that sufficient connectors are present so that excessive local permanent deformation of the concrete in the vicinity of stud connectors is minimized. If this provision was not used local deterioration of the concrete could result which would adversely influence the fatigue strength of stud connectors. Channel shear connectors have sufficient bearing area so that it is doubtful that excessive local permanent deformation would occur.

In simple beams the stress range values for stud and channel connectors will govern the design and it would not ordinarily be necessary to calculate both values since the fatigue criterion is the more critical condition. This is also true in continuous beams for unshored construction.

The minimum number of shear connectors required between the points of maximum positive moment and the end supports or dead load points of contraflexure, and between points of maximum negative moment and the dead load points of contraflexure is given by

$$N_i = \frac{H_i}{\phi q_u} \tag{13}$$

where

N_i = the minimum number of shear connectors between points of maximum positive moment and adjacent end supports or dead load points of contraflexure or between points of maximum negative moment and adjacent dead load points of contraflexure.

ϕ = a reduction factor = 0.85.

q_u = ultimate shear connector loads given by Eqs. 11 or 12.

H_i = smaller value of H_1 and H_2 (Eqs. 8 or 9) for: simple beams; continuous beams between points of maximum positive moment and the end supports; and continuous beams between points of maximum positive moment and points of dead load contraflexure.

= H_3 (Eq. 10) for continuous beams between points of dead load contraflexure and interior supports.

If the number of shear connectors given by Eq. 13 exceeds the number provided by the spacing given by Eq. 7, additional connectors should be added to insure that the ultimate strength is achieved.

SUMMARY AND CONCLUSIONS

1. Tests of 35 push-out specimens having the concrete slab connected to the steel beam section with $^3/_4$-in. stud shear connectors, 9 tests with $^7/_8$-in. stud connectors, and 12 tests with 4-in., 5.4-lb channel connectors were made to determine the fatigue behavior of the connectors.

2. A mathematical model expressing the logarithm of the fatigue life as a linear function of stress range was found to fit the test data. An analysis of variance indicated that minimum stress was a significant variable only for stress reversal. If the reversal portion was neglected the stress range was by far the most important independent variable.

3. Concrete strength did not significantly influence the fatigue strength of either the stud or the channel shear connector.

4. The push-out specimen developed for this study provided test results which overlap the earlier beam tests. The lower limit of dispersion for the beam tests overlaps the upper limit of dispersion for the push-out test. Hence, the lower limit of dispersion of the beam tests is about equal to the mean behavior of the push-out specimens. Push-out tests therefore represent a lower bound for connector failure.

5. A design criterion for shear connectors is proposed which recognizes both the static and fatigue behavior of the shear connectors for composite steel and concrete members.

6. A design procedure is developed which provides a simpler and more economical design for the shear connectors of composite beams.

ACKNOWLEDGMENTS

The work described in this report is part of an investigation on the design of shear connectors for highway bridges being conducted at the Fritz Engineering Laboratory, Department of Civil Engineering, Lehigh University. Prof. William J. Eney is head of the Department and Prof. Lynn S. Beedle is director of the laboratory. The project is sponsored by the American Iron and Steel Institute.

The authors are indebted to E. L. Erickson, E. W. Gradt, K. H. Jensen, B. F. Kotalik, R. J. Posthauer, A. A. Toprac, members, and I. M. Viest, Chairman, of the Project's Advisory Committee for their advice and guidance. Thanks are also extended to Mrs. Carol Kostenbader who typed the manuscript and to R. N. Sopko and his staff for the photography and preparation of the drawings.

REFERENCES

1. Slutter, R. G., and Driscoll, G. C., Jr. Flexural Strength of Steel and Concrete Composite Beams. Jour. Struct. Div., ASCE, Vol. 91, No. ST2, April 1965.
2. King, D. C., Slutter, R. G., and Driscoll, G. C., Jr. Fatigue Strength of ½-Inch Diameter Stud Shear Connectors, Highway Research Record 103, pp. 78-106, 1965.
3. Toprac, A. A. Fatigue Strength of ¾-Inch Stud Shear Connectors. Highway Research Record 103, pp. 53-77, 1965.
4. AASHO. Standard Specifications for Highway Bridges. AASHO, Washington, 1961.
5. Viest, I. M., Fountain, R. S., and Siess, C. P. Development of the New AASHO Specification for Composite Steel and Concrete Bridges. HRB Bull. 174, pp. 1-17, 1958.
6. Siess, C. P., Viest, I. M., and Newmark, N. M. Studies of Slab and Beam Highway Bridges, Part III: Small Scale Tests of Shear Connectors and Composite T-Beams. Univ. of Illinois Eng. Exp. Sta. Bull. 396, 1952.
7. Thurlimann, B. Fatigue and Static Strength of Stud Shear Connectors. Jour. ACI, Vol. 30, No. 12, June 1959.
8. Culver, C., and Coston, R. Tests of Composite Beams With Stud Shear Connectors. Jour. Struct. Div., ASCE, Vol. 87, No. ST2, Feb. 1961.
9. Highway Research Board. The AASHO Road Test, Report 4: Bridge Research. HRB Spec. Rept. 61D, 1962.
10. Viest, I. M., Fountain, R. S., and Singleton, R. C. Composite Construction in Steel and Concrete. McGraw-Hill Book Co., New York, 1958.

A Study of Splices in Tensile Reinforcing Bars

E. P. SEGNER, JR., Professor of Civil Engineering, University of Alabama

•THE NEED for reliable, practical and economical methods of splicing tensile reinforcing bars has long been known. In the field of precast concrete, such a connection or splice would lead to continuity for precast members resulting in increased strength, rigidity, and economy. In many long-span, flexural and eccentrically loaded compression members, it is frequently necessary to splice tensile reinforcing bars.

In the past this problem has been taken care of by lapping or butt-welding individual bars. Both of these approaches can adequately transfer the axial stress, but each has inherent undesirable characteristics. Lap splices usually initiate diagonal tensile cracks or failure at the point of cutoff of the stressed bars unless extra stirrups or ties are supplied in this region. Butt-welding of the ends of reinforcing bars is generally considered too expensive to be practical. Because of these undesirable features, other means of tensile splicing would gain wide acceptance if proper design criteria could be developed through research.

In response to this design need, several mechanical connectors have appeared on the market. However, due to the absence of proper research and testing, only limited acceptance has been gained. This is evidenced by the fact that most codes do not recognize such splices. In Sec. 1.7.5(c) of the 1961 AASHO specifications, the following statement appears:

> Tensile reinforcement shall not be spliced at points of maximum stress. When the reinforcement is spliced, the spliced bars shall lap sufficiently to develop the full strength in bond.

A further statement appears in Sec. 2.5.6:

> Splicing of bars, except where shown on the plans, will not be permitted without the written approval of the engineer. Splices shall be staggered as far as possible. Unless otherwise shown on the plans, bars in the bottom of beams and girders, and in walls, columns and haunches shall be lapped 20 diameters and bars near the top of beams and girders having more than 12 inches of concrete under the bars shall be lapped 35 diameters, to make the splice.

The 1963 code of the American Concrete Institute does not recommend the splicing of tensile bars at points of maximum stress, but such a splice when used is required to develop the full computed stress in the bar based on not more than ¾ of the permissible bond value. In addition, a minimum lap is specified for each of several grades of steel bars. To meet the 1963 ACI code, a welded butt splice or other approved positive connection must develop in tension at least 125 percent of the specified yield strength of the bar.

If mechanical splices are to have general acceptance, data must be obtained on the relative merits of mechanical splices compared with lap or butt-welded splices. The collection of these data and the critical evaluation of some of these types of connections were the objectives of the research reported in this paper.

Present Status of Research

In 1959 Eriksson (5) studied the sleeve splice. His testing program of 200 samples included only static tests, but treated extensively the variables of sleeve configuration,

Paper sponsored by Committee on Concrete Superstructures and presented at the 45th Annual Meeting.

curing time, and grout strength, type, and thickness. Both tension and compression tests were performed. These tests showed the splices to have excellent reliability under compression loading and to react in a satisfactory manner to tension loadings. Eriksson's tests indicated that the splice was quite insensitive to the variables of mortar thickness, grout type and strength, and curing durations above 7 days, but highly sensitive to the splice sleeve length in the range of 2 to 10 bar diameters. Eriksson also recommended the use of nonshrinking mortar grout.

Other references dealt with lapped splices and with bond stresses. Although lapped splices have long been an accepted construction practice, the literature in this area was rather limited. The problems of bar spacing, type of bar deformations and lap length were investigated by Chamberlin (2), Walker (9), and Chinn et al (3). Kluge and Tuma (7) conducted tests on lapped splices of bar sizes up to No. 8.

There is extensive literature on the subject of bond stresses and tension pull-out specimens. One of the earliest reports is by Abrams (1), who developed many ideas on the nature of bond resistance and conducted extensive tests on pull-out and beam specimens. He illustrated the progressive nature of bond stress development and described the effect of bar deformations on maximum bond stresses.

Following the paper by Abrams, a number of investigators conducted tests on the bond resistance of various types and sizes of reinforcing bars. Among the most significant reports are those by Watstein (10), Clark (4), Mylrea (8), and Ferguson et al (6).

Scope of This Investigation

The results reported in this paper are divided into 2 main groups—40-ksi nominal yield strength deformed bars (ASTM A 15 and ASTM A 408) and 60-ksi (ASTM A 432) nominal yield strength deformed bars. All bars used were from the same mill and thus had the same deformation pattern. A series of control bars (continuous bars) and a series of each type connection were tested using Nos. 9, 10, 11 and 14S bars in each group. The control bars were from the same heat number as the spliced bars of the same size and yield strength. Thus any variation in performance between the control bar and each type of the connection could reasonably be attributed to the connection alone. Two control samples of each particular size and yield strength were tested. The results of these 2 tests were also compared with the mill test reports supplied by the fabricator.

Two samples of each bar size and steel grade of the butt-welded bars were tested. These results also were compared with the other splicing devices. After some study it was decided to limit the new type connections to 3 basic types and to designate them as exothermic No. 1, exothermic No. 2, and sleeve-with-metal-filler. Three identical samples of each bar size and steel grade were included.

As a secondary study sleeves filled with epoxy and sleeves filled with expanded cement grout were also included in the investigation. Since it was felt that these connections would have to compare favorably with the sleeve-with-metal-filler connection to have significant practical value, each utilized the same sleeve which corresponded to the sleeve-with-metal-filler connection of the same bar size and steel grade. All bars in this secondary study were deformed No. 9 bars of 40-ksi nominal yield strength (ASTM A 15). Five sleeve samples filled with the expanded cement grout and at least 3 samples of each of 3 epoxy formulations were tested.

FABRICATION AND TESTING OF TENSILE SPLICES

The fabrication of the connections required a device to hold the 2 bars in rigid alignment during the splicing operation and a jig was constructed to fill this need (Fig. 1a). This jig could be used to make either vertical or horizontal connections, depending on its position. The sleeve-with-metal-filler connections were made with the axis of the reinforcing bar in a vertical position with the jig set on its end; all other connections were made with the axis of the reinforcing bar horizontal. In the case of the sleeve-with-metal-filler splices, either horizontal or vertical can be made. Although the investigation did not verify it, the supplier of this splice indicated that the splicing position does not affect the structural properties of the splice.

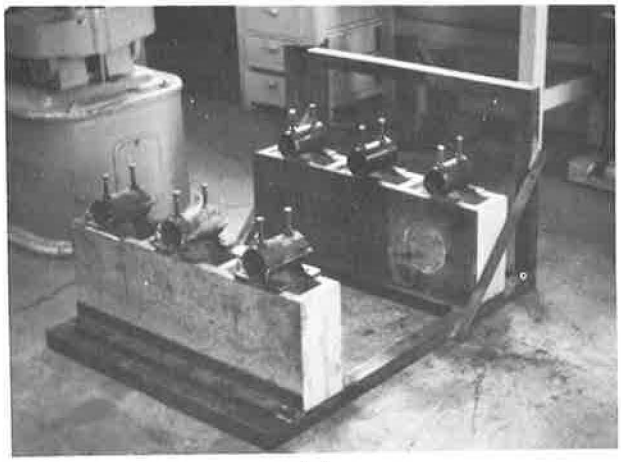

(a)

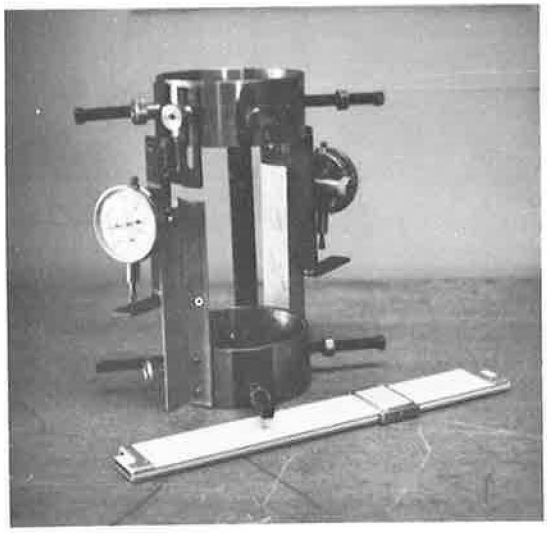

(b)

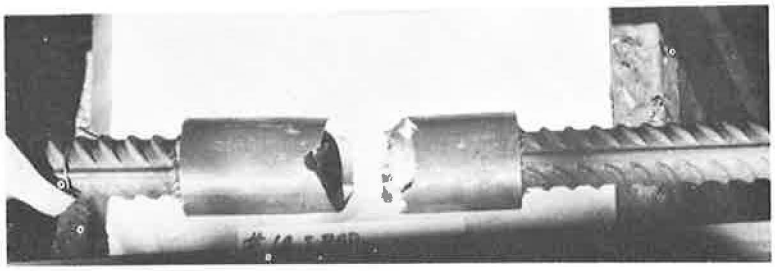

(c)

Figure 1. (a) Alignment jig. (b) Tensile extensometer. (c) Typical sleeve failure using sleeve-with-metal-filler type connection.

(d)

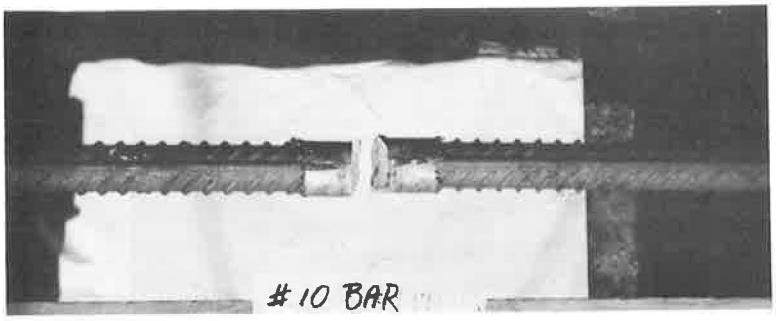

(e)

(f)

Figure 1. (d) Typical bar failure using sleeve-with-metal-filler type connection. (e) Typical exothermic No. 2 failure. (f) Typical exothermic splicing operation.

(g)

(h)

(i)

Figure 1. (g) Exothermic No. 1 connections being formed. (h) Surplus slag metal on exothermic No. 1 connection after its removal. (i) Typical cross section of exothermic No. 1 connection after failure.

TABLE I

TYPES AND NUMBER OF SAMPLES TESTED

NOMINAL YIELD STRENGTH (psi)	40,000				60,000				TOTAL
ASTM DESIGNATION	A-15	A-15	A-15	A-408	A-432	A-432	A-432	A-432	SAMPLES
BAR SIZE	#9	#10	#11	#14S	#9	#10	#11	#14S	TESTED
CONTROL BARS	2	2	2	2	2	2	2	2	16
BUTT WELDED	2	2	2	2	2	2	2	2	16
SLEEVE WITH METAL FILLER	3	3	3	3	3	3	3	3	24
EXOTHERMIC #1	3	3	3	3	3	3	3	3	24
EXOTHERMIC #2	3	3	3	3	3	3	3	3	24
EPOXY #1	5								5
EPOXY #2	5								5
EPOXY #3	3								3
EXPANDED GROUT	5								5
TOTAL NUMBER OF SAMPLES TESTED									122

The jig used for fabrication was relatively light and portable, which was convenient because the exothermic-type connections had to be made outdoors. These connections spewed bits of molten metal and produced a great deal of smoke from the mold during the reaction. In contrast, the sleeve-with-metal-filler connection generated a relatively small amount of heat and negligible smoke, and the fire hazard from the spewing bits of reactant material was minimal.

Two control bars were tested for each size and grade of steel used in this investigation (Table 1). The control bars consisted of 24-in. lengths cut from stock of the same heat used to make the other connections and were tested exactly the same way.

Connections

Butt Weld. —Two butt-welded connections were prepared and tested for each bar size and steel grade. In ordering the samples in this series of connections, each welded joint was specified to have sufficient strength so as to develop the full tensile strength of the bar, per American Welding Society specification D12.1, "Recommended Practices for Welding Reinforcing Steel, Metal Inserts, and Connections in Reinforced Concrete Construction." During the testing program, a value of 125 percent of the nominal yield strength of the bar was also considered, per 1963 ACI code Sec. 805(d).

Exothermic No. 1. —The exothermic No. 1 consisted essentially of a sand mold filled with reactant powder which, when ignited, reacted rather violently and changed to a molten state which flowed by gravity around and between the ends of the bars. A sealing paste was applied to the contact faces of the mold halves to prevent leakage. The bars were aligned with a $\frac{3}{8}$-in. gap between their ends by a spacer and the mold positioned so that the metal flow channel was directly over this gap. The ends of the mold around the reinforcing rod were luted with sealing sand and two metal discs were placed in the space provided at the bottom of the mold. The reactant powder was then poured into the mold and ignited. The reaction reached an extremely high temperature (4600 F) which melted the metal discs, thus allowing the molten metal to flow between and around the bars so as to weld them together. After a few minutes the remains of the mold, which is itself destroyed, can be removed, but a longer waiting period is recommended to permit the refractory portion of the mold to stress-relieve the weld area. Removal of flash and excess metal is not required but may be accomplished if space limitations demand it.

Exothermic No. 2. —The exothermic No. 2 connection very closely resembles the exothermic No. 1 connection. Both used luted sand molds with a reactant powder; both required a $\frac{3}{8}$-in. gap between bars, and both literally welded the bars together. There were some minor differences, however, in the physical procedure in making the two connections. The exothermic No. 2 used no sealing paste on the contact surfaces of

each half mold. A tight seal was obtained by clamping the half molds together with 2-in. C-clamps. Also, the molds fit rather loosely around the bars and small wooden wedges were placed at each end of the mold between the bar and the mold. This tended to stabilize the mold in the correct position and prevent rotation. After ignition of the reactant powder, the actual weld is formed in the same manner as the exothermic No. 1.

Sleeve-With-Metal-Filler. —This method of connecting reinforcing bars together consists of inserting the ends of both bars into a common sleeve and filling the sleeve with a metal filler material which mechanically locks the bars together. The ends of the bars must be clean, dry and free of rust, grease, dirt, etc. However, tightly adhering mill scale need not be removed. For vertical connections, as were used in this study, the bottom alignment fitting is positioned on the lower bar so that the gap between the bars will be at the center of the sleeve. Asbestos wicking or packing is placed around the bar at the top of the bottom alignment fitting (which supports the sleeve) and also at the top of the sleeve. The asbestos wicking at the top of the sleeve is positioned against the sleeve by the top alignment fitting. The pouring basin is then attached tightly around the small opening in the center of the sleeve. The crucible is then placed on top of the pouring basin. A small steel disc is placed in the bottom of the crucible over the tap hole and the filler cartridge of reactant powder is poured into the crucible. A small amount of starting powder is then placed on top of the reactant powder and ignited with a flint. Upon completion of the reaction in the basin the disc is melted, and the molten alloy metal flows into the sleeve through the small opening in the center of the sleeve. It cools, thus locking or keying the sleeve (through the internal grooves) to the reinforcing bars (through the bar deformations). It should be emphasized that this is a mechanical connection, not a weld. The sleeves used were proportioned in order to develop at least the ultimate tensile strength of each bar size and steel grade. Table 2 summarizes the geometric and physical properties of the splice sleeve.

TABLE 2

PROPERTIES OF SLEEVES USED

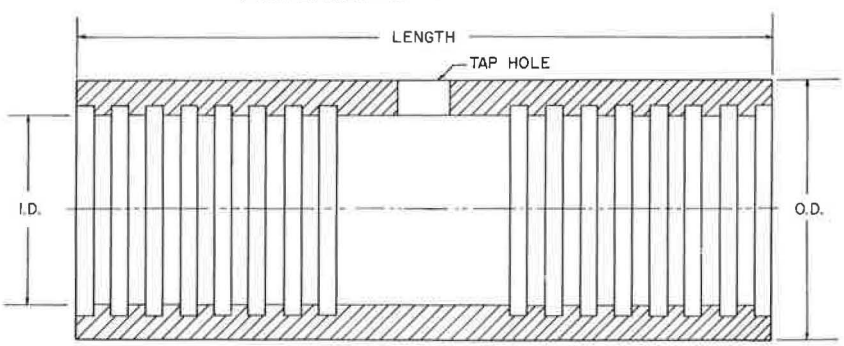

SLEEVE CROSS-SECTION

SPLICE SLEEVE						TENSILE STRENGTH OF SPLICE BASED ON AREA OF REBAR
BAR SIZE	NOMINAL YIELD STRENGTH OF REBAR (k.s.i.)	LENGTH (in)	O.D. (in)	I.D. (in)	AREA OF SLEEVE AT TAP HOLE (in^2)	$\frac{\text{AREA SLEEVE}}{\text{AREA REBAR}}$ x 80,000 p.s.i.
14S	60	7	2-3/4	2	2.564	91,200
	40	7	2-5/8	2	2.075	73,800
11	60	6	2-3/8	1-3/4	1.869	95,800
	40	6	2-1/4	1-3/4	1.446	74,200
10	60	5	2-1/4	1-5/8	1.746	110,000
	40	5	2-1/8	1-5/8	1.348	84,900
9	40 or 60	5	2	1-1/2	1.250	100,000

Sleeves With Epoxy No. 1, No. 2 and No. 3. —All epoxy connections used identical No. 9 bar sleeves as supplied by the manufacturer for the sleeve-with-metal-filler connections for bars meeting ASTM A 15 specifications. The epoxy served as the locking material in the sleeve and connected the bars together much as the sleeve-with-metal-filler connection. Although none of the epoxies were formulated for this particular purpose, it was desired to investigate their possible value in this area. Because of the limited amount of epoxy No. 3 available, only 3 samples of this type were made, but 5 samples each were made using epoxy No. 1 and No. 2.

Epoxy No. 1 and epoxy No. 3 were commercial formulations, while epoxy No. 2 was formulation 991-67 (General Purpose Adhesive) as outlined in American Railway Engineering Association Bulletin No. 573. When mixed, each epoxy had the consistency of a lightweight grease.

The epoxies presented some special handling problems as the pot life averaged only approximately 15 minutes and no special equipment was available to force it into the sleeves. In order to reduce the possibility of voids, each sleeve was filled with epoxy and then one bar was inserted, which forced out some excess epoxy. Then the second bar was inserted which forced out an additional excess quantity of epoxy. It was felt that a satisfactory procedure for filling the sleeves could be developed if the preliminary results of this limited test program should warrant it. The connections were tested one week from the date of fabrication after being cured at room temperature and humidity, and the stress-strain diagrams plotted when sufficient data resulted.

Sleeve With Expanded Cement Grout. —The sleeve-filled-with-grout connections also used the No. 9 bar sleeves supplied by the sleeve-with-metal-filler manufacturer. The bars were of ASTM A 15 material. The grout consisted of one part commercial expanding cement additive and one part of Type I portland cement. Enough water was added to render the mixture suitable for use in the sleeves. The method of fabrication was similar to the epoxy connections, i.e., one bar at a time was inserted into the grout-filled sleeve. Five samples were made. They were tested at 28 days after curing at room temperature in a moist chamber for 7 days followed by 21 days in air.

Testing Procedure

All tests conducted during this investigation were static tensile tests using a standard 8-in. gage length with the connection approximately centered within this length. All bar cross-sectional area calculations were based on the measured diameter of the bar at the base of the deformations. The special type of extensometer which was designed and constructed consisted of 2 rings, 8 in. apart (c/c of bolts), each fastened rigidly to the test specimen by 4 radial bolts (Fig. 1b). Two 0.0001-in. Ames dial gages were attached between the 2 rings and diametrically opposite each other, so that the average total strain recorded would be that of the centerline of the test specimen.

The loading rate was approximately 2000 lb per min for all tests. Because of their dependability against sudden failure, the sleeve-with-metal-filler connections were tested to the nominal yield strength before the gages were removed. After damaging several Ames dials due to premature failures of the exothermic-type connection, all subsequent test specimens were preloaded to approximately two-thirds of their nominal yield strength before the gages were set in place. When the connection had sufficient plastic strength to elongate the bar an appreciable amount after removal of the Ames dial gages large dividers and a 0.01-in. scale were used to obtain strain measurements until failure. All tests were conducted on a 200,000-lb Baldwin Universal testing machine which was calibrated before the investigation began.

Photographs of the test equipment and typical test samples are shown in Figure 1.

DISCUSSION OF TEST RESULTS

Control Bar

As expected, the control bars established the upper stress limits. A summary of all test results is shown in Figure 2. Also note the stress-strain curves for each sample shown in the Appendix, Figures A-1 through A-58. Each sample is compared with a bar without a splice (labeled control bar or theoretical bar).

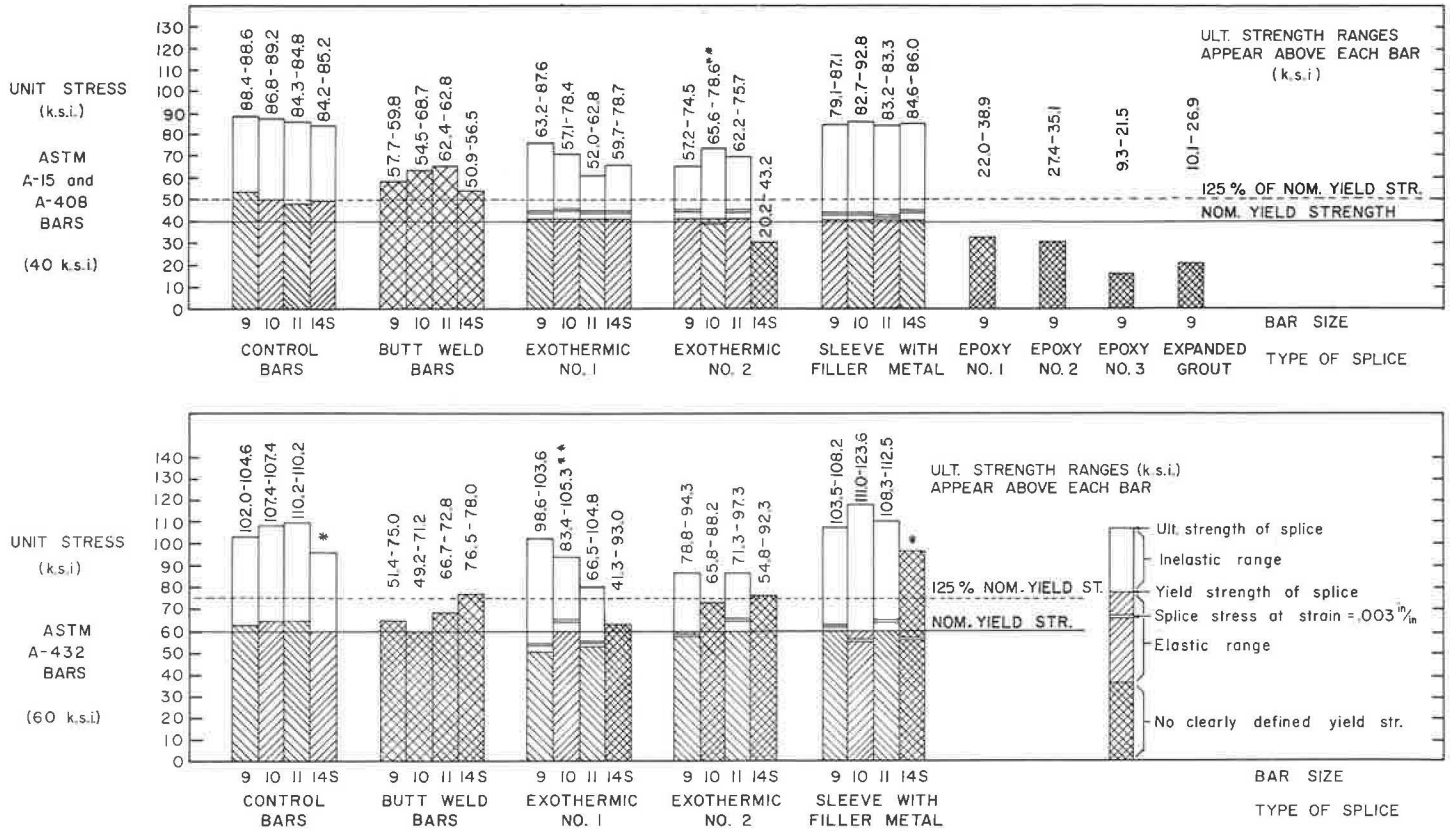

* 1. Bars did not break as they exceeded the 200 kip limit of the testing machine.
2. Each control bar column and each butt weld column is the average of two test samples.
3. Each exothermic column and each sleeve with filler metal column is the average of three test samples.
4. Each epoxy column (nos. 1 and 2) is the average of five test samples using the same sleeve as used with the metal filled sleeve.
5. Each epoxy column (no. 3) is the average of three test samples using the same sleeve as used with the metal filled sleeve.
6. For No. 9 bars butt welded, insufficient data was available to determine yield strength or unit stress corresponding to .003 in/in of strain.
7. Epoxy no. 3 samples all failed during the preload test of approximately one-half the yield strength.
8. Expanded grout column is the average of five test samples using the same sleeve as used with the metal filled sleeve.

** 9. One sample separated when the mold was removed.

Figure 2. Summary of splice test results.

Butt-Welded Splice

The average values of the maximum stress indicate that the butt-welded connections exceeded the 125 percent of nominal yield strength criteria for 40-ksi nominal yield steel but failed to do so for the 60-ksi yield steel. With the 40-ksi yield steel, data in Figure 2 indicate that the welds were satisfactory but tend to mask some rather erratic test results since an average of 2 samples is shown. The individual stress-strain curves in the Appendix must be taken into account for an accurate analysis. All samples failed in the weld area which, in nearly all cases, showed porosity and a lack of full penetration.

Exothermic No. 1 Splice

All exothermic No. 1 connections proved satisfactory with the exception of the No. 14S bars of 60-ksi nominal yield strength. An average of these 3 samples gives an ultimate strength of just over the nominal yield strength.

All but 2 samples failed in the connection itself. An examination of the cross section after failure revealed a large variation in appearance ranging from uniformly solid to a honeycombing effect with relatively large voids. Oddly enough, no correlation could be established between the presence or absence of the voids and the ultimate strength. The 2 samples that did not fail in the connection itself were the No. 9 bar connections—the bar failed in both cases. One bar was of 40-ksi nominal yield strength, the other was of 60-ksi nominal yield strength.

It should also be noted that one of the 24 exothermic No. 1 connections failed to join the bar together. When the mold was removed, the bars simply fell apart. The reason for this was not determined. The tips of both bar ends were covered with reactant metal which seemed to indicate that they were approximately in the correct position with respect to the metal flow channel.

Exothermic No. 2 Splice

In general, the exothermic No. 2 connections were not as satisfactory as the exothermic No. 1 connections. In the 40-ksi grade group, the No. 14S bars failed prematurely. The reason for this is difficult to determine. The break, which always occurred in the general weld area, appeared solid and free of voids but had a very even, fine-grained appearance somewhat different from the control bar breaks. Some failures were located slightly outside of the original gap between bars, indicating that the tip of one bar had separated. However, the average ultimate stresses of the other bars in this group were all above the 125 percent yield strength level.

Like the exothermic No. 1, one of the 24 exothermic No. 2 connections was a total failure and fell apart when the mold was removed. However, the reason seemed to be a leak in the mold which allowed considerable molten metal to be lost.

Sleeve-With-Metal-Filler Splice

For ultimate strength and reliability, this connection equaled the control bars. There were no premature failures. Of the 24 samples tested, only 2 failures occurred in the sleeves and then at very high stresses. In all other samples, the bars themselves failed and did so at a stress comparable to that of the control bars. Like the No. 14S control bars of the 60 ksi group, the comparable connections did not break but reached the 200,000-lb limit of the testing machine (corresponding to a unit tensile stress of approximately 89 ksi).

Strain may prove detrimental, as the 0.003 in. per in. strain level was reached before the nominal yield strength in 2 of the 4 sizes of bars tested in the 60-ksi group while all of the bars of 40-ksi material passed the nominal yield strength before reaching this strain level.

Sleeves Filled With Epoxy No. 1, No. 2, No. 3 and Expanded Cement Grout

This was actually a splinter project of this study. As epoxies are fairly new and apparently quite versatile, it was decided to examine the feasibility of using typical

epoxies as filler material for sleeve-type tensile connections. For the same reason, a sleeve filled with commercial expanded cement grout was tested. All tests failed at such disappointingly low loads that this area was not explored further. Each sample failed in shear at the interface between the inside sleeve surface and the surface of the reinforcing bar.

PRELIMINARY CONCLUSIONS

Butt-Welded Splices

Because of the wide variation in the test results in this study as well as the cost involved, this type of splice was not completely satisfactory. This is especially true in the case of the ASTM A 432 bars. Under ideal welding conditions, ASTM A 15 and A 408 butt-welded splices may be acceptable.

Sleeve-With-Metal-Filler Splices

Based on the results of this study, the sleeve-with-metal-filler connection will, for all practical purposes, equal the ultimate strength of both 40-ksi and 60-ksi nominal yield strength bars. Their consistently high quality was remarkable, and, if the recommended procedure is followed, it appears that this splice can be used with complete confidence. However, the allowable strain may be a limiting factor when the higher strength ASTM A 432 bars are used since the metal filler allows much more strain than did the control bars. Thus, some of the advantage of high strength bars may be lost if local concrete cracking around the connection results. With ASTM A 15 and A 408 bars the nominal yield strength of the steel was reached before the connection strained 0.003 in. per in. and excessive strain may not be objectionable.

A very definite advantage of this type connection is that its quality can be ascertained with accuracy by visual inspection; i.e., if the filler metal is visible at each end of the sleeve after removal of the asbestos packing, it can reasonably be assumed that the sleeve contains the proper amount of filler. In addition, the connection is relatively quick and easy to make since only approximately 5 minutes are required before the equipment can be removed for the next setup. As the sleeve and filler metal are the only items consumed, no troublesome cleanup is necessary. The fire hazard is minimal due to the relatively mild reaction in the crucible and the use of a splash guard.

Exothermic Splices

Based on the samples tested, these connections do not appear to possess the high reliability of the sleeve-with-metal-filler connection, but the exothermic connections did give reasonable average values of maximum stress. However, the averaging of samples tends to hide a wide variation between individual samples. For example, exothermic No. 1 splice of 40-ksi nominal yield strength steel failed at stresses ranging from approximately 52,000 to 88,000 psi and for 60 ksi nominal yield strength steel, from 41,000 to 105,000 psi. The exothermic No. 2 splice of 40-ksi nominal yield strength steel failed at stresses ranging from approximately 20,000 to 79,000 psi and for 60 ksi nominal yield strength steel, from 55,000 to 97,000 psi.

Both of the exothermic splices strained relatively little up to the point of failure, which from the standpoint of deflection and cracking is a real advantage.

A definite disadvantage of this type connection appears to be its immunity from accurate visual inspection. Very little can be determined about its load-carrying capabilities by observing it visually. All samples of this type looked identical, but they failed over a wide range of stresses.

More time is required to make the exothermic connections than the sleeve-with-metal-filler type. Both exothermic-type connections are very similar and both require approximately 10 minutes per connection, but the clean-up time, i.e., removing the molds, could extend this somewhat. In addition, the fire hazard in the immediate vicinity of the reaction could be a problem around wooden formwork.

Epoxy No. 1, No. 2, No. 3 and Expanded Grout Splices

On the basis of this limited study, these connections appear to be totally inadequate and should not be used for tensile splicing of reinforcing bars unless the length of the splicing sleeve is significantly increased compared with the sleeve used in the metal-filled sleeve splice.

ACKNOWLEDGMENTS

The project, which was the basis for this first of a series of papers, was sponsored jointly by the Oklahoma State Highway Department and the U. S. Bureau of Public Roads under a contract between the University of Oklahoma Research Institute and the Oklahoma State Highway Department. For this sponsorship, grateful acknowledgment is given.

The experimental phase of the project was conducted in the Structural Laboratory of the University of Oklahoma while the author was there as Professor of Civil Engineering.

Research assistants serving on the project were Richard L. Gilbert, Ronald D. Wickens, and Robert P. Williams, all students of civil engineering at the University of Oklahoma.

REFERENCES

1. Abrams, Duff A. Tests of Bond Between Concrete and Steel. University of Illinois Eng. Expt. Sta. Bull. No. 71, Dec. 1913.
2. Chamberlin, S. J. Spacing of Spliced Bars in Beams. Jour. ACI, Vol. 29, No. 8, Feb. 1958; Proc., Vol. 54, pp. 689-697.
3. Chinn, J., Ferguson, P. M., and Thompson, J. N. Lapped Splices in Reinforced Concrete Beams. Jour. ACI, Vol. 27, No. 2, Oct. 1955; Proc., Vol. 52, pp. 201-213.
4. Clark, Arthur P. Bond of Concrete Reinforcing Bars. Jour. ACI, Vol. 21, No. 3, pp. 161-183, Nov. 1949.
5. Eriksson, Owe. The Sleeve Method of Splicing Reinforcing Bars. Ingenioren, International Edition, Vol. 4, Dec. 1960.
6. Ferguson, P. M., Turpin, R. D., and Thompson, J. N. Minimum Bar Spacing as a Function of Bond and Shear Strength. Jour. ACI, Vol. 25, No. 10, pp. 869-887, June 1954.
7. Kluge, R. W., and Tuma, E. C. Lapped Bar Splices in Concrete Beams. Jour. ACI, Vol. 17, No. 1, pp. 13-36, Sept. 1945.
8. Mylrea, T. D. Bond and Anchorage. Jour. ACI, Vol. 19, No. 7, March 1948; Proc., Vol. 44, pp. 521-527.
9. Walker, William T. Laboratory Tests of Spaced and Tied Reinforcing Bars. Jour. ACI, Vol. 22, No. 5, Jan. 1951; Proc., Vol. 47, pp. 365-375.
10. Watstein, David. Bond Stress in Concrete Pull-Out Specimens. Jour. ACI, Vol. 13, No. 1, pp. 37-50, Sept. 1941.

Appendix

STRESS-STRAIN CURVES

The individual stress-strain curves for each sample, shown in Figures A-1 through A-58, should be taken into account for an accurate analysis, since the average values used in the text might tend to mask erratic results.

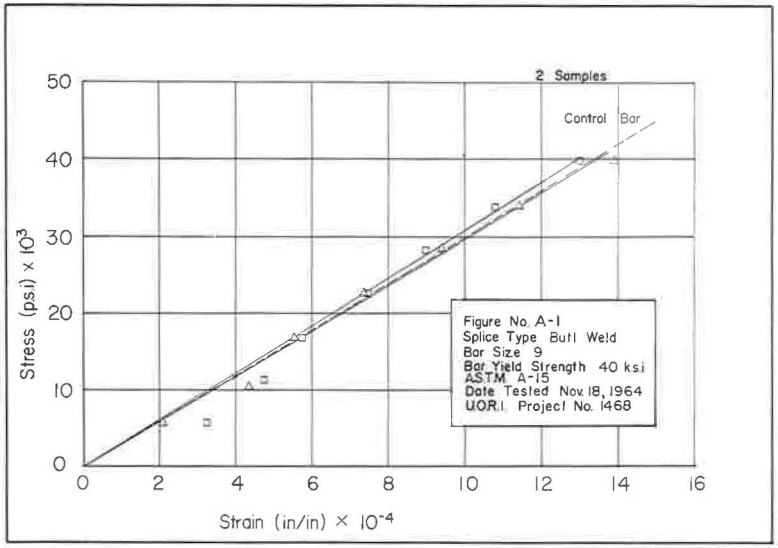
2 Samples
Control Bar
Stress (psi) x 10^3
Strain (in/in) x 10^{-4}
Figure No. A-1
Splice Type Butt Weld
Bar Size 9
Bar Yield Strength 40 ksi
A.S.T.M. A-15
Date Tested Nov. 18, 1964
U.O.R.I. Project No. 1468

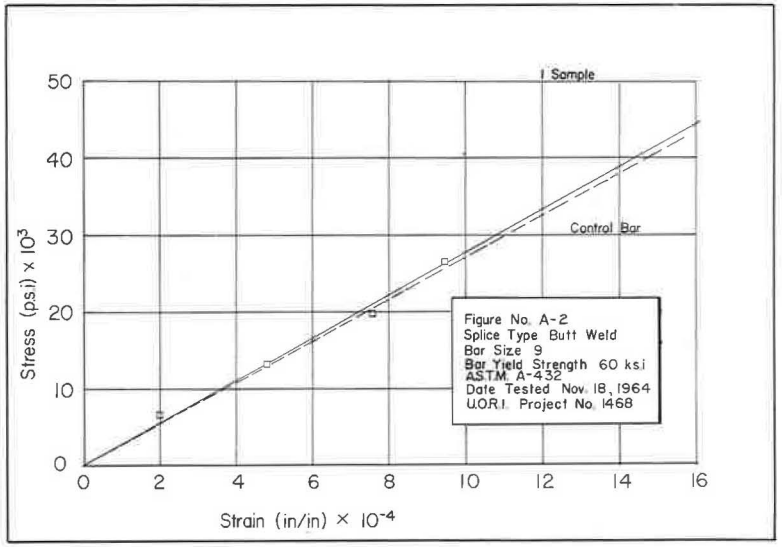
1 Sample
Control Bar
Stress (psi) x 10^3
Strain (in/in) x 10^{-4}
Figure No. A-2
Splice Type Butt Weld
Bar Size 9
Bar Yield Strength 60 ksi
A.S.T.M. A-432
Date Tested Nov. 18, 1964
U.O.R.I. Project No. 1468

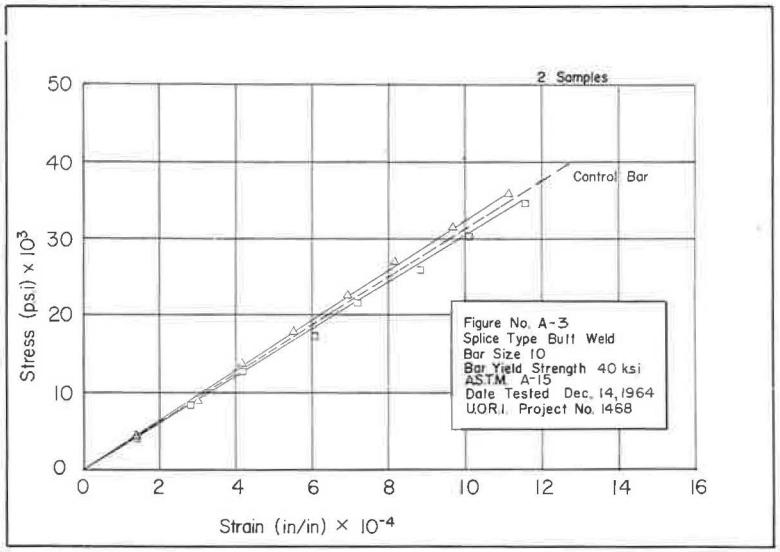
2 Samples
Control Bar
Stress (psi) x 10^3
Strain (in/in) x 10^{-4}
Figure No. A-3
Splice Type Butt Weld
Bar Size 10
Bar Yield Strength 40 ksi
A.S.T.M. A-15
Date Tested Dec. 14, 1964
U.O.R.I. Project No. 1468

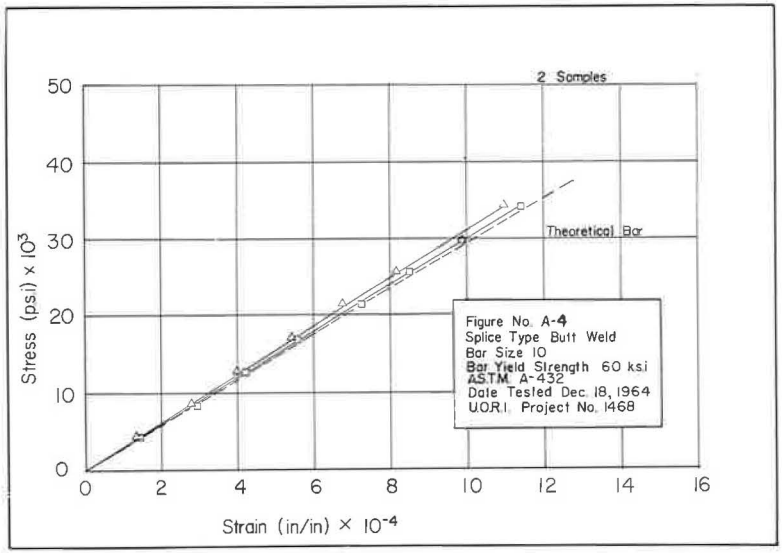
2 Samples
Theoretical Bar
Stress (psi) x 10^3
Strain (in/in) x 10^{-4}
Figure No. A-4
Splice Type Butt Weld
Bar Size 10
Bar Yield Strength 60 ksi
A.S.T.M. A-432
Date Tested Dec. 18, 1964
U.O.R.I. Project No. 1468

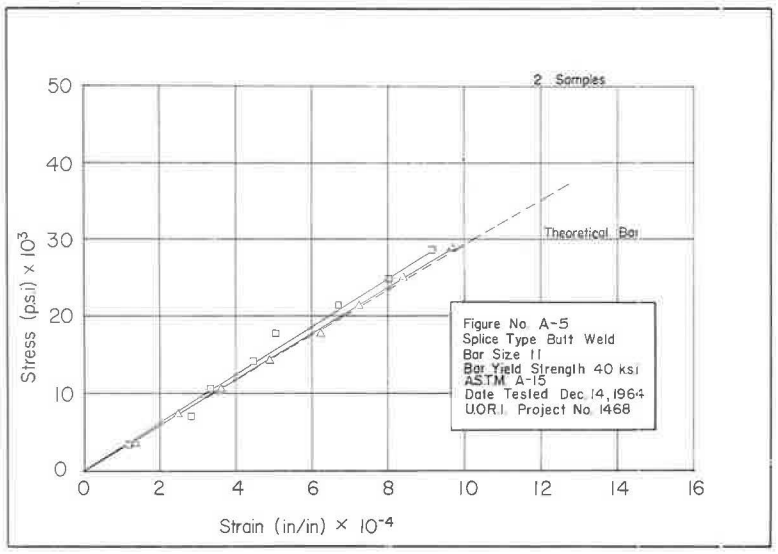
2 Samples
Theoretical Bar
Figure No. A-5
Splice Type Butt Weld
Bar Size 11
Bar Yield Strength 40 ksi
A.S.T.M. A-15
Date Tested Dec. 14, 1964
U.O.R.I. Project No. 1468
Stress (p.s.i) x 10^3
Strain (in/in) x 10^{-4}

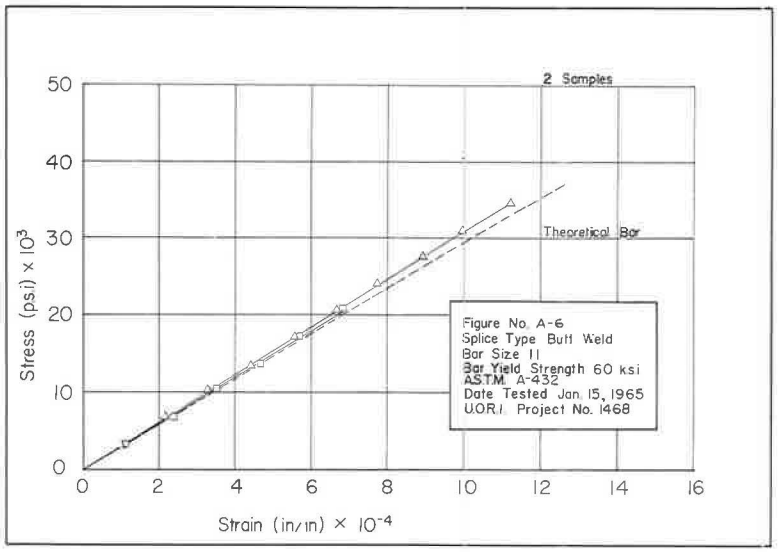
2 Samples
Theoretical Bar
Figure No. A-6
Splice Type Butt Weld
Bar Size 11
Bar Yield Strength 60 ksi
A.S.T.M. A-432
Date Tested Jan. 15, 1965
U.O.R.I. Project No. 1468
Stress (p.s.i) x 10^3
Strain (in/in) x 10^{-4}

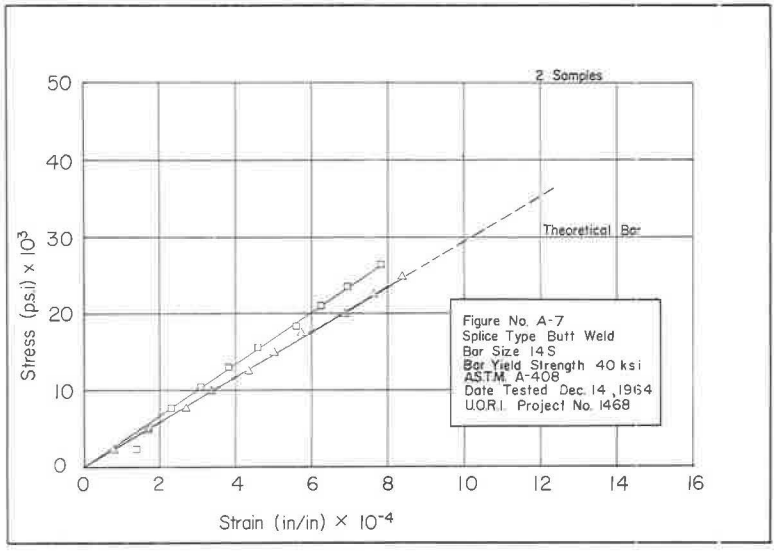
2 Samples
Theoretical Bar
Figure No. A-7
Splice Type Butt Weld
Bar Size 14S
Bar Yield Strength 40 ksi
A.S.T.M. A-408
Date Tested Dec. 14, 1964
U.O.R.I. Project No. 1468
Stress (p.s.i) x 10^3
Strain (in/in) x 10^{-4}

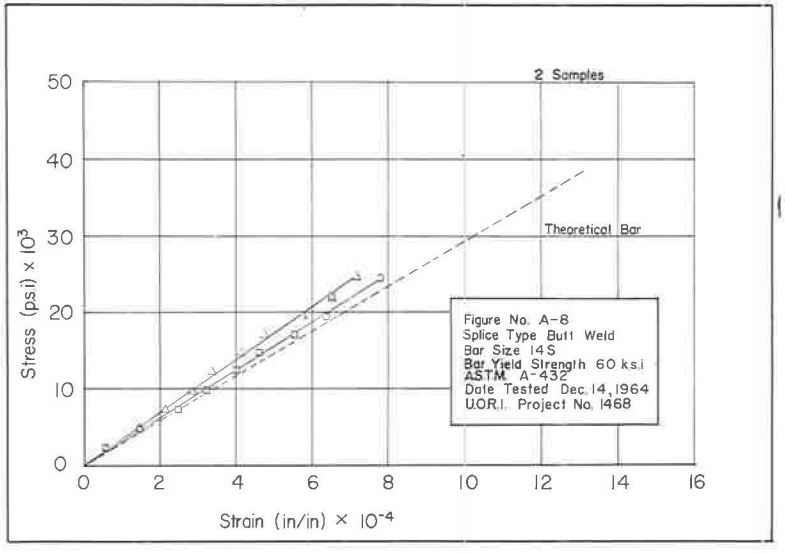
2 Samples
Theoretical Bar
Figure No. A-8
Splice Type Butt Weld
Bar Size 14S
Bar Yield Strength 60 ksi
A.S.T.M. A-432
Date Tested Dec. 14, 1964
U.O.R.I. Project No. 1468
Stress (p.s.i) x 10^3
Strain (in/in) x 10^{-4}

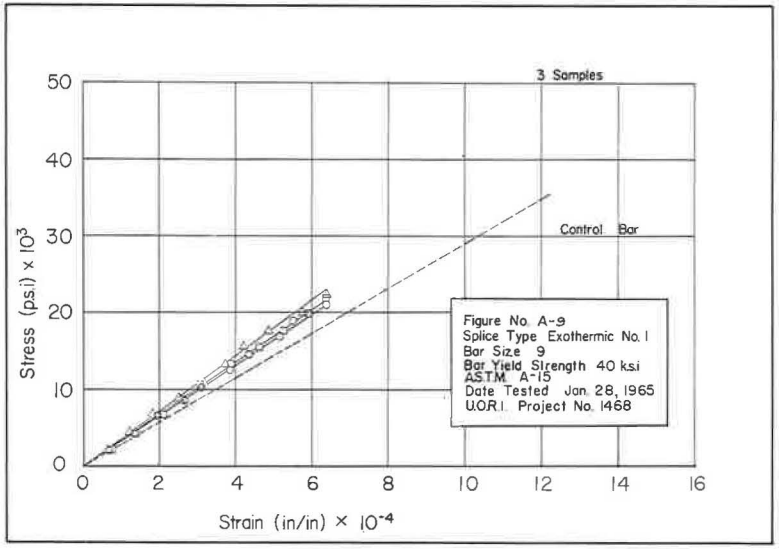
3 Samples
Control Bar
Stress (p.s.i) x 10^3
Strain (in/in) x 10^{-4}
Figure No. A-9
Splice Type Exothermic No. 1
Bar Size 9
Bar Yield Strength 40 k.s.i
A.S.T.M. A-15
Date Tested Jan. 28, 1965
U.O.R.I. Project No. 1468

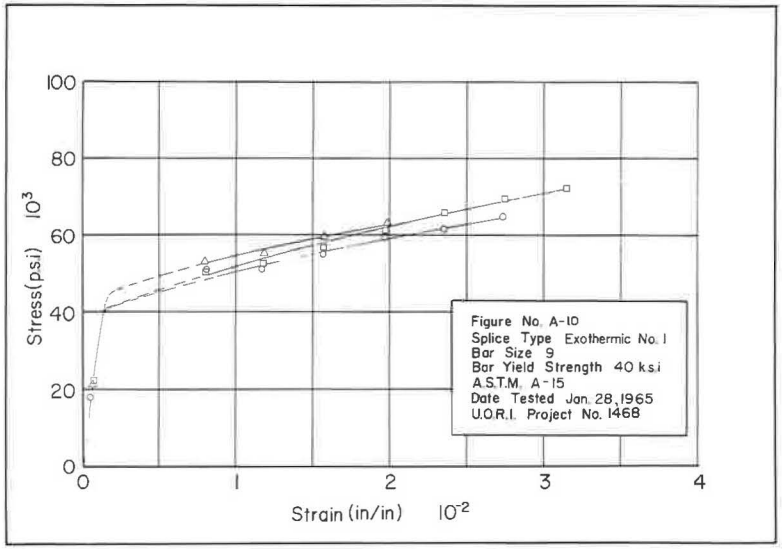
Stress(p.s.i) 10^3
Strain (in/in) 10^{-2}
Figure No. A-10
Splice Type Exothermic No. 1
Bar Size 9
Bar Yield Strength 40 k.s.i
A.S.T.M. A-15
Date Tested Jan. 28, 1965
U.O.R.I. Project No. 1468

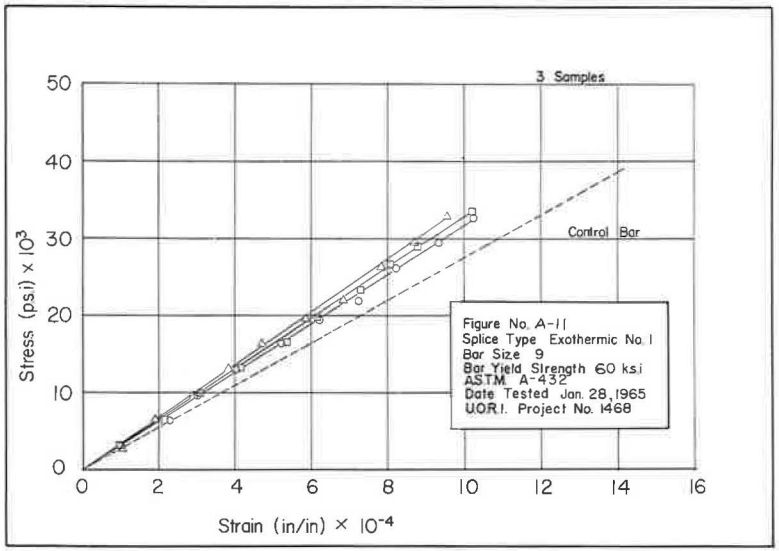
3 Samples
Control Bar
Stress (p.s.i) x 10^3
Strain (in/in) x 10^{-4}
Figure No. A-11
Splice Type Exothermic No. 1
Bar Size 9
Bar Yield Strength 60 k.s.i
A.S.T.M. A-432
Date Tested Jan. 28, 1965
U.O.R.I. Project No. 1468

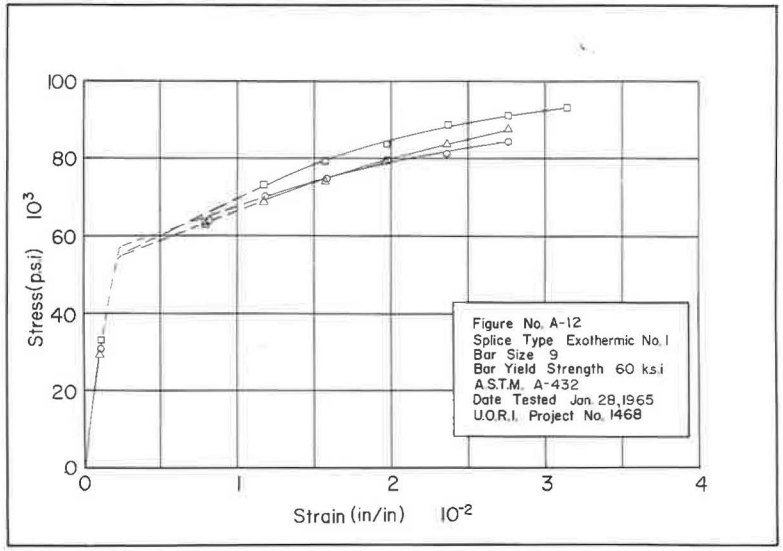
Stress(p.s.i) 10^3
Strain (in/in) 10^{-2}
Figure No. A-12
Splice Type Exothermic No. 1
Bar Size 9
Bar Yield Strength 60 k.s.i
A.S.T.M. A-432
Date Tested Jan. 28, 1965
U.O.R.I. Project No. 1468

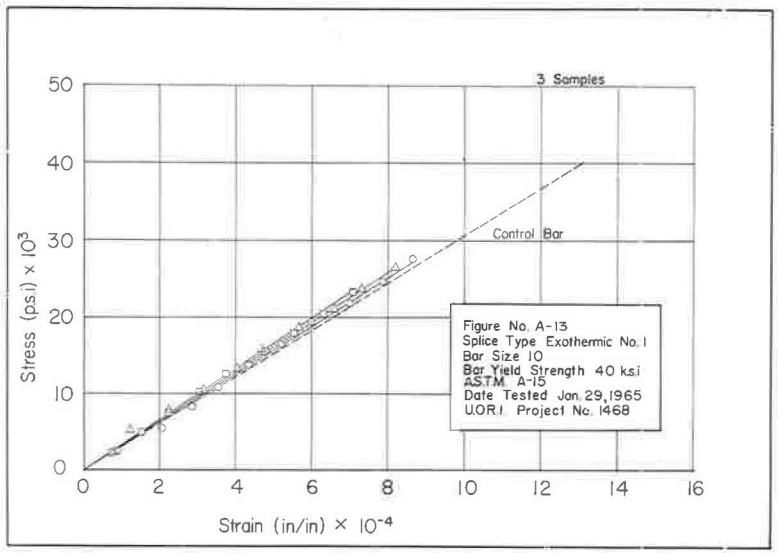
3 Samples
Control Bar
Stress (p.s.i) x 10^3
Strain (in/in) x 10^{-4}
Figure No. A-13
Splice Type Exothermic No. 1
Bar Size 10
Bar Yield Strength 40 k.s.i
A.S.T.M. A-15
Date Tested Jan. 29, 1965
U.O.R.I. Project No. 1468

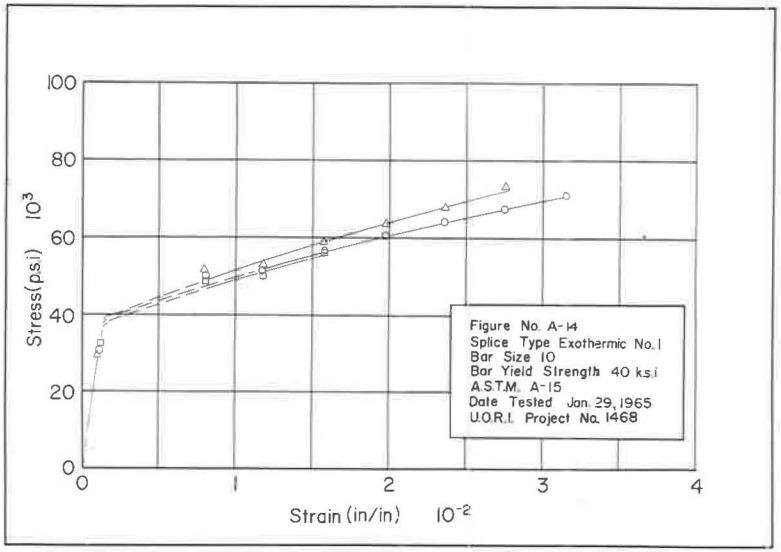
Stress(p.s.i) 10^3
Strain (in/in) 10^{-2}
Figure No. A-14
Splice Type Exothermic No. 1
Bar Size 10
Bar Yield Strength 40 k.s.i
A.S.T.M. A-15
Date Tested Jan. 29, 1965
U.O.R.I. Project No. 1468

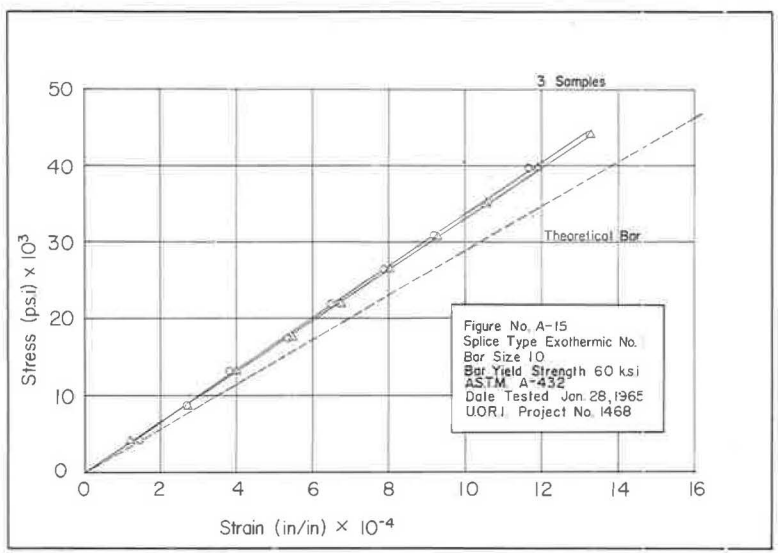
3 Samples
Theoretical Bar
Stress (p.s.i) x 10^3
Strain (in/in) x 10^{-4}
Figure No. A-15
Splice Type Exothermic No.
Bar Size 10
Bar Yield Strength 60 k.s.i
A.S.T.M. A-432
Date Tested Jan. 28, 1965
U.O.R.I. Project No. 1468

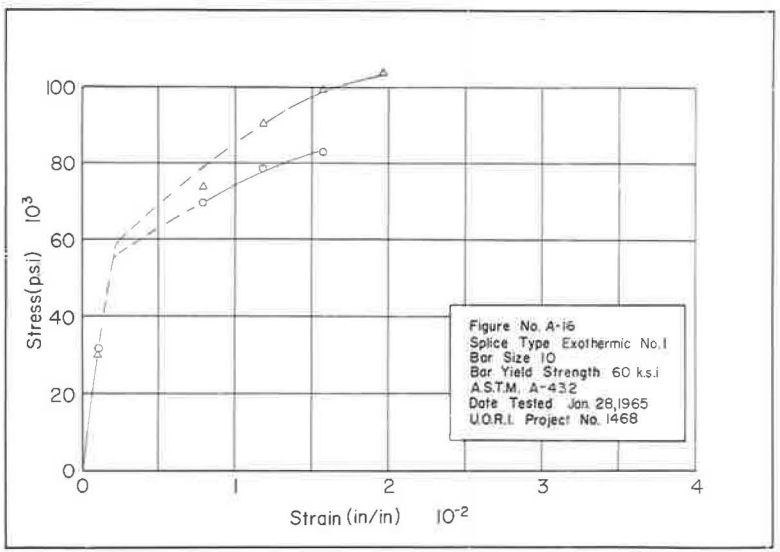
Stress(p.s.i) 10^3
Strain (in/in) 10^{-2}
Figure No. A-16
Splice Type Exothermic No. 1
Bar Size 10
Bar Yield Strength 60 k.s.i
A.S.T.M. A-432
Date Tested Jan. 28, 1965
U.O.R.I. Project No. 1468

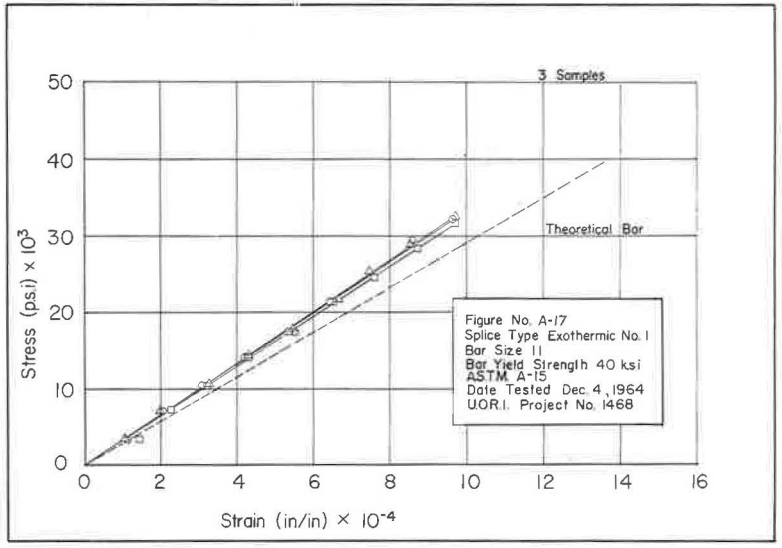
3 Samples
Theoretical Bar
Figure No. A-17
Splice Type Exothermic No. 1
Bar Size 11
Bar Yield Strength 40 k.s.i
A.S.T.M. A-15
Date Tested Dec. 4, 1964
U.O.R.I. Project No. 1468
Stress (p.s.i) x 10^3
Strain (in/in) x 10^{-4}

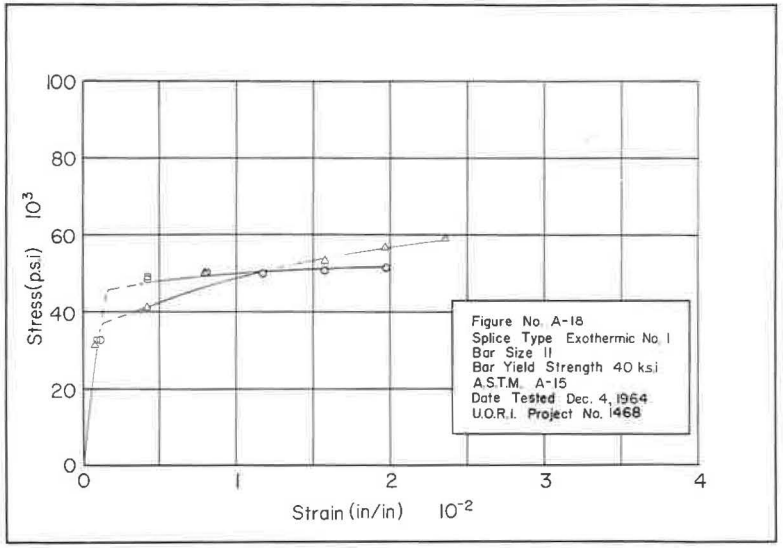
Figure No. A-18
Splice Type Exothermic No. 1
Bar Size 11
Bar Yield Strength 40 k.s.i
A.S.T.M. A-15
Date Tested Dec. 4, 1964
U.O.R.I. Project No. 1468
Stress(p.s.i) 10^3
Strain (in/in) 10^{-2}

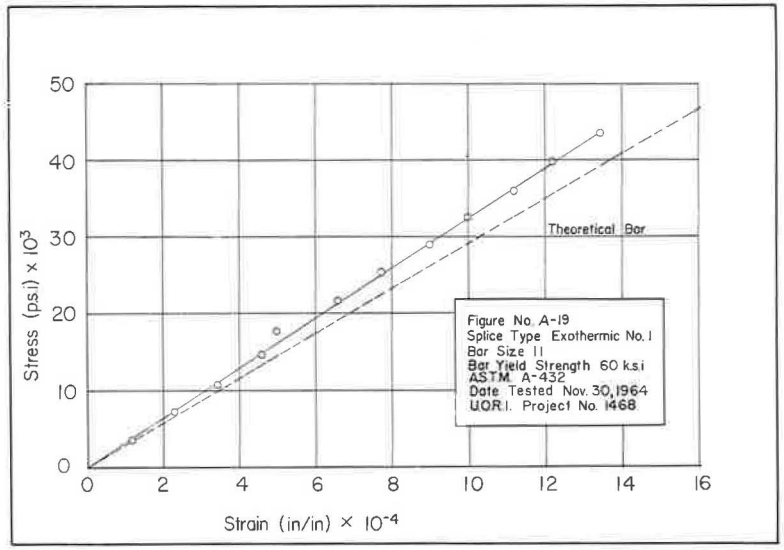
Theoretical Bar
Figure No. A-19
Splice Type Exothermic No. 1
Bar Size 11
Bar Yield Strength 60 k.s.i
A.S.T.M. A-432
Date Tested Nov. 30, 1964
U.O.R.I. Project No. 1468
Stress (p.s.i) x 10^3
Strain (in/in) x 10^{-4}

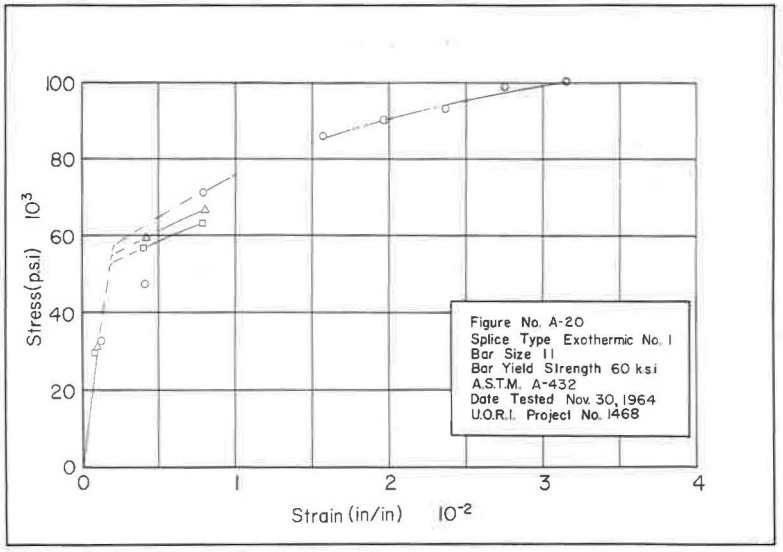
Figure No. A-20
Splice Type Exothermic No. 1
Bar Size 11
Bar Yield Strength 60 k.s.i
A.S.T.M. A-432
Date Tested Nov. 30, 1964
U.O.R.I. Project No. 1468
Stress(p.s.i) 10^3
Strain (in/in) 10^{-2}

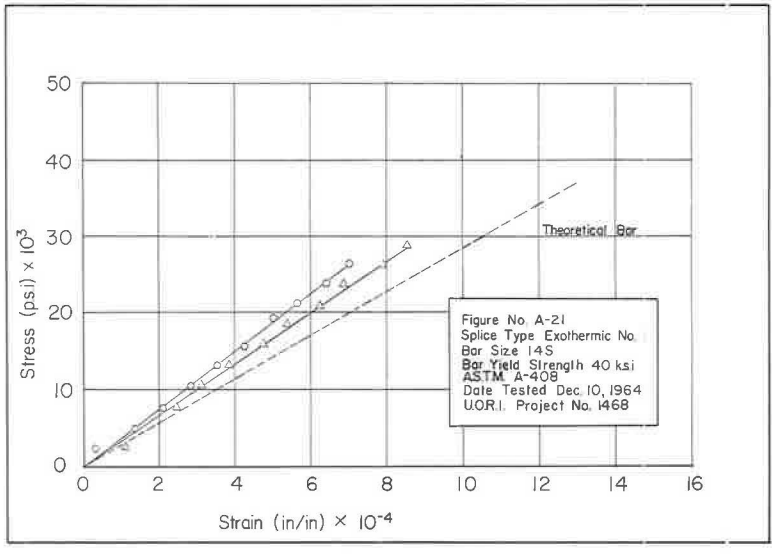
Stress (psi) x 10^3
Strain (in/in) x 10^{-4}
Theoretical Bar
Figure No. A-21
Splice Type Exothermic No.
Bar Size 14S
Bar Yield Strength 40 k.s.i
A.S.T.M. A-408
Date Tested Dec. 10, 1964
U.O.R.I. Project No. 1468

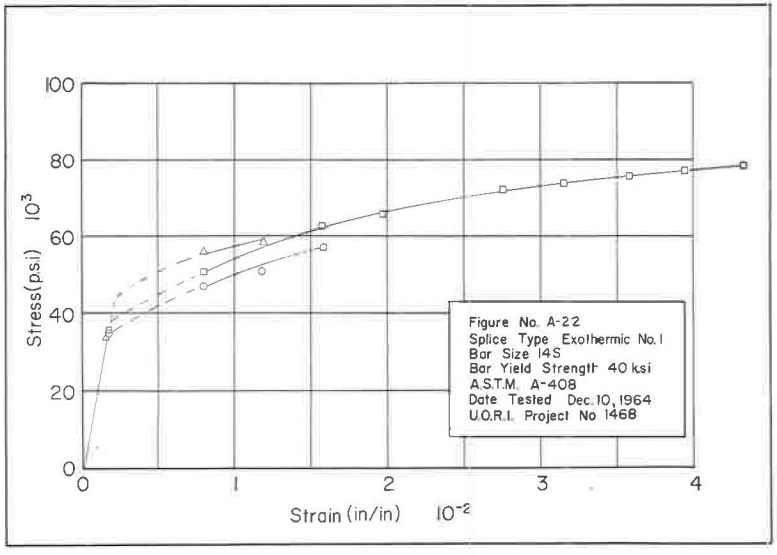
Stress(psi) 10^3
Strain (in/in) 10^{-2}
Figure No. A-22
Splice Type Exothermic No. I
Bar Size 14S
Bar Yield Strength 40 k.s.i
A.S.T.M. A-408
Date Tested Dec. 10, 1964
U.O.R.I. Project No 1468

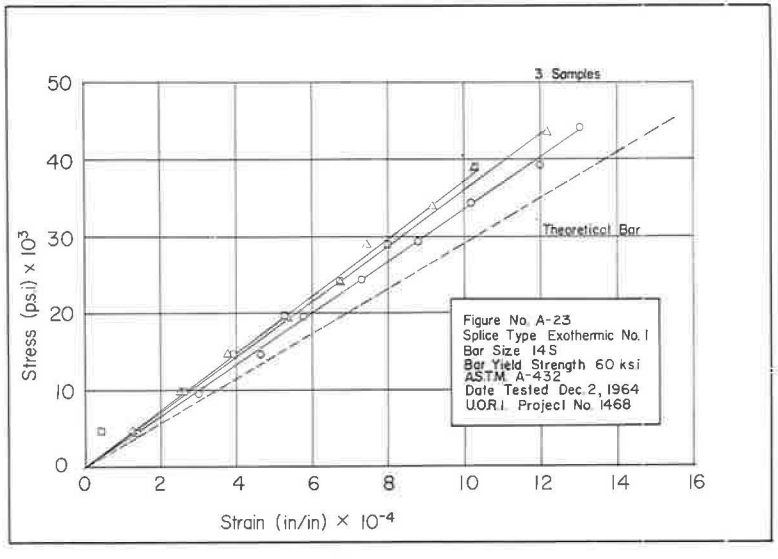
3 Samples
Stress (psi) x 10^3
Strain (in/in) x 10^{-4}
Theoretical Bar
Figure No. A-23
Splice Type Exothermic No. I
Bar Size 14S
Bar Yield Strength 60 k.s.i
A.S.T.M. A-432
Date Tested Dec. 2, 1964
U.O.R.I. Project No. 1468

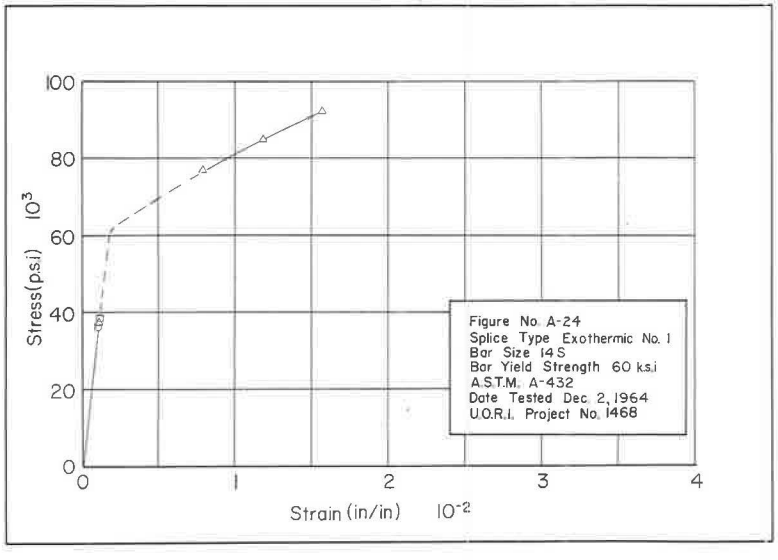
Stress(psi) 10^3
Strain (in/in) 10^{-2}
Figure No. A-24
Splice Type Exothermic No. I
Bar Size 14S
Bar Yield Strength 60 k.s.i
A.S.T.M. A-432
Date Tested Dec. 2, 1964
U.O.R.I. Project No. 1468

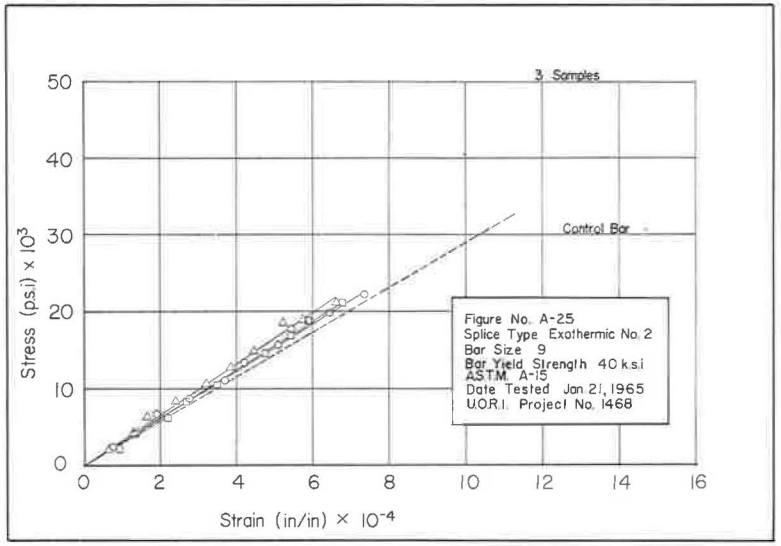
3 Samples
Control Bar
Stress (p.s.i) x 10^3
Strain (in/in) x 10^{-4}
Figure No. A-25
Splice Type Exothermic No. 2
Bar Size 9
Bar Yield Strength 40 k.s.i
A.S.T.M. A-15
Date Tested Jan 21, 1965
U.O.R.I. Project No. 1468

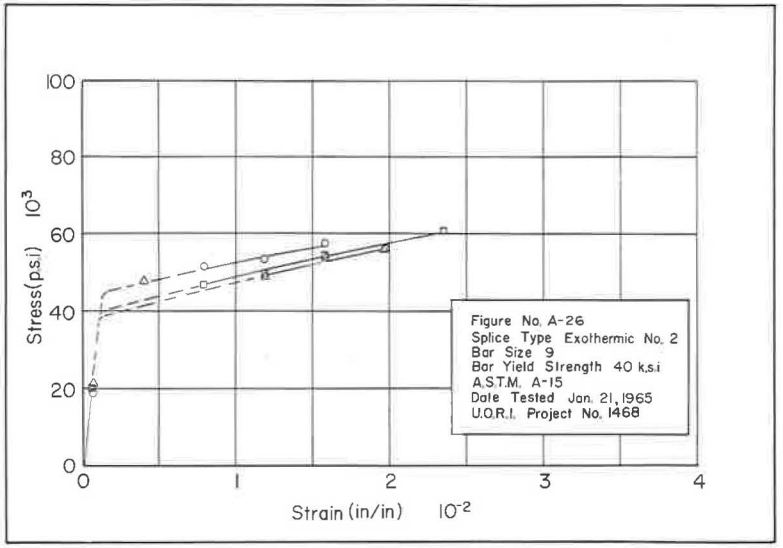
Stress(p.s.i) 10^3
Strain (in/in) 10^{-2}
Figure No. A-26
Splice Type Exothermic No. 2
Bar Size 9
Bar Yield Strength 40 k.s.i
A.S.T.M. A-15
Date Tested Jan. 21, 1965
U.O.R.I. Project No. 1468

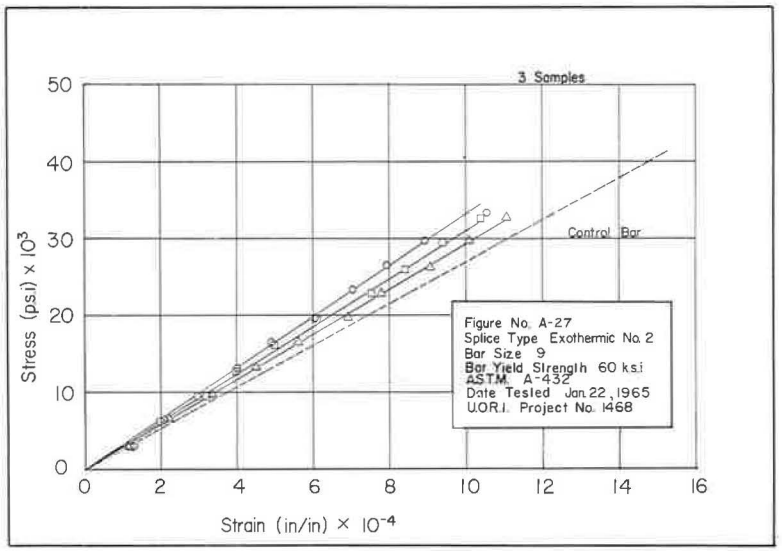
3 Samples
Control Bar
Stress (p.s.i) x 10^3
Strain (in/in) x 10^{-4}
Figure No. A-27
Splice Type Exothermic No. 2
Bar Size 9
Bar Yield Strength 60 k.s.i
A.S.T.M. A-432
Date Tested Jan. 22, 1965
U.O.R.I. Project No. 1468

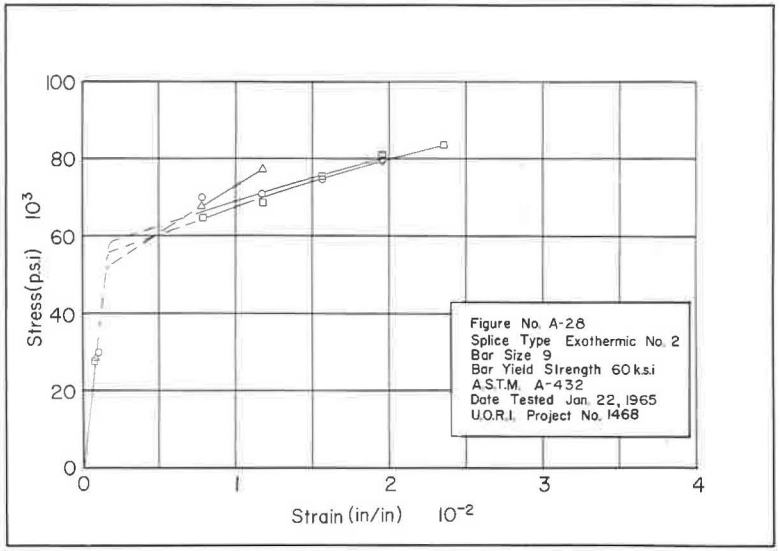
Stress(p.s.i) 10^3
Strain (in/in) 10^{-2}
Figure No. A-28
Splice Type Exothermic No. 2
Bar Size 9
Bar Yield Strength 60 k.s.i
A.S.T.M. A-432
Date Tested Jan. 22, 1965
U.O.R.I. Project No. 1468

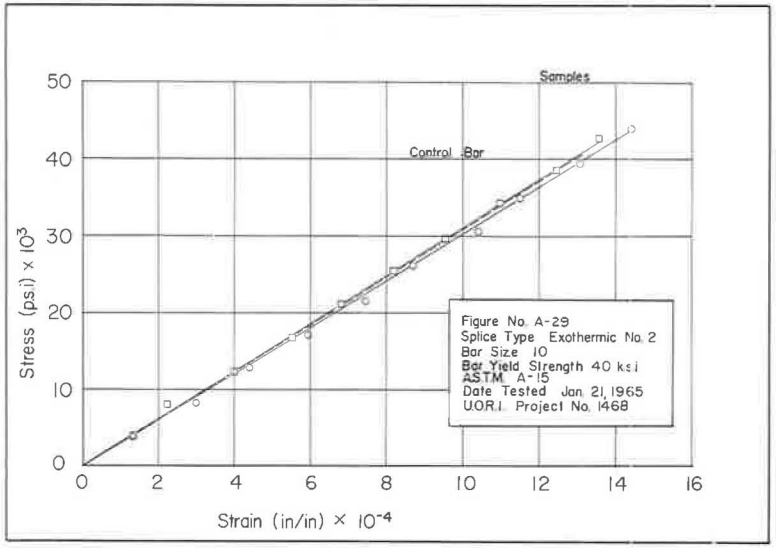
Samples
Control Bar
Stress (psi.) x 10^3
Strain (in/in) x 10^{-4}
Figure No. A-29
Splice Type Exothermic No. 2
Bar Size 10
Bar Yield Strength 40 ksi
A.S.T.M. A-15
Date Tested Jan. 21, 1965
U.O.R.I. Project No. 1468

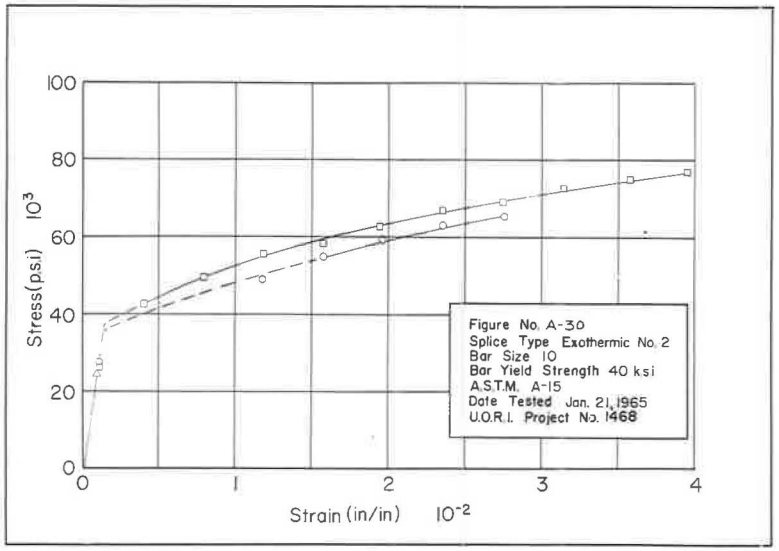
Stress(psi) 10^3
Strain (in/in) 10^{-2}
Figure No. A-30
Splice Type Exothermic No. 2
Bar Size 10
Bar Yield Strength 40 ksi
A.S.T.M. A-15
Date Tested Jan. 21, 1965
U.O.R.I. Project No. 1468

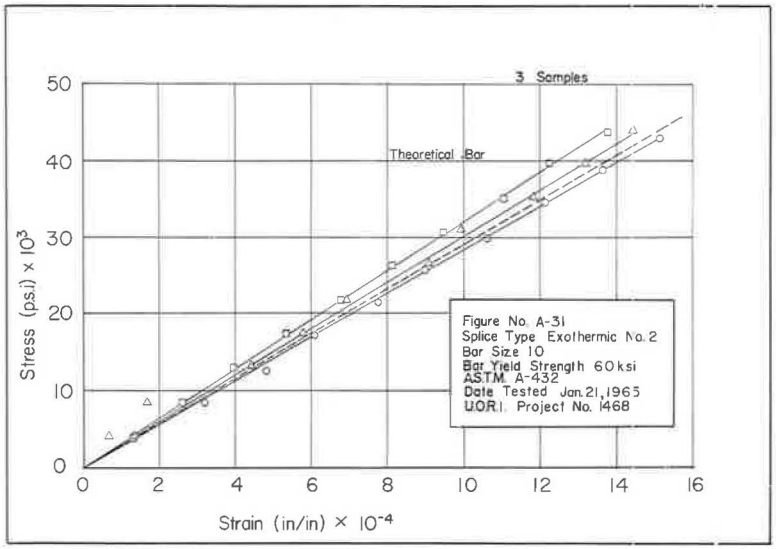
3 Samples
Theoretical Bar
Stress (psi.) x 10^3
Strain (in/in) x 10^{-4}
Figure No. A-31
Splice Type Exothermic No. 2
Bar Size 10
Bar Yield Strength 60 ksi
A.S.T.M. A-432
Date Tested Jan. 21, 1965
U.O.R.I. Project No. 1468

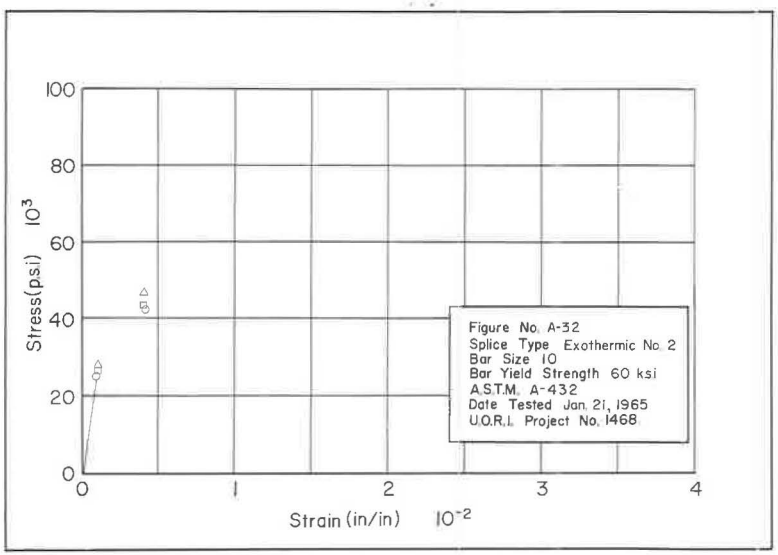
Stress(psi) 10^3
Strain (in/in) 10^{-2}
Figure No. A-32
Splice Type Exothermic No. 2
Bar Size 10
Bar Yield Strength 60 ksi
A.S.T.M. A-432
Date Tested Jan. 21, 1965
U.O.R.I. Project No. 1468

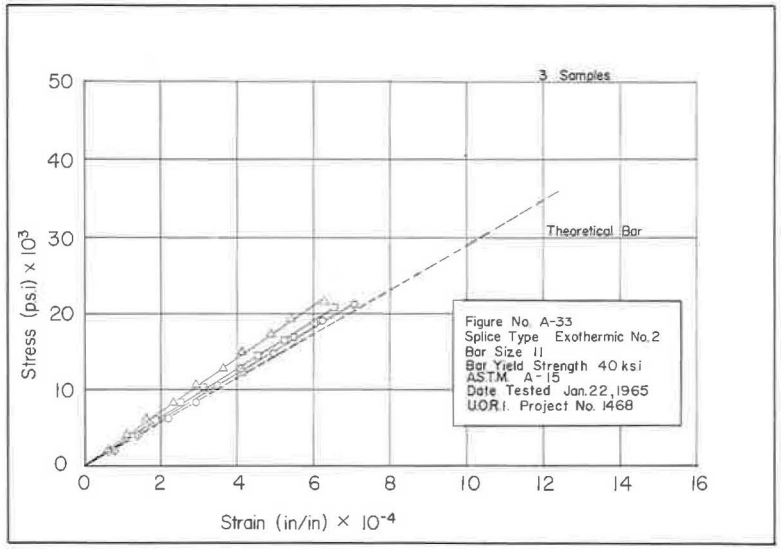
3 Samples
Theoretical Bar
Stress (psi) x 10^3
Strain (in/in) x 10^{-4}
Figure No. A-33
Splice Type Exothermic No. 2
Bar Size 11
Bar Yield Strength 40 k.s.i
A.S.T.M. A-15
Date Tested Jan. 22, 1965
U.O.R.I. Project No. 1468

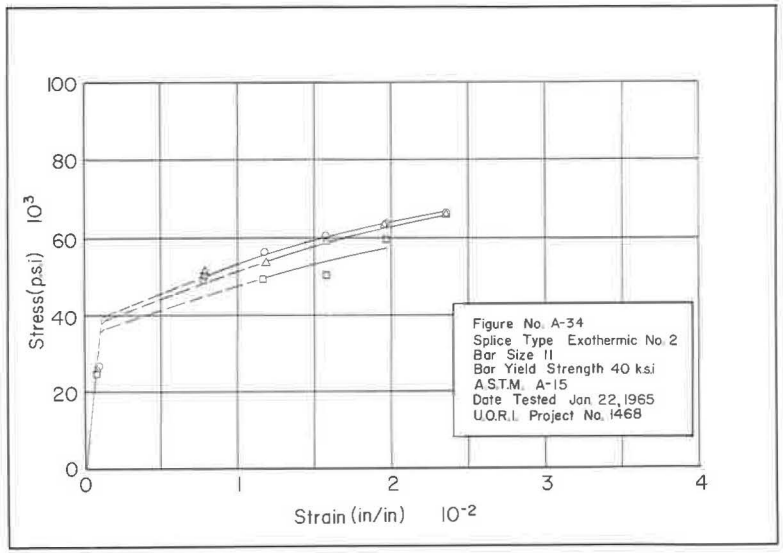
Stress(p.s.i) 10^3
Strain (in/in) 10^{-2}
Figure No. A-34
Splice Type Exothermic No. 2
Bar Size 11
Bar Yield Strength 40 k.s.i
A.S.T.M. A-15
Date Tested Jan. 22, 1965
U.O.R.I. Project No. 1468

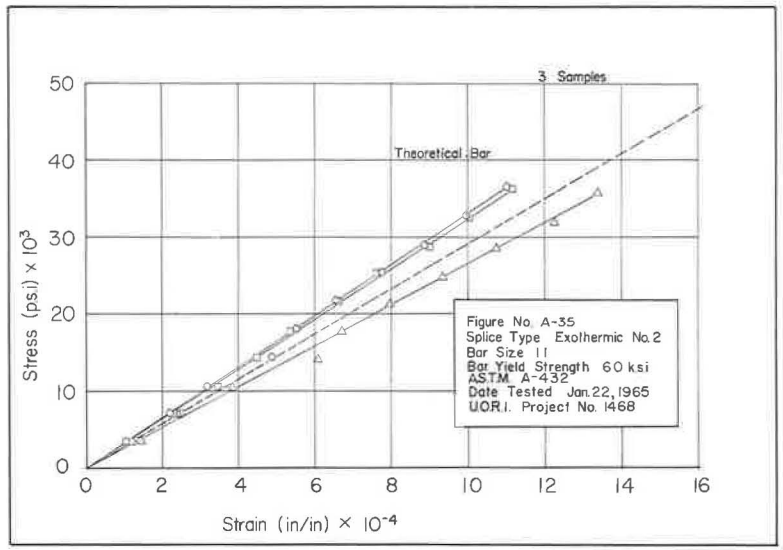
3 Samples
Theoretical Bar
Stress (psi) x 10^3
Strain (in/in) x 10^{-4}
Figure No. A-35
Splice Type Exothermic No. 2
Bar Size 11
Bar Yield Strength 60 k.s.i
A.S.T.M. A-432
Date Tested Jan. 22, 1965
U.O.R.I. Project No. 1468

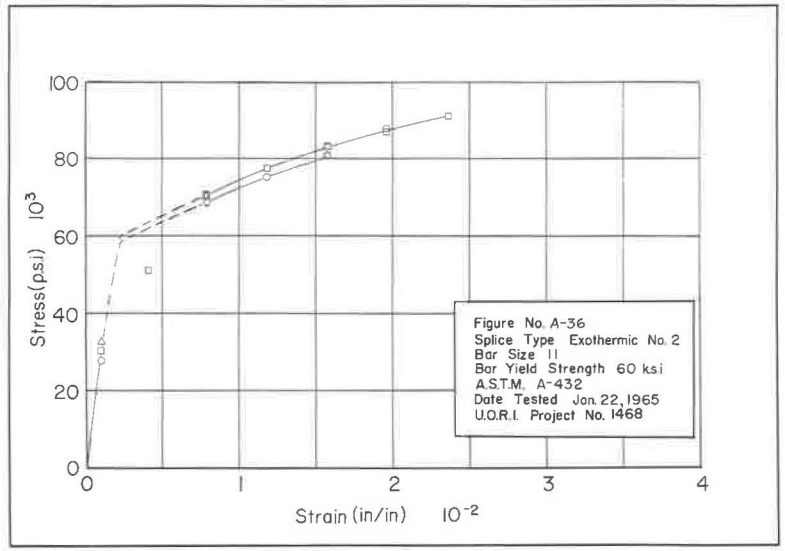
Stress(p.s.i) 10^3
Strain (in/in) 10^{-2}
Figure No. A-36
Splice Type Exothermic No. 2
Bar Size 11
Bar Yield Strength 60 k.s.i
A.S.T.M. A-432
Date Tested Jan. 22, 1965
U.O.R.I. Project No. 1468

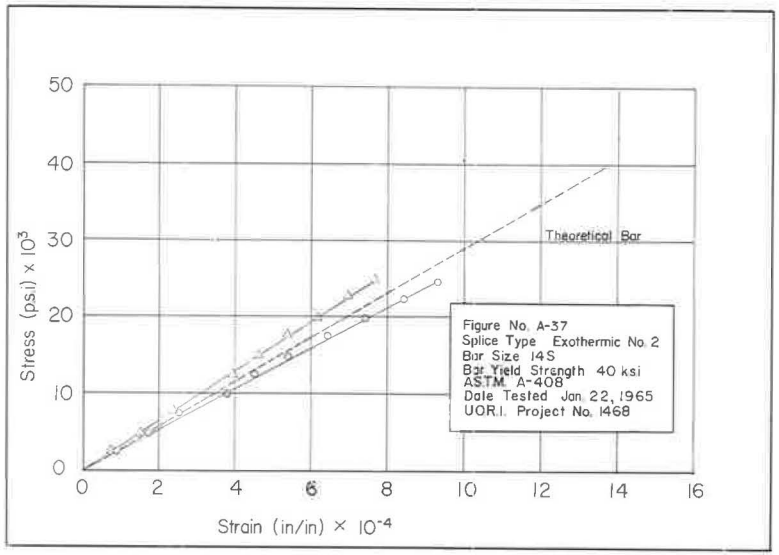

EXOTHERMIC NO. 2

BAR SIZE - 14S

BAR YIELD STRENGTH - 40KSI

ASTM - A408

(FAILED BELOW NOMINAL YIELD STRENGTH)

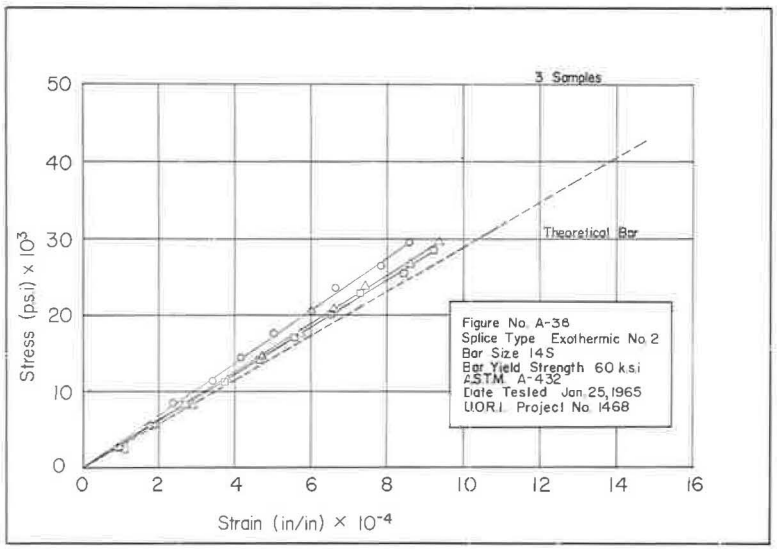

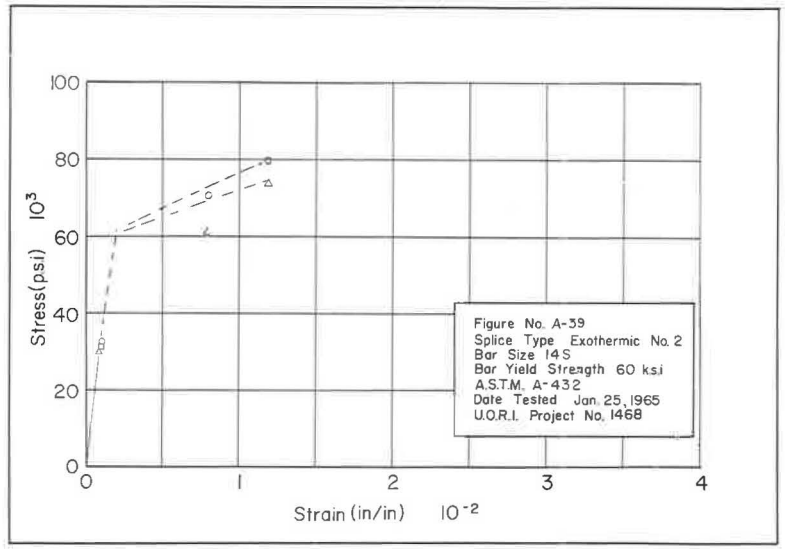

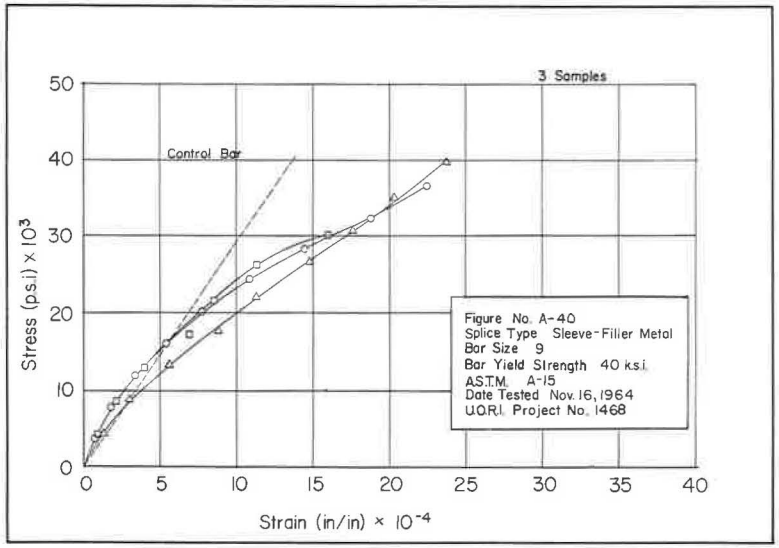
3 Samples
Control Bar
Stress (p.s.i.) x 10³
Strain (in/in) x 10⁻⁴
Figure No. A-40
Splice Type Sleeve-Filler Metal
Bar Size 9
Bar Yield Strength 40 k.s.i.
A.S.T.M. A-15
Date Tested Nov. 16, 1964
U.O.R.I. Project No. 1468

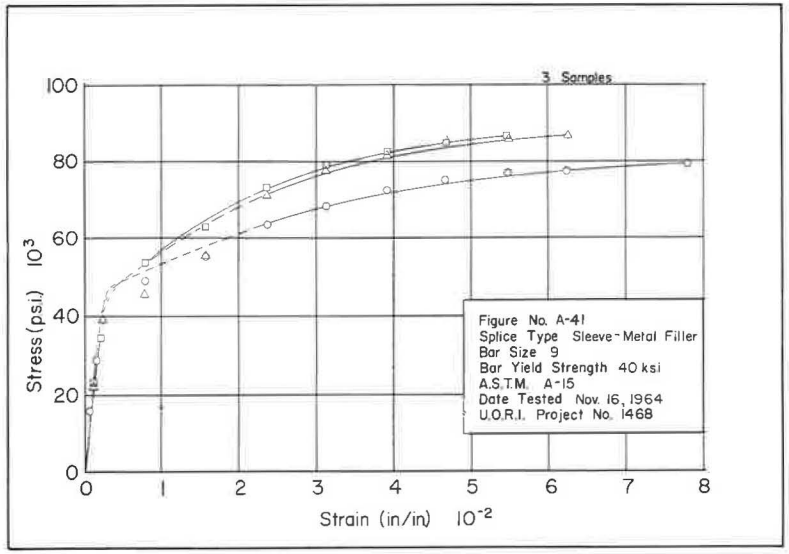
3 Samples
Stress (p.s.i.) 10³
Strain (in/in) 10⁻²
Figure No. A-41
Splice Type Sleeve-Metal Filler
Bar Size 9
Bar Yield Strength 40 k.s.i
A.S.T.M. A-15
Date Tested Nov. 16, 1964
U.O.R.I. Project No. 1468

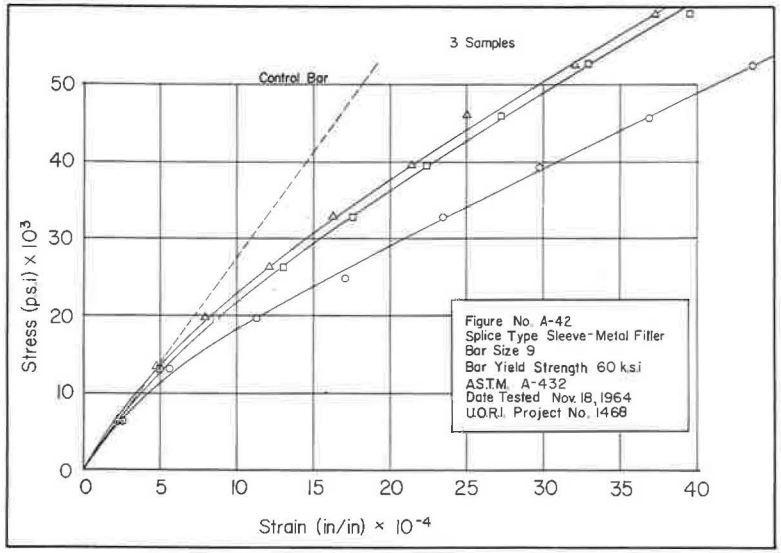
3 Samples
Control Bar
Stress (p.s.i.) x 10³
Strain (in/in) x 10⁻⁴
Figure No. A-42
Splice Type Sleeve-Metal Filler
Bar Size 9
Bar Yield Strength 60 k.s.i
A.S.T.M. A-432
Date Tested Nov. 18, 1964
U.O.R.I. Project No. 1468

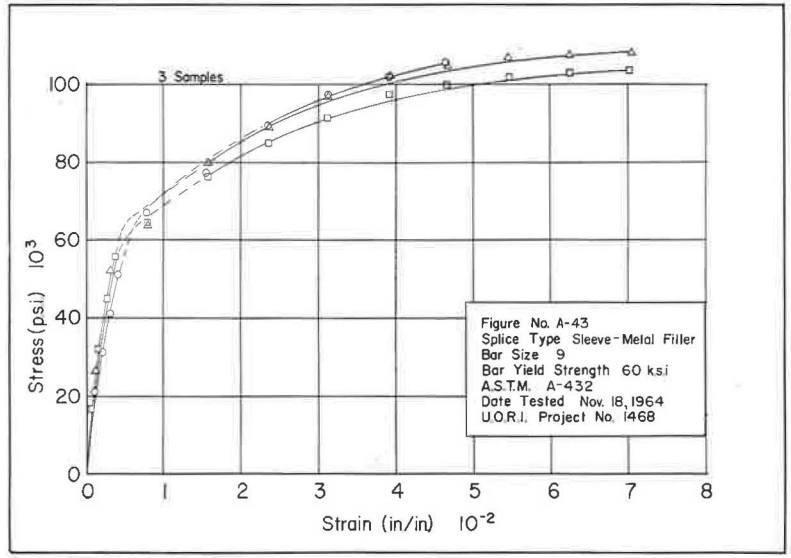
3 Samples
Stress (p.s.i.) 10³
Strain (in/in) 10⁻²
Figure No. A-43
Splice Type Sleeve-Metal Filler
Bar Size 9
Bar Yield Strength 60 k.s.i
A.S.T.M. A-432
Date Tested Nov. 18, 1964
U.O.R.I. Project No. 1468

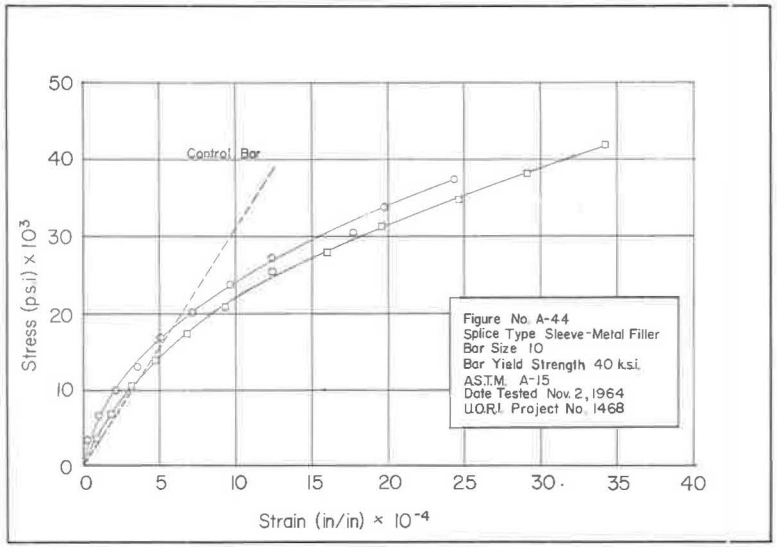
Control Bar
Stress (p.s.i.) x 10³
Strain (in/in) x 10⁻⁴
Figure No. A-44
Splice Type Sleeve-Metal Filler
Bar Size 10
Bar Yield Strength 40 k.s.i.
A.S.T.M. A-15
Date Tested Nov. 2, 1964
U.O.R.I. Project No. 1468

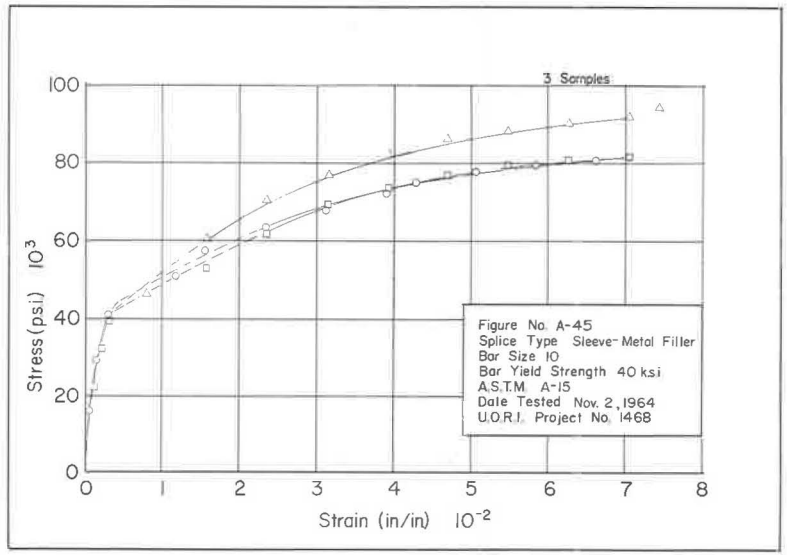
3 Samples
Stress (p.s.i.) 10³
Strain (in/in) 10⁻²
Figure No. A-45
Splice Type Sleeve-Metal Filler
Bar Size 10
Bar Yield Strength 40 k.s.i
A.S.T.M. A-15
Date Tested Nov. 2, 1964
U.O.R.I. Project No. 1468

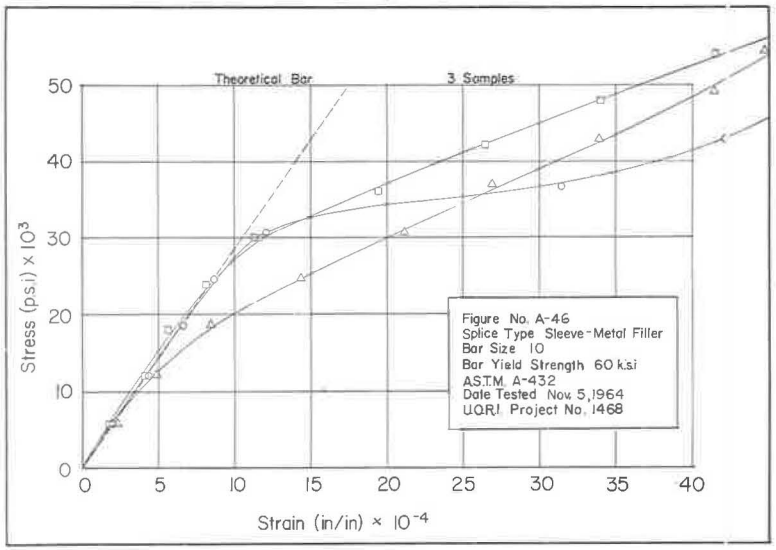
Theoretical Bar
3 Samples
Stress (p.s.i.) x 10³
Strain (in/in) x 10⁻⁴
Figure No. A-46
Splice Type Sleeve-Metal Filler
Bar Size 10
Bar Yield Strength 60 k.s.i
A.S.T.M. A-432
Date Tested Nov. 5, 1964
U.O.R.I. Project No. 1468

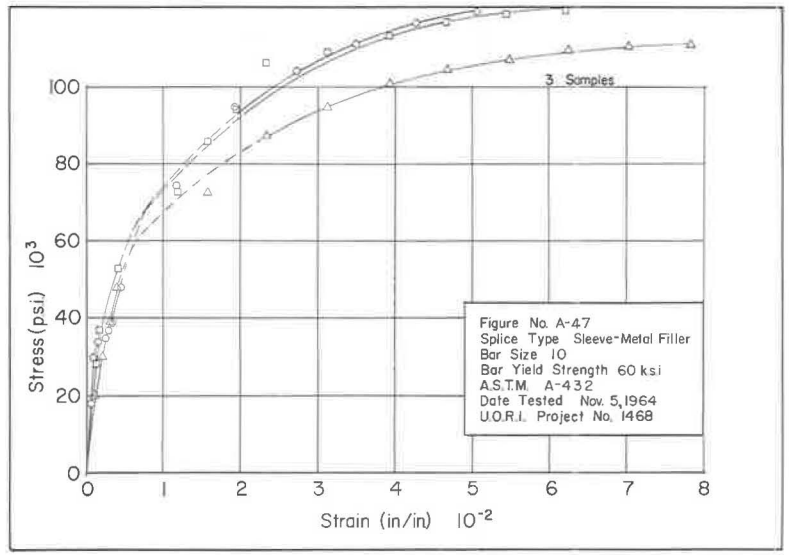
3 Samples
Stress (p.s.i.) 10³
Strain (in/in) 10⁻²
Figure No. A-47
Splice Type Sleeve-Metal Filler
Bar Size 10
Bar Yield Strength 60 k.s.i
A.S.T.M. A-432
Date Tested Nov. 5, 1964
U.O.R.I. Project No. 1468

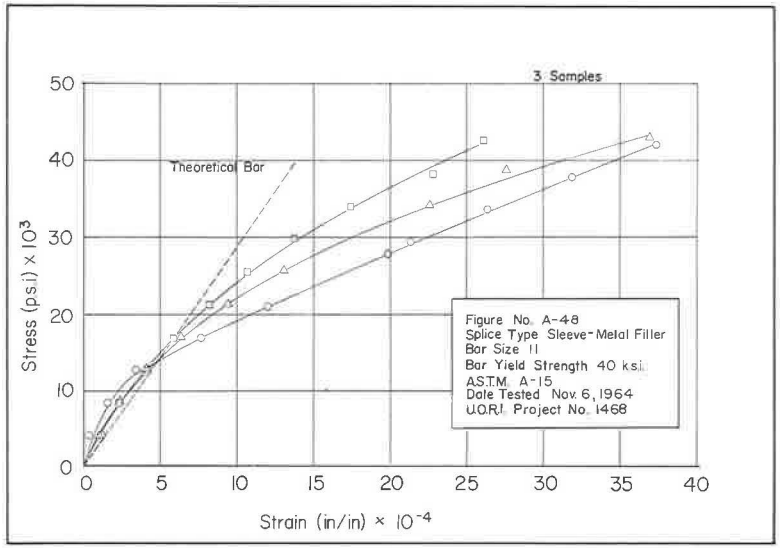
3 Samples
Theoretical Bar
Stress (p.s.i) x 10³
Strain (in/in) x 10⁻⁴
0
10
20
30
40
50
0
5
10
15
20
25
30
35
40
Figure No. A-48
Splice Type Sleeve-Metal Filler
Bar Size 11
Bar Yield Strength 40 k.s.i.
A.S.T.M. A-15
Date Tested Nov. 6, 1964
U.O.R.I. Project No. 1468

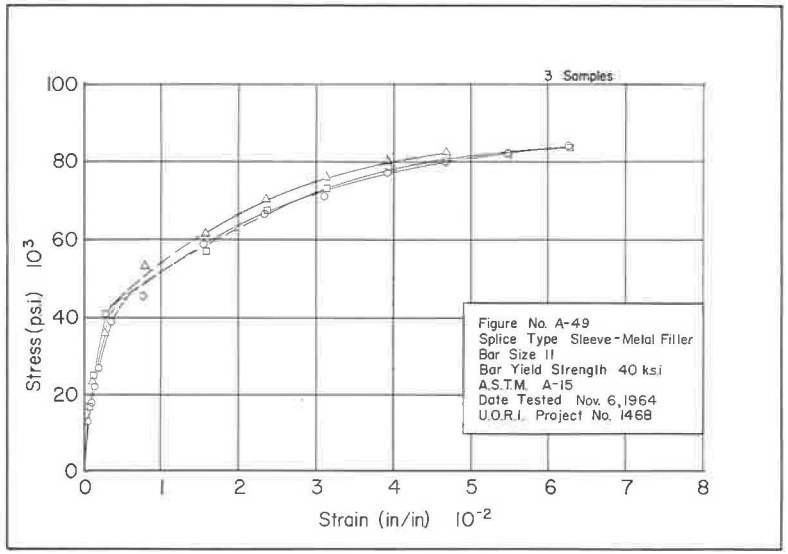
3 Samples
Stress (psi) 10³
Strain (in/in) 10⁻²
0
20
40
60
80
100
0
1
2
3
4
5
6
7
8
Figure No. A-49
Splice Type Sleeve-Metal Filler
Bar Size 11
Bar Yield Strength 40 k.s.i
A.S.T.M. A-15
Date Tested Nov. 6, 1964
U.O.R.I. Project No. 1468

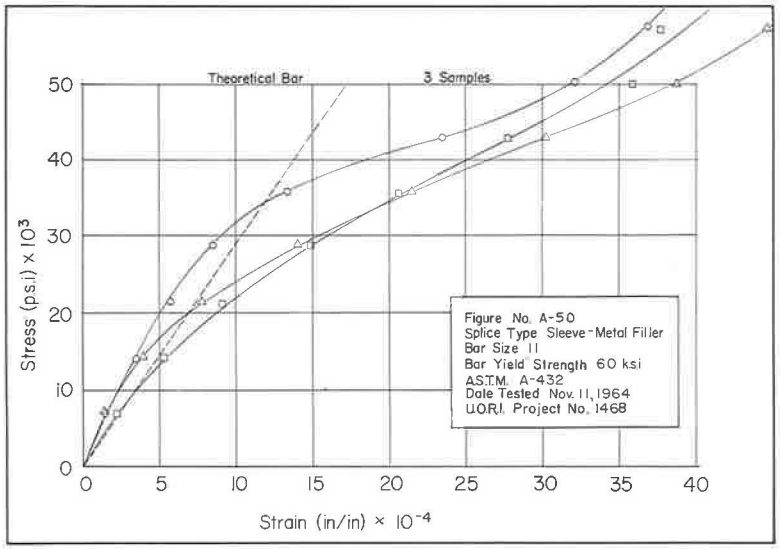
Theoretical Bar
3 Samples
Stress (p.s.i) x 10³
Strain (in/in) x 10⁻⁴
0
10
20
30
40
50
0
5
10
15
20
25
30
35
40
Figure No. A-50
Splice Type Sleeve-Metal Filler
Bar Size 11
Bar Yield Strength 60 k.s.i
A.S.T.M. A-432
Date Tested Nov. 11, 1964
U.O.R.I. Project No. 1468

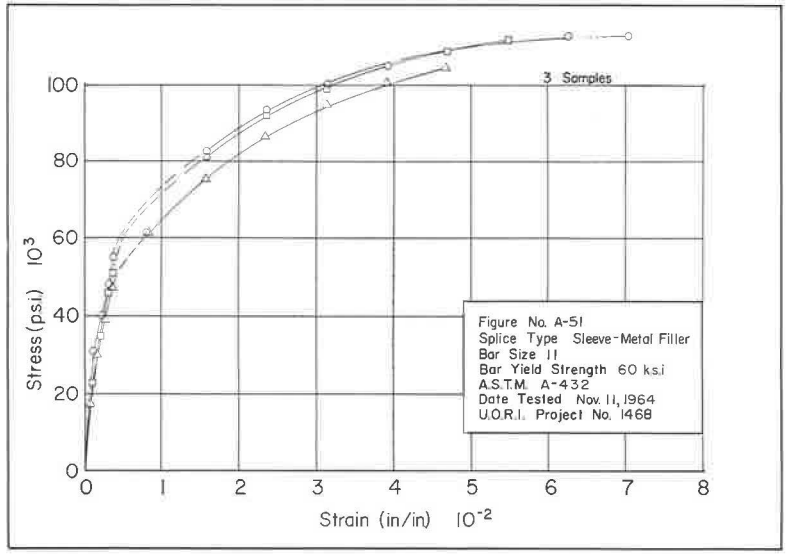
3 Samples
Stress (psi) 10³
Strain (in/in) 10⁻²
0
20
40
60
80
100
0
1
2
3
4
5
6
7
8
Figure No. A-51
Splice Type Sleeve-Metal Filler
Bar Size 11
Bar Yield Strength 60 k.s.i
A.S.T.M. A-432
Date Tested Nov. 11, 1964
U.O.R.I. Project No. 1468

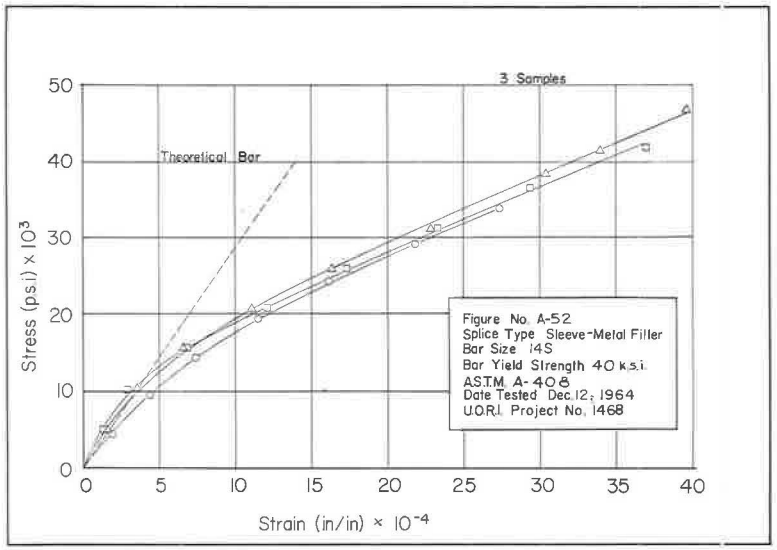
3 Samples
Theoretical Bar
Stress (psi.) x 10³
Strain (in/in) x 10⁻⁴
Figure No. A-52
Splice Type Sleeve-Metal Filler
Bar Size 14S
Bar Yield Strength 40 k.s.i.
A.S.T.M. A-408
Date Tested Dec. 12, 1964
U.O.R.I. Project No. 1468

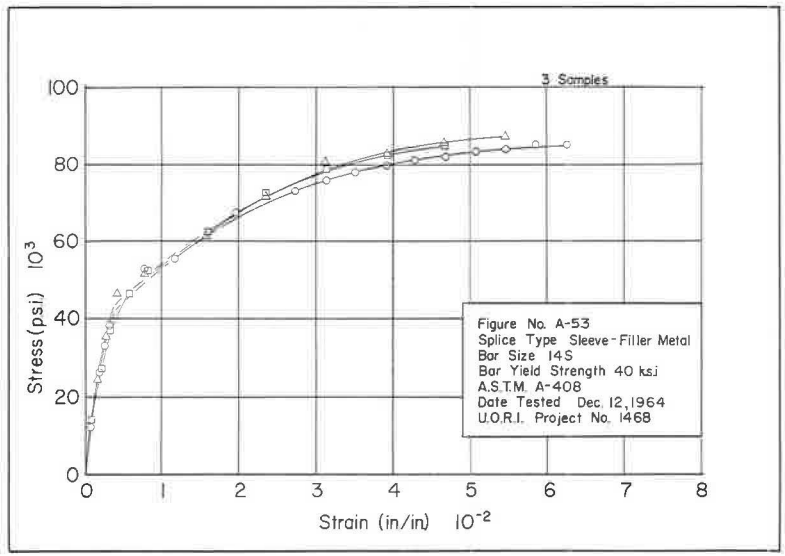
3 Samples
Stress (psi.) 10³
Strain (in/in) 10⁻²
Figure No. A-53
Splice Type Sleeve-Filler Metal
Bar Size 14S
Bar Yield Strength 40 ksi
A.S.T.M. A-408
Date Tested Dec. 12, 1964
U.O.R.I. Project No. 1468

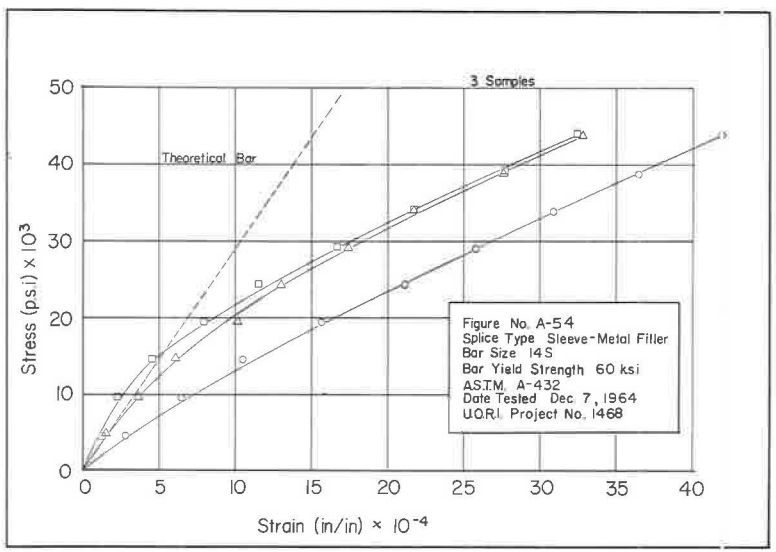
3 Samples
Theoretical Bar
Stress (psi.) x 10³
Strain (in/in) x 10⁻⁴
Figure No. A-54
Splice Type Sleeve-Metal Filler
Bar Size 14S
Bar Yield Strength 60 ksi
A.S.T.M. A-432
Date Tested Dec. 7, 1964
U.O.R.I. Project No. 1468

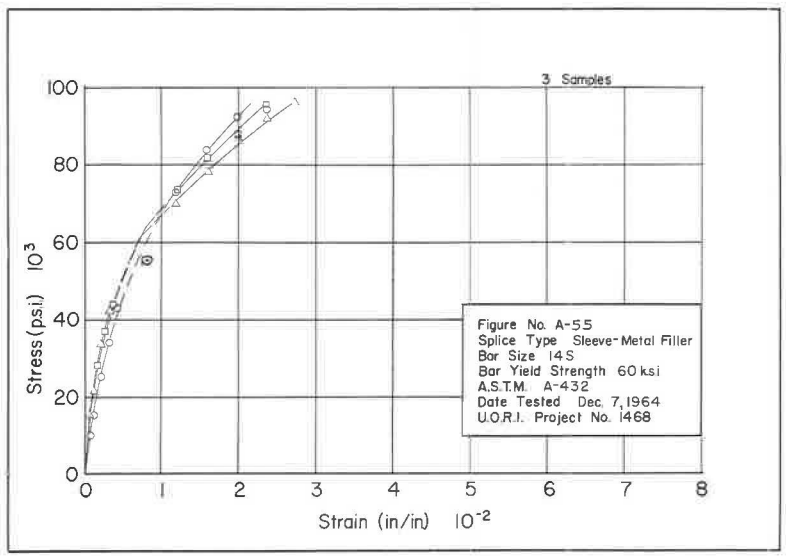
3 Samples
Stress (psi.) 10³
Strain (in/in) 10⁻²
Figure No. A-55
Splice Type Sleeve-Metal Filler
Bar Size 14S
Bar Yield Strength 60 ksi
A.S.T.M. A-432
Date Tested Dec. 7, 1964
U.O.R.I. Project No. 1468

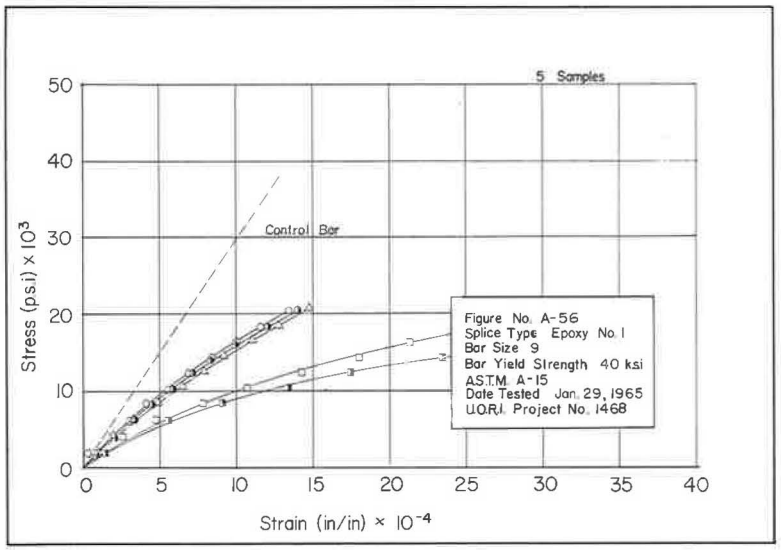

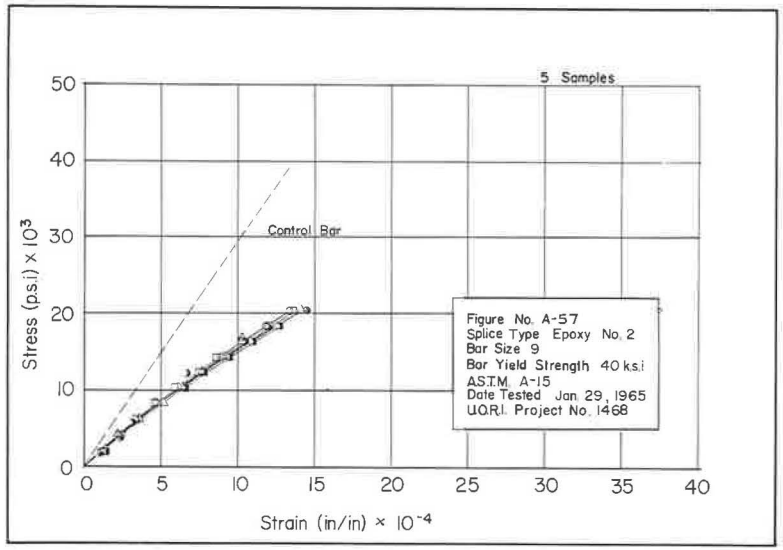

EPOXY SPLICE NO. 3

BAR SIZE - 9

BAR YIELD STRENGTH - 40KSI

ASTM - A15

(NO DATA TAKEN - FAILED PREMATURELY)

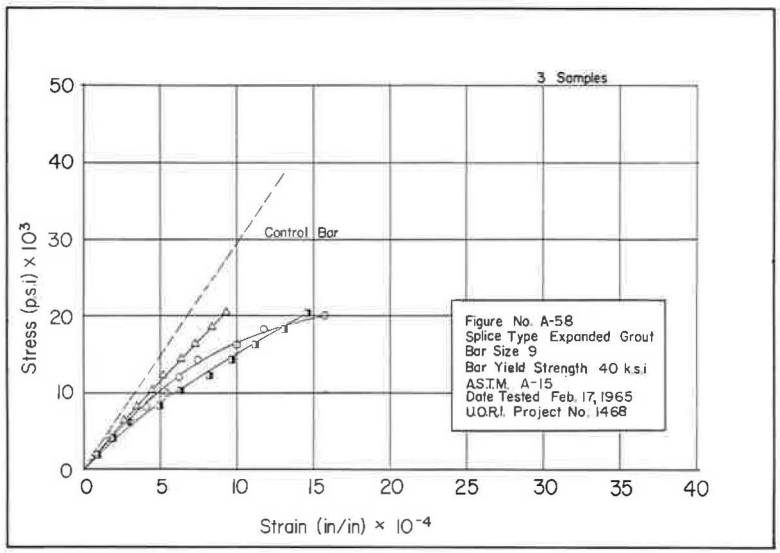

Design Criteria for Overhanging Ends of Bent Caps—Bond and Shear

PHIL M. FERGUSON, Center for Highway Research, University of Texas

A program of 36 bent cap sections of 36-in. depth were tested in an investigation primarily directed toward the bond and shear strengths which should be used in design. Intermediate, A 432, and A 431 grade steels were used. Even though the final failures were often classified as bond or shear, only 8 percent of the specimens failed at less than the calculated f_y steel stress. The average f_s developed was between $1.15f_y$ and $1.20f_y$.

In shear it was found that an ultimate v much higher than allowed by current specifications was feasible for loads placed between 0.5d and 1.2d from the support. Vertical stirrups added no perceptible strength but horizontal web steel was effective.

In bond it was found that the nominal bond stress in the length between load and support was not important, but that an end anchorage distance beyond the load was essential. With an end anchorage of 15 in. for No. 11 bars or 12 in. for No. 8 bars, there seemed to be no problem in developing a 75-ksi steel.

The width of web cracks was only slightly less than that of flexural cracks on the tension face and suggested the desirability of using horizontal stirrups in these cantilever ends.

•THE OVERHANGING end of a bent cap is a short cantilever beam with large depth relative to its projection. Elastic methods of analysis indicate that such cantilever members must be classified as deep beams with flexural stress distributions far from linear. In such elastic beams under negative moment the resultant of compressive stress rises above mid-depth as the length decreases to provide an internal couple with a lever arm much less than 0.5d rather than the usual arm of around 0.9d for ordinary concrete beams. For a uniformly loaded member, the horizontal unit flexural stresses would be as shown in Figure 1a. There is very little information on how the usual flexural cracking of reinforced concrete modifies this elastic stress distribution.

DESIGNING BENT CAP CANTILEVER ENDS

It is customary to design such short cantilever members at the support as though ordinary flexure and bond formulas applied. However, it is usually realized that these steel stresses will not decrease as rapidly as the moment at sections closer to the load. Instead, the resultant compression tends to slope from the bottom of the beam at the support and trend towards the load point at the top (Fig. 1b), much the same as if the cantilever were somewhat more triangular in shape. This implies considerable tension in the bars at the load point (Fig. 1c) and thus much smaller flexural bond stresses ($u = V/\Sigma o\, jd$) between the support and the load than this formula indicates. Likewise it requires that the tension at the load be anchored by bond stress beyond the load, that is, by what is usually designated as end anchorage.

Paper sponsored by Committee on Concrete Superstructures and presented at the 45th Annual Meeting.

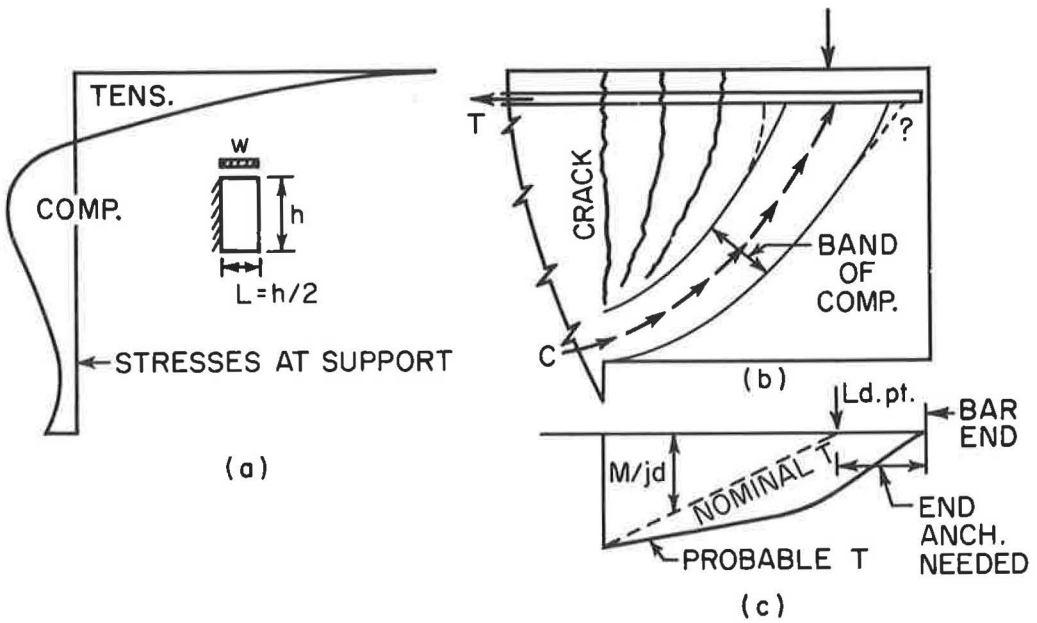

Figure 1. (a) Elastic stress distribution by deep beam theory. (b) The practical case. (c) Probable distribution of bar tension.

In the calculation of shear stress near the support there are traditional methods which can included the effect of the sloping bottom of a bracket or short cantilever and which result in lower calculated critical stresses. These assume that the resultant compression is sloping, parallel to the compression face. The compression thus has a vertical component which balances part of the external shear and only the remaining remnant of the shear causes diagonal tension, which is the real critical stress for design. As already indicated (Fig. 1) it is certain, even with no bottom slope, that the resultant compression does slope and thereby reduces the critical shear stress. With any reasonable proportions (even for a sloping bottom), experience shows that shear failure always involves the total depth at support. The present investigation was planned to establish, in part, proper numerical values of such shear strength for a load applied on top of the cap and a reaction applied to the bottom of the cap, that is, for the typical bent cap design situation.

Bottom slopes on bent caps are usually small and compression capacity normally exceeds tension capacity. Since these bottom slopes probably have no influence on the member capacity and very little influence on the stresses at a given loading, this entire study has been presented on the basis of nominal stresses calculated as though the member were of uniform depth and of considerable length.

Since the critical behavior of the cantilever always follows the usual cracking in reinforced concrete, the cracking invalidates all the assumptions and conclusions of elastic deep beam theory. At no part of the investigation would the use of deep beam theory serve to explain member behavior better than ordinary beam calculations. Hence no further mention of deep beam theory will be made.

OBJECTIVE AND SCOPE OF INVESTIGATION

The purpose of this investigation was to establish reasonable and safe design procedures and stresses, especially shear and bond stresses, which could be applied in designing overhanging cantilever ends having proportions typical for highway structures. Although the conclusions are not intended to be limited to a particular member depth, all the members tested were 36 in. deep overall and all were reinforced with moment steels having pf_y values in a narrow range of some 380 to 450 psi, i.e., p values approximately 0. 0094 to 0. 0110 for an intermediate grade steel but p values lower for

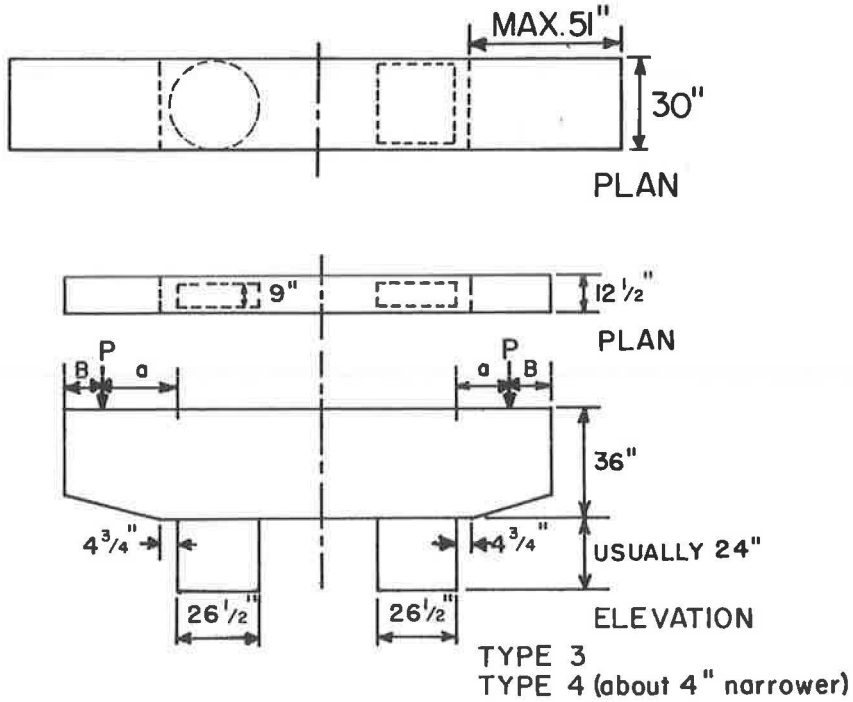

Figure 2a. Types of specimens and nominal dimensions.

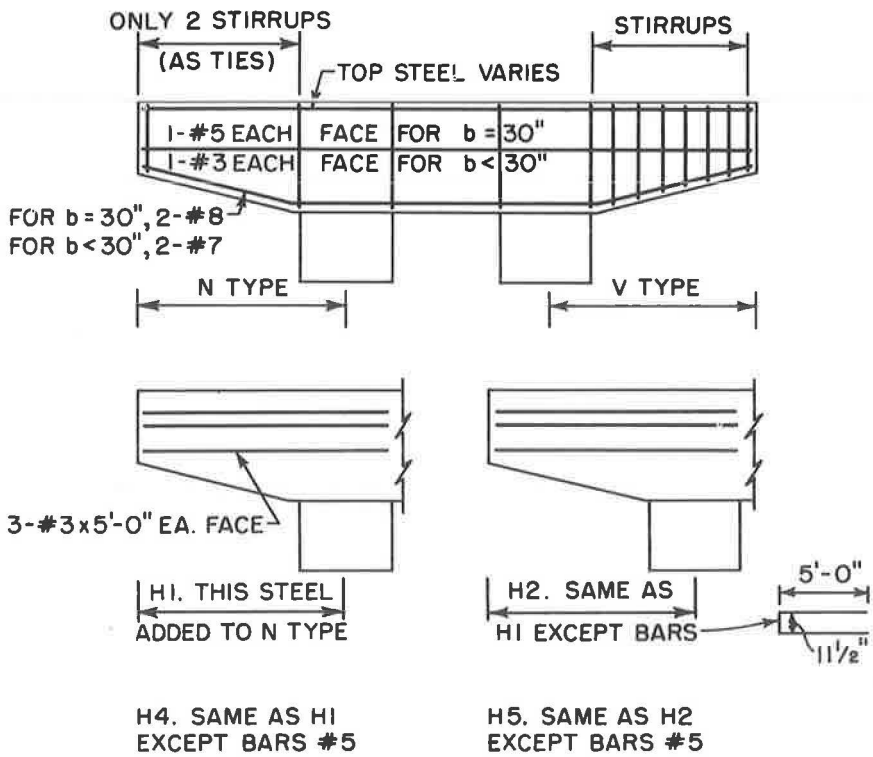

Figure 2b. Reinforcement patterns.

higher yield point steels. All loads were applied to the top of the members and the investigation is not intended to relate to cases where bridge girders might be monolithic with and at the same height as bent caps and thus would deliver their loads through a shear surface.

A total of 36 overhanging ends was made and tested (34 beams are reported here) with the following variables represented:

1. Distance of load from support.
2. Member length beyond center of load.
3. Grades of steel.
4. Type of web reinforcement, and with no web reinforcement.
5. A slight variation in bar size.
6. A limited comparison between circular and rectangular column supports.

TEST SPECIMENS AND PROCEDURE

All specimens had the same depth at the critical section (Fig. 2a). The distance a out to the load (called the shear span) and the extension B beyond the load (called the end anchorage length) were varied when casting the specimen merely by omitting any unwanted portion of the outer end. The bent proportions matched one of the Texas Highway Department standards.

Other than in length, there were many variations based on this standard. Among these variations were the following (Figs. 2a and 2b):

1. The shaft or column support was round (Type 1) with diameter equal to cap thickness (30 in.) or rectangular of the same cross-sectional area (Type 2).

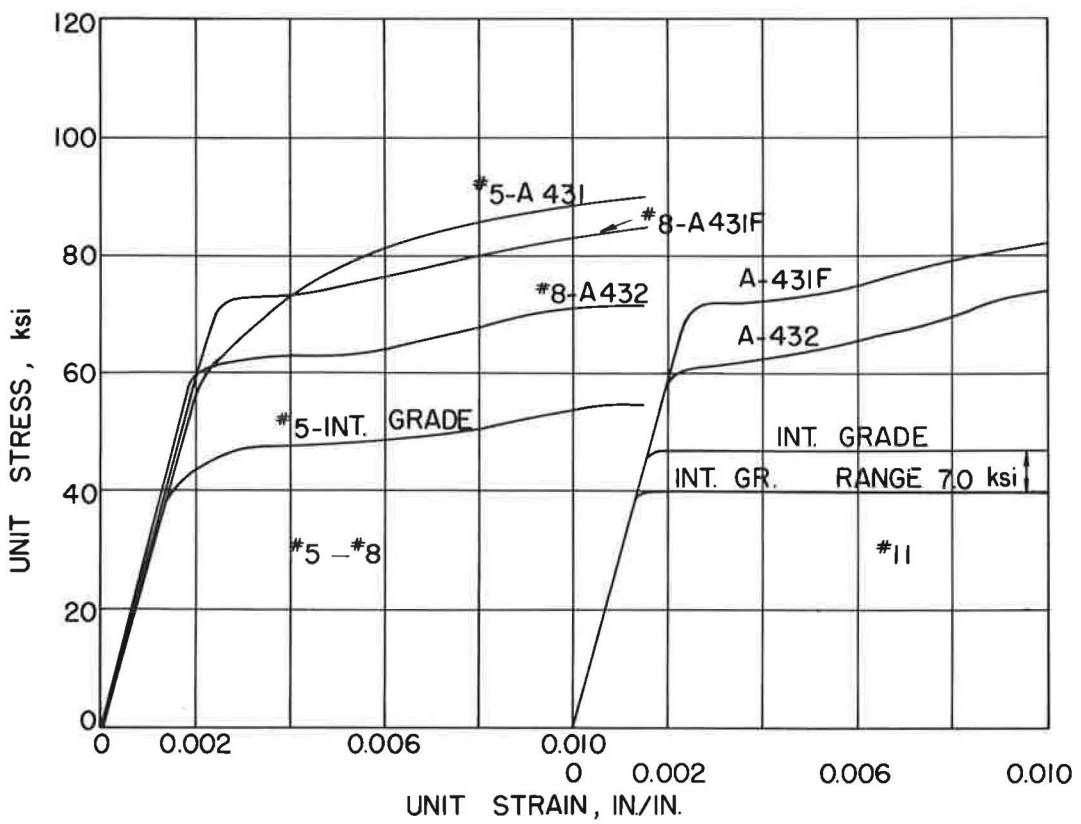

Figure 3. Reinforcing steels used.

2. The cap thickness, which was initially 30 in., was reduced to about 12. 5 in. (Type 3) with many of the rectangular columns, and for a few to 8. 5 in. (Type 4) without changing the reinforcement ratio. This was chiefly for convenience in testing.

3. The grade of main tension steel was varied between intermediate grade, ASTM A 432 and A 431 steels (Fig. 3), in each case maintaining nearly the same effective steel ratio pf_y/f_c'.

4. Bar size of main steel was usually No. 11, but No. 8 bars were also used with higher strength steels, and in a few cases a No. 5 bar was added with No. 8 bars to make up the desired tension capacity.

5. Stirrups were varied slightly in their ratio r, but primarily by complete omission or by placing horizontal steel in lieu of vertical stirrups, as in Figure 2b.

For convenience different specimens were cast at opposite ends of a common unit. An attempt was made to keep concrete strength constant, but transit-mixed concrete was used in all cases and controls were not adequate at times.

The specimens are listed in Table 1 in the Appendix with exact dimensions and reinforcing. The specimens are numbered in the sequence tested, but they are grouped according to type of specimen and reinforcement and are coded according to the following plan: First—the test serial number; second—type of specimen (Fig. 2a); third—pattern of reinforcing (Fig. 2b); fourth—quality of steel (4 for intermediate, 6 for A 432, 8 for A 431). Thus 31-1-V-4 indicates the 31st specimen tested, 30 in. wide with a round column, vertical stirrups, and main steel of intermediate grade.

Specimens and cylinders were cast from the following mix: High-early strength cement, 5 sacks (all quantities per cubic yard); Puzzolith, 5 quarts; Darex (air entraining), 2 oz; coarse aggregate (gravel), 2130 lb; fine aggregate, 1150 lb; water, 21. 4 gal. They were cast in wooden forms and cured in the forms under plastic covering until the day before the test (usually until the sixth day), and then tested the following day. The specimen, shown to the left in Figure 4b, was placed on its side on rollers and jacked against an anchor beam using steel yokes. The active jack and yoke is shown in the foreground. Since the cantilever end was statically determined, the location of the anchor yoke and jack was not critical and was usually over the other column. Load was applied, in increments, to failure except when failure required more than the 400k jack capacity. Crack lengths and widths were marked as the test progressed.

DATA

The ultimate loads and mode of failure are given in Table 2 in the Appendix. Also in this table are values of stresses calculated by standard ultimate strength methods as though for members of uniform depth:

$$f_s = M_u/(A_s\ 0.9d)$$
$$v = V_u/bd$$
$$u = V_u/(\Sigma o\ 0.9d)$$

These relations for f_s and for u were also used for beams with horizontal bars for web steel, thus ignoring the help this horizontal web steel should contribute towards f_s and and u stresses.

Since there was some scattering of f_c' values, corrections of v and u values were made to stresses corresponding to $f_c' = 4500$ psi by use of the relations $v_{4.5} = v\sqrt{4500/f_c'}$ and $u_{4.5} = \sqrt{4500/f_c'}$, which assume that v and u vary as f_c'.

Comparison of Round and Square Column Effects

In this investigation, as often is done in design, it was assumed that a round support might be replaced by a square support of the same cross-sectional area. The first variation introduced into the tests was an attempt to check the validity of this engineering

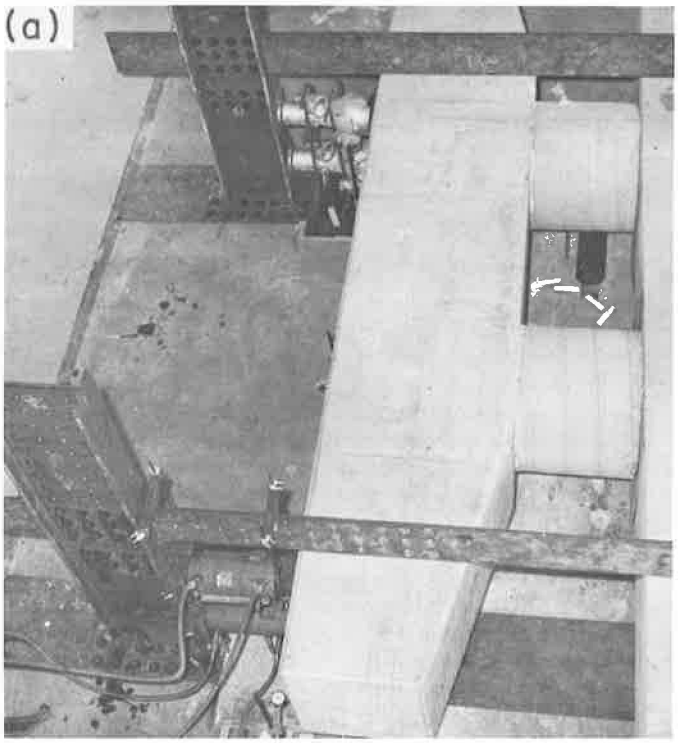

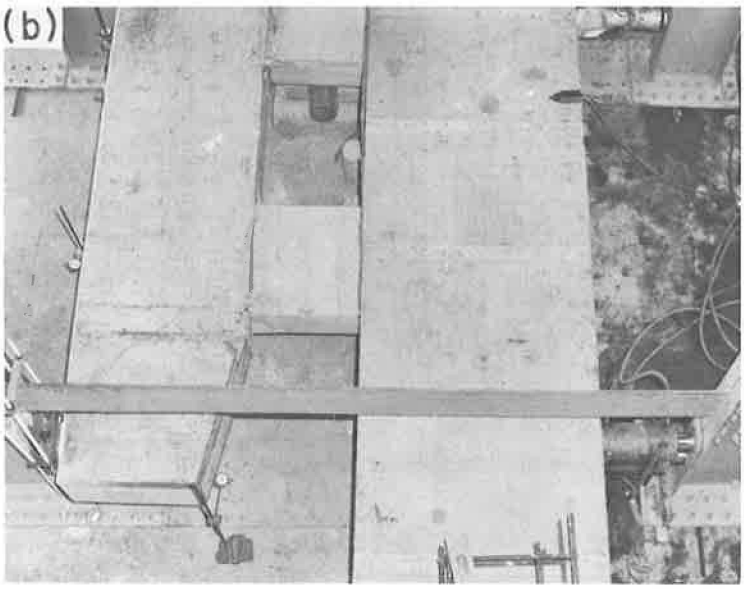

Figure 4. Test setup—load is applied at the near end. The jack position in (b) is the more stable. The load is applied to specimen through a 1-in. square rod between bearing plates in lower left corner.

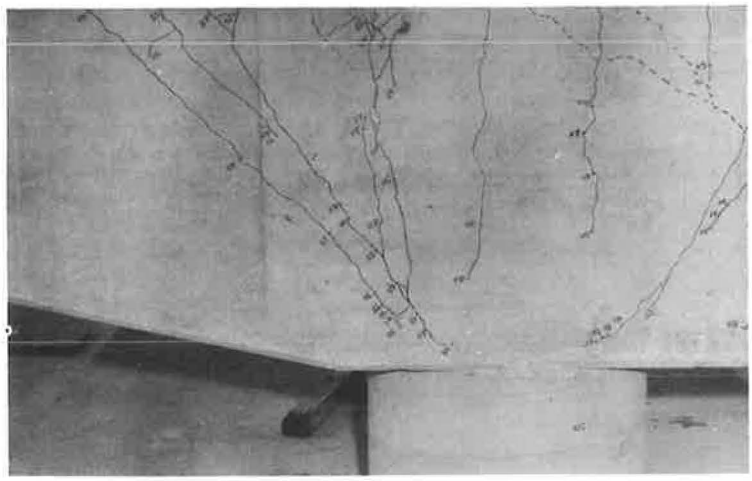

Figure 5. Side cracks tended to turn so as to intrude back into support area.

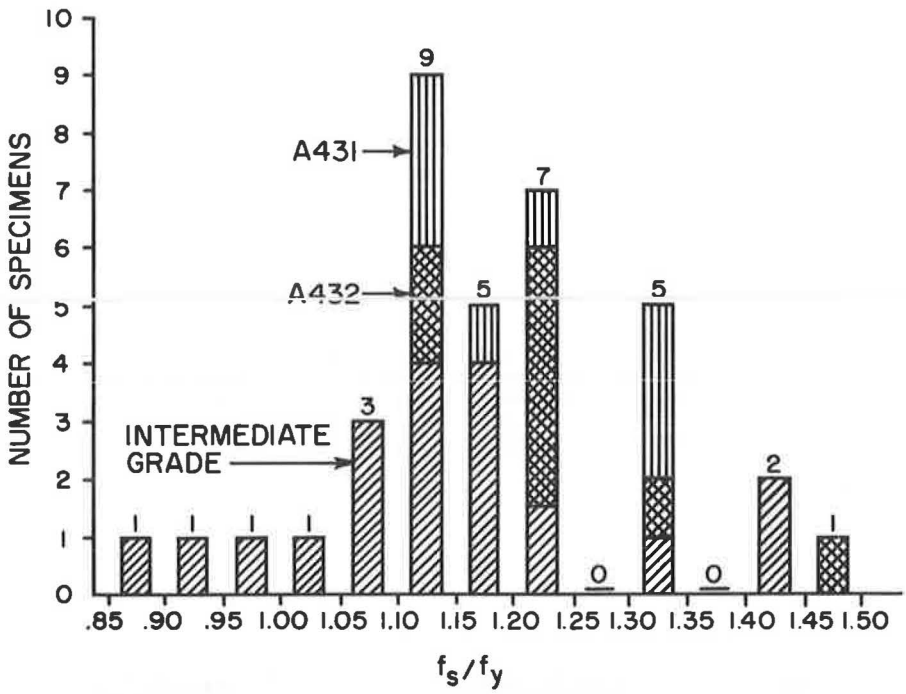

Figure 6. Histogram of ultimate f_s attained.

assumption. Specifically, specimens 1 and 3 with round columns were compared with specimen 4 with a square column, and similarly specimen 5 with specimen 6.

Unfortunately, in these early tests conclusive evidence of yielding of the main longitudinal steel was taken as evidence of flexural failure and the loading was not carried to secondary compression failure. This was only in part a technical decision, since the test equipment established a 400k limit. Specimens 1, 3, and 5 reached 399k, 402k, and 391k, respectively, before the tests were stopped.

These comparisons were not conclusive but they showed no difference greater than 6 percent and the differences were in opposite directions for the 2 sets, with developed steel stresses of 119 to 120 percent of yield strength. Accordingly, the later specimens generally used rectangular columns and a reduced width which brought most specimens well within the capacity of the test equipment, even for loads closer to the support.

It was observed that both round and square columns introduced a cracking phenomenon different from that which would have accompanied a square support extending all across the cap. In the latter, flexure cracks would tend to run to the support edge and very little inside it. In the tests reported here, these cracks extended 6 to 8 in. inside the support (Fig. 5), and this was more apparent with the circular columns than with the square columns. This suggests that with both types the crack surface inside the cap is probably not a plane surface from side face to side face.

Flexural Strength

In only 3 out of 36 specimens did members fail in any fashion before reaching the calculated yield point of the longitudinal steel. In only 5 cases did failure occur at less than 1.09 f_y. Thus in the following discussion of ultimate shear and bond it must be kept in mind that the failures were chiefly in members already well past their computed flexural capacity. This is illustrated by the bar charts in Figure 6 showing the distribution of calculated f_s/f_y for the 3 separate steel grades. These charts show that the concrete strains associated with high-strength steels constituted no handicap insofar as flexural strength was concerned, the low f_s/f_y values being for specimens failing in bond or shear. Crack width is discussed separately in a later section.

Shear Strength

When all failure points or maximum load points are plotted in terms of shear (Fig. 7), there is considerable scatter, with a general trend of higher values showing for small shear spans (the distance as shown in Fig. 2a). All shear values are much higher than ordinarily used in design. Each of these points constitutes a fair "proof load" measure of capacity in shear, but the bond failures and flexural failures cannot properly be used in setting the lower limit for shear capacity. When such failures are culled out of the lower regions (Fig. 8), the number of points is more limited but is adequate to support the dotted curve as a safe lower boundary. Within this limited a/d range and for an f_c' of 4500 psi this curve can be defined by the equation

$$v_u = 320 + 140d/a \qquad (\text{for } 0.5 < a/d < 1.2)$$

These shear stresses are quite large in terms of the usual accepted design values.

The Joint ACI-ASCE Committee on Shear and Diagonal Tension reported that it would be safe to design beams on the basis of shear stresses at a distance d from the face of the support and then to use the same web reinforcement (if any) back to the support. The next section in the present report indicates that vertical stirrups as actually used contributed little or no strength although their contribution to the calculated ultimate strength was from 135 psi to 160 psi for the various specimens. The Joint Committee recommended that shear on the concrete itself be limited to the diagonal cracking stress, which is approximately $2\sqrt{f_c'}$, or 136 psi for an f_c' of 4500 psi. Thus the sum of these 2 components might be calculated as 136 plus 160 (maximum) for a total of 296 psi. In contrast, the value proposed here (without stirrups) becomes 460 psi for an a/d of 1.00. This is no discredit to the Joint Committee report, which was not aimed at the short a/d values of importance in the design of the overhanging end of a bent cap.

Influence of Web Reinforcement

The data can be analyzed further for the influence of horizontal or vertical web reinforcing. To simplify the comparison, Figure 9 has been prepared from Figure 8

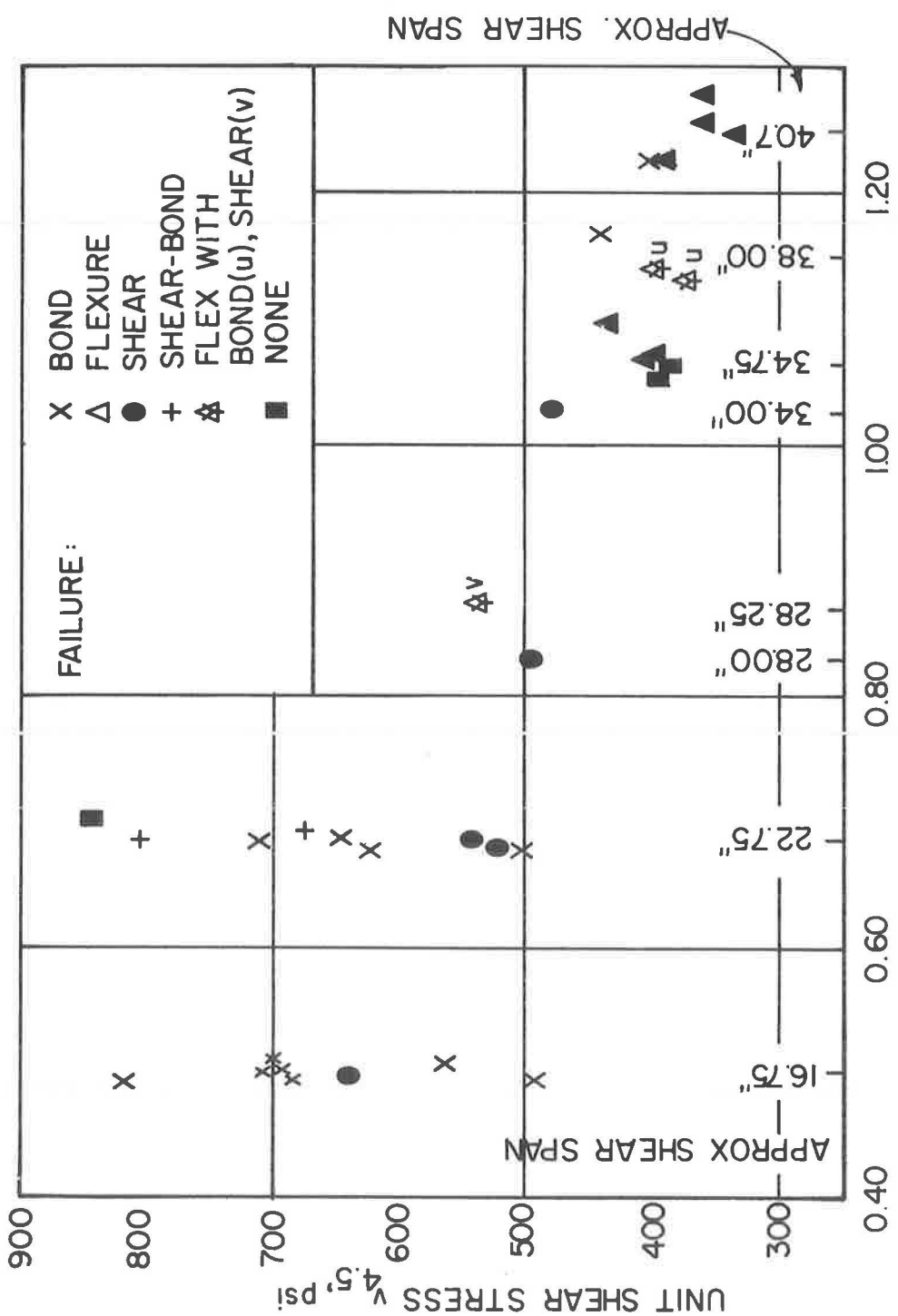

Figure 7. Ultimate shear stress, including all types of failure.

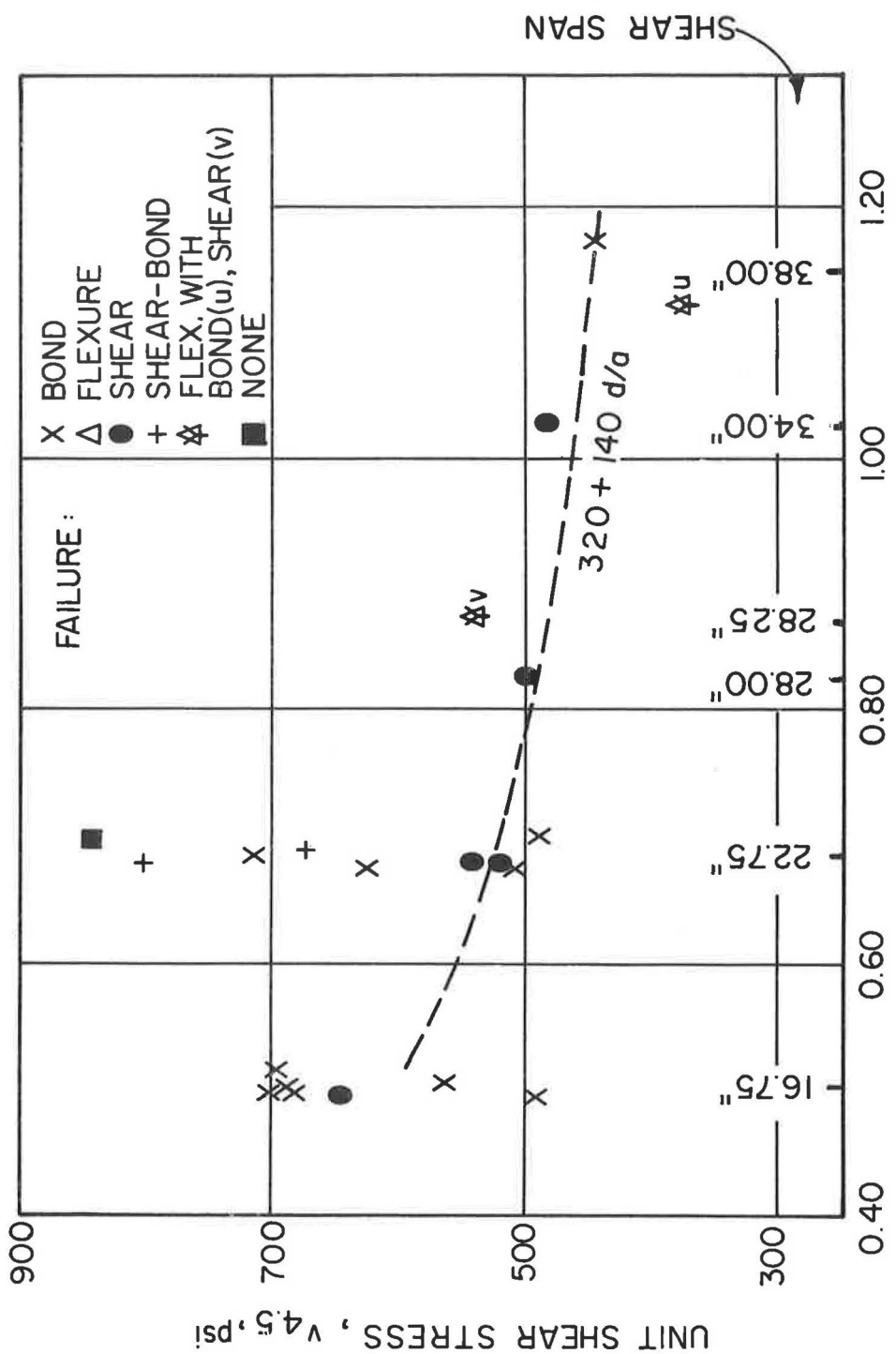

Figure 8. Ultimate $v_{4.5}$ for shear failures and for bond failures which also serve as proof loads.

to show only a comparison between vertical stirrups (V) and no stirrups at all (N). The X marks represent bond failures and thus the 3 low points on the left are shown only to account for all members made without stirrups. In the upper left are 4 bond failures which do have significance as proof loads, to show at least this much shear capacity.

The direction of cracks in early tests had indicated that very few stirrups were crossed by the critical cracks. Hence it was suspected that the stirrups were nearly ineffective. In Figure 9 a detailed comparison at each given a/d indicates that the vertical stirrups either add nothing to the strength, or, more probably, that the amount they add is so small that it is lost in the ordinary scatter of the experimental data.

The steepness of the observed "diagonal" cracks suggested that horizontal steel would be more effective than vertical steel in improving shear strength.[1] Unfortunately all horizontal steel was used in specimens having a small end anchorage beyond the load (B in Fig. 2a) and thus probably failed to show the full potential of this shear reinforcement.

The effect of U-shaped horizontal steel is shown in Figure 8 by points H4-22 and H5-28. The first of these, of No. 3 bars, failed in bond but with a shear strength 35 percent above the lower bounding curve. The second, of No. 5 bars, did not fail in the cap because of a premature column failure, but it reached a shear stress 60 percent above the bounding curve. Of the 3 specimens made with horizontal side bars not having either hooks or end loops, 2 definitely failed in bond (one at a shear 6 percent below the curve, one at a shear 36 percent above) and one failed in combined shear and bond at very satisfactory shear stresses.

These data strongly support the idea that vertical stirrups are of little value and that looped horizontal stirrups can add substantial shear strength. The scope of this investigation did not permit complete evaluation of the horizontal bars. It is even possible that the high shear capacity shown without any web reinforcement makes the higher value with horizontal web reinforcement of little practical importance.

Flexural Bond Stress

When all the calculated bond stresses at failure are plotted, excluding definite flexure failures and shear failures (Fig. 10), the overall picture is still somewhat confusing. The very fact that bond stresses of 1500 to 1900 psi were calculated on No. 11 bars is evidence that these are not real stresses, because No. 11 bars do not have this bond capacity. The calculated values emphasize the comment in the opening paragraphs of this report to the effect that steel tensile stress increases at a less rapid rate than moment such that $u = V/(\Sigma o\ jd)$ is a purely nominal calculation for these short cantilevers. At the same time many calculated values are quite reasonable, around 600 to 800 psi, and a couple are in the 400 to 500 psi range, a little low.

Closer investigation indicated that not a single beam having an end anchorage (B in Fig. 2a) in excess of 9 in. failed in bond and only one beam having an end anchorage as small as 5. 5 in. (Specimen No. 16[2]) escaped without a bond failure. Thus it appears that bond failure can be avoided by the simple expedient of extending the bars more than 9 in. beyond the center of the applied load. The tests show that 14 or 15 in. is adequate end anchorage even though the developed steel stress is quite high. It is probable that even a 12-in. end anchorage is adequate, based on the trend of the data, although there are no tests of this length. With adequate end anchorage there seems to be no reason to calculate the ordinary bond stress at all.

In spite of the fact that it appears the best design technique is to avoid bond problems by using end anchorage, there were some interesting trends indicated by the bond failures. It was first suspected that the high bond values might relate to No. 8 bars

[1] In spite of the fact that German tests with highly stressed webs in I-shapes have shown that horizontal web bars lowered the compression "diagonal" strength and resulted in lower shear strengths because of diagonal compression failures.

[2] Specimen 16 had to be classified as a combined shear and bond failure, which means it could have been a shear failure.

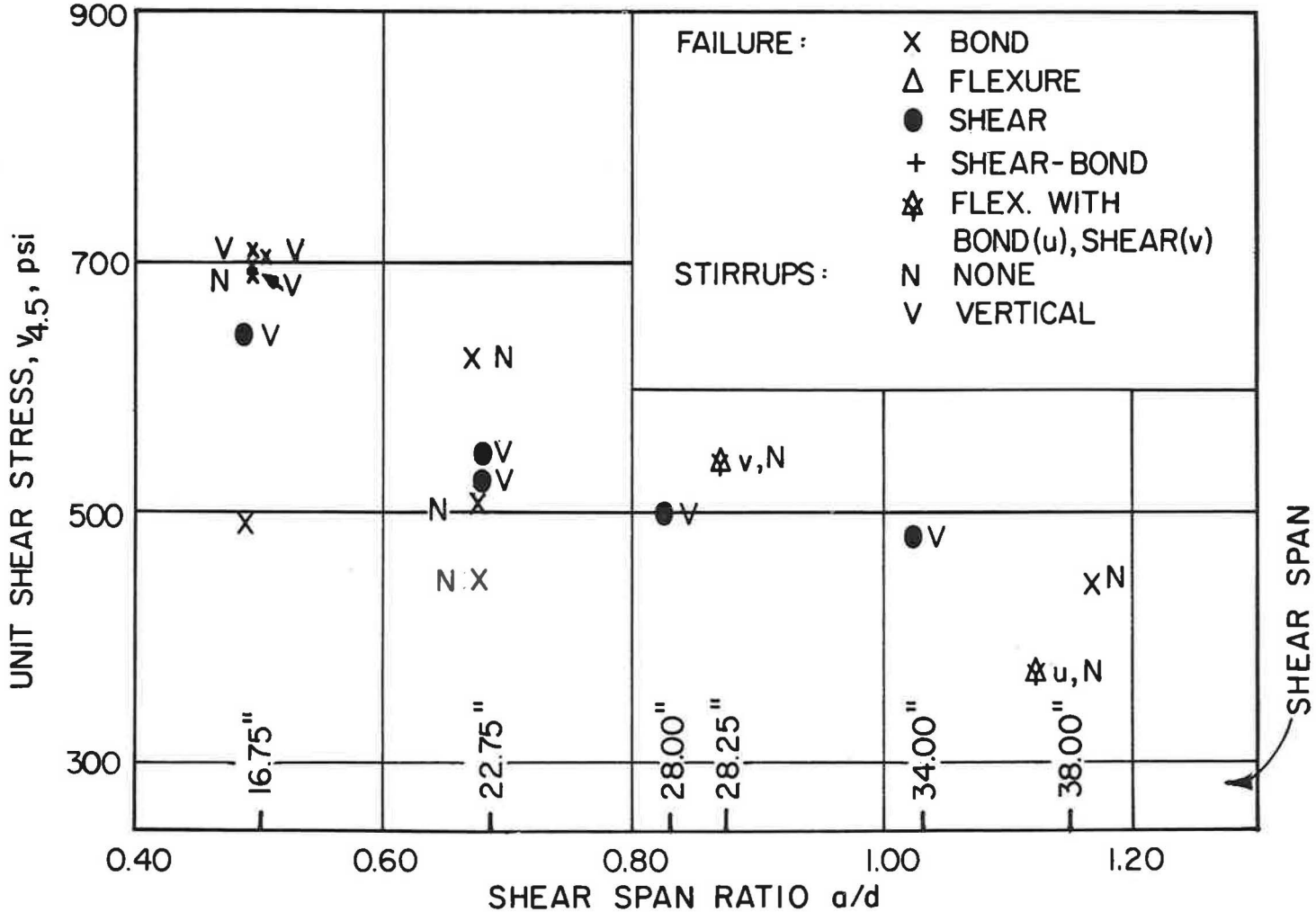

Figure 9. Ultimate $v_{4.5}$ comparing vertical stirrups with no web steel.

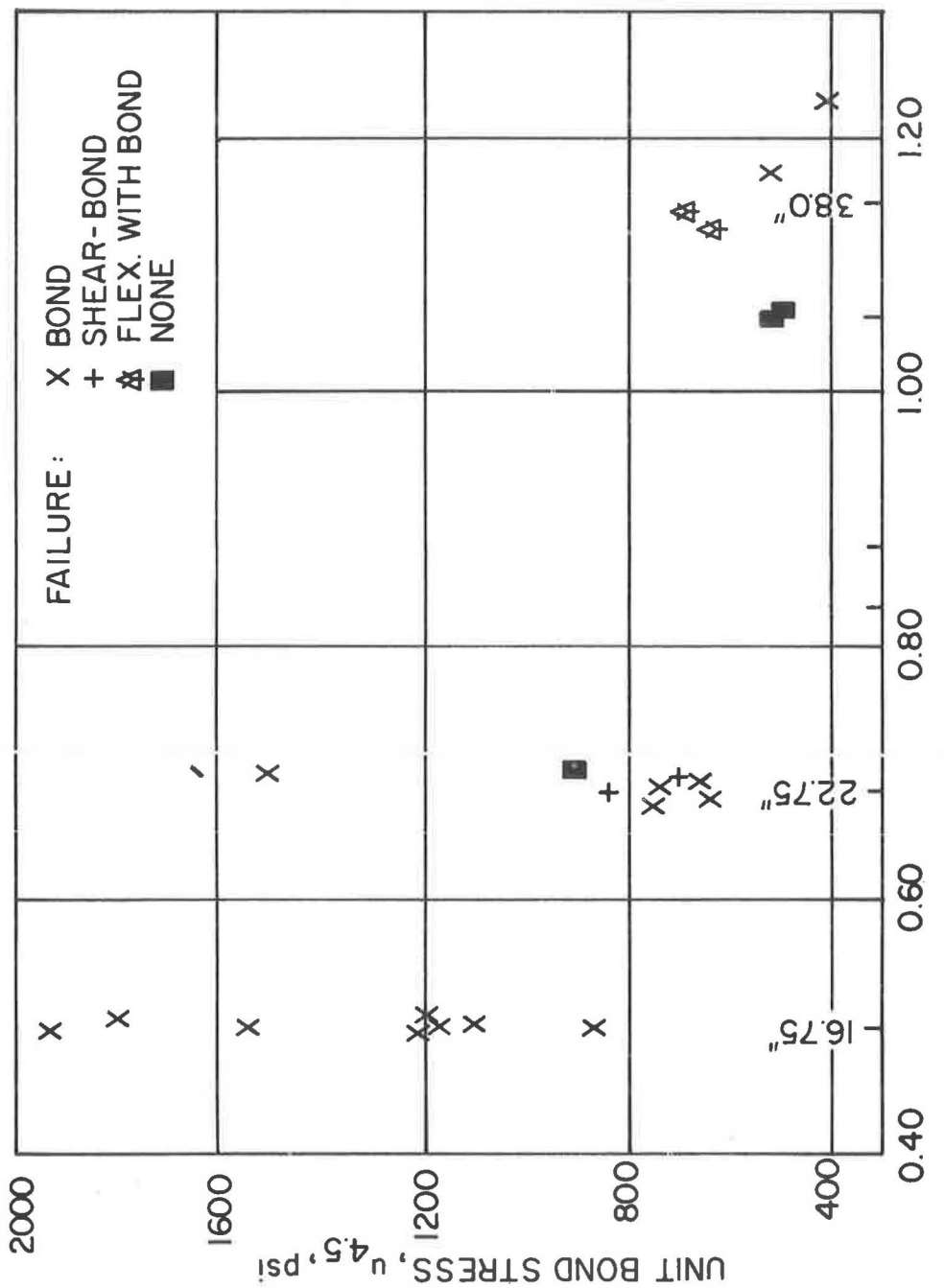

Figure 10. Bond strength related to shear span.

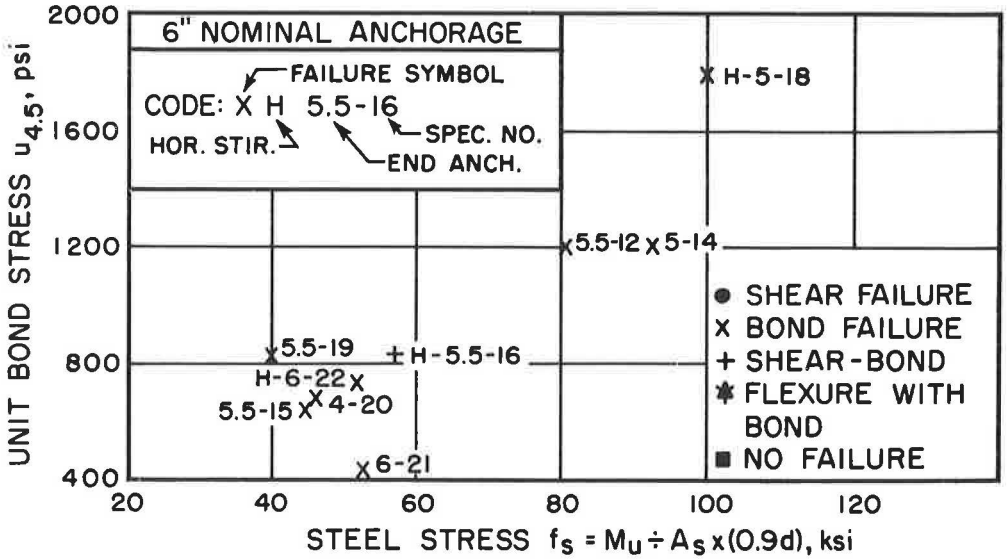

Figure 11. Variation of bond strength with steel stress for 6-in. anchorage.

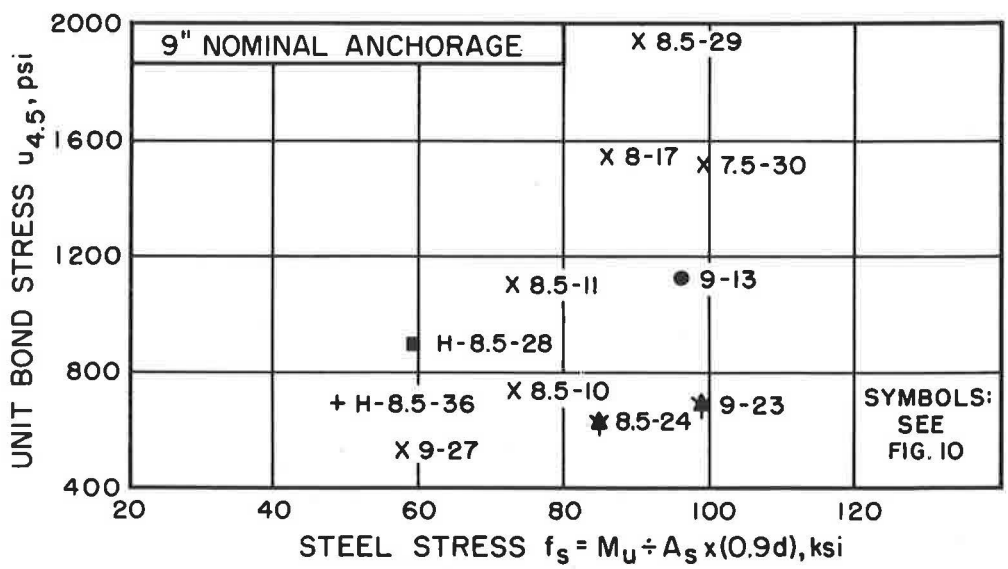

Figure 12. Variation of bond strength with steel stress for 9-in. anchorage.

and the low ones to No. 11 bars, but it was found that both the highest and the lowest values applied to No. 11 bars and the No. 8 bars fell in between. The larger shear span ratios showed lower minimum bond values and the smaller shear spans showed higher minimum values, all within the 400 to 800 psi bond stress range.

It must be noted that the only 3 recorded values of ultimate $f_S/f_y < 1.0$ were caused by bond failures and represented anchorage lengths of 4 to 5. 5 in. In general all other bond failures came after the calculated steel stress was much greater than f_y, a condition generally thought to be adverse to bond strength. This situation was explored further. Figure 11 plots the developed bond stress against ultimate f_S for all end

anchorages of 6 in. or less; it shows much higher bond stresses for higher steel stresses. The values for nominal anchorages of 9 in. in Figure 12 show a similar trend, although there are also 2 low specimens in the 85-100 ksi steel stress range (which showed rather minor evidence pointing toward the possibility of bond failure and possibly do not belong in this figure). These figures may be taken as further evidence that it is not really calculated bond stress which caused failure, but something else, such as end anchorage.

Examination of these bond values in excess of 1000 psi, 8 specimens in all, showed that 6 represented A 431 steel and two A 432 steel. The A 431 steels developed from 1. 14 to 1. 34 times their nominal yield stress before failing in bond stress. The A 432 steels developed 1. 13 to 1. 24 times the measured yield point. Thus it could be said, even for these short end anchorages, that all these 8 cases were primary flexural failures with a secondary failure in bond. The interpretation which is here preferred is that, even with fairly small end anchorages, the steel can develop to high values of strain (and high stress in high strength steels) before failing at the end anchorage. Thus a 12- or 15-in. end anchorage beyond the center of load could develop almost any commercial reinforcing steel and still not fail in bond.

The bond stress data are presented in another manner in Figure 13, which plots the ultimate bond stress against the ratio of end anchorage to the shear span a. This shows high bond strengths attainable for an anchorage-arm ratio from 0. 30 to 0. 55, but there are also lower values included in the ratio range of 0. 30 to 0. 40. It is interesting to note that all bond values in excess of 1000 psi were in beams with calculated f_s values of 73 to 100 ksi.

The most serviceable conclusion that can be noted from the study of bond stress is that in only a few cases (and then for very high bond stresses) did splitting seem to work along the bars all the way to their end. In most cases the failure was a sudden one suggesting that the end of the anchorage slipped and permitted an entirely new diagonal crack to develop as evidence of this failure (Fig. 14). Empirically the data seem to indicate that, if end anchorage of as much as 12 or 15 in. is provided, one can forget bond stress completely in evaluating the strength of the cantilever. A number of specimens with a 9-in. end anchorage did not fail in bond, indicating that for the No. 8 and the No. 11 bars used here this was about the breakpoint between bond and other types of failure.

Effect of Embedding Column Shaft in Cap

Specimens 31 and 32 were made identical with the early full-size specimens except that the precast round and square shafts were each extended 6 in. into the cap form before the cap was cast. It was thought that this type of specimen might show some sign of weakness or a reduced effective depth. These 2 tests were only partially effective. The concrete strength was some 8 percent greater than on the original specimens and the full capacity of the loading frame and jacks was not enough to bring the specimen to failure. However, crack widths of 0. 5 mm and 0. 6 mm were attained and it was estimated that flexure failure would have occurred with not over 5 or 10 percent more load. Although the earlier specimens had been marked as flexure failures, they were not actually carried to their secondary failure in compression.

Up to the 400-k load the specimens with the 6-in. embedment of the shafts performed quite similarly to those where the cap was cast just in contact with the top of the shaft. The shear $v_{4.5}$ sustained was 399 psi and 393 psi at a shear span of 34. 75 in., which can be compared with a calculated v_u of 454 psi suggested in Figure 8 as a minimum for design. The embedded specimens thus came within 12 percent of the expected shear strength and showed no evidence of impending shear distress. A complete check on shear strength of embedded specimens would require more specimens, including short shear spans, and the present equipment would not be adequate for this large a load. In other words, the length actually tested would normally lead to a flexure failure, as indicated for these specimens.

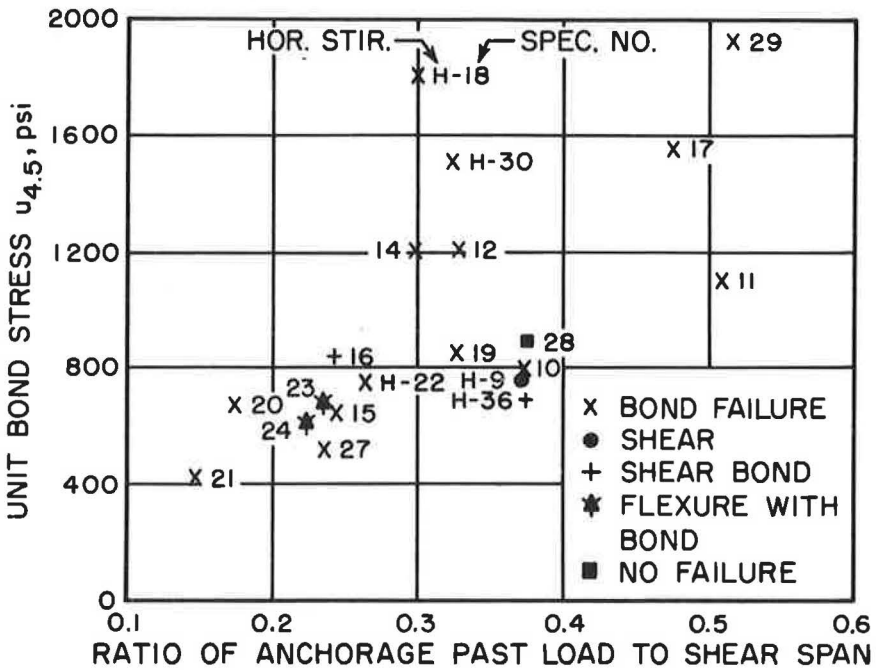

Figure 13. Variation of bond stress with position of load.

Crack Widths in Flexure

In the use of steels stronger than intermediate grade, the crack width at service load becomes important. Crack widths were carefully measured and recorded, but must be interpreted somewhat cautiously. Crack width always varies from point to point. Occasionally a crack splits into 2 branches and occasionally it is joined by a meandering neighboring crack. To all to these problems, although measuring devices are subdivided to 0. 2 mm and distances can easily be estimated to 0. 04 mm (0. 0016 in.), the cracks have ragged or jagged edges to such an extent it seems useless to record cracks this closely. Records were made in terms of "small" (less than 0. 5 mm), 0. 1 mm, 0. 2 mm, etc. Crack widths were recorded at points where a crack crossed one of the grid lines, which were 6 by 6 in. on the sides and top for the 30-in. width, and 6 by 4 in. centered on the top of the 12. 5- and 8. 5-in. widths.

In Table 3 in the Appendix the steel stress calculated for the loading which first produced a surface crack width of 0. 2 mm (0. 008 in.) at any one point is tabulated for each specimen, grouped by grade of steel, size of bar, and the presence of horizontal web steel. This crack width is approximately the maximum that would be universally acceptable for construction not protected from the weather. Since some might accept a wider crack width the same table shows comparable data for a crack width of 0. 4 mm and also the steel stress at initial cracking. The average values of stress are plotted separately for each classification in Figure 15 and the curves for No. 11 bars are grouped together in Figure 16. The higher a curve the more favorable it is, because it means the member sustained a higher f_s before developing a crack of the width plotted. Average concrete strengths are marked for A 431 and A 432 steel specimens. For the intermediate grade steel the strengths averaged nearly the same, 5030 psi for the specimens with horizontal web steel, 4750 psi for the others.

It was somewhat of a surprise to find that the A 431 steel sustained a higher stress before reaching each crack width. It is easy to see that the calculated stress at initial cracking should be higher for this steel. The cracking moment itself is influenced only slightly by the area of steel present. At cracking the total tension originally

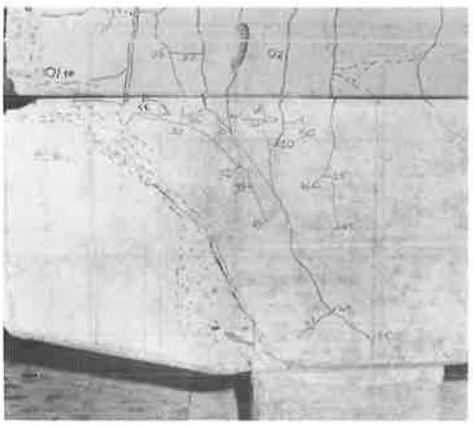

Figure 14. Bond failure (end anchorage failure).

carried in the concrete (about the same for all steel grades) must move into the steel. Thus the smaller the steel area, the higher will be the calculated steel stress at the cracking load. However, it is not evident why A 431 No. 11 bars stressed to a nominal 40 ksi produced a crack width (at 0. 008 in.) no greater than intermediate grade No. 11 bars developed at 26 ksi. At the 0. 008-in. crack width only one intermediate bar specimen had reached a calculated stress as high as 37. 6 ksi and no A 431 bar showed less than 37. 4 ksi.

In terms of design it is probable that average crack width should be considered. In these data the widest measured point on each specimen is reported and the average

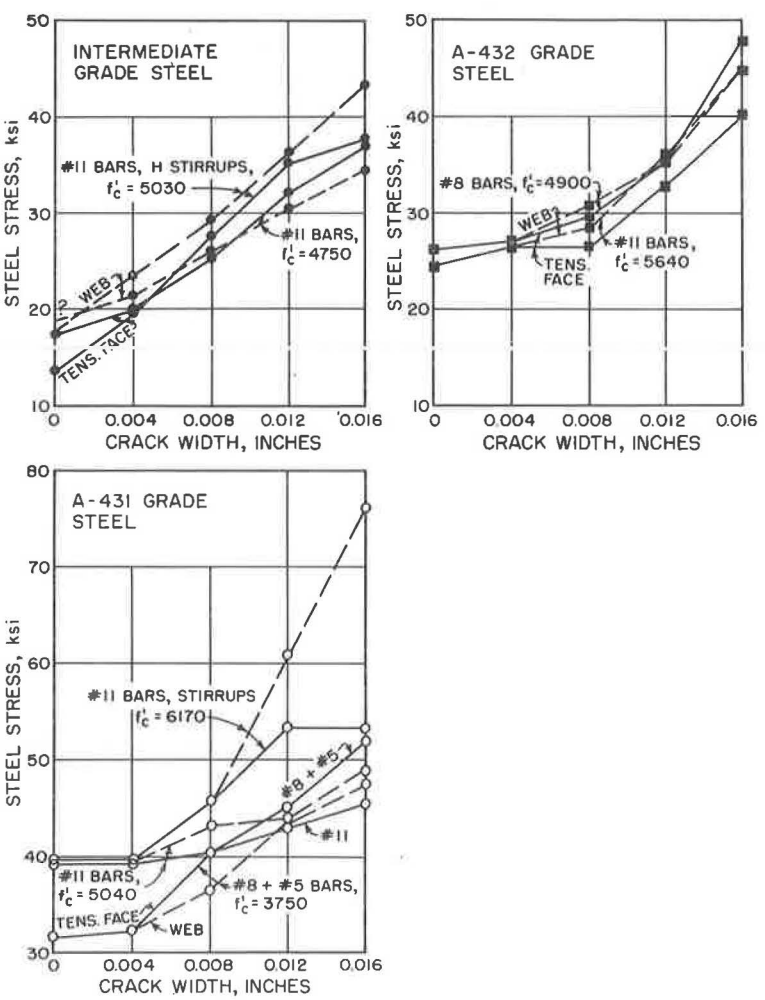

Figure 15. Crack widths with and without horizontal web reinforcing.

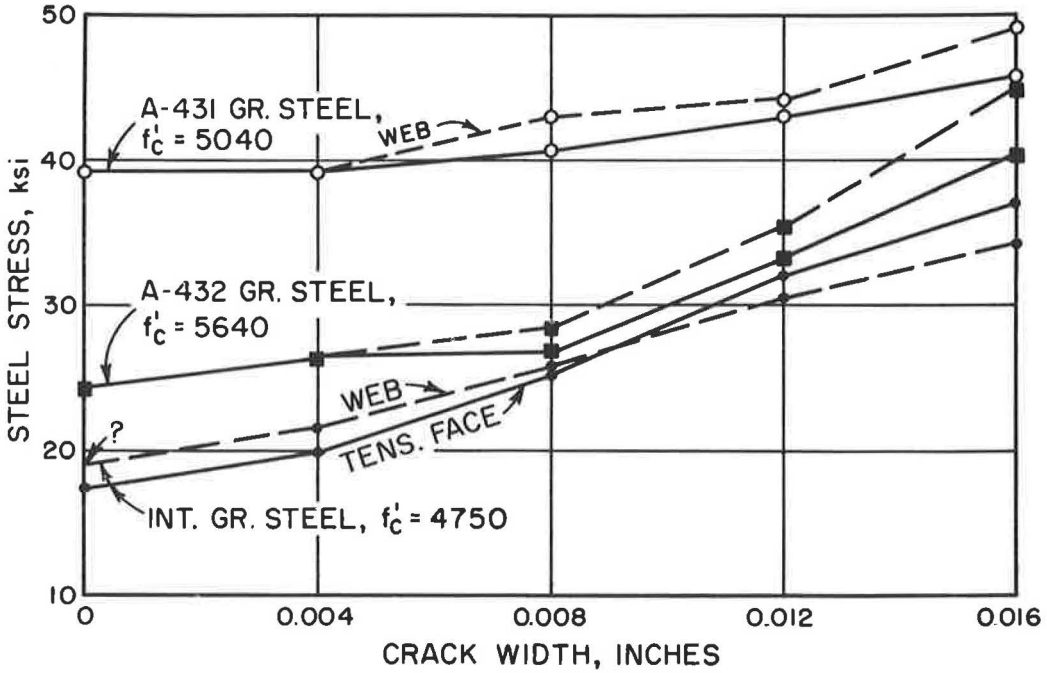

Figure 16. Crack widths for various grades of steel, No. 11 bars.

given is an average including only these worst points. Hence it is a little severe to use these data. Nevertheless, on this basis Figure 16 indicates the following unit stresses would give reasonable crack widths with No. 11 bars for a service load equal to half the ultimate design load:

Grade	No. 11 bars	No. 8 bars
Intermediate grade	f_s = 25 ksi = 0.62f_y	—
A 432 grade	f_s = 26 ksi = 0.43f_y	29 ksi = 0.48f_y
A 431 grade	f_s = 40 ksi = 0.53f_y	40 ksi = 0.53f_y

In general these data support the use of a working stress design based on half the minimum yield point, although this is somewhat high for the A 432 data (especially for No. 11 bars) and somewhat conservative for the A 431 grade. With intermediate steel, flexural crack width is apparently no problem.

Crack Widths on Sides of Cap

In advanced cases of shear distress it is commonplace to observe in laboratory research diagonal cracks which are wider than flexural cracks, especially on small shear spans. However, it was noticeable in these deep beams that side crack width near mid-depth was from the beginning nearly as wide as the cracks on the tension face, and this is not commonly observed. This was in spite of the standard use of the equivalent of one horizontal No. 5 bar on each face at mid-height (for a 30-in. width specimen). This excessive side cracking suggested the need for more horizontal side steel.

Five specimens were further reinforced with horizontal side bars and these did show more favorably, that is, higher calculated steel stresses were reached in these specimens before developing any given crack width. The increase in nominal steel

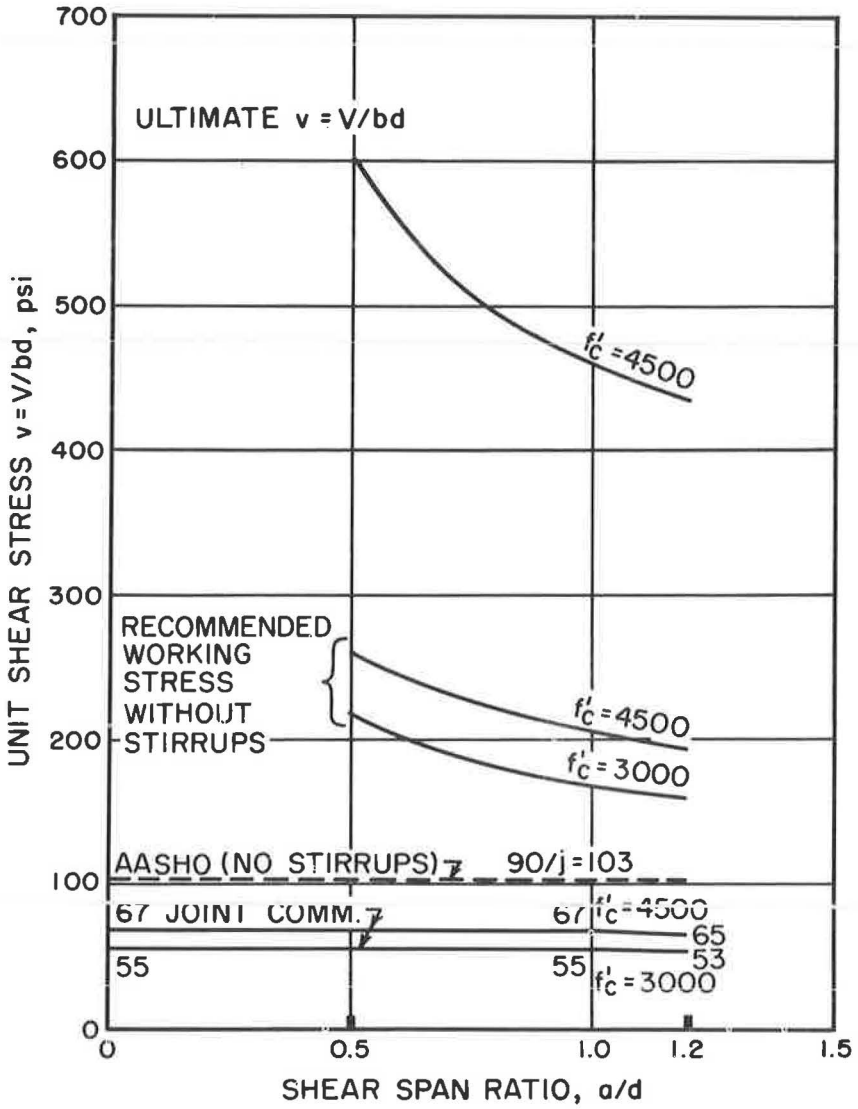

Figure 17. Recommended shear stress comparison.

stress averaged upwards from 16 percent and was greater when No. 5 bars were used than for No. 3 bars. Part of the increase was purely nominal; part was the effect of a higher f_c' (for A 431 steel); but part must represent the effect of better directed reinforcement. The calculated steel stress was based solely on the nominal area of steel, ignoring the horizontal web steel. While actual steel stresses would be lower than these calculated values, a more exact calculation would account for not over half of the benefit observed.

DESIGN CONCLUSIONS

Behavior of Present Designs

The bent cap from which the tests were modeled behaved excellently in the tests, its only deficiency being in wider side cracks than were expected. Even these side cracks were not wider than commonly accepted on the tension face in flexure.

Flexure

In flexure the use of ordinary beam theory, without any correction for variable depth, gave f_s values which seemed to be in good agreement with test results. The moment was calculated from the face of a square support having the same area as the circular column. It appears that no modifications in ordinary flexural theory (for uniform depth members) are needed for these short-span cantilevers so long as they are designed to fail in tension rather than compression. This should be a normal procedure since ultimate strength design theory shows that a beam balanced by working stress methods will always fail in tension. Furthermore, beams designed for compression failure are expensive and are undesirable because of their sudden failure mode.

Beams designed in flexure with A 432 steel (minimum f_y of 60 ksi) would be more economical than beams using intermediate grade steel. While crack widths with such steel may not make a 30-ksi design stress (working stress) desirable, certainly 24 or 26 ksi appears entirely feasible. The upper boundary of usable stress might be raised further by additional studies with this grade of steel.

Shear Strength

Within a shear span-depth ratio of 0. 5 to 1. 2, the ultimate shear strength may be conservatively evaluated much higher than used in the past, for f_c' of 4500 psi as

$$v_u = V/bd = 320 + 140\ d/a$$

For working stress design with a factor of safety, say, of 2. 25 this becomes

$$v = V/bd = 142 + 62.5\ d/a \text{ (for } f_c' = 4500 \text{ psi)}$$
$$v = V/bd = 116 + 51\ d/a \text{ (for } f_c' = 3000 \text{ psi)}$$

The latter value assumes that v varies as the $\sqrt{f_c'}$, as is now commonly accepted. These values compare with AASHO allowable values of 90 psi for V/(bjd), or 103 psi for V/bd, for either grade of concrete without stirrups, as plotted in Figure 17.

The more recent Joint ACI-ASCE Committee recommendation was more conservative, for $d/a \leq 1$ an ultimate shear of

$$v_u = 1.9\sqrt{f_c'} + 2500\ p^*$$

For $f_c' = 4500$ psi and 6 No. 11 bars in a 30-in. width ($p = 0.00945$) this becomes

$$v_u = 1.9\sqrt{4500} + 2500 \times 0.00945 = 127 + 24 = 151 \text{ psi}$$

With the same 2. 25 factor used above this reduces to 67 psi for f_c' of 4500 psi and 55 psi for f_c' of 3000 psi, substantially lower than the AASHO allowable values. However, the Joint Committee was not primarily interested in these small a/d ratios; the recommendations suggested here are only for $0.5 < a/d < 1.2$.

The recommendation from these tests would thus substantially raise the presently specified shear capacity without stirrups for $a/d < 1.2$, as Figure 17 shows.

Stirrups

It is noted that the above comparisons have been made without stirrups. Vertical stirrups did little good insofar as the test observations showed. Specimens without any stirrups were on the whole as good as those with vertical stirrups (which ordinary

*The last term is $2500\ p\frac{Vd}{M}$ for $a/d > 1$.

working stress theory would value at 67 psi). Horizontal web reinforcing with one closed end did reduce crack width and raise the strength in shear. The data here are inadequate to do more than support a recommendation that if web reinforcement is used, as probably is desirable, the same metal placed horizontally over the upper 60 percent of the effective depth will serve a more useful purpose than vertical stirrups. The greatly increased shear values recommended make web reinforcement much less necessary.

Bond Strength

The tests indicate that bond stress between load and support constitutes no problem for these small a/d ratios, even with the small perimeter furnished by high strength steel. On the other hand, end anchorage beyond the center of the outermost load is essential. All specimens with a 6-in. end anchorage failed in the anchorage in bond. Since no bond failure occurred with a 15-in. end anchorage and only about half of the 9-in. end anchorages showed distress even at high f_s values, it appears amply safe to specify a 15-in. end anchorage for No. 11 bars and a 12-in. end anchorage for No. 8 bars. This assumes that no bar is cut off within the shear span and that all bars extend for the stated end anchorage.

If the above conditions, that is, both small a/d and adequate end anchorage, are met, it appears that no limit needs to be set on allowable u calculated from $u = V/(\Sigma o\ jd)$. The calculation is not an indication of whether the member is safe or unsafe; safety depends on the end anchorage.

This end anchorage distance could probably be reduced by a cross bar welded across the end or some other type of end anchor. Such devices should be tested before their use is recommended. The Portland Cement Association has had good success with the welded crossbar in research.

ACKNOWLEDGMENTS

The tests described here were conducted as part of the overall research program of the University of Texas Center for Highway Research. The work was sponsored jointly by the Texas Highway Department and the U. S. Bureau of Public Roads under an interagency contract between the University of Texas and the Texas Highway Department. Liaison with the Texas Highway Department was maintained through the advisory committee for this project consisting of Wayne Henneberger, Robert L. Reed, and Larry G. Walker.

Appendix

TABLE 1 SPECIMEN PROPERTIES

Specimen Code	b in.	d in.	Clear Cover, in.	f'_c psi	f_y ksi	A_s	Arm a, in.	Bar Extension B, in.	Stirrups
Flexure failures - full width specimens									
1-1-V-4	30.1	31.6	3.69	4200	45.4	6-#11	34.75	21	#5@6"
2-1-V-4	30.1	32.0	3.35	4340	45.4	6-#11	40.75	15	#5@6"
3-1-V-4	30.2	32.7	2.74	4470	46.4	6-#11	34.75	21	#5@6"
4-2-V-4	30.1	32.5	2.98	4470	46.4	6-#11	34.75	21	#5@6"
5-1-V-6	30.2	32.7	2.99	5520	66.5	4-#11	40.75	15	#5@6"
6-2-V-6	30.2	32.6	2.93	5750	66.5	4-#11	40.75	15	#5@6"
Flexure failures - narrow specimens									
7-3-V-6	12.25	33.3	2.65	4700	64.9	3-#8	40.75	7	#3@4¼"
Combined flexure + shear - narrow specimens									
35-3-N-4	12.25	32.4	3.17	5050	39.8	3-#11	28.25	8.7	None
Combined flexure + bond - narrow specimens									
23-3-V-8	12.62	33.8	2.28	3290	75.4	2-#8, 1-#5	38.50	9	#3@4¼"
24-3-N-8	12.44	33.9	2.19	2860	75.4	2-#8, 1-#5	38.00	8.5	None
Flexure failure approached (loading stopped) - 6" embedment									
31-1-V-4	30.25	33.0	2.83	4820	43.8	6-#11	34.75	21	#5@6"
32-2-V-4	30.25	32.8	2.54	4820	43.8	6-#11	34.75	21	#5@6"
Shear failures - narrow specimens									
9-3-N-6	12.87	33.5	2.45	5330	64.9	3-#8	22.75	14	None
8-3-V-6	13.25	33.4	2.51	4980	64.9	3-#8	22.75	15	#3@4¼"
13-3-V-8	12.94	33.8	2.55	4470	75.4	2-#8	16.75	9	#3@4¼"
					47.8	1-#5			
26-6-V-4	8.62	33.8	2.03	5000	45.7	2-#11	28.0	27.75	#3@6"
33-5-V-4	12.75	33.2	2.59	4320	42.5	3-#11	34.0	15.75	#3@4¼"
Combined shear + bond - narrow specimens[1]									
16-3-HI-4	12.50	33.2	2.29	5100	47.1	3-#11	22.75	5.5	3-#3ea. fa.
36-3-H2-4	12.31	32.7	3.07	5370	39.8	3-#11	22.75	8.5	3-#3ea. fa.
Bond failures - narrow specimens[2]									
12-3-V-6	14.50	33.2	2.55	4540	64.9	3-#8	16.75	5.5	#3@4¼"
14-3-V-8	12.88	33.6	2.50	4390	75.4	2-#8	16.75	5	#3@4¼"
					47.8	1-#5			
15-3-N-4	12.37	33.6	2.40	5100	47.1	3-#11	22.75	5.5	None
18-3-HI-8	12.62	33.3	2.44	6170	75.8	1-#11	16.75	5	3-#3ea. fa.
19-3-V-4	12.56	33.9	1.98	4340	45.0	3-#11	16.75	5.5	#3@4¼"
20-3-V-4	12.50	33.2	2.43	4800	45.0	3-#11	22.87	4	#3@4¼"
21-3-V-4	12.38	33.5	2.14	5330	46.0	3-#11	40.94	6	#3@4¼"
22-3-H4-4	12.50	33.3	2.49	5160	46.0	3-#11	22.75	6	3-#5ea. fa.
10-3-N-6	12.62	33.8	2.14	5330	64.9	3-#8	22.75	8.5	None
11-3-V-6	13.25	33.5	2.50	4540	64.9	3-#8	16.75	8.5	#3@4¼"
17-3-N-8	12.50	33.9	2.00	6170	75.8	1-#11	16.75	8	None
27-3-N-4	14.00	32.5	3.02	4820	41.0	3-#11	38.0	9	None
29-3-N-8	11.25	33.4	2.38	4480	75.8	1-#11	16.5	8.5	None
30-3-N-8	12.12	33.3	2.25	4480	75.8	1-#11	23.25	7.5	None
Loading stopped short of failure[3]									
28-3-H5-4	12.62	32.4	3.15	4820	41.0	3-#11	22.62	8.5	3-#5ea. fa.

1. See also #35 under combined flexure and shear.
2. See also #23, 24 under combined flexure and bond.
3. See also #21, 32 under flexure failure approached (loading stopped).

TABLE 2 ULTIMATE LOADS AND CALCULATED STRESSES

Specimen Code	f_c'	f_y	Bar Extension B	P_u	M_u	$f_s = \frac{M_u}{A_s(.9)d}$	$v = \frac{V}{bd}$	$v_{4.5} = \frac{u}{\Sigma o(.9)d}$		$u_{4.5}$
	psi	ksi	in.	kips	k-in.	ksi	psi	psi	psi	psi
Flexure failures - full width specimens										
1-1-V-4	4200	45.4	21	399	13,870	52.1	420	435	528	547
2-1-V-4	4340	45.4	15	340	13,860	51.4	353	360	444	453
3-1-V-4	4470	46.4	21	402	13,970	50.7	407	408	514	515
4-2-V-4	4470	46.4	21	391	13,590	49.6	400	401	503	504
5-1-V-6	5520	66.5	15	370	15,080	82.1	375	338	709	639
6-2-V-6	5750	66.5	15	393	16,010	87.5	399	353	756	668
Flexure failures - narrow specimens										
7-3-V-6	4700	64.9	7	165	6,730	94.7	405	396	584	571
Combined flexure + shear - narrow specimens										
35-3-N-4	5050	39.8	8.7	227	6,420	47.0	572	540	585	552
Combined flexure + bond - narrow specimens										
23-3-V-8	3290	75.4	9	147	5,640	98.2	343	401	584	683
24-3-N-8	2860	75.4	8.5	127	4,840	83.9	302	379	505	634
Flexure failure approached (loading stopped) - 6" embedment										
31-1-V-4	4820	43.8	21	412	14,320	51.5	413	417	522	527
32-2-V-4	4820	43.8	21	404	14,040	50.8	407	377	515	477
Shear failures - narrow specimens										
9-3-N-6	5330	64.9	14	246	5,600	78.4	570	524	866	796
8-3-V-6	4980	64.9	15	254	5,780	81.1	574	545	897	852
13-3-V-8	4470	75.4 47.8[4]	9	280	4,690	86.4	640	642	1118	1120
26-6-V-4	5000	45.7	27.75	153	4,280	45.1	525	498	568	538
33-5-V-4	4320	42.5	15.75	200	6,780	48.5	471	481	503	513
Combined shear + bond - narrow specimens[1]										
16-3-H1-4	5100	47.1	5.5	356	8,100	57.9	858	774	898	810
36-3-H2-4	5370	39.8	8.5	296	6,750	49.0	735	673	757	693
Bond failures - narrow specimens[2]										
12-3-V-6	4540	64.9	5.5	340	5,700	80.5	706	703	1207	1201
14-3-V-8	4390	75.4 47.8[4]	5	298	4,990	93.4	689	697	1195	1210
15-3-N-4	5100	47.1	5.5	276	6,280	44.4	664	651	687	673
18-3-H1-8	6170	75.8	5	280	4,700	100.5	665	567	2110	1800
19-3-V-4	4340	45.0	5.5	340	5,700	40.1	799	813	839	854
20-3-V-4	4800	45.0	4	276	6,310	45.1	665	644	695	673
21-3-V-4	5330	46.0	6	183	7,490	53.1	442	406	457	420
22-3-H4-4	5160	46.0	6	318	7,250	51.7	764	713	799	745
10-3-N-6	5330	64.9	8.5	234	5,320	73.8	548	504	817	751
11-3-V-6	4540	64.9	8.5	314	5,260	73.6	708	705	1105	1100
17-3-N-8	6170	75.8	8	246	4,130	86.8	580	495	1818	1550
27-3-N-4	4820	41.0	9	210	7,980	58.3	462	446	540	521
29-3-N-8	4480	75.8	8.5	258	4,260	90.8	686	687	1936	1939
30-3-N-8	4480	75.8	7.5	200	4,650	99.5	495	496	1508	1510
Loading stopped short of failure[+]										
28-3-H5-4	4820	41.0	8.5	357	8,080	59.2	873	843	921	890

1. See also #35 under combined flexure and shear.
2. See also #23, 24 under combined flexure and bond.
4. Through error the #5 bar of Specimens 13 and 14 was of intermediate grade.

[+]See also #31, 32 under flexure failure approached (loading stopped).

TABLE 3 CALCULATED STEEL STRESSES (ksi)
AT VARIOUS CRACK WIDTHS

Specimen Code	Tension Face Crack			Web Cracks		
	Initial Crack	0.008"	0.016"	0.008"	0.012"	0.016"
Intermediate grade steel						
#11 bars						
1-1-V-4	19.4	22.2	30.5	27.7	30.5	33.3
2-1-V-4	19.3	22.5	35.3	22.5	28.9	35.3
3-1-V-4	18.7	29.4	40.2	24.1	29.4	34.8
4-2-V-4	18.9	24.3	37.8	29.7	37.8	37.8
15-3-N-4	13.7	20.5	----	20.5	27.3	30.7
19-3-V-4	10.5	22.6	----	22.6	22.6	27.6
20-3-V-4	17.3	29.5	39.9	20.8	22.5	24.3
21-3-V-4	16.1	26.0	----	26.0	40.8	50.6
26-6-V-4	16.3	37.6	----	31.3	37.6	37.6
27-3-N-4	18.3	23.6	30.6	28.3	28.3	33.0
31-1-V-4	18.6	26.6	42.5	26.6	31.9	37.2
32-2-V-4	21.4	24.1	42.8	32.1	32.1	33.5
33-5-V-4	20.6	25.8	41.3	25.8	36.1	36.1
35-3-N-4	13.2	22.0	28.6	22.0	22.0	26.4
Ave. f_s	17.3	25.5	37.0	25.7	30.6	34.2
#11 with H-stirrups						
16-3-HI-4	15.2	24.1	----	20.7	31.0	37.9
22-3-H4-4	17.3	31.0	41.4	41.4	44.8	48.3
28-3-H5-4	12.7	26.1	33.1	26.1	36.6	43.7
36-3-H2-4	10.5	28.1	38.6	28.1	31.6	35.1
Ave. f_s	13.9	27.3	37.7	29.1	36.0	41.3
A432 grade steel						
#8 bars						
7-3-V-6	26.7	30.4	42.5	30.4	36.4	48.5
8-3-V-6	25.7	35.2	51.4	29.8	40.6	55.5
9-3-N-6	28.4	33.8	51.4	33.8	37.8	51.4
10-3-N-6	26.9	26.9	60.5	33.6	33.6	33.6
11-3-V-6	21.9	24.9	49.8	24.9	29.9	44.8
12-3-V-6	27.2	27.2	32.2	32.2	32.2	37.2
Ave. f_s	26.1	29.7	48.0	30.8	35.1	45.2
#11 bars						
5-1-V-6	24.6	24.6	42.5	28.3	33.1	47.3
6-2-V-6	24.6	28.4	37.8	28.4	37.8	42.5
Ave. f_s	24.6	26.5	40.2	28.4	35.4	44.9
A431 grade steel						
#8 + #5 bars						
13-3-V-8	26.2	32.7	50.0	32.7	45.8	50.0
14-3-V-8	30.0	40.0	50.3	40.0	46.7	46.7
23-3-V-8	37.0	48.4	62.6	37.0	42.7	48.4
24-3-N-8	32.2	39.2	44.7	35.6	39.2	44.7
Ave. f_s	31.4	40.1	51.9	36.3	43.6	47.5
#11 bars						
17-3-N-8	33.7	37.4	52.4	44.9	44.9	56.2
29-3-N-8	41.7	41.7	41.7	41.7	44.7	47.7
30-3-N-8	42.4	42.4	42.4	42.4	42.4	42.4
Ave. f_s	39.3	40.5	45.5	43.0	44.0	48.8
#11 with H-stirrups						
18	39.6	45.7	53.3	45.7	60.9	76.2

Ultimate Design of Prestressed Concrete Beams

NARBEY KHACHATURIAN, Professor of Civil Engineering, and
GERMAN GURFINKEL, Civil Engineering Department, University of Illinois, Urbana

A method is presented by which prestressed concrete beams can be designed on the basis of strength and ductility. The requirements of strength and ductility are developed in a general form and their influence on the dimensions of the beam is studied. The influence of compression steel on ductility and the required area of the beam is presented. Numerical examples are included to show the practical application of the method in design.

•IN PRESENT design practice, prestressed concrete beams are almost always designed and proportioned by working stress design. The provisions of ultimate design are used to check the flexural strength of a section that has already been designed. It can be shown that the provisions of ultimate design can be used to proportion a section with a rigorous control of both strength and ductility. The provisions of working stress design can then be used to check the stresses at transfer, and at service loads in the section so designed. A rational design of a section is considerably simpler by ultimate design than by service load design.

A simply supported bonded beam is considered, and it is assumed that the strength of the beam is measured by flexure. It is assumed that the only loads acting—in addition to the prestressing force—are the weight of the beam, the superimposed dead load and live load.

NOTATION

The following symbols have been adopted for use in this paper:

- a = distance from the neutral axis to the top fiber
- A = gross cross-sectional area of the beam
- A_s = area of prestressed steel
- A'_s = area of non-prestressed compression steel
- b = width of compression zone or top flange
- b' = web thickness
- d = distance from the center of gravity of prestressed steel to the top fiber
- d' = distance from the center of gravity of the non-prestressed compression steel to the top fiber
- $F(\epsilon_{su})$ = f_{su}, equation of the stress-strain diagram of prestressed steel
- $f(\epsilon)$ = stress in the concrete, equation of the stress-strain diagram of concrete
- f'_c = cylinder strength of concrete at 28 days
- f_{su} = stress in prestressed steel at failure
- f'_{su} = stress in non-prestressed compression steel at failure
- f_y = yield point of non-prestressed compression steel
- $G(\epsilon'_{su})$ = f'_{su} equation of the stress-strain diagram of non-prestressed compression steel
- h = overall depth of the beam

Paper sponsored by Committee on Concrete Superstructures and presented at the 45th Annual Meeting.

L = span length of a simply supported beam
M_g = moment due to the weight of the beam
M_ℓ = moment due to the live load
M_s = moment due to the superimposed dead load or slab
M_w = moment due to any dead load acting on the roadway slab
M_u = required flexural strength of the beam
M_{cu} = flexural strength of composite section
N_d = load factor for the dead load
N_ℓ = load factor for the live load
p = percentage of prestressed steel, A_s/bd
p' = percentage of non-prestressed compression steel, A_s'/bd
Q = $M_u/bd^2 f_c'$
S = effective width of slab in composite section
t = flange thickness
t_s = thickness of slab
γ = unit weight of concrete
ϵ = strain
ϵ_{ce} = strain in concrete at the level of steel due to effective prestress
ϵ_{se} = strain in the prestressed steel due to effective prestress
$\epsilon_{s\ell}$ = limiting strain in prestressed steel
ϵ_{su} = strain in the prestressed steel at ultimate
ϵ_{su}' = strain in the non-prestressed compression steel at ultimate
ϵ_u = ultimate strain of concrete in flexural compression
ϵ_y = strain at yield of non-prestressed steel
φ = curvature of the section
ψ = a dimensionless shape factor, A/bh

ANALYSIS OF PRESTRESSED CONCRETE BEAMS AT ULTIMATE

Analysis of a prestressed concrete beam at ultimate is discussed for beams having an idealized section as shown in Figure 1. The section considered is flanged, the prestressed steel is assumed to be bonded to concrete, and in addition to prestressed steel the section is assumed to have non-prestressed compression steel. Detailed studies of flexural strength of prestressed concrete beams have been reported previously (1, 2, 3); the presentation here is brief, and is in a form suitable for ultimate design.

The calculation of the ultimate moment is based on the following assumptions:

1. The strain distribution in concrete varies linearly with depth in the compression zone of the beam.
2. The stress-strain diagrams for the prestressed as well as non-prestressed reinforcement are known; the stress-strain diagram for concrete is known and is the same for all fibers in the compression zone.
3. Failure occurs when the strain in concrete at the top fiber reaches a limiting value.
4. The strain in non-prestressed compression steel is equal to the strain in concrete at the level of compression steel.
5. The average strain in steel is not greatly different from the maximum strain, hence the area of steel is concentrated at its centroid.

In addition to the above assumptions, the tension contributed by concrete is usually neglected since it is small at ultimate.

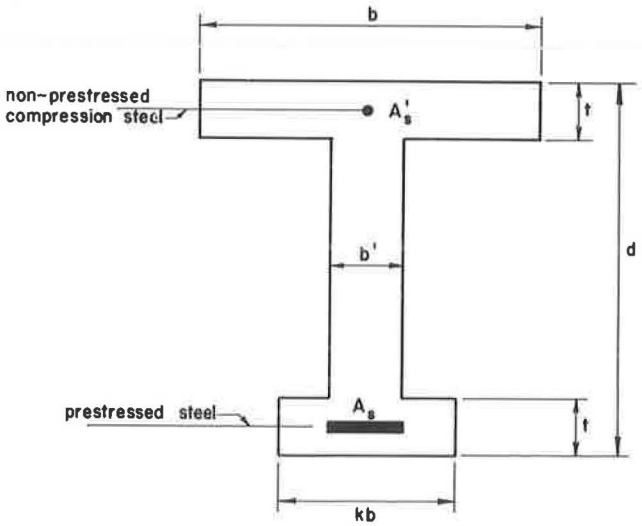

Figure 1. Idealized I-section.

The neutral axis at failure may be either in the flange or below the flange depending on the dimensions of the beam, the amount of steel and the properties of steel and concrete. The case in which the neutral axis falls in the flange is considered first.

Flexural Strength of Section in Which the Neutral Axis at Ultimate Falls in the Flange

In this case the width of the compression zone is constant and is equal to b (Fig. 2). The equation for the stress-strain diagram for concrete is expressed as $f = f(\epsilon)$. Since the width of the compression zone is constant and the strain distribution is assumed to be linear with depth in the compression zone, equations of equilibrium of moments and forces in the section may be written as

$$\frac{a^2 b}{\epsilon_u^2} \int_0^{\epsilon_u} \epsilon f(\epsilon) d\epsilon + A_s f_{su}(d - a) + A'_s f'_{su}(a - d') = M_u \tag{1}$$

$$\frac{ab}{\epsilon_u} \int_0^{\epsilon_u} f(\epsilon) d\epsilon + A'_s f'_{su} = A_s f_{su} \tag{2}$$

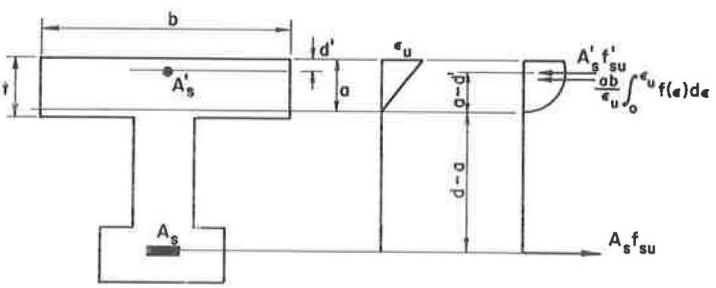

Figure 2. Flanged section, neutral axis in the flange.

where

M_u = ultimate moment,
a = distance from neutral axis to the top fiber,
ϵ_u = limiting strain at the extreme fiber of the beam which defines the condition of flexural failure,
f_{su} = stress in prestressed steel at failure,
f'_{su} = stress in non-prestressed compression steel at failure,
b = width of compression zone or top flange,
d = distance from the center of gravity of prestressed steel to the top fiber,
d' = distance from the center of gravity of the non-prestressed compression steel to the top fiber,
A_s = area of prestressed steel, and
A'_s = area of non-prestressed compression steel.

The strain in prestressed steel and non-prestressed compression steel is given by

$$\epsilon_{su} = \epsilon_{se} + \epsilon_{ce} + \frac{\epsilon_u}{a} (d - a) F \tag{3}$$

and

$$\epsilon'_{su} = \frac{\epsilon_u}{a} (a - d') \tag{4}$$

where

ϵ_{su} = strain in prestressed steel at failure,
ϵ_{se} = strain in prestressed steel due to effective prestress,
ϵ_{ce} = strain in concrete at the level of steel due to effective prestress,
ϵ'_{su} = strain in non-prestressed compression steel at failure, and
F = a strain compatibility factor taken as unity.

The stress-strain relations for prestressed and non-prestressed compression steel are given by

$$f_{su} = F(\epsilon_{su}) \tag{5}$$

$$f'_{su} = G(\epsilon'_{su}) \tag{6}$$

The first term on the left side of Eqs. 1 and 2 is the force and moment contributed by concrete respectively and does not take into account the area of concrete replaced by the compression steel. This effect is small and if necessary can be taken into account.

In order to analyze a beam with given dimensions and a specified value for ϵ_u, Eqs. 1 through 6 can be solved simultaneously for the 6 unknowns, M_u, a, ϵ_{su}, f_{su}, ϵ'_{su} and f'_{su}.

Flexural Strength of Section in Which the Neutral Axis at Ultimate Falls Below the Flange

When the neutral axis at ultimate falls below the flange Eqs. 1 and 2 should be replaced by the following 2 equations:

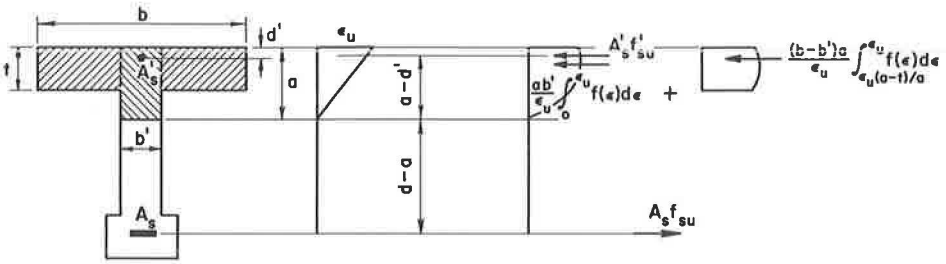

Figure 3. Flanged section, neutral axis below the flange.

$$M_u = \frac{b'a^2}{\epsilon_u^2}\int_0^{\epsilon_u} \epsilon f(\epsilon)d\epsilon + \frac{(b-b')\,a^2}{\epsilon_u^2}\int_{\epsilon_u(a-t)/a}^{\epsilon_u} \epsilon f(\epsilon)d\epsilon$$

$$+ A_s f_{su}(d-a) + A'_s f'_{su}(a-d') \qquad (7)$$

$$\frac{b'a}{\epsilon_u}\int_0^{\epsilon_u} f(\epsilon)d\epsilon + \frac{(b-b')a}{\epsilon_u}\int_{\epsilon_u(a-t)/a}^{\epsilon_u} f(\epsilon)d\epsilon + A'_s f'_{su} = A_s f_{su} \qquad (8)$$

where

b' = the web thickness, and
t = the flange thickness.

Equations 7 and 8 describe the equilibrium of moments and horizontal forces respectively. Figure 3 shows the forces in the section.

Expressions for Ultimate Moment in Dimensionless Form

For convenience in design Eqs. 1 and 2 will be expressed in dimensionless form as follows:

$$Q = \frac{M_u}{bd^2 f'_c} = \frac{(a/d)^2}{f'_c\,\epsilon_u^2}\int_0^{\epsilon_u} \epsilon f(\epsilon)d\epsilon + p\frac{f_{su}}{f'_c}\left(1-\frac{a}{d}\right) + p'\frac{f'_{su}}{f'_c}\left(\frac{a}{d}-\frac{d'}{d}\right) \qquad (1a)$$

$$\frac{a/d}{\epsilon_u f'_c}\int_0^{\epsilon_u} f(\epsilon)d\epsilon + p'\frac{f'_{su}}{f'_c} = p\frac{f_{su}}{f'_c} \qquad (2a)$$

where $p = \frac{A_s}{bd}$, $p' = \frac{A'_s}{bd}$, and f'_c = cylinder strength of concrete at 28 days.

Similarly Eqs. 7 and 8 may be expressed in dimensionless form:

$$Q = \frac{M_u}{bd^2 f'_c} = \frac{(b'/b)(a/d)^2}{f'_c \epsilon_u^{\,2}} \int_0^{\epsilon_u} \epsilon f(\epsilon) d\epsilon + \frac{(1 - b'/b)(a/d)^2}{f'_c \epsilon_u^{\,2}} \int_{\epsilon_u(a-t)/a}^{\epsilon_u} \epsilon f(\epsilon) d\epsilon$$

$$+ p \frac{f_{su}}{f'_c} \left(1 - \frac{a}{d}\right) + p' \frac{f'_{su}}{f'_c} \left(\frac{a}{d} - \frac{d'}{d}\right) \tag{7a}$$

and

$$\frac{(b'/b)(a/d)}{\epsilon_u f'_c} \int_0^{\epsilon_u} f(\epsilon) d\epsilon + \frac{(1 - b'/b)(a/d)}{\epsilon_u f'_c} \int_{\epsilon_u(a-t)/a}^{\epsilon_u} f(\epsilon) d\epsilon + p' \frac{f'_{su}}{f'_c} = p \frac{f_{su}}{f'_c} \tag{8a}$$

ULTIMATE DESIGN

Ultimate design of a prestressed concrete beam is based on the ultimate moment and ductility of the section. The section is proportioned in such a way that the ultimate moment is greater than the moment developed under service loads by a prescribed quantity, and that it deforms a certain amount before it fails.

These concepts may be stated in the form

$$M_u \geq N_d (M_g + M_s) + N_\ell M_\ell \tag{9}$$

and

$$\epsilon_{su} \geq \epsilon_{s\ell} \tag{10}$$

where

M_u = flexural strength of the beam,

N_d = load factor for the dead load,

M_g = moment due to weight of the beam,

M_s = moment due to the superimposed dead load,

N_ℓ = load factor for the live load,

M_ℓ = moment due to the live load,

ϵ_{su} = strain in steel at ultimate, and

$\epsilon_{s\ell}$ = limiting strain in steel.

Expression 9 states that the required flexural strength of the beam should be at least equal to $N_d(M_g + M_s) + N_\ell M_\ell$, which is a requirement for the strength of the beam.

Expression 10 states that the ductility of the beam should be large enough so that the strain in steel at ultimate is at least equal to a given limiting value designated as $\epsilon_{s\ell}$. Ductility is usually measured by the curvature at ultimate, which may be defined as follows:

$$\varphi = \frac{\epsilon_u}{a} = \frac{\epsilon_{su} - \epsilon_{se} - \epsilon_{ce} + \epsilon_u}{d}$$

where φ is the curvature of the section. For given values of ϵ_{se}, ϵ_{ce}, ϵ_u and d, ϵ_{su} may be used as a measure of ductility.

Determination of the Area of the Beam

Expression 9 can be written as an equation in the following form:

$$Qbd^2f'_c = N_d (M_g + M_s) + N_\ell M_\ell$$

Substituting $A/h\psi$ for b where A is the gross cross-sectional area of the beam, h is the over-all depth, and ψ is a dimensionless shape factor, the following is obtained:

$$M_g = \frac{\gamma AL^2}{8} = Q \frac{A}{h\psi} d^2 f'_c \frac{1}{N_d} - \frac{N_\ell}{N_d} M_\ell - M_s$$

and

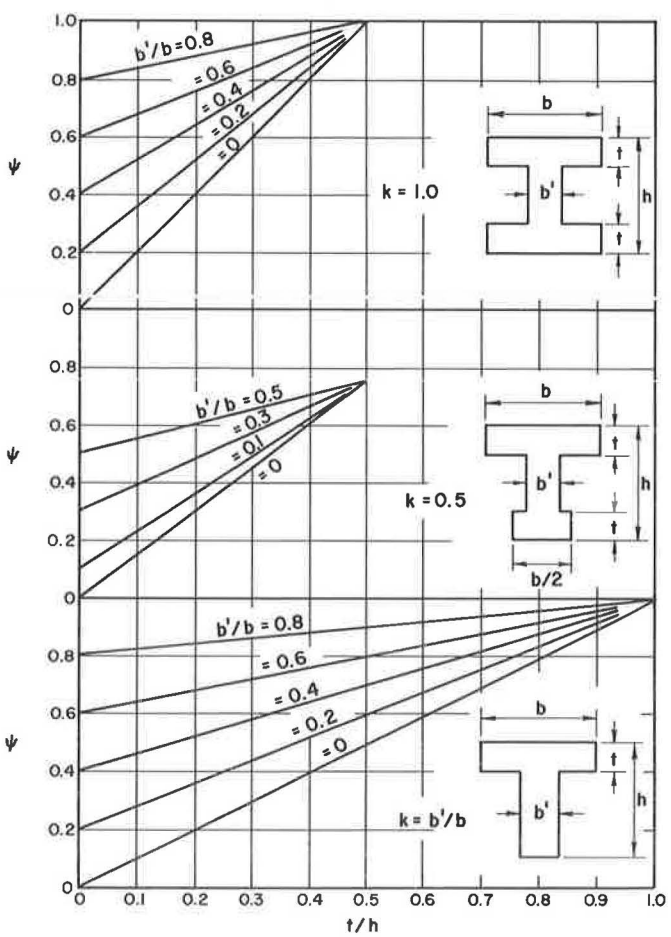

Figure 4. Relationship between ψ and geometric parameters of the section.

$$A = \frac{M_s + \frac{N_\ell}{N_d} M_\ell}{\frac{d^2 f'_c Q}{h\psi\ N_d} - \frac{\gamma L^2}{8}} \tag{11}$$

where γ is the unit weight of concrete.

For the idealized I-section shown in Figure 1, ψ is given by

$$\psi = \frac{t}{h}\ (1 + k) + \frac{b'}{b}\left(1 - 2\frac{t}{h}\right) \tag{12}$$

The quantity k in Eq. 12 is the ratio of the width of bottom flange to that of top flange. Equation 12 is plotted in Figure 4 for typical sections.

A study of Eq. 11 indicates that for a given design problem, in which the depth and type of concrete are specified, A depends on ψ and Q only. It can be seen that A decreases with Q and increases with ψ; i.e., to decrease the area of the beam it is necessary to increase Q and decrease ψ, or to increase the ratio Q/ψ.

The quantities t/d and b′/b usually decrease with increasing Q/ψ; hence they should be made small, without causing the dimensions of the beam to become unreasonably thin.

From Eq. 12 it can be seen that ψ increases and Q/ψ decreases with k. Therefore a small bottom flange is desirable. However, since the bottom flange of the beam should be large enough to permit the placing of steel, k cannot be reduced indefinitely.

From Eqs. 1a and 7a it can be seen that Q increases with a/d and hence it is desirable to make a/d as large as possible; however, Expression 10 for the required ductility sets the upper limit for a/d. Since Expression 10 sets the required minimum ductility of the beam at a strain in steel equal to $\epsilon_{s\ell}$, the required maximum a/d consistent with the required ductility can be computed from Eq. 3 as follows:

$$(a/d)_{max} = \frac{\epsilon_u}{\epsilon_{s\ell} - \epsilon_{se} - \epsilon_{ce}\quad \epsilon_u} \tag{3a}$$

Equation 3a contains the quantity ϵ_{se}, the strain in steel due to effective prestress. It can be seen that since ϵ_{se} increases with the maximum value of a/d, it should be taken as large as practicable. The practical upper limit for ϵ_{se} for the materials used in pretensioned construction is about 0.005.

It should be pointed out that d/h also influences A, the area of the beam, and from Eq. 11 it can be seen that A decreases with d/h. In most practical problems, however, d/h cannot exceed 0.9.

Design Procedure

In the design method presented here it is assumed that the span length, the acting load, the load factors, the strength and unit weight of concrete are given. It is further assumed that the limiting strain in concrete ϵ_u, the requirement of ductility $\epsilon_{s\ell}$, the effective prestrain ϵ_{se}, as well as the stress-strain relations for all materials are given. Hence for a selected value of h, the calculation of A from Eq. 11 means determination of d^2Q/ψ. The quantities d, ψ and Q may be determined as follows:

1. Assign a reasonable value to d as close to h as the arrangement of strands would permit.
2. Assign values to b′/b, t/h and k, and calculate ψ from Eq. 12. These values should be as small as possible.
3. Calculate a/d from Eq. 3a based on the given values of ϵ_u, ϵ_{se} and $\epsilon_{s\ell}$.

4. Calculate $p(f_{su}/f'_c)$ from either Eq. 2 a or 8a, whichever applies.
5. Calculate Q from Eq. 1a or 7a, whichever applies.

EXAMPLES OF APPLICATION

Example 1

The following example illustrates the procedure for the ultimate design of a prestressed concrete beam and shows the influence of the required ductility on the dimensions of the beam so designed.

Given a simply supported beam of 54-ft span subjected to a superimposed dead load of 1.0 klf and a live load of 0.6 klf which produce midspan moments of M_s = 4370 in-k and M_ℓ = 2630 in-k respectively. The load factors are N_d = 1.5 and N_ℓ = 1.8. Design the section (a) for a minimum ductility corresponding to $\epsilon_{s\ell}$ = 0.01, and (b) for a mini-

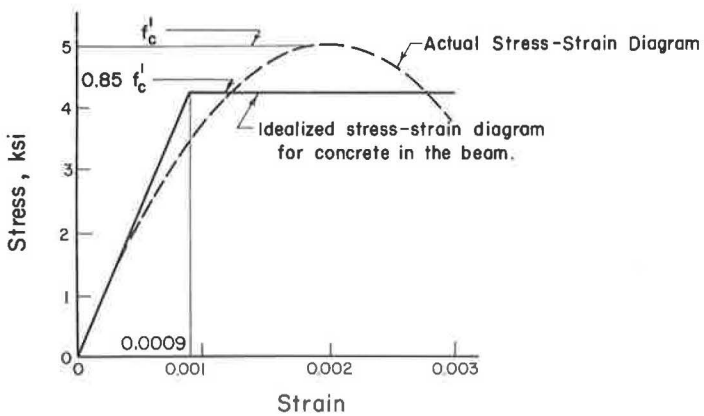

Figure 5. Stress-strain diagram for concrete.

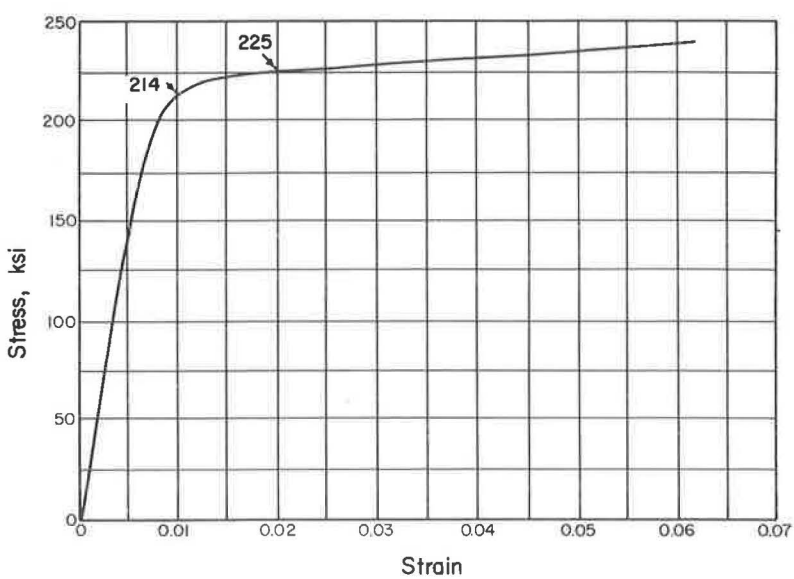

Figure 6. Stress-strain diagram for steel.

mum ductility corresponding to $\epsilon_{s\ell} = 0.02$. Non-prestressed compression steel is not to be used.

The effective prestress or the prestress after losses is given as 145 ksi, which corresponds to a transfer prestress of 170 ksi. The strain due to effective prestress is $\epsilon_{se} = 0.0048$. The quantity ϵ_{ce} is approximated as 0.0005 initially, which may be verified after the section is designed. The limiting strain in concrete is given as $\epsilon_u = 0.003$, unit weight of concrete as $\gamma = 0.15$ kcf, and overall depth as h = 36 in. The strength of concrete f'_c is specified as 5 ksi. The stress-strain diagram for concrete and steel are as shown in Figures 5 and 6 respectively.

1a. Section With Minimum Required Ductility Corresponding to $\epsilon_{su} = 0.01$.—It was shown before that the quantities t/h, b′/b and k increase with A, and thus they should be taken as small as possible. Here they will be taken as t/h = 1/6 (or t = 6 in.), b′/b = 0.3 and k = 1.0. Substitution of these values in Eq. 12 gives $\psi = 0.533$. It is further assumed that d/h = 0.9, which for h = 36 in. yields d = 32.4 in. For the given ductility, $\epsilon_{su} = \epsilon_{s\ell} = 0.01$, Eq. 3a gives depth to the neutral axis as a = 12.64 in. Since in this case the neutral axis is in the web, Eqs. 7a and 8a apply.

From Figure 5, $f(\epsilon) = 4722\epsilon$ when $\epsilon \leq 0.0009$, and $f(\epsilon) = 4.25$ when $\epsilon \geq 0.0009$, the quantity $p(f_{su}/f'_c)$ may be calculated from Eq. 8a as follows:

$$p\frac{f_{su}}{f'_c} = \frac{(0.3)(0.390)}{(0.003)\ (5)}\left[\int_0^{0.0009} 4722\epsilon d\epsilon + \int_{0.0009}^{0.003} 4.25\ d\epsilon\right]$$

$$+ \frac{(0.70)(0.390)}{(0.003)\ (5)}\int_{0.00158}^{0.003} 4.25\ d\epsilon = 0.085 + 0.11 = 0.195$$

For the above value of $p(f_{su}/f'_c)$, in a similar way Q is obtained from Eq. 7a:

$$Q = \frac{(0.3)(0.390)^2}{(5)\ (0.003)^2}\left[\int_0^{0.0009} 4722\ \epsilon^2 d\epsilon + \int_{0.0009}^{0.003} 4.25\ \epsilon d\epsilon\right]$$

$$+ \frac{(1-0.3)(0.390)^2}{(5)\ (0.003)^2}\int_{0.00158}^{0.003} 4.25\ \epsilon d\epsilon + 0.195\ (1-0.390) = 0.171$$

From Eq. 11 the area of the beam is 284 in^2. In addition, the following quantities are obtained: b = b′ = 14.8 in.; b′ = 0.3 × 14.8 = 4.4 in.

The stress-strain diagram for steel (Fig. 6) yields $f_{su} = 214$ ksi. The amount of prestressing can be found from $p(f_{su}/f'_c) = 0.195$ to be p = 0.00455 from which A_s = 2.18 in^2. A total of sixteen ½-in. strands is needed. Each ½-in. strand has an area of 0.1438 in^2. The final dimensions of the section in this solution are shown in Figure 7a. The bottom flange has been widened to properly accommodate the reinforcement, and it is tapered to facilitate construction. The final width of the top flange is taken the same as that of bottom flange to maintain the symmetry of the section originally assumed. The properties of the gross section and the transformed section as well as the stresses at the top and bottom fibers before and after losses for both assumptions are given in Table 1.

1b. Section With Minimum Required Ductility Corresponding to $\epsilon_{su} = 0.02$.—The ultimate strain in the steel required for this example is large, and is not necessarily

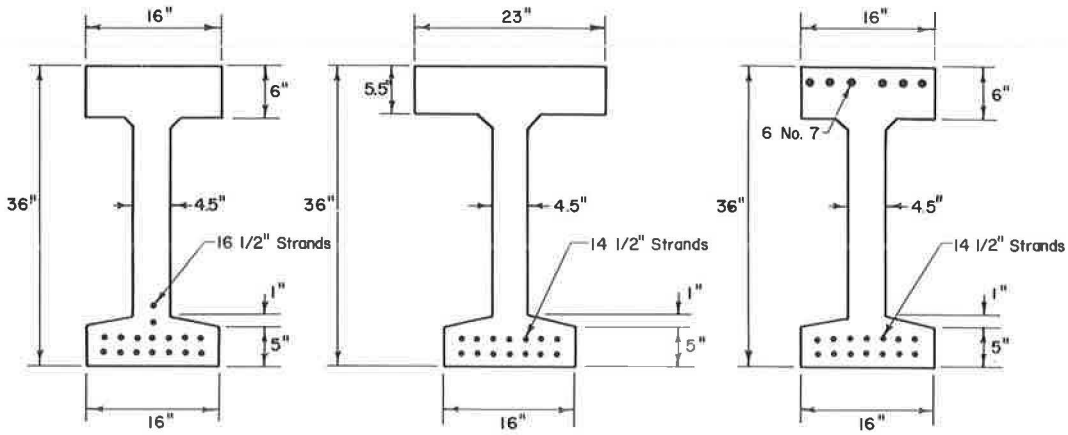

EXAMPLE 1a
Low Ductility ϵ_{su}=0.01
Weight 307 lb/ft
Fig. 7a

EXAMPLE 1b
High Ductility ϵ_{su}=0.02
Weight 341 lb/ft
Fig. 7b

EXAMPLE 2
High Ductility ϵ_{su}=0.02
Weight 307 lb/ft
Fig. 7c

Figure 7. Sections of design examples.

TABLE 1

SUMMARY OF SECTION PROPERTIES AND STRESSES FOR SECTIONS OBTAINED BY ULTIMATE DESIGN
(For each example the results shown are based first on the gross area of the section and second on the transformed section assuming n = 7. Negative stresses are tensile.)

Section	A (in^2)	y_t (in.)	y_b (in.)	I (in^4)	A_s (in^2)	A_s' (in^2)	Weight (lb/ft)	Stress Before Losses (Transfer) (ksi)		Stress After Losses (ksi)	
								Top (Tens.)	Bottom (Comp.)	Top (Comp.)	Bottom (Tens.)
Example 1a	294	17.76	18.24	48,080	2.30	—	307	-0.34	3.04	2.37	-0.13
ϵ_{su} = 0.01	308	18.43	17.57	51,040				-0.27	2.73	2.37	-0.14
Example 1b	327	16.20	19.80	55,230	2.01	—	341	-0.23	2.60	1.92	-0.37
ϵ_{su} = 0.02	339	16.81	19.19	58,610				-0.18	2.36	1.92	-0.35
Example 2	294	17.76	18.24	48,080	2.01	3.60	307	-0.30	2.66	2.40	-0.46
ϵ_{su} = 0.02	328	17.29	18.71	56,270				-0.22	2.41	2.02	-0.34

A = area; y_t = distance from centroidal axis to top fiber; y_b = distance from centroidal axis to bottom fiber; I = moment of inertia; A_s = area of prestressed steel; A_s' = area of non-prestressed compressive steel; n = modular ratio for both types of steel; f_c' = strength of concrete; f_{ci}' = strength of concrete at transfer; prestress at transfer = 170 ksi; effective prestress after losses = 145 ksi. The underlined quantities correspond to the results obtained on the basis of the transformed section.

used in practice. It has been selected to show that direct design for the largest levels of ductility is possible, and to study how it affects the shape of the section.

All the quantities are the same as in Example 1a except that in this case $\epsilon_{su} = 0.02$, which corresponds to a higher ductility. Since a higher required ductility results in a wider top flange, and the bottom flange need only be large enough to accommodate the reinforcement, k is taken as 0.75 in this case. For a similar reason the quantity b'/b is taken as 0.2. Taking t = 5.5 in., t/h = 0.153, Eq. 12 yields $\psi = 0.407$. As before, d = 32.4 in.

From Eq. 3a we obtain a = 5.49 in., which places the neutral axis in the flange. For the stress-strain diagram adopted for concrete from Eq. 2a we have $p(f_{su}/f_c') = 0.122$,

and from Eq. 1a we obtain Q = 0.113. From Eq. 11, A = 336 in.^{2}, and b = 22.9 in., b′ = 4.6 in., kb = 17.2 in.

From the stress-strain diagram for steel (Fig. 6), f_{su} = 225 ksi. From $p(f_{su}/f'_c)$ = 0.122, p = 0.00271, from which A_s = 2.01 in.^{2} Fourteen ½-in. are strands needed. Figure 7b shows the final section of the beam. The dimension of the bottom flange is the minimum required to accommodate the prestressing steel at the required depth. As kb turned out to be larger than necessary, only the minimum required was used, because the bottom flange does not contribute to the strength and ductility of the section. Had the adjustment of the dimensions been large, recalculation may have been necessary to improve the shape of the section. The properties of the section and the stresses before and after losses for this part are given in Table 1.

Example 2

In order to show that the non-prestressed compressive reinforcement increases the ductility without increasing the area of the section, the following example is presented. It is required to design the section in Example 1 in such a way that for a ductility corresponding to ϵ_{su} = 0.02, the area of the section will be the same as that for a ductility corresponding to ϵ_{su} = 0.01. The yield point stress of the compressive reinforcement may be assumed as f_y = 50 ksi. The section designed in Example 1a has a ductility corresponding to ϵ_{su} = 0.01. The problem is to determine how much compressive steel of the type given should be placed so that the ductility of the section will reach that corresponding to ϵ_{su} = 0.02.

The distance of the neutral axis from the top fiber was determined as a = 5.49 in. in Example 1b for the same required ϵ_{su}. Since in this case the neutral axis falls in the flange, Eqs. 1a and 2a may be used with Q = 0.171, as in Example 1a, and d′ = 2 in., to write the following independent relations between $p(f_{su}/f'_c)$ and $p(f'_{su}/f'_c)$:

$$0.171 = 0.012 + p\frac{f_{su}}{f'_c}(1 - 0.170) + p'\frac{f'_{su}}{f'_c}(0.170 - 0.062) \qquad (1a)$$

$$0.122 + p'\frac{f'_{su}}{f'_c} = p\frac{f_{su}}{f'_c} \qquad (2a)$$

The simultaneous solution of the above equations yields $p(f_{su}/f'_c)$ = 0.183 and $p'(f'_{su}/f'_c)$ = 0.061.

From Figure 6, ϵ_{su} = 0.02 corresponds approximately to f_{su} = 225 ksi. Therefore, p = 0.00407 and A_s = 1.95 in.^{2} A total of fourteen ½-in. strands is needed. Since the strain in compression steel is 0.003(3.49/5.49) = 0.0019 > ϵ_y the intermediate grade steel has yielded and the net f'_{su} is 50 - 4.25 = 45.75 ksi. Therefore, p′ = 0.00666, A'_s = 3.20 in.^{2} and six No. 7 bars of intermediate grade steel are required. The length of these non-prestressed bars need not be the total span of the beam. Theoretically they are not needed at a section where the required Q is that of the section without the compression reinforcement. The properties of the section and the stresses before and after losses for this example are shown in Table 1; Figure 7c shows the beam section.

A reduction in the amount of non-prestressed compression reinforcement is possible with a section having a wider top flange. The parameter $p(f'_{su}/f'_c)$ is related to $p(f_{su}/f'_c)$ by Eq. 2a. Selection of a smaller value of p (f'_{su}/f'_c) would fix $p(f_{su}/f'_c)$ and permit the determination of the required Q by Eq. 1a. The area of the section and its final shape can be determined as usual from Eq. 11. If the proper values of t/h, b′/b, and k were selected, the new section will present a flange wider than that of Example 1a, but not as large as that of Example 1b. Also, the compressive reinforcement required will be smaller than that of Example 2. This solution would show that to obtain high ductility a compromise section can be obtained if some increment of weight is tolerated with a smaller amount of non-prestressed compression steel.

Comparison of the Three Solutions

It has been shown that ultimate strength design provides a convenient procedure which leads to well-proportioned sections. The desired ductility and strength were used as the fundamental constraints for proportioning the sections, while the stresses at transfer and under service loads were checked.

An examination of Table 1 shows interesting details. The beam of Example 1a with a required ductility corresponding to $\epsilon_{su} = 0.01$ required more prestressing steel (2 strands) than the beams of Examples 1b and 2 with a required ductility corresponding to $\epsilon_{su} = 0.02$.

For the stress-strain diagram of prestressing steel adopted in these examples, any increase in ductility is accompanied by an increase in stress in steel at ultimate. For the larger ductility considered here the stress in steel increases at ultimate from 214 ksi to 225 ksi. This increase in steel stress causes a decrease in the required area of prestressing steel.

The beam of Example 1b shows that by increasing the width of the top flange and thereby adding concrete area to the compression zone, high ductility can be obtained. This, however, increases the weight of the section by 11 percent, but decreases the amount of prestressing steel to 14 strands. The increase in stress in steel at ultimate not only supports the additional weight of the beam, but also permits a reduction in the required area of steel. Under the service loads this beam shows, however, a tendency for a larger tensile stress at the bottom fiber due to the smaller amount of prestressing force.

The beam of Example 2 shows a different way of obtaining high ductility. Six No. 7 intermediate grade bars are added to the top flange of the low ductility section of Example 1a. This increment in compression area raises the neutral axis and increases the lever arm of the resisting couple by approximately 7 percent. In addition the stress in the steel at ultimate is increased from 214 ksi to 225 ksi, approximately 5 percent. These 2 factors combined explain the 12 percent reduction in the number of prestressing strands, from 16 to 14, since the required tensile force at ultimate can be obtained with less area of steel at a higher stress and a larger lever arm. The non-prestressed bars also provide additional tensile strength for the top part of the beam at transfer and during handling operations. Furthermore, they have a tendency to reduce the inelastic deflections due to creep.

SUMMARY AND CONCLUSIONS

A method is presented by which a prestressed concrete beam can be proportioned by ultimate design. Particular emphasis has been placed on the requirement of ductility and its influence on the dimensions of the section. The design examples presented show the actual method of proportioning as well as the influence of ductility on the dimensions of the beam.

The following conclusions may be drawn from the study.

1. A prestressed concrete beam can be proportioned for given required minimum flexural strength and ductility. The stresses at transfer and at service conditions may be checked in a section thus obtained.
2. The dimensions of a section are influenced greatly by the required ductility. An increase in the required ductility results in an increase in the required area of the section, unless compression steel is provided.
3. Compression steel contributes appreciably to the ductility of the section. Example 2 shows that the most expeditious way for increasing the ductility of a section is by placing non-prestressed compression reinforcement as near the top fiber as possible.

For a large required ductility considerable saving in the area of the beam may be effected by use of non-prestressed compression steel. Compression steel has additional advantages such as its contribution to the crack stability of the top fiber, its use as spacer for the web reinforcement and its function in providing more safety for the beam during transportation and erection.

REFERENCES

1. Hognestad, E., Hanson, N. W., and McHenry, D. Concrete Stress Distribution of Ultimate Strength Design. Jour. ACI (Proc.), Vol. 52, pp. 455-479, Dec. 1955.
2. Warwaruk, J., Sozen, M. A., and Siess, C. P. Strength and Behavior in Flexure of Prestressed Concrete Beams. Univ. of Illinois Eng. Exp. Sta. Bull. No. 464, 1962.
3. Gurfinkel, G., and Khachaturian, N. Ultimate Design of Prestressed Concrete Beams. Univ. of Illinois Eng. Exp. Sta. Bull. No. 478, 1965.

Appendix

DESIGN OF COMPOSITE SECTIONS

The method discussed in the preceding sections may be used to design composite prestressed concrete beams on the basis of safety and ductility. Composite construction, which is used extensively in highway bridges, consists of a reinforced concrete slab cast in place on top of precast prestressed concrete stringers. It is assumed that the shear connection between slab and stringer is strong enough to develop the flexural strength of the composite section.

Design of stringers in highway bridges is based on the assumption that a known portion of the loads acts on each stringer, and that a strip of the roadway slab contributes to support any load which comes on the bridge after the roadway concrete has set. Thus the problem is reduced to the design of a stringer with a slab of given width, thickness and strength at the top. The slab becomes an integral part of the stringer section for all the loads acting after the slab concrete has hardened. The loads as well as the effective slab section available for each stringer are different for the end and intermediate stringers.

The strength of a composite section, which consists of the stringer and the slab of known width and thickness, is calculated assuming that it is a unit all by itself. Strength calculated in this fashion provides only a measure of safety, and should not be confused with the safety of the entire bridge for the intended loads.

In the discussion that follows it will be assumed that a concrete deck of known thickness is cast on top of parallel stringers at a given spacing, and that a portion of the deck slab behaves compositely with each stringer. The design of the stringer is to be based on the prescribed strength and ductility of the composite section as well as that of the stringer section by itself.

The stringer should be designed such that the following two inequalities are satisfied in the composite section:

$$M_{cu} \geq N_d(M_g + M_s + M_d + M_w) + N_\ell M_\ell \tag{9a}$$

and

$$\epsilon_{csu} \geq \epsilon_{s\ell} \tag{10a}$$

The above inequalities are similar to Inequalities 9 and 10. The quantity M_{cu} is the flexural strength of the composite section; ϵ_{csu} is the strain in the prestressing steel at failure of the composite section; M_s denotes the moment caused by the weight of that portion of the slab which contributes to the composite section; M_d is the moment due to any additional dead load that may be present before the slab concrete has set, and M_w is the moment due to any dead load (such as wearing surface) that may act on the structure after the slab concrete has set.

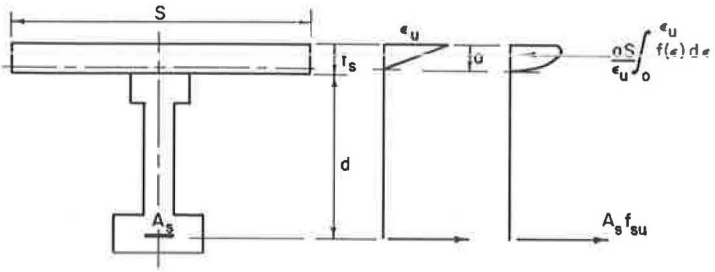

Figure 8. Composite section.

In addition, the following inequality should be satisfied in the stringer section:

$$M_u \geq N_d (M_g + M_s + M_d) \tag{9b}$$

Thus Inequalities 9a, 10a and 9b constitute the basis of design.

The condition expressed by Inequality 10a can easily be satisfied in a composite section, since a comparatively large area of concrete is available in the compression zone. Figure 8 shows a ductile beam in which the neutral axis at failure is in the slab. It can be seen that a considerable compression force may be developed in the slab if the width of slab is large, even though the strength of concrete in the slab is usually in the neighborhood of 3000 psi.

The effective width of slab is usually taken as the center-to-center spacing of stringers, which ranges between 4 and 7 ft. A width of this order of magnitude for the slab provides large compression forces even for high ductilities. On the other hand the higher the ductility, the smaller the available compression force and the required area of prestressing steel. Hence if the ductility is too high, the requirement expressed by Inequality 9a may no longer be satisfied. Thus it can be seen that although high ductility is available, Inequality 9a provides an upper limit for it. In practice the highest ductility compatible with Inequality 9a should be used.

The requirement expressed by Inequality 9b assures that the flexural strength of the stringer section is adequate. Where the available area of slab is large, this requirement is automatically satisfied.

Determination of Area and Prestressing Force

The preceding discussions may be expressed conveniently in algebraic form for use in design. It is assumed that the neutral axis of the composite section at failure will fall in the slab. Ignoring the effect of non-prestressed compression reinforcement, if any, and designating S and t_s respectively as the width and thickness of the slab, from Eqs. 1 and 2 the following can be derived:

$$M_{cu} = \frac{a^2 S}{\epsilon_u^2} \int_0^{\epsilon_u} \epsilon f(\epsilon) d\epsilon + A_s f_{su} (d - a) \tag{1b}$$

and

$$A_s f_{su} = \frac{aS}{\epsilon_u} \int_0^{\epsilon_u} f(\epsilon) d\epsilon \tag{2b}$$

where

$$a = \frac{\epsilon_u}{\epsilon_{s\ell} - \epsilon_{se} - \epsilon_{ce} + \epsilon_u}(d + t_s) \tag{3b}$$

The substitution of Eq. 1b for M_{cu} and $(A\gamma L^2)/8$ for M_g in Inequality 9a yield the following expression for A, the area of the stringer:

$$A \leq \frac{8}{\gamma L^2}\left[\frac{a^2 S}{N_d \epsilon_u^2}\int_0^{\epsilon_u} \epsilon f(\epsilon)d\epsilon + \frac{A_s f_{su}(d-a)}{N_d} - \frac{N_\ell}{N_d} M_\ell - M_s - M_d - M_w\right] \tag{13}$$

Inequality 13 provides an upper bound for A.

Since Inequality 9b for the stringer section is similar to non-composite design, a lower bound for A may be obtained by expressing 9b in the following form:

$$A \geq \frac{M_s + M_d}{\frac{d^2 f'_c Q}{h\psi N_d} - \frac{\gamma L^2}{8}} \tag{11a}$$

Since Inequality 11a seldom governs in practical problems, it is more convenient to check the flexural strength of the stringer section directly by Inequality 9b.

The steps to be taken in the determination of A and A_s may be summarized as follows:

1. On the basis of a ductility greater than or equal to the prescribed ductility calculate a from Eq. 3b.
2. Calculate A_s from Eq. 2b using the given stress-strain diagram for concrete.
3. Find the upper bound of A from Inequality 13. If A is too large it means that the ductility may be increased further. On the other hand if A is unreasonably small the ductility should be decreased.
4. Determine the proportions of the section and check Inequality 9b.

Example 3

Given a simply supported bridge of 54-ft span consisting of precast prestressed concrete stringers and cast-in-place slab; the roadway slab is 6½ in. thick and the structure is to be designed for H20-S16-44 loading. It is anticipated that the structure will have to support a 2-in. wearing surface. The bridge will have one diagram at midspan connecting the stringers, whose weight is equivalent to a concentrated load of 1.25 k per intermediate stringer. Design an intermediate stringer assuming a center-to-center spacing of 5 ft 0 in. and overall depth of 36 in.

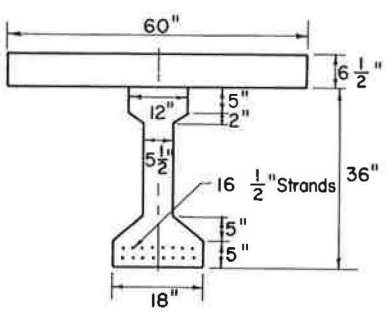

Figure 9. Design Example 3.

The following are given: for slab, f'_c = 3000 psi; for stringer, f'_c = 5000 psi; ϵ_{se} = 0.0048; ϵ_u = 0.003; γ = 0.15 kcf.

The quantity ϵ_{ce} may be taken as 0.0005. The stress-strain diagrams for concrete and prestressing steel are as shown in Figures 5 and 6 respectively.

The moments may be calculated as follows:

TABLE 2

SUMMARY OF SECTION PROPERTIES AND STRESSES IN EXTREME FIBERS OF STRINGER

Section		A (in^2)	y_t (in.)	y_b (in.)	I (in^4)	Stress Before Losses (Transfer) (ksi)		Stress After Losses (ksi)	
						Top (Tens.)	Bottom (Comp.)	Top (Comp.)	Bottom (Tens.)
Gross	Stringer	330.8	20.24	15.76	48050	-0.23	2.16	1.10	-0.03
	Composite	642.8	8.85	27.15	137960				
Transformed	Stringer	344.6	20.78	15.22	50190	-0.17	1.98	1.14	-0.04
	Composite	656.6	9.36	26.64	145800				

In the above calculation the ratio of modulus of elasticity of concrete in the slab to that in the stringer is taken as 0.8. The properties of the transformed section are calculated assuming N = 7 and $A_s = 2.3\ in^2$.

$$M_s = 0.406 \times \frac{(54)^2}{8} \times 12 = 1775 \text{ in. k}$$

$$M_d = 1.25 \times \frac{(54)}{4} \times 12 = 203 \text{ in. k}$$

$$M_e = \tfrac{1}{2} \times 699.3 \times \frac{5}{5} \times 1.28 \times 12 = 5370 \text{ in. k}$$

$$M_w = 0.125 \times \frac{(54)^2}{8} \times 12 = 546 \text{ in. k}$$

Assume $\epsilon_{s\ell} = 0.031$, and $d + t_s - 33 + 6.5 = 39.5$ in. From Eq. 3b, $a = 4.12$ in., from Eq. 2b, $A_s = 2.33\ in^2$; from Inequality 13, $A \leq 330\ in^2$.

To provide the required area for prestressing steel, sixteen ½-in. strands are used. Figure 9 shows the stringer section and the arrangement of strands. The web is taken as 5½ in. to provide sufficient room for draping. The top flange is made 12 in. wide in order to provide sufficient area to transmit the shearing stresses which occur between slab and stringer in the composite section.

It can be shown that the section of Figure 9 satisfies Inequality 9b. Table 2 shows a summary of the section properties and stresses in the stringer before and after losses.

In the example the effect of non-prestressed reinforcement either in slab or stringer is not taken into account. The non-prestressed compression reinforcement increases the ductility of the stringer section, but is usually under tensile stress at the failure of the composite section. The longitudinal reinforcement in the slab increases the ductility of the composite section, if placed at the top of the slab.

Time Dependent Deformations of Two Lightweight Aggregate Concretes

GORDON W. BEECROFT, Associate Professor of Civil Engineering, Oregon State University

A research project was conducted by the Oregon State Highway Department in cooperation with the U.S. Bureau of Public Roads to determine the creep and shrinkage characteristics of 2 expanded shale aggregate concretes. For the earlier phase of the project, measurements were made for about 8 years on specimens subjected to a constant compressive stress. Other prisms were subjected to a compressive stress which was permitted to diminish as creep and shrinkage of the concrete occurred. Deformations of the latter prisms were measured over a 5-year period.

To provide a basis for comparison, the relaxing stress phase of the project included identical specimens cast from normal-weight, sand and gravel aggregate concrete. The magnitudes of creep, shrinkage, and loss of prestress measured on the lightweight prisms are compared with the values measured on the normal-weight prisms.

The various measurements for both the constant stress and the relaxing stress specimens are presented and the significance of the values as applied to design is discussed.

For the specimens subjected to a relaxing prestress force, the loss of prestress was 50 percent greater in the lightweight prisms than in the normal-weight prisms.

•THE PURPOSE of this project was to evaluate the suitability of lightweight concretes, using aggregates readily available in Oregon, for use in prestressed concrete bridge members. The project consisted of 3 phases: first, a rather limited investigation of mix design; second, a long-term investigation of time deformations of concrete prisms subjected to a constant stress; and third, determining the deformations of prisms under a relaxing prestress force. In addition to the studies of lightweight aggregates, the latter phase included identical specimens cast from sand and gravel aggregates to obtain comparable values of deformations between lightweight and normal-weight concretes.

Many engineers concerned with the design and construction of bridges and other structures have recognized potential advantages that would result from the use of lightweight aggregate concrete in prestressed members. However, lightweight aggregates have not been used extensively in prestressed work because of the limited knowledge of the physical properties of the lightweight concretes, particularly with regard to creep and shrinkage. During recent years, a number of studies have been undertaken to broaden the engineer's knowledge of the physical properties of structural quality lightweight concretes.

During 1955 the Oregon State Highway Department initiated a research project to study the characteristics of concretes manufactured from lightweight aggregates that are readily available within the state. The objectives included the design of concrete

Paper sponsored by Committee on Concrete Superstructures and presented at the 45th Annual Meeting.

mixtures having suitable strength and workability for use in prestressed members and the measurement of time dependent deformations in specimens cast from selected concrete mixtures. One group of test prisms was maintained under constant stress for approximately 8 years. During this time periodic measurements of the change in length of the specimens were made. Another group of prisms was subjected to a gradually reducing prestress force for a period of over 5 years. Progress reports on both groups of prisms have been published (1, 2). The rate of deformation has now reduced to the point that future deformations would appear to be insignificant, and the project is therefore being terminated.

AGGREGATES

The aggregates investigated in connection with the project were volcanic cinders, pumice, and 2 expanded shale aggregates produced commercially in Oregon and marketed under trade names. For this project, the expanded shales have been designated as aggregate A and aggregate B. The normal-weight aggregate used in the control specimens was Santiam River sand and gravel.

The expanded shale aggregates are the products of crushing and burning Keasey shales. Before burning, aggregate A is crushed to a 2-in. maximum size and aggregate B to a 3-in. maximum size. Both materials are expanded by heating them to about 2,000 F in rotary horizontal kilns. After burning, the aggregates are crushed to the desired sizes for marketing. The resulting material is primarily uncoated; that is, most of the larger particles and many of the small ones have porous faces. Initial studies were made using $3\frac{3}{4}$-in. maximum particle sizes in the expanded shales, but the mixes chosen for time deformation studies used $\frac{3}{8}$-in. to $\frac{3}{16}$-in. and $\frac{3}{16}$-in. to 0. The grain size analyses of the various aggregates used in the time deformation studies are given in the progress reports (1, 2).

The maximum particle size used in the sand and gravel concrete was $\frac{3}{4}$ in. These normal-weight materials are sound and durable and have a good service record as concrete aggregates.

The pumice and volcanic cinders were obtained from natural deposits in central Oregon and subsequently crushed to desired gradings.

MIX DEVELOPMENT

In the beginning stages of the project, concrete mixes made with the 2 expanded shales, with cinders, and with a combination of cinders and pumice were cast in standard cylinders and tested at ages of 28 and 60 days to determine the ultimate compressive strengths of the concrete. In addition, the various mixes were judged for workability and the slump and wet weights were measured. In designing the mixtures, it was decided the concrete should have a minimum 28-day ultimate strength of 4,500 psi to be economically feasible for the intended purpose. Cement contents were varied between 6 and 9 sacks per cu yd and the coarse and fine aggregate proportions were varied to evaluate the effect on workability.

Several trial mixes were made using volcanic cinders. This material is very sharp and concrete produced with it was considered too harsh for use in prestressed members. The wet weight of the concrete was about 122 pcf, somewhat higher than was desirable. Because of the harshness and the weight of the concrete, mixes with a full range of cement content were not made. A 7-sack mix had a 28-day ultimate strength of about 3,000 psi.

To reduce the weight and improve the workability, pumice were used as the fine aggregate and cinders as the coarse aggregate. This combination produced concrete that was much lighter (101 pcf wet) and the workability was somewhat improved, but the concrete still seemed somewhat harsh and the ultimate strength of these mixes fell far short of meeting the desired 4,500-psi 28-day strength. Because of the unsatisfactory strength and workability, no time deformation studies were made on these concretes.

The initial trial mixes with expanded shale aggregate A used $\frac{3}{4}$-in. to $\frac{3}{8}$-in. material for the coarse fraction and $\frac{3}{8}$-in. to 0 for the fine fraction. Other mixes were made with only the $\frac{3}{8}$-in. to 0 material. For later mixes the manufacturer supplied $\frac{3}{8}$-in. to

3/16-in. and 3/16-in. to 0 material and these were used as the coarse and fine fractions. Because of a slight harshness of these mixes and influenced by previous experience of the manufacturer, 2 cu ft of natural sand per cubic yard of concrete were combined with the 3/8-in. to 3/16-in. and the 3/16-in. to 0 aggregates. Using these components, a 9-sack mix having excellent workability and adequate ultimate strength were selected for a study of time deformation characteristics.

The most extensive experimentation with the various aggregates was with aggregate B, for which 16 trial mixes were made. Several mix designs developed by an independent testing laboratory were obtained and used as a basis for the earlier mixes developed in connection with this project. Initially the aggregate was furnished in 3 sizes—3/4- to 3/8-in., 3/8- to 3/16-in., and 3/16-in. to 0. In many of the mixes all 3 sizes were used in varying proportions but a stronger, more workable concrete resulted from using 3/8 in. as the maximum particle size. To provide a margin of safety on the desired ultimate strength, a 9-sack mix was selected for use in the time deformation studies. Details of the concrete mixes used in the time deformation studies are given in Table 1. Aggregates for prisms numbered 7 through 12 were obtained at a different time than those that were used in prisms 1 through 6 and although the volume ratios of coarse aggregate to fine aggregate were maintained the same for a given aggregate, variations in gradation and unit weight caused significant differences in the resulting concrete mixes.

To obtain high-strength concrete with the expanded shale aggregates used in this study, it was found that a rather high cement factor was required. An objective of the project was to develop mixes having high ultimate strength and suitable workability to make the placing of the concrete feasible using conventional field techniques. By using lower water-cement ratios or higher proportions of coarse aggregate in relation to the amount of fine aggregate, concretes having satisfactory strengths can be produced with lower cement factors; however, these mixtures did not seem suitable for field placement. For the construction of members in a casting yard, where rigid controls and adequate vibration can be assured, the drier, harsher mixes can be used to economical advantage.

Because the absorption of water by lightweight aggregates fluctuates widely, depending on the porosity and the moisture content of the particles, it was found impractical to design a mixture with a rigid water-cement ratio. To control consistency to a specified slump is more satisfactory. For comparable workability, the lightweight concretes will have appreciably less slump than corresponding sand and gravel concretes. In this study, it was found that expanded shale concretes having a slump of 1 1/2 in. were easily placed and tended to flow readily under the action of a vibrator. It was estimated

TABLE 1

CONCRETE MIXTURES USED IN TIME DEFORMATION STUDIES

Property	Mixture					
Aggregate type	A	A	B	A	B	Sand & Grav.
Prism numbers	1, 2	3, 4	5, 6	7, 8	9, 10	11, 12
Coarse aggregate, 3/8 in. -3/16 in., lb per cu yd	311	283	366	307	431	—
Coarse aggregate, cu ft per cu yd	8.2	8.5	8.3	9.2	7.9	—
Fine aggregate, 3/16 in. -0, lb per cu yd	960	986	1,213	1,056	1,183	—
Fing aggregate, cu ft per cu yd	19.0	19.6	21.7	21.2	20.7	—
Gravel, 3/4 in. -3/16 in., lb per cu yd	—	—	—	—	—	2,220
Gravel, cu ft per cu yd	—	—	—	—	—	20.0
Natural sand, lb per cu yd	186	159	0	173	0	907
Natural sand, cu ft per cu yd	2.0	2.0	0	2.0	0	9.0
Cement factor, sacks per cu yd	8.6	8.8	9.0	9.5	8.6	7.5
Admixture, lb per sack	0.25	0.25	0.25	0.25	0.25	0.25
Water/cement ratio, total water, gal per sack	7.3	7.1	6.2	6.4	7.5	4.7
Wet weight, pcf	102	103	107	108	104	153
Slump, in., average	2 1/2	1 7/8	1 1/2	1 3/4	1 1/2	2 1/4
28-day compressive strength, psi	4,450	5,078	5,690	6,260	5,880	6,420
Secant modulus of elasticity at 28 days, psi	1,722,000	2,014,000	2,069,000	2,244,000	2,233,000	5,010,000

that the consistency of this concrete was similar to sand and gravel concrete having a slump of about 3 in.

Of concern to designers of prestressed concrete members is the modulus of elasticity of the concrete. The secant modulus of elasticity, calculated at 2,000-psi stress level, was determined for most of the trial mixes as well as the mixes used in the time deformation studies. Values of modulus of elasticity vs ultimate strength are plotted for aggregate A in Figure 1 and for aggregate B in Figure 2. The straight-line equations that best represent the modulus of elasticity of these concretes were determined by the method of least squares to be:

1. for aggregate A, $E = 420,000 + 320\, f'_c$, and
2. for aggregate B, $E = 560,000 + 275\, f'_c$.

Since the cylinder strengths used in obtaining these equations varied only from about 4,000 to 7,000 psi, the equations can only be assumed to be applicable within this range.

The modulus of elasticity values of concretes from both of the expanded shale aggregates were consistently lower than the values calculated from the equation $E = w^{1.5}\sqrt{f'_c}$, contained in the 1963 ACI Building Code revision (3), where w is the weight of the concrete in pounds per cubic foot and E and f'_c are in pounds per square inch. The measured values are approximately 80 percent as great as values calculated from this equation.

For the limited data available from the concretes tested on this project, an equation of the type proposed by the ACI Code committee that fits the values for the lightweight

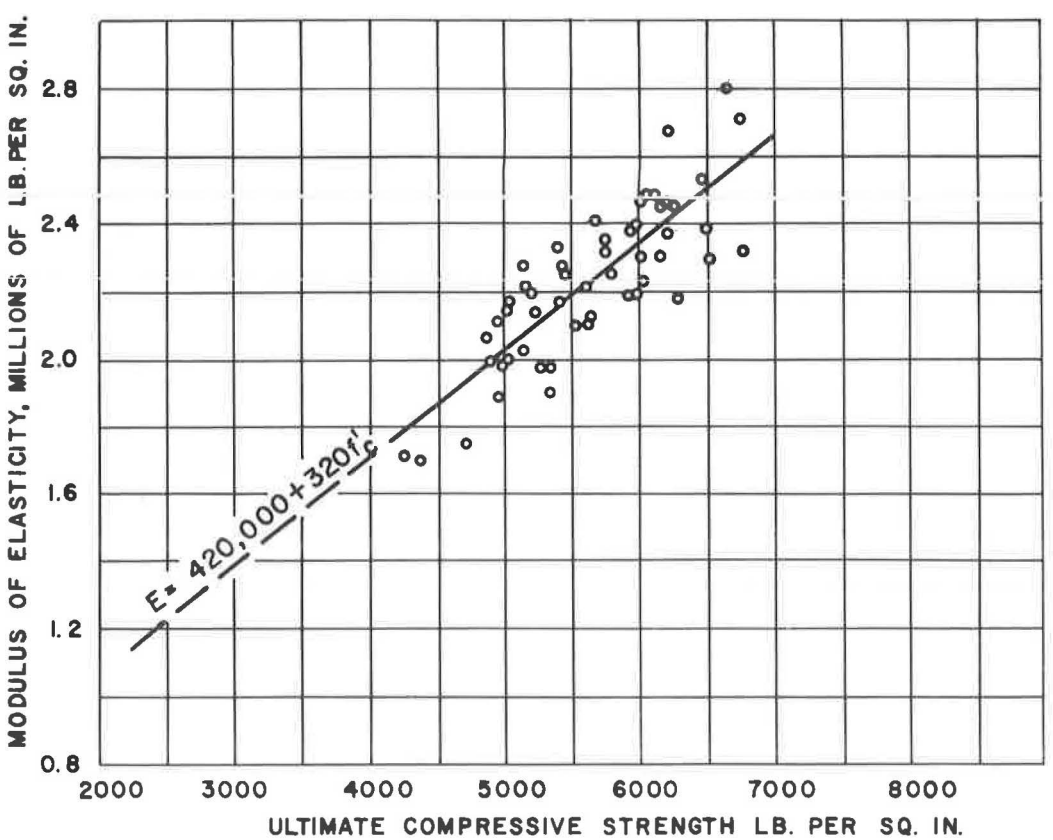

Figure 1. Modulus of elasticity vs ultimate strength for concrete using aggregate A.

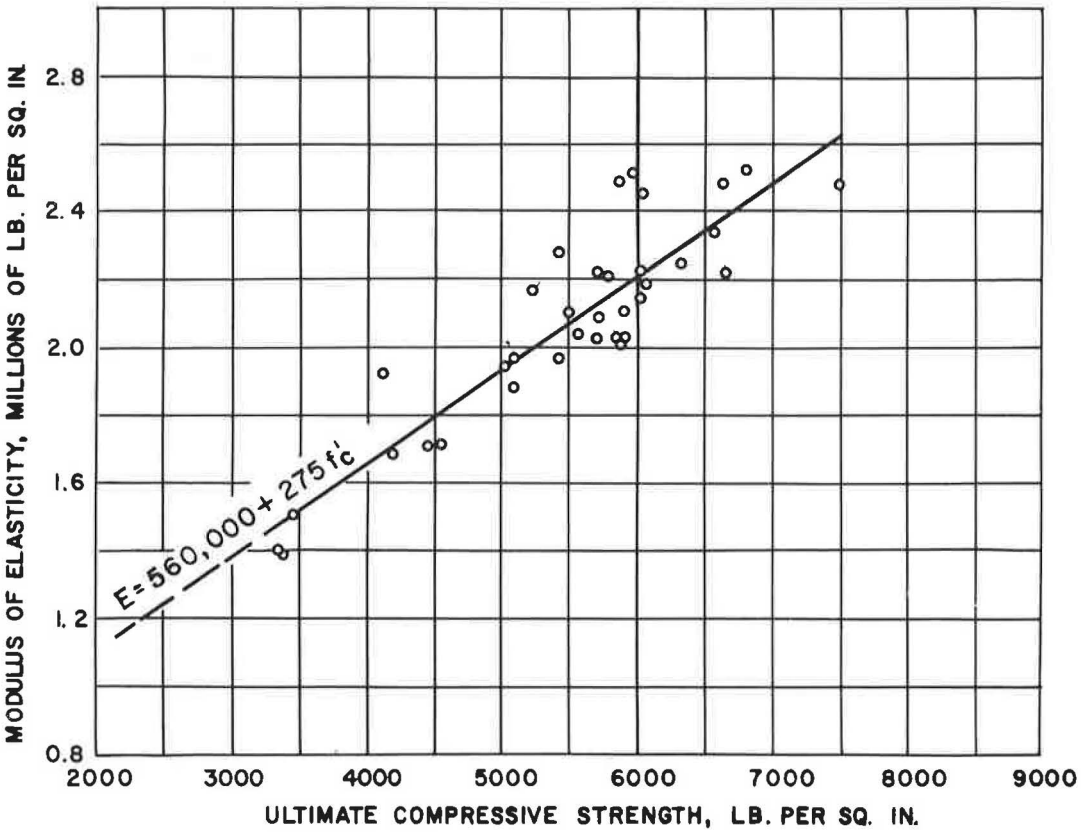

Figure 2. Modulus of elasticity vs ultimate strength for concrete using aggregate B.

concretes with less error and also fits the sand and gravel concrete is $E = 1.1\ w^{2.18}\sqrt{f'_c}$ This equation is presented for purposes of comparison only. Although it provides reasonably good values for the concretes used in this study, its general applicability is unknown.

PROCEDURE FOR CREEP AND SHRINKAGE STUDIES

To determine the total time deformation in the concrete mixtures that were chosen for these studies, rectangular prisms 5 in. by 6 in. by 107 in. were cast. A flexible metal conduit was cast into the prisms along the longitudinal axis to permit the introduction of reinforcement for stressing. Four steel bars, 2 near each end, were cast in the prisms perpendicular to the axis of the prisms. These bars protruded from each side of the prisms and provided 4 pairs of gage points 100 in. center-to-center for each specimen. The gage points were 1 in. from the top and bottom surfaces of the prisms. The gage used for length measurements consisted of an Invar rod with a dial indicator graduated to 0.001 in. mounted at one end and a pointed stud and clamp at the opposite end. During the measurements, the gage was supported at the ends and at 4 intermediate points so that deflection of the Invar rod was practically eliminated.

The prisms were cast and stored in timber racks. To reduce resistance to creep and shrinkage, the prisms were supported by aluminum covered members on which a parting compound was used to prevent bond between the aluminum and the concrete. The side forms were removed 24 hours after casting the prisms. The ends of the prisms were provided with load distributing plates $1\frac{1}{4}$ in. thick having the same areal dimensions as the prism cross section. These plates served as the end forms in casting the members.

In the portion of the study in which specimens were subjected to a constant stress, 2 prisms were cast from aggregate B concrete and 4 prisms from aggregate A concrete. These prisms were numbered 1 through 6; the mix details are given in Table 1.

To determine the time deformation of concretes subjected to a relaxing prestress force, 6 additional 107-in. prisms were cast—2 each from aggregate A, aggregate B, and sand and gravel concretes. In this latter study, 2 shorter prisms were cast from each of the 3 mixes to provide shrinkage specimens. The shrinkage prisms had the same cross-sectional dimensions as the longer prisms and, to maintain the same area-perimeter ratio, they also had a flexible conduit at the longitudinal axis. The shrinkage specimens had a 24-in. gage length but otherwise the arrangement of the gage points was the same as those on the longer prisms. To obtain adequate sensitivity, dial indicators graduated to 0.0001 in. were used on gages for measuring shrinkage.

Twelve standard cylinders were cast from each of the concrete mixes at the time the prisms were poured to provide information on strength and modulus of elasticity. All concrete for the project was mixed in a Lancaster laboratory mixer in batches of about 1.3 cu ft. Consistency was controlled by a slump test on each batch. Average slumps are given in Table 1. Except for prisms 3 and 4, the concrete was consolidated in the forms by means of hand rodding and tamping. An electrically operated laboratory vibrator was used for prisms 3 and 4 but because of some difficulty in using the vibrator in the restricted forms and higher initial time deformations in the prisms on which it was used, its use was discontinued. The cylinders were cured in a moist room until tested and the prisms were cured by maintaining a wet burlap covering over them for a 2-week period. Approximately 24 hours after casting the various prisms, the side forms were removed and initial measurements of length were made. To detect any differential shrinkage or creep, measurements were always made at each of the 4 gage positions on each prism. Periodic measurements were made on all of the prisms during a 28-day curing period preceding the stressing of the longer prisms.

PRESTRESSING DETAILS

The first 6 prisms were stressed to 2,000 psi and, within narrow limits, this stress has been retained. These prisms are referred to as being subjected to a constant stress although the actual stress varied between values of 1,900 and 2,100 psi. The variation seldom exceeded 75 psi, from a low of 1,950 to a high of 2,025 psi. To apply the stress, a 1-in. diameter Stressteel bar was introduced at the longitudinal axis through the metal conduit cast into each prism. The bars were tensioned by means of a calibrated, center-hole ram and pump and stress adjustments were made through the anchorage nuts on the threaded bar ends. The bars were retensioned at intervals so that a relatively constant stress was maintained.

To study creep under conditions similar to those that exist in typical prestressed members where the stress intensity is gradually diminished as creep and shrinkage of the concrete and relaxation of the steel occur, an initial stress of approximately 1,820 psi was applied to a series of 6 prisms and natural relaxation was permitted to occur. To provide this stress a standard Prestressing Inc. unit having six 0.25-in. diameter wires was inserted through the conduit in each prism. The wires in these units have double buttons at the ends—an outer button for stressing and an inner one for anchoring. The standard anchorage and stressing hardware was used. To provide precise adjustment at the anchorage, a threaded bearing collar was used instead of shims. Because some seating deformation of the buttons was anticipated, the cables were stressed, anchored, restressed, and, after adjusting the threaded collar, anchored again.

In an effort to measure the difference in stress of various wires in a given wire group, type A-12, SR-4 resistance strain gages were installed on each wire. These gages have a 1-in. gage length and a trim width of $\frac{1}{8}$ in. Some difficulty was encountered in installing the gages on the small-diameter wires. The gages were sensitive to strain and in most instances reasonable readings were obtained from them; however, the variation in readings was large enough that the difference in stress in individual wires of a group was more or less obscured by the experimental errors in measurement. These data are not considered reliable. The initial total force calculated from

the strains measured in the individual wires varied from 91.5 percent to 94.9 percent of the design load with the average being 93.4 percent of design load. The reduction in strain measured on the individual wires as creep and shrinkage of the concrete occurred was not as great as the reduction in total force on the prisms would indicate. To summarize, the initial SR-4 gage strain readings were low, on the average, and the indicated change in strain as losses occured was also low, but not by a consistent ratio.

To measure the total loss of stress in the wires as creep and shrinkage of the concrete and relaxation of the steel occurred, pressure cells were installed between the end anchorage and the bearing plate on each prism. These cells were fabricated from 12-in. lengths of AISI 4130 Shelby tubing $2\frac{1}{2}$ in. in diameter with 11-gage walls. On opposite sides of each prism dial indicators graduated to 0.0001 in. were installed to measure strain over a 10-in. gage length. One division on the dial indicators represented a change in load of about 280 lb. This sensitivity is equal to approximately 0.5 percent of the initial applied load. Prior to use, the pressure cells were preloaded briefly to reduce the relaxation of the steel in the cells and were calibrated in a hydraulic testing machine.

Immediately before and after stressing a given prism, length measurements were made and readings were taken on the pressure cells and SR-4 gages. Since the design load was applied by a calibrated ram, these various measurements provided several methods of evaluating the initial force. Agreement within 1 percent was obtained between the force indicated by hydraulic ram and pressure cell on all but one prism. On the one prism, the pressure cell indicated an initial force about 8 percent higher than the hydraulic indication. It appears an erroneous zero reading was obtained for this cell, perhaps because of some slight damage during stressing.

RESULTS OF SHRINKAGE MEASUREMENTS

On the group of 6 prisms that were subjected to a constant stress, no provision was made to measure shrinkage separately. Shrinkage was measured during the 28-day curing period preceding stressing, but subsequently only the combination of creep and shrinkage was obtained. During the 2-week period that moist burlap was kept over them, a slight growth was measured in most of the prisms. After 28 days, all prisms had some shrinkage. The average values for the individual pairs were as follows: prisms 1 and 2, 0.75 ten-thousandths in. per in.; prisms 3 and 4, 0.60 ten-thousandths in. per in.; and prisms 5 and 6, 1.10 ten-thousandths in. per in. These pairs of prisms were cast at different times and it is likely that slight variations existed in the amount of water available to the concrete from the moist burlap so the differences in shrinkage existing at the time of stressing were not considered to be significant. In each of the prisms, higher shrinkage was measured at the upper gage points than at the lower points. This difference is attributed to a more rapid drying near the top since the prisms rested on aluminum sheets, preventing loss of moisture at the bottom.

Shrinkage specimens were cast to accompany the prisms subjected to a relaxing prestress force. During the 28-day curing period, periodic length measurements were made on the shrinkage specimens and the longer prisms that were prepared for stressing. During the 2-week period that the prisms were kept moist, some swelling occurred in those cast from expanded shales, whereas those cast from sand and gravel showed some shrinkage. The longer prisms showed less change in length during the curing period than the shorter shrinkage specimens. The longer prisms of sand and gravel concrete had a very slight shrinkage during the initial 2-week period and the longer prisms of lightweight concretes show less growth than the shorter prisms of the same concrete. All prisms received identical treatment, but slight variations in available moisture are likely and the frictional resistance of the longer prisms to changes in length would be greater than for the shorter prisms. Figure 3 shows the average shrinkage for each of the concretes as measured on the shrinkage specimens. The initial measurements were made immediately after the side forms were removed and the study on these specimens was continued for over 5 years. The prisms were numbered to correspond with the same concrete in the longer prisms. Prisms 7 and 8 are from aggregate A concrete, prisms 9 and 10 from aggregate B, and prisms 11 and 12

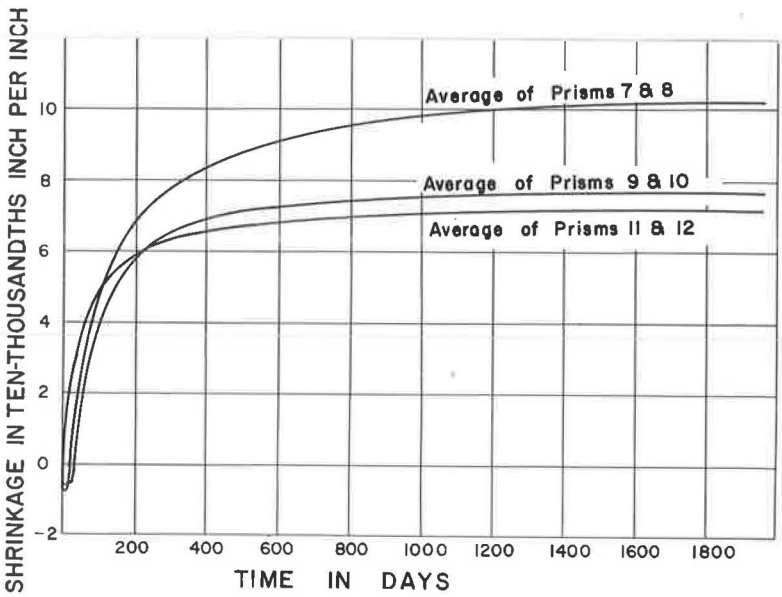

Figure 3. Average shrinkage of prisms.

from sand and gravel. Slight variations in shrinkage existed between the individual prisms cast from a given concrete, but these differences were considered insignificant, and only the average values for each pair are shown. The shrinkage of the aggregate B concrete exceeds that of the normal-weight concrete by only 4 percent but the shrinkage of the aggregate A concrete is 41 percent greater than that of the normal-weight mixture. The reason for the significant difference in shrinkage between the 2 lightweight concretes cannot be established from the limited scope of this study. However, reports of other studies suggest several items that probably contributed to the greater shrinkage of the aggregate A concrete. Jones and Hirsch (4) found that mixtures having a higher cement content, with aggregate type and gradation and consistency of the concrete being the same, had higher shrinkage. Also, it has been found that high percentages of fine particles in the aggregate result in higher shrinkage of the concrete. The aggregate A concrete had a higher cement content and a higher percentage of material passing the No. 100 sieve than the aggregate B mix. Aside from the greater shrinkage of prisms 7 and 8, the difference in shape of the normal-weight concrete curve from those of the lightweight concretes is significant. In considering the loss of prestress due to shrinkage, it is the shrinkage that occurs after the tendons are stressed that is of importance. In a post-tensioned application, where the tendons may not be stressed for 3 or 4 weeks after the concrete is cast, the measurements on the prisms indicate appreciably less subsequent shrinkage for the normal-weight concrete than for either of the lightweight concretes.

The values of ultimate shrinkage measured on this project exceed by a wide margin the usual allowance contained in recommendations for the design of prestressed members. For normal-weight concrete, the recommendations of different authorities usually vary between 0.0002 and 0.0004 in. per in. for shrinkage allowance. No recommended allowances are presented for lightweight concrete.

A number of studies conducted on structural quality concretes during recent years report shrinkage strains comparable to those measured on this project. A paper by Raymond E. Davis and Harmer E. Davis (5) reports that unstressed specimens stored at 50 percent relative humidity showed a shrinkage of 0.00061 in. per in. at an age of one year. Shideler (6) reports ultimate shrinkage values for normal-weight concrete ranging from 0.00073 in. per in. for a 4,500-psi mixture to 0.00053 in. per in. for a

7,000-psi mixture. For corresponding lightweight concretes, Shideler found shrinkage values ranged from 6 to 38 percent higher than for normal-weight mixes. These tests were conducted at 50 percent relative humidity. In a paper by Staley and Peabody (7) shrinkage of 0.00087 in. per in. is reported for normal-weight concrete bars stored at 70 F and 50 percent relative humidity. Shrinkage values for various lightweight concretes ranging from a high of about 0.0009 in. per in. to a low of about 0.0004 in. per in. are reported by Jones and Hirsch (4) for specimens stored at an average relative humidity of 60 percent. The higher values were for the richer concrete mixes. A paper by Corley, Sozen, and Siess (8) shows shrinkage values of about 0.0006 to 0.0007 in. per in. for laboratory specimens stored at 70 F and 50 percent relative humidity.

On this project, no control of temperature and relative humidity was maintained. Temperatures were recorded each time measurements were made and these values indicate the average temperature was about 72 F. From occasional measurements of relative humidity, it is estimated this value averaged around 50 percent. The average relative humidity of the storage area would be somewhat lower and much more uniform than that which would be expected in a typical outdoor installation in Oregon. This lower relative humidity would accelerate the time rate of shrinkage and probably increase the total amount. The paper by Jones and Hirsch compares the shrinkage of laboratory-stored specimens with identical specimens that were stored outdoors where they were exposed to rain, fog, and light freezing. Even though the average relative humidity and the average temperature was almost the same for both exposures, the field specimens show less than one-third as much shrinkage as the laboratory specimens. This extreme variation makes it difficult to estimate how much shrinkage should be anticipated for concrete in a bridge member. The deck would provide shelter from direct precipitation, but fog and condensation would probably reduce the shrinkage far below the laboratory measured values for bridges constructed in other than a very arid climate. Further research is needed in this area.

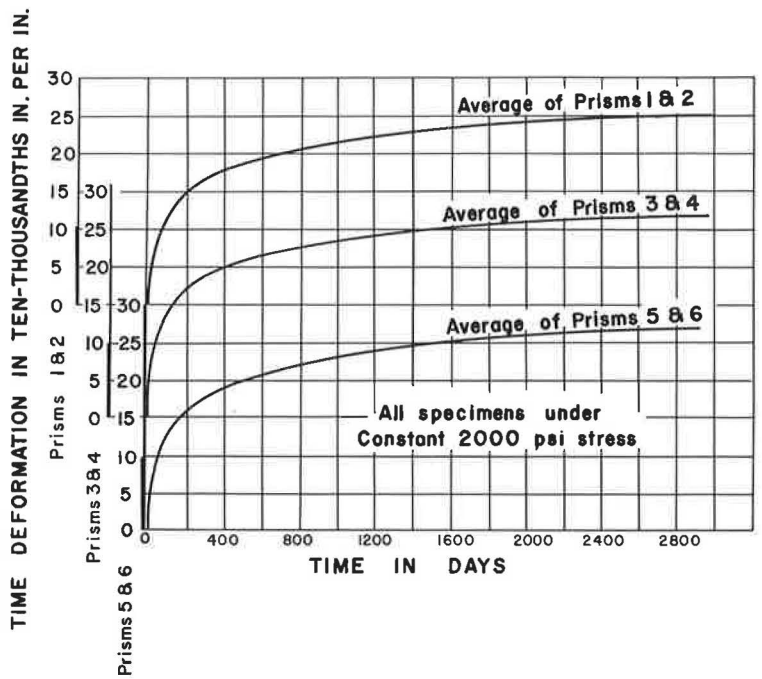

Figure 4. Time deformation curves.

TIME DEFORMATION OF SPECIMENS

The unit change in length for the prisms subjected to constant stress is shown in Figure 4. This deformation includes both creep and shrinkage and will be referred to as "time deformation." The origin of the ordinate on these curves is based on the length measured immediately after the initial stressing, and the abscissa originates from the day of this stressing. For purposes of comparison, the instanteous, or elastic, deformation is shown as a bar on the left side of each curve. Prisms 1, 2, 3, and 4 were cast from aggregate A concrete, 2 each from 2 slightly different mixes. Prisms 5 and 6 were from aggregate B concrete. Deformations of the individual prisms of the various pairs were very similar. The greatest difference was between prisms 1 and 2 where the variation was about 5 percent. The average deformation of the different pairs is also quite similar. At an age of 8 years, the averages were 0.00252 in. per in. for prisms 1 and 2; 0.00268 in. per in. for prisms 3 and 4; and 0.00270 in. per in. for prisms 5 and 6. Although the difference is hardly significant, it is interesting to note that prisms 1 and 2, having the lowest time deformation, were from concrete having lower ultimate strength, higher slump, higher water-cement ratio, but also, a lower cement content.

The values of time deformation at the termination of the measurements can be considered ultimate values with very little error. It is frequently estimated that approximately 75 percent of the ultimate creep will occur during the first year. These prisms had one-year values of creep plus shrinkage that ranged from 68 percent to 73 percent of the ultimate values—similar to the 75 percent estimate.

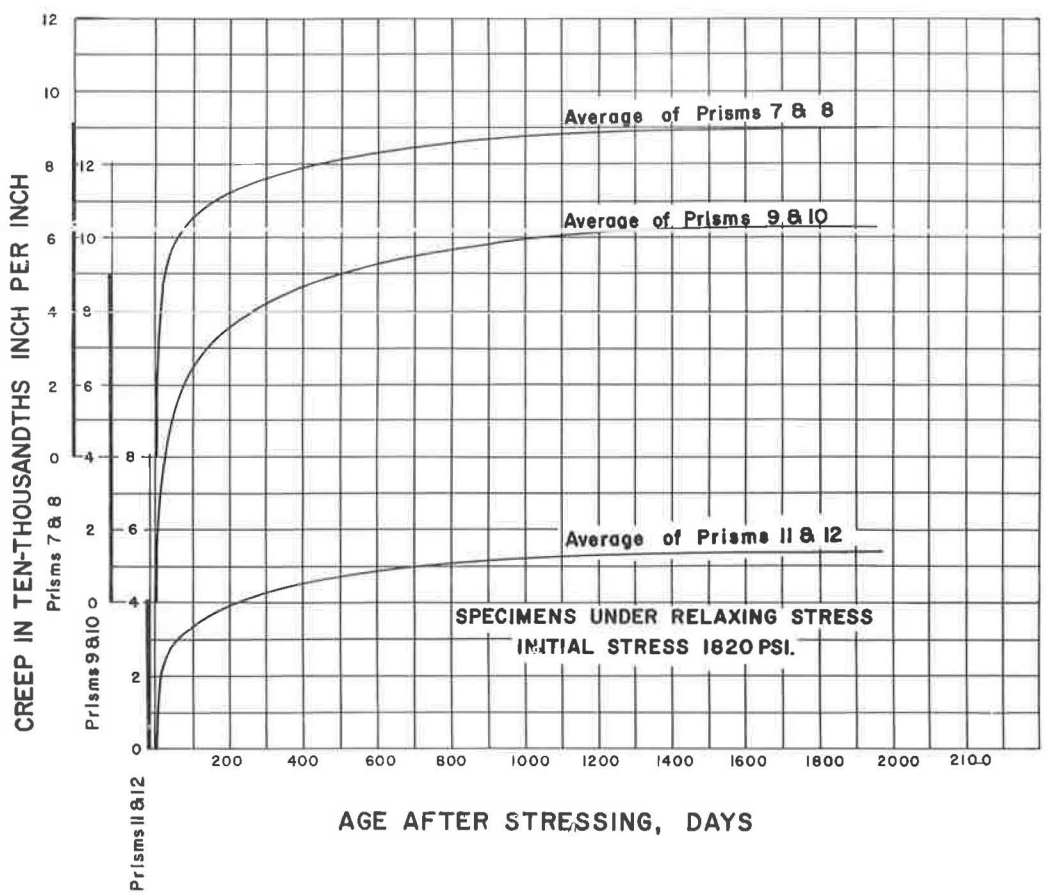

Figure 5. Creep deformation of prisms.

For the prisms subjected to a relaxing prestress force, companion specimens remained unstressed to measure the shrinkage of the concrete. The creep was determined by subtracting the shrinkage from the measured total deformation. The average unit creep for these pairs of prisms is shown in Figure 5. In this group, prisms 7 and 8 were made with aggregate A, prisms 9 and 10 with aggregate B, and prisms 11 and 12 with sand and gravel concrete. The measurements extend over a period of about 5.3 years and from the present slope of the curves it would seem that any future creep would be insignificant. As would be expected, the fact that these prisms were under a relaxing force caused them to attain a condition of equilibrium at an earlier age than those prisms that were under a uniform stress. The deformations of the individual prisms from a given concrete were all quite similar. A maximum difference of 7 percent occurred between prism 9 and prism 10, which were cast using aggregate B. The average elastic deformation of each pair of prisms is shown as a bar on the ordinate. Comparing the different concretes, the average unit creep at the conclusion of measurements was 0.00091 in. per in. for prisms 7 and 8, 0.00103 in. per in. for prisms 9 and 10, and 0.00054 in. per in. for prisms 11 and 12. On these prisms, the measured creep for the aggregate A concrete is 69 percent greater than that for the sand and gravel concrete and the aggregate B concrete is 90 percent greater than the value for the sand and gravel concrete. Comparing the total deformations (creep plus shrinkage), the differences among the 3 concretes are not as great. On this basis, the total deformations are 52 percent greater for aggregate A and 41 percent greater for aggregate B than the value measured for the sand and gravel concrete.

LOSS OF PRESTRESS

The designer of prestressed concrete members must estimate the magnitude of the initial prestressing force required to assure the retention of some minimum design value after the ultimate creep and shrinkage of the concrete and the ultimate relaxation of the steel have occurred. The decrease in prestress can be estimated with reasonable accuracy if sufficient information about the physical characteristics of the concrete and steel is available. For the prisms subjected to a relaxing prestress force, pressure cells were installed to measure the loss of prestress directly. Figure 6 shows the change in prestress expressed in terms of the initial prestress remaining. The measurements cover over 5 years and it appears that the ultimate values have been attained. The average values for the different aggregates indicate a 30.1 percent loss for aggregate A prisms, a 29.9 percent loss for aggregate B, and a 19.8 percent loss for the normal-weight concrete. Calculations of loss of prestress based on the measured time deformations of the concrete indicate average losses of 26.0 percent for aggregate A, 24.2 percent for aggregate B, and 17.0 percent for the normal-weight concrete prisms. Comparing the values of measured and calculated losses, the difference indicates average losses from relaxation of the steel of 4.1 percent for the pair of prisms from aggregate A, 5.7 percent for aggregate B, and 2.8 percent for the sand and gravel concrete. These are not unreasonable values for relaxation losses; however, since all of the steel was from the same lot and stressed to the same level, the relaxation losses should be very nearly equal for all prisms. The variations are probably the result of experimental errors in measurements.

The value of loss of prestress measured on the test prisms would require some modification to permit their application in the design of prestressed concrete members, even though the same stress intensity were applied. In the test specimens, the concrete portions of the prisms were 105 in. long whereas the length of the stressed steel was approximately 125 in., the difference being the combined length of pressure cell, bearing plates and miscellaneous anchorage hardware. In a typical beam of commercial dimensions, the difference in length between the concrete and the stressed steel is an insignificant percentage of the total length, whereas in the test prisms the steel was 19 percent longer than the concrete. The stress losses caused by shortening of the concrete would be increased by this amount if steel and concrete were the same length, all other factors being equal.

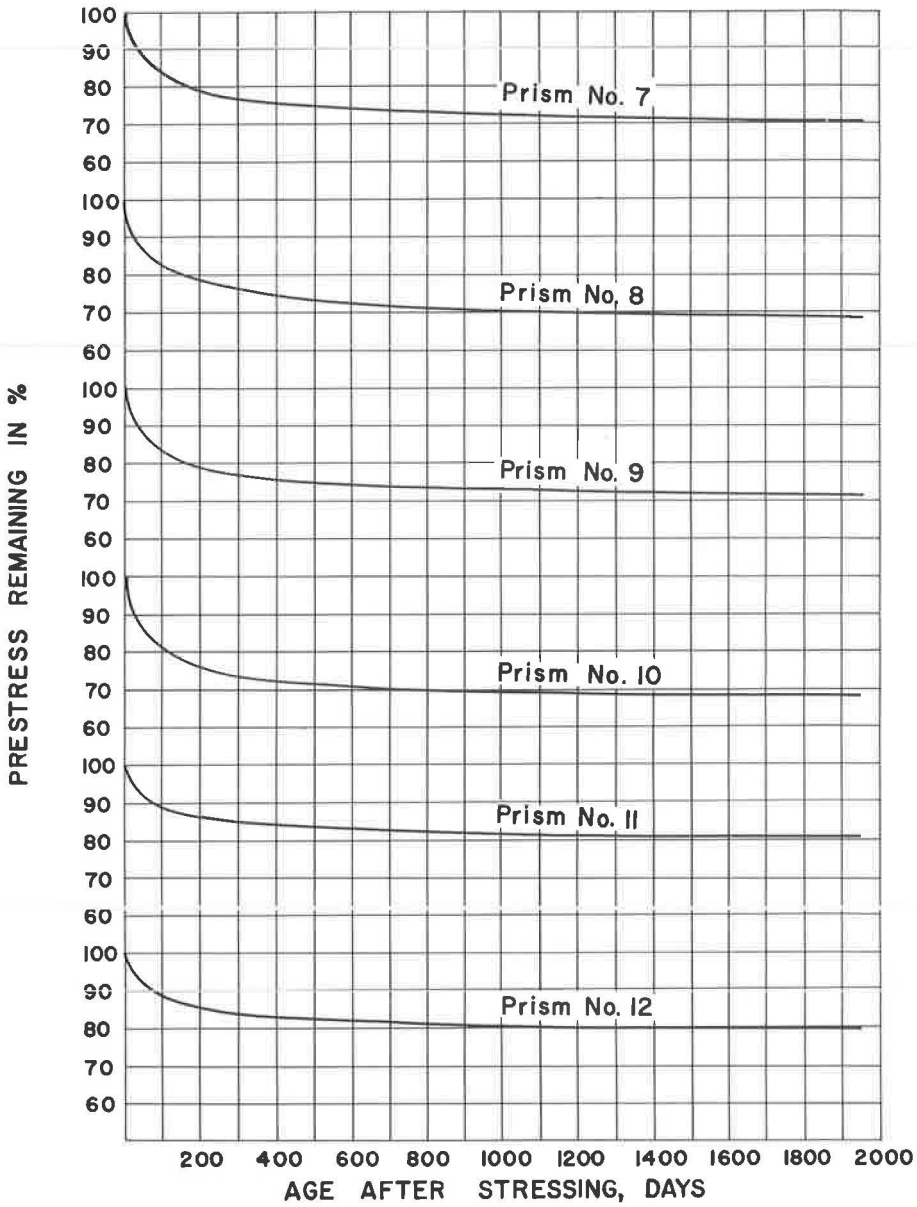

Figure 6. Loss of prestress curves.

COMPARISON OF CONSTANT STRESS AND RELAXING STRESS

To provide a basis for comparison of the prisms subjected to constant stress with those under a relaxing stress, it is necessary to assume values of shrinkage for the constant-stress prisms. The best estimate is probably provided by assuming that the shrinkage of the constant-stress prisms was the same as that of the concretes used in the relaxing-stress phase of the project. The differences between the concretes used in the studies leave some doubt about the accuracy of such an assumption; however, the magnitude of error should not be great.

After correction for shrinkage, the constant-stress prisms yield an average creep coefficient of 0.79 microinches per in. per psi for aggregate A concrete and 0.97 microinches per in. per psi for aggregate B concrete. The constant-stress studies did not include normal-weight concrete prisms so no comparisons are available between the normal-weight and lightweight materials.

To obtain a visualization of the effect of the diminishing stress intensity as compared with specimens under constant stress, the coefficients for the relaxing-stress study can be computed on the basis of the initial stress level. On this basis, the average creep coefficients for the different prisms were 0.50 microinches per in. per psi for aggregate A, 0.57 microinches per in. per psi for aggregate B, and 0.30 microinches per in. per psi for the normal-weight concrete. Numerous investigators have determined a linear or near linear relationship between stress and creep. This fact permits the use of such coefficients to predict losses that may occur under stress intensities different from those used in the tests. Since these latter coefficients were evaluated under a relaxing stress condition that would resemble the stress changes occurring in a prestressed member, they could be used to estimate the ultimate creep of prestressed members constructed from similar concretes by considering only the initial stress conditions. Some variation would result for different amounts of shrinkage and relaxation since these factors would influence the magnitude of the effective stress existing over a period of time. However, the effect of such differences would be minor.

A comparison between the creep coefficients obtained for the constant stress prisms and the latter coefficients computed on the basis of the initial stress reveals the latter are about 60 percent of the former. This comparison demonstrates the reduction in creep deformation that occurred in the lightweight prisms subjected to a relaxing prestress force. A smaller difference would exist with the normal-weight prisms since the stress reduction was less for the material.

In utilizing prestressed members, different increments of dead load may be applied at significantly different times, an illustration being the time elapsing between prestressing of beams and casting of deck on bridges. In some instances the total load is applied in a short time and the assumption that it was all applied at the same time would be satisfactory for calculating losses. In other cases, where more time elapses between the application of increments of load, it is necessary to consider the effect of the individual loads. For this condition, the shape of the creep curve is involved and an equation to express the shape is convenient. For the prisms subjected to constant stress, the deformation curves had the shape:

$$\Delta = 0.150 \log_e (t + 3) - 0.19$$

where Δ = fraction of the total deformation from creep plus shrinkage, and t = time after stressing in days.

This equation is equal to 1.00 at 2,800 days which can be assumed to cover the total deformation. Actually, a semilog plot of the data is still linear at the termination of the measurements. Thus no finite terminal value is indicated; however, the rate of increase is negligible. Creep and shrinkage were not separated on this portion of the project so the equation is for the total deformation in the lightweight concrete prisms. There is no significant difference between the shape of curves for the different lightweight aggregates.

SIGNIFICANCE OF MEASUREMENTS AS APPLIED TO DESIGN

The designer of prestressed members must estimate the magnitude of creep, shrinkage, and relaxation losses that may occur in the materials he intends to use. Typical allowances are available for normal-weight concrete, but the information about the properties of lightweight concrete is limited. Present AASHO specifications permit the use of an assumed total loss in the prestressing steel of 25,000 psi for posttensioned members and 35,000 psi for pretensioned members constructed from typical normal-weight concrete. Values for lightweight concretes must be estimated from tests on

mixtures from the particular aggregates. The AASHO values for loss of stress are similar in magnitude to those calculated from recommended allowances in other literature on prestressed concrete design.

In most of the design literature, recommended allowances for shrinkage range from 0.0002 to 0.0004 in. per in. On this project the shrinkage of the normal-weight concrete was 0.00072 in. per in. which results in a stress loss from shrinkage much greater than that anticipated by the design recommendations. Although the measured shrinkage seems high, many investigators have measured similar values on good quality concretes. Studies of concretes in an outdoor exposure where free moisture in the form of rain or fog is periodically available have shown lower values of shrinkage (4) than laboratory stored specimens even though the average relative humidity was the same in each case. Except for very sheltered locations or use in arid climates, shrinkage allowances somewhat lower than the laboratory-measured values should be satisfactory. Values of about 0.0004 in. per in. were measured on specimens studied in connection with the AASHO Road Test. An allowance of this magnitude would seem reasonable for normal-weight concrete in typical outdoor exposures.

The total shrinkage of the concrete using aggregate B was very similar to that of the normal-weight concrete, but initially, the lightweight concretes increased in length while the normal-weight concrete decreased. For posttensioned members, this initial swelling leaves more of the shrinkage to occur after stressing, resulting in a proportionally greater loss of prestress.

Under like storage conditions, the prisms cast from aggregate A had a total shrinkage about 35 percent greater than aggregate B prisms and 40 percent greater than the normal-weight prisms. For concrete in an outdoor exposure, this percentage difference would probably remain similar so that if an allowance of 0.0004 in. per in. is satisfactory for normal-weight concrete, about 0.0006 in. per in. should be anticipated in aggregate A concrete.

The measured values of shrinkage occurring after the prisms were stressed would cause stress losses of about 14,000 psi for the sand and gravel concrete, 21,000 psi for the aggregate B concrete, and 28,000 psi for the aggregate A concrete, assuming a modulus of elasticity of 28×10^6 psi for the steel.

The average end-to-end stress at the centroid of the prestressing steel will undoubtedly vary appreciably between beam designs, but a value of about 1,000 psi was determined for several beams that were reviewed. If an average stress of 1,000 psi is assumed and the creep coefficients based on the initial stress are applied, the loss of stress from creep would be about 8,400 psi for normal-weight concrete, 16,000 psi for aggregate B concrete, and 14,000 psi for aggregate A concrete.

If a 4 percent relaxation loss is assumed for the steel and the steel is stressed to 170,000 psi, the relaxation loss would be 6,800 psi for all beams. Summing the values from shrinkage, creep, and relaxation gives a total indicated loss of 29,200 psi for normal-weight concrete, 43,800 psi for aggregate B concrete, and 48,000 psi for aggregate A concrete. These values are for a posttensioned application in which the shrinkage characteristics resembled those of the laboratory specimens. For beams in an outdoor exposure, the shrinkage would probably be reduced appreciably which would, in turn, reduce the loss of prestress.

If concretes having the same properties were used in pretensioned members which were subsequently stored in the laboratory atmosphere, the loss of prestress would be about 41,400 psi for the sand and gravel concrete, 57,600 psi for aggregate B concrete, and 63,500 psi for aggregate A concrete. These values are based on the measured deformations, an assumed initial stress of 1,000 psi in the concrete, initial steel stress of 170,000 psi, 4 percent relaxation loss, and sheltered indoor storage.

For posttensioned members, a comparison of values in the preceding paragraphs shows that the loss of prestress of aggregate A concrete is about 67 percent greater than the normal-weight concrete and the loss for aggregate B concrete is about 50 percent greater than the normal-weight concrete. For pretensioned applications, a comparison shows the losses are 53 percent greater for aggregate A concrete and 39 percent greater for aggregate B concrete than the value estimated for the sand and gravel concrete. The high shrinkage of the aggregate A concrete is responsible for the higher losses in this concrete.

SUMMARY

These tests have shown that concretes produced with expanded shale aggregates can provide adequate strength and workability for use in prestressed bridge members. The cement requirement is rather high for the aggregates and gradations used in this study. A nominal cement factor of 9 sacks per cu yd was used. With carefully controlled construction, drier, harsher mixes could probably be used to advantage. With a smaller proportion of fine aggregate, suitable strengths can be obtained with less cement. A reduction in the cement paste would be expected to reduce the shrinkage and probably improve the creep characteristics of the concrete.

For concretes having similar strengths and workability, the use of expanded shale aggregates permits a reduction in weight of approximately 30 percent. The wet weights of the different expanded shale concretes ranged from 102 pcf to 108 pcf while the wet weight of the sand and gravel concrete was 153 pcf. The reduced weight of expanded shale members would make their transportation and erection more economical and in some instances, the reduced weight may permit design alternatives not possible with normal-weight concrete.

The modulus of elasticity of concretes produced from expanded shales is less than one-half as great as for normal-weight concrete of similar strength. The values for the lightweight concretes in this study were around 2×10^6 psi. The low modulus of elasticity is an important consideration in several aspects of design. In pretensioned members, the elastic deformation contributes directly to loss of prestress. Also, the magnitude of camber and deflection would be increased in members having a low modulus of elasticity.

The shrinkage of the concretes used in this study was higher than would ordinarily be anticipated for structural quality concrete in an outdoor application, although other investigators have found similar values in laboratory studies. The shrinkage of the aggregate A concrete was about 41 percent greater than that of the sand and gravel mixture whereas the aggregate B concrete exceeded the sand and gravel concrete by only 4 percent. The amount of shrinkage occurring in the test prisms represents a source of appreciable loss of prestress. An outdoor exposure would probably reduce the shrinkage. Also, concretes having lower mixing water contents would probably exhibit less shrinkage.

By subtracting the measured shrinkage from the total deformation and dividing the remaining creep deformation by the initial stress, creep coefficients were obtained for the prisms subjected to a relaxing prestress force. From these values, the creep of the concrete from aggregate A was 67 percent higher than the normal-weight concrete and the creep of the aggregate B concrete was 90 percent higher than the value for the sand and gravel concrete.

The ultimate loss of prestress indicated by the pressure cells averaged 30 percent for each of the lightweight aggregates, whereas the value for the normal-weight aggregate was 20 percent. Thus, the measured losses are 50 percent greater in each of the lightweight concretes than in the normal-weight concrete. These values include losses due to shrinkage, creep, and relaxation and, although some variation might be expected for different stress levels and different exposures, the percentage difference is likely to remain close to this value. The calculated values discussed earlier indicated total deformations of the lightweight concretes exceeding the normal-weight by 50 percent for aggregate B and 67 percent for aggregate A. Although the values for aggregate A concrete differ, the general range is indicated.

The greater deformations occurring in the lightweight concretes and the resultant increases in loss of prestress would obviously be significant in design; however, with knowledge of the approximate magnitude of the deformations, the expanded shale aggregate concretes can be used satisfactorily in prestressed members. In some applications, the reduced weight would offer important benefits.

ACKNOWLEDGMENTS

This project was conducted by the Oregon State Highway Department in cooperation with the U.S. Bureau of Public Roads.

The project was initiated under the administrative supervision of G.S. Paxson, now retired, and under the direct supervision of Roy C. Edgerton, now Assistant Director for Technical Activities, Highway Research Board. The later stages of the project were conducted under the supervision of P. M. Stephenson, Assistant State Highway Engineer, and John C. Jenkins, Assistant Engineer of Materials and Research, Oregon State Highway Department. The advice of these individuals is greatfully acknowledged. Also, the assistance of Charles R. Chandler, Research Assistant, was greatly appreciated.

REFERENCES

1. Beecroft, G. W. Time Deformation Studies on Two Expanded Shale Concretes. HRB Proc., Vol. 37, pp. 90-105, 1958.
2. Beecroft, G. W. Creep and Shrinkage of Two Lightweight Aggregate Concretes. HRB Bull. 307, pp. 26-41, 1962.
3. American Concrete Institute. Building Code Requirements for Reinforced Concrete. ACI 318-63, June 1963.
4. Jones, T. R., Jr., and Hirsch, T. J. Creep and Shrinkage in Lightweight Concrete. HRB Proc., Vol. 38, pp. 74-89, 1959.
5. Davis, R. E., and Davis, H. E. Flow of Concrete Under the Action of Sustained Loads. Proc. ACI, Vol. 27, pp. 837-901, 1931.
6. Shideler, J. J. Lightweight-Aggregate Concrete for Structural Use. Jour. ACI, Vol. 29, pp. 299-328, 1957.
7. Staley, H. R., and Peabody, D., Jr. Shrinkage and Plastic Flow of Prestressed Concrete. Proc. ACI, Vol. 42, pp. 229-244, 1946.
8. Corley, W. G., Sozen, M. A., and Siess, C. P. Time-Dependent Deflections of Prestressed Concrete Beams. HRB Bull. 307, pp. 1-25, 1962.